

CRYSTAL DYNAMICS AND ANHARMONIC PROPERTIES

OF

Bi-Pb-Tl ALLOYS

CRYSTAL DYNAMICS AND ANHARMONIC PROPERTIES

OF

Bi-Pb-Tl ALLOYS

by

ADITYA PRASAD ROY, M.Sc.

A Thesis

Submitted to the Faculty of Graduate Studies

in Partial Fulfilment of the Requirements

for the Degree

Doctor of Philosophy

McMaster University

September 1970

DOCTOR OF PHILOSOPHY (1970)
(Physics)

McMASTER UNIVERSITY
Hamilton, Ontario

TITLE: Crystal Dynamics and Anharmonic Properties of
Bi-Pb-Tl Alloys.

AUTHOR: Aditya Prasad Roy, M.Sc. (University of Bombay)

SUPERVISOR: Professor B.N. Brockhouse, F.R.S.

NUMBER OF PAGES: xiv, 209

SCOPE AND CONTENTS:

The crystal dynamics and anharmonic properties have been investigated in disordered alloys of Bi-Pb-Tl using slow neutron spectrometry. Damping of phonons caused by phonon-phonon interaction and the effect of the force constant disorder on the lifetime of the phonons have been studied in the alloys. Measurements of the coefficients of thermal expansion are reported. An experimental method of determining the lattice frequency spectra by coherent inelastic scattering of neutrons from polycrystalline materials is described.

ACKNOWLEDGEMENTS

I would like to thank, above all, my research supervisor Professor B.N. Brockhouse, F.R.S., for his guidance and encouragement throughout the course of this work. His inspiring lectures and the many stimulating discussions have contributed greatly to my understanding of the field of solid state physics. I am also indebted to Dr. P.K. Iyengar for initiating me into the field of neutron physics.

I am grateful to Dr. D.W. Taylor for a reading of part of the manuscript and for his advice. I wish to thank Dr. J.P. Carbotte and Dr. E.R. Cowley for many helpful discussions.

To my colleagues at McMaster University, Dr. E.D. Hallman, Dr. A.P. Miiller, Dr. S.C. Ng, Mr. J.R.D. Copley, Mr. J. Couper, Mr. D.H. Dutton, Mr. R. Dymond, Mr. W.A. Kamitakahara, Mr. A. Larose and Mr. H.C. Teh go my sincere thanks for their assistance with the experiments and data analyses, and for many of the computer programs used in this work. The participation of Dr. S.C. Ng in some of the earlier experiments is gratefully acknowledged.

I have appreciated the use of facilities and the cooperation of the staff at Atomic Energy of Canada Ltd.; in particular Dr. G.A. Bartholomew, Dr. A.D.B. Woods and Dr. R.A. Cowley.

I wish to thank the Canadian International Development Agency for financial support and Bhabha Atomic Research Center for granting me study leave.

To Mrs. S. McQueen go my sincere thanks for her cooperation in typing the thesis from a difficult manuscript.

Thanks are due to Mrs. S. Duke and Mr. J. Ho for drawing a number of diagrams.

Finally I wish to thank my wife, Banashree, for her continued patience and encouragement during the course of this work.

TABLE OF CONTENTS

	page
CHAPTER I.	
<u>INTRODUCTION</u>	
A. General Survey	1
B. Outline of the Thesis	4
CHAPTER II.	
<u>CRYSTAL DYNAMICS</u>	
A. Introduction	6
B. Adiabatic approximation	7
C. Born-von Kármán theory	10
D. Anharmonic effects in Thermodynamic Properties	15
E. Fundamental theories of Metals	20
F. Disordered Alloys	30
G. Damping of Phonons	37
CHAPTER III.	
<u>INTERACTION OF THERMAL NEUTRONS WITH SOLIDS</u>	
A. Introduction	39
B. Scattering Cross Section	41
C. Scattering from Perfect and Imperfect Crystals	44
D. Experimental Procedures	51
CHAPTER IV.	
<u>CRYSTAL DYNAMICS OF Bi-Pb-Tl ALLOYS</u>	
A. Introduction	56
B. Dispersion Curves in $Pb_{33}Tl_{67}$ and $Bi_{20}Pb_{60}Tl_{20}$	60

	page
C. Temperature dependence of the dispersion curves in Pb and $Pb_{40}Tl_{60}$.	68
D. Anharmonic damping of phonons in $Pb_{40}Tl_{60}$ and $Bi_{10}Tl_{90}$.	83
E. Anharmonic effects in thermo- dynamic properties--Thermal expansion.	98
F. Kohn anomaly and electron-phonon interaction in Bi-Pb-Tl alloys.	113
G. Phonon frequency spectra of Pb and $Pb_{40}Tl_{60}$ by coherent scattering of neutrons from polycrystalline materials.	136
H. Force constant disorder in the ternary alloy-- $Bi_{20}Pb_{60}Tl_{20}$.	158
APPENDIX I.	
<u>CHARACTERIZATION OF THE</u>	
<u>SPECIMEN SINGLE CRYSTALS</u>	172
APPENDIX II.	
<u>SENSITIVITY FUNCTION AND THE</u>	
<u>RESOLUTION FUNCTION OF THE</u>	
<u>TRIPLE-AXIS SPECTROMETER</u>	180
APPENDIX III.	
<u>TEMPERATURE VARIATION OF THE</u>	
<u>FREQUENCY OF LONGITUDINAL</u>	
<u>INTER-PLANAR OSCILLATIONS IN</u>	
<u>PYROLITIC GRAPHITE.</u>	193
References	199

List of Figures

	Page
Fig. 3.1	Layout of the spectrometers at the McMaster University Reactor. 54
Fig. 3.2	A schematic diagram of the McMaster University triple-axis spectrometer at Chalk River. 55
Fig. 4.1	The phonon dispersion curves for $\text{Pb}_{33}\text{Tl}_{67}$ in the four major symmetry directions at 100°K. 63
Fig. 4.2	The dispersion curves for $\text{Bi}_{20}\text{Pb}_{60}\text{Tl}_{20}$ at 100°K along the symmetry directions. 66
Fig. 4.3	The dispersion curves of Pb at 296°K and 100°K along the symmetry directions. 71
Fig. 4.4	The dispersion curves for $\text{Pb}_{40}\text{Tl}_{60}$ along the symmetry directions at 296°K and 100°K. 74
Fig. 4.5	Bare-ion Coulomb frequencies and the renormalized phonon frequencies in Pb and $\text{Pb}_{40}\text{Tl}_{60}$ along various symmetry directions. 77
Fig. 4.6	The pseudopotential form factors in $\text{Pb}_{40}\text{Tl}_{60}$. 79
Fig. 4.7	The dispersion curves for $\text{Pb}_{40}\text{Tl}_{60}$, calculated at 100°K and 296°K using the Heine-Abarenkov model pseudopotential. Experimental measurements at a few selected points are also shown. 81

- Fig. 4.8 Neutron groups in $\text{Pb}_{40}\text{Tl}_{60}$ at two different temperatures illustrating the temperature dependent background arising from the multiphonon processes. 85
- Fig. 4.9 Typical neutron groups, corrected for the analyzer sensitivity, in $\text{Pb}_{40}\text{Tl}_{60}$ at 100°K and 296°K . 88
- Fig. 4.10 Phonon widths in $\text{Pb}_{40}\text{Tl}_{60}$ at 296°K arising mainly from the anharmonic broadening. 91
- Fig. 4.11 Phonon widths and frequency shifts in $\text{Bi}_{10}\text{Tl}_{90}$. 93
- Fig. 4.12 Typical neutron groups in $\text{Bi}_{10}\text{Tl}_{90}$ at 100°K and 296°K along the $[\zeta 00]\text{L}$ symmetry direction. 94
- Fig. 4.13 Lattice constants measured as a function of temperature for the Bi-Pb-Tl alloys. 102
- Fig. 4.14 Comparison between the calculated and the measured coefficient of thermal expansion for $\text{Pb}_{40}\text{Tl}_{60}$. 107
- Fig. 4.15 Frequency distribution functions of $\text{Pb}_{40}\text{Tl}_{60}$ at 100°K and 296°K , computed using an eight neighbour force constant model. 109
- Fig. 4.16 Calculated lattice specific heat of $\text{Pb}_{40}\text{Tl}_{60}$ at constant pressure (including the anharmonic contribution). 112

	Page
Fig. 4.17	The Fermi surface of $\text{Pb}_{80}\text{Tl}_{20}$ in the $(1\bar{1}0)$ plane. 119
Fig. 4.18	Experimental observation of Kohn anomalies in $\text{Pb}_{80}\text{Tl}_{20}$ along a line parallel to $[\zeta\zeta\zeta]$ but in an off-symmetry direction. 120
Fig. 4.19	Observation of Kohn anomaly along an off-symmetry direction in $\text{Pb}_{80}\text{Tl}_{20}$. 121
Fig. 4.20	Temperature dependence of Kohn anomaly in Pb. 125
Fig. 4.21	The second moments of the frequency distributions for Bi-Pb-Tl alloys, plotted as a function of the average valence. 127
Fig. 4.22	Neutron groups for some Bi-Pb-Tl alloys at two different temperatures, for the $[\zeta 00]\text{T}$ zone-boundary mode. 130
Fig. 4.23	Temperature shifts of the $[\zeta 00]\text{T}$ zone-boundary phonon frequencies for the Bi-Pb-Tl alloys. 132
Fig. 4.24	Plot of v_{exp}^2 ($[\zeta 00]\text{T}$ zone-boundary) against average valence for some alloys. 134
Fig. 4.25	Reciprocal space diagram illustrating double scattering events. 141
Fig. 4.26	Debye-Scherrer lines at 296°K from polycrystalline specimens of Pb and the Pb-Tl alloy. 143

- Fig. 4.27 Observed neutron spectra scattered from Pb powder at 90°K over an energy transfer of 3.2×10^{12} cps and an angular range of 90-142°. 145
- Fig. 4.28 Accumulated data for Pb and $\text{Pb}_{40}\text{Tl}_{60}$, obtained from superposition of all the individual energy distributions recorded at various scattering angles. 148
- Fig. 4.29(a) Comparison of $g(\nu)$ for Pb obtained from the powder experiment with $\alpha^2(\nu)g(\nu)$ from the tunneling measurements. 150
- Fig. 4.29(b) Comparison of $g(\nu)$ for Pb obtained from the powder experiment with that from the neutron scattering results of Stedman et al. 151
- Fig. 4.30(a) Comparison of $g(\nu)$ for $\text{Pb}_{40}\text{Tl}_{60}$ obtained from the powder experiment with $\alpha^2(\nu)g(\nu)$ from the tunneling measurements. 154
- Fig. 4.30(b) Comparison of $g(\nu)$ for $\text{Pb}_{40}\text{Tl}_{60}$ obtained from the powder experiment with $g(\nu)$ computed from an eight neighbour tensor force model. 155
- Fig. 4.31 A scattering diagram in reciprocal space for the powder experiment. 157

	page	
Fig. 4.32	observed neutron spectrum from $\text{Bi}_{20}\text{Pb}_{60}\text{Tl}_{20}$ at 100°K, at the reciprocal lattice point (222).	160
Fig. 4.33	The frequency distribution function for $\text{Bi}_{20}\text{Pb}_{60}\text{Tl}_{20}$ at 100°K, calculated using an eight-neighbour force constant model, with and without energy smearing.	162
Fig. 4.34	"Constant-Q" measurement at $(a/2\pi)\underline{Q} = (2.5, 2.5, 2.5)$ for $\text{Bi}_{20}\text{Pb}_{60}\text{Tl}_{20}$ at 296°K with different tilts of the (110) crystallographic axis with respect to the vertical.	163
Fig. 4.35	Comparison of neutron groups between $\text{Pb}_{80}\text{Tl}_{20}$ and $\text{Bi}_{20}\text{Pb}_{60}\text{Tl}_{20}$ corresponding to the $[\zeta\zeta\zeta]$ zone-boundary phonons.	166
Fig. 4.36	Phonon widths (arising from force constant disorder) plotted as a function of the wavevector along the $[\zeta 00]\text{T}$ branch in $\text{Bi}_{20}\text{Pb}_{60}\text{Tl}_{20}$.	169
Fig. Al.1	Lead solutions (Pb-Tl and Pb-Bi) lattice spacings at 20°C.	173
Fig. Al.2	A family of rocking curves for $\text{Bi}_{10}\text{Tl}_{90}$ -- (400) reflection.	175
Fig. Al.3	Plots of the maximum intensity of the ψ -rocking curves for some of the alloy crystals, as a function of the scattering angle.	176

	Page
Fig. A1.4	Observed widths vs lattice plane spacing. 178
Fig. A2.1	Neutron spectra as measured after thermalization of monoenergetic neutron beams incident on a large paraffin block. Sensitivity function of the analyzing spectrometer obtained from these measurements is also shown. 181
Fig. A2.2	Comparison between the paraffin moderator experiment and the results of Dymond and Brockhouse (1970) for the integrated reflectivity of the analyzing crystal as a function of wavelength. 183
Fig. A2.3	Comparison between the calculated and the experimentally determined sections of the resolution ellipsoid. 187
Fig. A2.4	Energy resolution of the Chalk River spectrometer. 192
Fig. A3.1	Plots of the peak intensity of the crystal rocking curves as a function of the scattering angle at two different temperatures, for pyrolytic graphite. 194
Fig. A3.2	Neutron groups observed at the point $(c/2\pi)Q = (003)$ at various temperatures in pyrolytic graphite. 196

List of Tables

	Page
Table 4.1 (a) Properties of the elements Bi, Pb, Tl.	58
Table 4.1 (b) Properties of the Bi-Pb-Tl alloys	59
Table 4.2 Phonon Frequencies for the symmetry branches in $Pb_{33}Tl_{67}$ at $100^{\circ}K$	62
Table 4.3 Phonon frequencies for the symmetry branches in $Bi_{20}Pb_{60}Tl_{20}$ at $100^{\circ}K$	65
Table 4.4 Atomic force constants for $Bi_{20}Pb_{60}Tl_{20}$ and $Pb_{33}Tl_{67}$ at $100^{\circ}K$	67
Table 4.5 Phonon frequencies for the symmetry branches in Pb at $296^{\circ}K$	70
Table 4.6 Phonon frequencies for the symmetry branches in $Pb_{40}Tl_{60}$ at $100^{\circ}K$ and $296^{\circ}K$	72
Table 4.7 (a) Phonon frequencies in $Bi_{10}Tl_{90}$ along the $[\zeta 00]$ symmetry direction at $100^{\circ}K$ and $296^{\circ}K$	96
Table 4.7 (b) Phonon widths at $296^{\circ}K$ in $Bi_{10}Tl_{90}$ along the $[\zeta 00]$ symmetry direction	97
Table 4.8 Lattice constants for Bi-Pb-Tl al- loys at some selected temperatures	103
Table 4.9 $[\zeta 00]T$ zone-boundary phonon frequencies in the Bi-Pb-Tl alloys measured at different temperatures.	131
Table 4.10 Phonon widths for the zone-boundary modes in $Bi_{20}Pb_{60}Tl_{20}$ at $100^{\circ}K$	168

	page	
Table A1.1	Compositions, homogeneities and lattice constants of the specimen single crystals.	179
Table A2.1	Instrumental Parameters of the triple-axis spectrometer at Chalk River.	186
Table A3.1	Phonon frequencies in pyrolytic graphite, measured at $(c/2\pi)Q=$ (003), as a function of temperature.	198

CHAPTER I
INTRODUCTION

A. General Survey

The atoms in a crystalline solid vibrate about their mean equilibrium positions as a result of thermal fluctuations at finite temperatures. Even at absolute zero there is zero-point motion. From a modern point of view, the foundations of the theory of crystal dynamics were laid down in a pioneering paper by Born and von Kármán (1912).

In the early days, interest in the thermal motions was mainly with a view to explain thermal properties like specific heat. In more recent times the emphasis has changed. The study of lattice dynamics is carried out mainly with a view to obtain better understanding of the nature of interatomic forces in crystals. This approach has been promoted with the advent of some new techniques which enable one to study the detailed motion of the vibrating atoms in crystals. Slow neutron spectroscopy is probably the most powerful tool now available for experimental studies of the internal dynamics of matter in condensed phases.

Einstein (1907) first applied the quantum hypothesis to a crystalline solid. Debye put forward his famous theory of specific heats in 1912. The distribution of frequencies in a solid was considered from the point of view of an elastic

continuum; the medium is assumed to be isotropic and dispersionless. At high temperature Debye theory reduces to the classical Dulong-Petit law and at low temperatures one gets the T^3 law of specific heat. This law was found to hold fairly well for many substances with the experimental results available at that time. The main reason for the success of this simple theory is due to the fact that the thermal properties are rather insensitive to the actual details of the frequency distribution function. The inadequacies of the Debye model were largely pointed out by Blackman (1935, 1941). He showed that considerable deviations from the Debye values exist at intermediate temperatures. He (1935) further pointed out that the experimental observation of T^3 variation in the range (10-50°K) was not related to the real T^3 region, which lies at a much lower temperature ($\sim 0^\circ\text{K}$).

The shortcomings of the Debye theory can be overcome by giving a proper discussion of the atomic motions taking into account the crystalline properties of the substance. In the formulation given by Born and von Kármán (1912), the discrete nature of the lattice and the dispersive property of the medium are taken into account. In a crystal, the atoms execute small oscillations. The motion of the atoms can be considered as superposition of the normal vibrations, the characteristic vibrations, of the crystal. The normal vibrations can be considered as standing waves (a bounded crystal) or travelling waves (an infinite one). The frequency ν or angular frequency ω of the normal

vibrations, and the wavevector \underline{q} are related through the dispersion relation

$$v = v_j(\underline{q}) \text{ or } \omega = \omega_j(\underline{q}) \quad (\text{I.1})$$

The index j characterizes the vibration branch. These lattice waves are quantized in energy and are termed as "phonons". The Born-von Kármán theory provides the link between the phonon dispersion relation and the forces between the atoms in the crystal.

According to the underlying atomic forces, crystalline solids may be classified into the following four principal types:

- (i) Ionic Crystals,
- (ii) van der Waals crystals,
- (iii) Covalent Crystals
- (iv) Metallic crystals.

Light is cast on the nature of the interatomic forces if the lattice vibrations are measured. Such measurements have been made, in particular by neutron inelastic scattering, for many substances (Brockhouse 1966; Dolling and Woods 1965). A study of the dynamics of the metallic alloys of Bi, Pb and Tl by neutron scattering forms the subject of this thesis.

Substitutional disordered alloys of bismuth, lead and thallium exist, with a face-centred-cubic structure. It is possible to vary the conduction electron concentration in these alloys from about 3.1 to 4.15 electrons per atom by varying the constituents and composition. This offers an interesting possibility of studying the effect of conduction electrons on the lattice dynamics (Ng and Brockhouse 1968).

B. Outline of the thesis

Chapter I (section A) summarizes the general background of lattice dynamics with a brief historical introduction.

Crystal dynamics of metals and alloys are discussed in Chapter II. A discussion of the anharmonic properties is also given.

Chapter III describes the theory of slow neutron scattering from solids with emphasis on alloys.

The work presented in these chapters is not original. These chapters are intended to provide a framework within which the experimental results obtained during the present course of work and their theoretical interpretation can be discussed.

The main body of work is contained in Chapter IV. The measurement of phonon dispersion curves in $\text{Pb}_{33}\text{Tl}_{67}$ is presented in Sec. B. The interest in this work lies in the fact that starting from Pb, for which the Fermi surface extends to the third zone, as the electron concentration is reduced by adding Tl the third zone is expected to become virtually empty for the binary alloy $\text{Pb}_{33}\text{Tl}_{67}$. This feature, in turn, manifests itself in the dispersion curves and is discussed in Sec. F along with a comparative study of the electron-phonon interaction in the Bi-Pb-Tl system. In that section we also describe a somewhat detailed experimental study of the Fermi surface in $\text{Pb}_{80}\text{Tl}_{20}$ by the neutron scattering technique which is perhaps the only tool available for investigating the Fermi surface in disordered alloys.

A comparison between the dispersion curves for the alloy $\text{Bi}_{20}\text{Pb}_{60}\text{Tl}_{20}$ and for pure Pb, which both have the same number of electrons per atom, is given in Sec. B. Further, the effect of the force constant disorder, present in the ternary alloy, on the phonon lifetime is discussed in Sec. H.

Anharmonic damping and the temperature induced frequency shifts have been studied in some selected alloys. Measurements of thermal expansion for the Bi-Pb-Tl alloys over a temperature range of 100°K - 400°K are reported.

An experimental method of obtaining the frequency distribution function, from neutron scattering results, for polycrystalline materials is described in Sec. G. This method has been used to obtain the lattice frequency spectra of Pb and $\text{Pb}_{40}\text{Tl}_{60}$.

Appendix I describes the characterisation of the alloy specimens used in the experiment by neutron diffraction technique. The determination of the sensitivity function and the resolution function of the triple-axis spectrometer installed at Chalk River is dealt with in Appendix II. Finally, Appendix III contains a study of temperature dependence of the zone-boundary mode propagating along the hexad axis in pyrolytic graphite. This latter work is not directly related to the main body of work presented in the thesis.

CHAPTER II
CRYSTAL DYNAMICS

A. Introduction

In a crystal, the atom may be considered to execute small oscillations. An important restriction on the validity of the theory of lattice vibrations is that the adiabatic approximation hold; this states that the electrons in the crystal follow the motion of the ions and adjust themselves instantaneously to the nuclear coordinates in the perturbed crystal.

Lattice dynamics is traditionally discussed within the framework of the Born-von Kármán theory. This is a phenomenological theory in which the analysis is carried out using a set of interatomic force constants, analogous to Hooke's spring constants in a mechanical system.

In metals, where the forces are relatively unknown the force constants may not always possess clear physical meaning. There have been reasonably successful attempts to study lattice dynamics of metals from a more fundamental point of view. We also discuss briefly these approaches in this chapter.

B. Adiabatic approximation

Since in this thesis we will be mainly concerned with the lattice vibrations in metals and metallic alloys where the conduction electrons play an important role, it will be worthwhile to examine the validity of the adiabatic approximation in metals.

In the free electron picture a metal can be considered an ordered arrangement of ions embedded in a uniform compensating background of conduction electrons. The core electrons belonging to an ion are assumed to move rigidly and cannot be excited at the energies available. The valence electrons respond easily to screen out the local charge fluctuations generated by the vibration of the positive ion. In other words, the electrons follow the nuclear motion and adjust their wave-functions adiabatically in the perturbed crystals. The exclusion principle forbids transitions from one state to another. Chester (1961) has pointed out that motion of the electrons will be essentially adiabatic, except for those few with energy close to the Fermi energy. The adiabatic approximation may then be expected to hold good for properties in which the entire distribution of electrons take part, such as for the frequencies of lattice vibrations*.

The adiabatic approximation introduces considerable simplification in the problem by separating the dynamical aspects of the electron and ion motion (Born and Oppenheimer

* The adiabatic approximation may break down in the region of Kohn anomaly--see Chapter IV.

1927). One finds (Sham and Ziman 1963) that the part of the potential energy of the ion system due to the presence of the conduction electrons is just the total energy of such an electron system. This electron energy is a function of the lattice coordinates only, though strictly speaking it also depends on the exact electron states. We will see later how the "bare" lattice frequencies (computed from the direct interaction between the ions--mainly Coulomb interaction) are to be "renormalized" to give the observed frequencies when the contribution from the electron gas is taken into account.

A rather independent justification of this decoupling procedure has been given by Migdal (1958) using techniques of many-body theory. Because phonon frequencies are so low compared with typical electron "frequencies" (being of the order of $\sqrt{m/M}$ where m is the electron mass and M is the ionic mass) the phonons may be regarded as an external field which is only weakly coupled to the electron gas. The corrections to the electron-phonon interaction may be shown to be of order $(m/M)^{1/2}$ relative to the terms one has kept. Finally, mention may be made of the concept of "neutral pseudo-atom" (an ion plus its screening charge) introduced by Ziman (1964) which makes the adiabatic approximation more plausible in metals. As the bare ion moves around, it carries its cloud of screening electrons with it. The field of an ion is however, not completely screened at moderately large distances. Friedel (1952) showed that at large distances the screened potential has an oscillatory behaviour. This is a possible source of the

long range interactions in metals (Langer and Vosko 1959).

Having discussed the justification of the adiabatic approximation we give a brief description of the elements of the classical theory of lattice dynamics to introduce the notation and terminology. Detailed discussions can be found in Born and Huang (1954), Maradudin et al. (1963), and Ludwig (1967).

C. Born-von Kármán approach

We shall consider a perfect crystal, having no impurities, vacancies or dislocations. Further, we confine ourselves to monatomic Bravais lattices* The interaction between the assembly of the particles is assumed to be completely described by a potential energy. This potential energy is supposed to be a function of the relative positions of the particles only.

It is often difficult to discuss finite crystals. Therefore one uses an infinite crystal in many considerations. But since the potential energy of an infinite crystal diverges, one divides this infinite crystal into "macrocrystals" simulating in this way a finite crystal. It can be shown (Maradudin et al. 1963) that for the discussion of bulk properties this procedure is alright since surface effects give negligible contributions. This infinite crystal can be described in terms of the basis vector \underline{a}_i ($i=1,2,3$). In equilibrium, all lattice sites are given by

$$\underline{R}^{\ell} = \sum_i \ell_i \underline{a}_i$$

where $\{\ell_i\}$ stands for the integer components of ℓ extending from $-\infty$ to $+\infty$.

With respect to every Bravais lattice there exists a reciprocal lattice which is defined by the basis vectors

$$\underline{a}_i \cdot \underline{b}_j = \delta_{ij} .$$

After specifying the equilibrium positions of the lattice we can give the expansion of the potential energy about these positions, \underline{u}^{ℓ} being the displacements of the ions from the equilibrium position.

* The substances discussed in this thesis fall in this category.

$$\Phi(\underline{R}^{\ell} + \underline{u}^{\ell}) = \Phi_0(\underline{R}^{\ell}) + \Phi_1 + \Phi_2 + \Phi_3 + \dots \quad (2.1)$$

with

$$\Phi_1 = \sum_{\alpha, \ell} \Phi_{\alpha}^{\ell} u_{\alpha}^{\ell}$$

$$\Phi_2 = \frac{1}{2!} \sum_{\substack{\alpha\beta \\ \ell\ell'}} \Phi_{\alpha\beta}^{\ell\ell'} u_{\alpha}^{\ell} u_{\beta}^{\ell'} \quad (2.2)$$

$$\Phi_3 = \frac{1}{3!} \sum_{\alpha\beta\gamma} \sum_{\ell\ell'\ell''} \Phi_{\alpha\beta\gamma}^{\ell\ell'\ell''} u_{\alpha}^{\ell} u_{\beta}^{\ell'} u_{\gamma}^{\ell''}$$

The subscripts α, β, γ denote Cartesian components; Φ_0 is just the static (equilibrium) potential energy of the crystal and

$$\phi_{\alpha}^{\ell} = \left. \frac{\partial \Phi}{\partial u_{\alpha}^{\ell}} \right|_0 ; \quad \phi_{\alpha\beta}^{\ell\ell'} = \left. \frac{\partial^2 \Phi}{\partial u_{\alpha}^{\ell} \partial u_{\beta}^{\ell'}} \right|_0 \dots \quad (2.3)$$

The subscript zero means that the derivatives are evaluated in the equilibrium configuration. For finite crystals, $\Phi(\underline{R}^{\ell} + \underline{u}^{\ell})$ is properly defined. In infinite crystals, one considers usually the potential energy of one periodicity volume in order to avoid divergences. In any case, the coupling parameters $\phi_{\alpha\beta}^{\ell\ell'}$ have a definite meaning:-- $\phi_{\alpha\beta}^{\ell\ell'} u_{\beta}^{\ell'}$ is the force acting on ion ℓ in α -direction if the ion ℓ' is displaced by $u_{\beta}^{\ell'}$.

A first approximation to lattice theory is obtained from (2.1) by dropping terms of higher than 2nd order in displacements. If one further takes the equilibrium positions defined by the minimum of the potential energy ($\phi_{\alpha}^{\ell} = 0$), independent of temperature then it is called a harmonic theory.

However, such a harmonic theory does not account for a number of effects, such as, thermal expansion, the temperature dependence of elastic constant, the difference between specific heat at constant volume and constant pressure and many other

effects. These effects are strongly related to anharmonic terms in the expansion of the potential energy with respect to the displacements. Therefore, it is convenient to use the following procedure: the expansion (2.1) is performed by starting with unknown equilibrium positions \underline{R}^ℓ which are treated as parameters to be determined later by the equilibrium condition which is the minimum of the Helmholtz free energy. Now, the equilibrium position does not coincide with the position of minimum potential energy and therefore the ϕ_1 -term does not vanish in general. However, for Bravais lattices it can still be shown (Leibfried and Ludwig 1961) that $\phi_\alpha^\ell = 0$ as a consequence of inversion symmetry. Therefore, limiting the expansion (2.1) to the quadratic terms

$$\Phi(\underline{R}^\ell + \underline{u}^\ell) = \Phi_0(\underline{R}^\ell) + \frac{1}{2!} \sum_{\substack{\alpha\beta \\ \ell\ell'}} \phi_{\alpha\beta}^{\ell\ell'} u_\alpha^\ell u_\beta^{\ell'} \quad (2.4)$$

This is called the quasiharmonic approximation because it is formally identical with the harmonic theory but the coupling parameters $\phi_{\alpha\beta}^{\ell\ell'}$ involve the temperature dependent equilibrium positions \underline{R}^ℓ .

The equations of motion are

$$M u_\alpha^\ell = - \sum_{\beta\ell'} \phi_{\alpha\beta}^{\ell\ell'} u_\beta^{\ell'} \quad (2.5)$$

The displacement \underline{u}^ℓ of an atom ℓ from its equilibrium position is given by the superposition of the displacements for the individual normal vibration, thus:

$$\underline{u}^\ell = \frac{1}{\sqrt{MN}} \sum_{\underline{q}j} A_j(\underline{q}) \underline{\xi}_j(\underline{q}) \exp[i(\underline{q} \cdot \underline{R}^\ell - \omega_j(\underline{q})t)] \quad (2.6)$$

The amplitudes A determine the amount of energy carried.

$\underline{\xi}_j(\underline{q})$ is a unit polarization vector and \underline{q} is a propagation vector with magnitude equal to $\frac{2\pi}{\lambda}$, λ being the wavelength of the lattice wave. Considering the contribution of one of the components (\underline{q}, j) of Eq. (2.6), we obtain from Eq. (2.5) a relation between the normal mode frequencies and the coupling parameters of second order,

$$\omega_j^2(\underline{q}) = \sum_{\alpha\beta} D_{\alpha\beta}(\underline{q}) \xi_{\alpha j}(\underline{q}) \xi_{\beta j}(\underline{q}) \quad (2.7)$$

with

$$D_{\alpha\beta}(\underline{q}) = \frac{1}{M} \sum_{\ell, \ell'} \phi_{\alpha\beta}^{\ell\ell'} \exp[-i\underline{q}(\underline{R}^{\ell} - \underline{R}^{\ell'})] \quad (2.8)$$

The three solutions $\omega_j(\underline{q})$, $j=1,2,3$ for each value of \underline{q} are obtained by finding the roots of the determinantal equation

$$\det |D - \omega^2 I| = 0$$

Using the translational invariance of the lattice, Eq. (2.8) can be rewritten as

$$D_{\alpha\beta}(\underline{q}) = \frac{1}{M} \sum_{\ell \neq \ell'} \phi_{\alpha\beta}^{\ell\ell'} [\exp(i\underline{q} \cdot \underline{R}^{\ell'}) - 1] \quad (2.9)$$

Because of the structural identity of all unit cells, the summation does not depend on ℓ , the position of the unit cell containing the "origin atom".

The different allowed values of \underline{q} are determined by the well known Born-von Kármán cyclic condition imposed on \underline{u}^{ℓ} .

The allowed \underline{q} values are given by

$$\underline{q} = 2\pi \sum_i (h_i/L_i) \underline{b}_i$$

where $L_i a_i$ are the dimensions of the Born-von Kármán repeat units.

In practical applications of the Born-von Kármán model, the interactions are assumed to exist between a particle and a limited group of neighbours. This limits the total number of force constants. The independent constants for a particular

neighbour are those permitted by symmetry considerations alone. Further reduction on the number of force constants can be achieved by postulating a form for the potential, eg, that the force constants be derivable from a spherically symmetric potential. Another useful way of analysing dispersion relations along symmetry directions in terms of interplanar force constants has been proposed by Foreman and Lomer (1957). Lucid discussions of these different force constant models can be found in the review articles by Brockhouse et al. (1968) and Joshi and Rajagopal (1968).

D. Anharmonic Effects in Thermodynamic Properties

Thermal Expansion: We can write the Helmholtz free energy in the quasiharmonic theory (see, for example, Ludwig (1967))

$$F_{\text{qh}} = \Phi_0(\underline{R}^\ell) + kT \sum_{\underline{qj}} \ln \left\{ 2 \sinh \frac{h\nu_j(\underline{q})}{kT} \right\} \quad (2.10)$$

which is again the harmonic free energy apart from the fact that Φ_0 and the frequencies $\nu_j(\underline{q})$ depend on the position parameters \underline{R}^ℓ . Now, we can determine the equilibrium positions by taking the derivative of F_{qh} as a function of cell parameter. It is more convenient to introduce the tensor of finite thermal strain $\epsilon_{\alpha\beta}$ to describe the temperature variation of the cell data. In cubic crystals with the assumption of isotropic expansion, we can write $\epsilon_{\alpha\beta} = \eta \delta_{\alpha\beta}$ where $\eta = \Delta a/a_0$, fractional change in lattice constant. Hence, in case of vanishing stresses in the equilibrium state

$$\frac{\partial F_{\text{qh}}}{\partial \eta} = 0 = \frac{\partial \Phi_0}{\partial \eta} + \sum_{\underline{qj}} \frac{\partial h\nu_j(\underline{q})}{\partial \eta} \left[\bar{n}_j(\underline{q}) + \frac{1}{2} \right] \quad (2.11)$$

since only $\nu_j(\underline{q})$ depends on the parameter \underline{R}^ℓ or η . In this expression $\bar{n}_j(\underline{q})$ is the mean thermal occupation number of an oscillator (\underline{q}, j), i.e. $\bar{n} = [\exp(h\nu/kT) - 1]^{-1}$.

If we introduce the mean thermal energy $\epsilon(\nu, T) = (\bar{n} + \frac{1}{2})h\nu$ of an oscillator we have,

$$\frac{\partial \Phi_0}{\partial \eta} + \frac{1}{2} \sum_{\underline{qj}} \frac{\partial \ln(\nu_j^2(\underline{q}))}{\partial \eta} \epsilon(\nu, T) = 0 \quad (2.12)$$

We define the Grüneisen constant

$$\gamma_j(\underline{q}) = -\frac{1}{6} \frac{\partial \ln v_j^2(\underline{q})}{\partial \eta} = -\frac{a_0}{6} \frac{\partial \ln v^2}{\partial a} = -\frac{\partial \ln v}{\partial \ln v} \quad (2.13)$$

where v is the volume of the unit cell. The change of ϕ_0 with thermal strain can be related to the elastic constants With zero mechanical stresses (Ludwig 1967)

$$\frac{\partial \phi_0}{\partial \eta} = \sum_{\alpha\beta} N C_{\alpha\alpha, \beta\beta} \eta v,$$

where $C_{\alpha\alpha, \beta\beta}$ are the elastic constants and N is the number of unit cells in the crystal. Further, in cubic crystals

$$\sum_{\alpha\beta} C_{\alpha\alpha, \beta\beta} = \frac{3}{\chi},$$

where χ is the compressibility. Solving for η from (2.12) we finally obtain

$$\eta = \frac{\chi}{Nv} \sum_{\underline{qj}} \gamma_j(\underline{q}) \varepsilon(v, T), \quad (2.14)$$

and the coefficient of thermal expansion

$$\beta(T) = \frac{\partial \eta}{\partial T} = \frac{\chi}{Nv} \sum_{\underline{qj}} \gamma_j(\underline{q}) \frac{\partial \varepsilon(v, T)}{\partial T}. \quad (2.15)$$

If we are interested in a rough overall estimate of temperature dependence then we may replace the Grüneisen constant by a mean value: $\gamma = \frac{1}{3N} \sum_{\underline{qj}} \gamma_j(\underline{q})$, and take it outside the summation. The expansion coefficient is then proportional to the specific heat in harmonic theory; vanishing as T^3 with $T \rightarrow 0$ and at high temperature ($T > \theta_D$) becomes a constant (Grüneisen 1926).

Entropy and Specific heat

Since the number of atoms in a crystal is very large and the eigenvalues are bounded and quasi-continuous, it is more convenient to deal with the frequency distribution function in discussing thermodynamic properties than with the individual frequencies. We define $g(v)dv$ to be the fraction of

frequencies in the interval $(\nu, \nu+d\nu)$ along with the normalization condition

$$\int g(\nu) d\nu = 3N$$

In the harmonic approximation, there are three alternative ways of calculating the heat capacity

$$C_V = T \left(\frac{\partial S}{\partial T} \right)_V = -T \left(\frac{\partial^2 F}{\partial T^2} \right)_V = \left(\frac{\partial E}{\partial T} \right)_V \quad (2.16)$$

where S is the entropy, F the free energy and E is the vibrational energy of the lattice. To obtain the anharmonic contribution, one can start with the harmonic expressions and allow the normal mode frequencies to vary with temperature. The correction derived from a harmonic expression for E approaches a constant value at high temperature (Stedman et al. 1967) whereas according to anharmonic theory it should vary as T . Cowley (1963) has found that harmonic expressions for free energy leads to a change in the temperature dependent part of the free energy which is twice the amount obtained by more proper consideration of phonon-phonon interaction. Now, Barron (1965) has shown that to a first approximation entropy is the appropriate quantity for calculating the thermodynamic properties of an anharmonic crystal; the entropy can be calculated by using the frequency distribution, determined by inelastic scattering, in the appropriate quasi-harmonic expression. Essentially this approach has been used to calculate the total lattice specific heat (including the anharmonic contribution) by Stedman et al. (1967b) for Al and Pb and by Miiller and Brockhouse (1968, 1970) for Pd and Cu.

The lattice entropy of a crystal is given by

$$S(T) = k \int_0^{\nu_m} \left\{ \frac{h\nu_T/kT}{(\exp(h\nu_T/kT)-1)} - \ln[1 - \exp(-\frac{h\nu_T}{kT})] \right\} g_T(\nu_T) d\nu_T \quad (2.17)$$

ν_T and $g_T(\nu_T)$ represent the frequencies and the distribution function as obtained in neutron scattering experiments at a temperature T . Since the measurements are normally carried out at constant pressure (essentially zero pressure) $S(T)$ refers to the entropy at constant pressure at the temperature T . It is useful to express the frequencies and the frequency distribution function in the above equation for $S(T)$ in terms of the quantities at some reference temperature T_0 . This reference temperature may be chosen to be the room temperature or some other convenient temperature for which detailed measurements of phonon frequencies are available so that the frequency distribution function is well determined at that temperature.

The temperature dependence of the normal mode frequencies can be described by

$$\nu_{\underline{qj}}(T) = \nu_{\underline{qj}}(T_0) G_{\underline{qj}}(T)$$

$G_{\underline{qj}}(T)$ has an implicit dependence on T_0 (reference temperature). Assuming that the relative frequency shifts of all modes are the same (this is equivalent to assuming an average Gruniesen constant for the crystal) we can write in a simplified notation

$$\nu_T = \nu_0 G(T) \quad (2.18)$$

also

$$g_T(\nu_T) d\nu_T = g_0(\nu_0) d\nu_0$$

Hence Eq. (2.17) can be rewritten as

$$S(T) = k \int d\nu_o g_o(\nu_o) \left\{ \frac{(h\nu_o/kT)G(T)}{(\exp[(h\nu_o/kT)G(T)]-1)} - \ln(1-\exp[-(h\nu_o/kT)G(T)]) \right\} \quad (2.19)$$

The lattice specific heat at constant pressure is then given by

$$C_\ell(T) = T \left(\frac{\partial S}{\partial T} \right) = k \int d\nu_o g_o(\nu_o) \frac{[(h\nu_o/kT)G(T)]^2 \exp[(h\nu_o/kT)G(T)]}{(\exp[(h\nu_o/kT)G(T)]-1)^2} \left\{ 1 - \frac{T(dG(T)/dT)}{G(T)} \right\} \quad (2.20)$$

Thus, it is seen that from a knowledge of the temperature dependence of normal mode frequencies one can calculate the total lattice specific heat at any temperature T using the frequency distribution function at some reference temperature T_o . This procedure automatically ensures inclusion of the anharmonic contribution in the calculation.

E. Fundamental Theories of Crystal Dynamics of Metals

It has been found experimentally that the Fermi surfaces of the polyvalent metals (eg Zn, Al, Pb) are remarkably close to the appropriate spherical surfaces corresponding to the free electron gas. This indicates clearly that the periodic potential of the lattice has only a relatively small effect upon the energy bands in metals. However, the lattice potential itself is certainly not small. Near an ion core the potential acting on a valence electron is very strong and attractive and the wavefunction of the electron has an oscillatory behaviour in this region arising from the orthogonalisation of the conduction electron wavefunctions to the core orbitals. Phillips and Kleinman (1959) noted that this orthogonalisation has the effect of a repulsive potential to be added to the true crystalline potential. The net effective potential has come to be called the pseudopotential which can be suitably chosen to be a weak potential. This feature makes it possible to use perturbation theory. Harrison (1962) applied such a calculation to a metal in a study of the band structure and the Fermi surface of zinc. Subsequently, this pseudopotential method has proved to be a reasonably successful tool in calculating band structure, phonon spectra and atomic properties of a large number of metals. In the general formulation, the pseudopotential is a nonlocal operator. Further, some kind of nonuniqueness is associated with the choice of the pseudopotential (Harrison 1966).

The Diffraction Model

We consider a metal containing N similar atoms, each atom contributing Z conduction electrons. The ions interact with each other through a central force potential $V_d(R)$ which we call the direct interaction. We use the small core approximation i.e. we assume that adjacent cores do not overlap. Hence, the only important contribution to $V_d(R)$ arises from Coulomb interaction.

At the same time, these ions interact with the conduction electrons through a weak central force potential $w^0(r)$. Summing over the ionic positions \underline{R}^ℓ ($\ell=1,N$), the potential energy $W^0(r)$ of an electron at r is given by

$$W^0(r) = \sum_{\ell} w^0(|\underline{r}-\underline{R}^\ell|) \quad (2.21)$$

It may be noted that at this stage we have not specified the arrangement of the ions. Hence, the model includes the case of perfect crystal i.e. a periodic array of atoms as well as a completely disordered system.

Next we evaluate matrix elements of $W^0(r)$ between plane wave states. We represent a normalised plane wave labelled by the state \underline{k} as

$$\psi_{\underline{k}}(r) = |\underline{k}\rangle = \frac{1}{\sqrt{N\Omega_0}} e^{i\underline{k}\cdot\underline{r}}$$

where Ω_0 is the atomic volume⁺ and N is the number of unit cells.

We find that

$$\langle \underline{k}+\underline{Q} | W^0(r) | \underline{k} \rangle = S(\underline{Q}) \langle \underline{k}+\underline{Q} | w^0(r) | \underline{k} \rangle \quad (2.22)$$

where \underline{Q} is a general vector in reciprocal space.

* We will see in the next section that $W^0(r)$ will be screened when we allow the electrons to interact with each other.

⁺ For a monatomic solid $\Omega_0 = v$ (volume of the unit cell)

The structure factor

$$S(\underline{Q}) = \frac{1}{N} \sum_{\ell} e^{-i\underline{Q} \cdot \underline{R}_{\ell}} \quad (2.23)$$

depends only upon the arrangement of the ions and is independent of the individual ionic potentials. The form factor

$$\langle \underline{k} + \underline{Q} | w^0(\underline{r}) | \underline{k} \rangle = \frac{1}{\Omega_0} \int e^{-i(\underline{k} + \underline{Q}) \cdot \underline{r}} w^0(\underline{r}) e^{i\underline{k} \cdot \underline{r}} d\tau \quad (2.24)$$

is quite independent of the arrangement of the ions (except through a change of volume, Ω_0). The form factors are simply the Fourier transforms of the individual ionic potentials. (As discussed before, the ion-electron interaction can be represented by a weak pseudopotential. However, this is immaterial for the present discussion). If we make the assumption that $w^0(\underline{r})$ is a local potential rather than an operator then the form will depend only on \underline{Q} and be independent of \underline{k} . Therefore, in the local approximation we arrive at the simple result

$$w^0(\underline{Q}) = \frac{1}{\Omega_0} \int e^{-i\underline{Q} \cdot \underline{r}} w(\underline{r}) d\tau. \quad (2.25)$$

A Simple Theory of Screening in Metals (Local Pseudopotential):--

So far we have neglected the electron-phonon interaction in the sense that the problem has been treated as an electrostatic one in which point ions move in a uniform distribution of negative charge which does not respond to their motion. If we consider the electron-electron interaction explicitly then the electrons follow the motion of the ions and screen out the interaction of the latter. This result

was first obtained by Bardeen (1937) in his classic paper. Screening plays such a fundamental role in the behaviour of metals that it has been aptly remarked by Harrison "that any understanding of metals which does not include a feeling for screening is in a sense illusory".

We first study the screening of an ion in an electron gas. For its interaction with an electron we represent the ion by a fictitious positive charge distribution $eZ(r)$ which is localised at the core. The ionic charge is given by

$$eZ = \frac{1}{\Omega_0} e \int_{\Omega_0} Z(\underline{r}) d\underline{r}$$

Assuming that the charge distribution is spherically symmetric, we obtain the corresponding potential from Poisson's equation $\nabla^2 w^0(\underline{r}) = -\frac{4\pi e^2}{\Omega_0} Z(r)$. Taking Fourier transforms we obtain

$$w^0(Q) = \frac{4\pi e^2}{\Omega_0 Q^2} Z(Q) \quad (2.26)$$

Now, electrons will pile up around the ion with a charge distribution $Z_e(r)$ and will tend to screen out the field of the ion at large distances. Let us write this potential due to the conduction electrons as $w_e(r)$. (This is a potential energy; it is the electrostatic potential times the electronic charge). It also follows that $w_e(Q) = \frac{4\pi e^2 Z_e(Q)}{\Omega_0 Q^2}$. We

finally obtain for the screened potential

$$\begin{aligned} w(Q) &= w^0(Q) + w_e(Q) \\ &= \frac{4\pi e^2}{\Omega_0 Q^2} [Z(Q) + Z_e(Q)] \end{aligned} \quad (2.27)$$

Applying first order perturbation theory to the wave equation for free electrons where $w(r)$ is the perturbing potential,

we obtain for the perturbed wavefunction

$$\psi_{\underline{k}}(\underline{r}) = \frac{1}{\sqrt{N\Omega_0}} \exp(i\underline{k} \cdot \underline{r}) + \frac{1}{\sqrt{N\Omega_0}} \sum_{\underline{Q}} \frac{\langle \underline{k} + \underline{Q} | w(\underline{r}) | \underline{k} \rangle}{E_{\underline{k}} - E_{\underline{k} + \underline{Q}}} \times \exp[i(\underline{k} + \underline{Q}) \cdot \underline{r}]$$

Now
$$z_e(\underline{r}) = \sum_{\underline{k} < k_F} [|\psi_{\underline{k}}(\underline{r})|^2 - 1] = \sum_{\underline{Q}} z_e(\underline{Q}) e^{i\underline{Q} \cdot \underline{r}},$$
 where the

summation is carried over the occupied states ie. over the Fermi surface. E_F and k_F denote the energy and wavenumber of an electron at the Fermi surface. Substituting the value of $\psi_{\underline{k}}(\underline{r})$, we obtain for a particular Fourier component of the electron density

$$z_e(\underline{Q}) = \frac{2}{N\Omega_0} w(\underline{Q}) \sum_{\underline{k} < k_F} \frac{1}{E_{\underline{k}} - E_{\underline{k} + \underline{Q}}}. \quad (2.28)$$

Now,

$$\begin{aligned} \sum_{\underline{k} < k_F} \frac{1}{E_{\underline{k}} - E_{\underline{k} + \underline{Q}}} &= \frac{2N\Omega_0}{(2\pi)^3} \int_{k_F} \frac{d\underline{k}}{\frac{\hbar^2}{2m} [k^2 - (\underline{k} + \underline{Q})^2]} \\ &= -\frac{N\Omega_0 k_F^3}{8\pi^2 E_F} \left[1 + \frac{1-\eta^2}{2\eta} \ln \left| \frac{1+\eta}{1-\eta} \right| \right], \\ \eta &= \frac{Q}{2k_F} \end{aligned}$$

$$\text{Defining } \epsilon(\underline{Q}) = 1 + \frac{me^2}{2\pi k_F \hbar^2 \eta^2} \left[1 + \frac{1-\eta^2}{2\eta} \ln \left| \frac{1+\eta}{1-\eta} \right| \right] \quad (2.29)$$

we can rewrite (2.28) as

$$z_e(\underline{Q}) = \frac{Q^2}{4\pi e^2} w(\underline{Q}) (1 - \epsilon(\underline{Q}))$$

Using Eq. (2.27)

$$z_e(\underline{Q}) = -z(\underline{Q}) \left(1 - \frac{1}{\epsilon}\right) \quad (2.30)$$

and

$$w(\underline{Q}) = w^0(\underline{Q}) / \epsilon(\underline{Q}) \quad (2.31)$$

$\epsilon(Q)$ may be termed the static dielectric function for a free electron gas in the Hartree approximation since we have neglected exchange and correlation effects. It should also be pointed out that the present analysis is valid only if w is a local potential; the result is slightly more complicated if this cannot be done (Sham and Ziman 1963). In the general case the scalar $\epsilon(Q)$ is a matrix $\epsilon(\underline{q} + \underline{G}, \underline{q} + \underline{G}')$ whose rows and columns are labeled by the reciprocal lattice vectors. Also, the Fourier components of the bare ionic potential are not screened independently in this case. We remark here that the logarithmic singularity in the screening at $Q = 2k_F$ gives rise to similar singularities in the dispersion curves (See Chapter IV(F) for a detailed discussion).

One can allow for exchange and correlation effects in the electron interaction in an approximate way without changing the form of Eq. (2.31). Based upon Hubbard's method, and as used by Sham (1965) and Heine and Abarenkov (1964), the exchange can be included in our formulation by writing

$$\epsilon(Q) = 1 + \frac{V(Q)\Pi_0(Q)}{1 - V(Q)f(Q)\Pi_0(Q)} \quad (2.32)$$

where $V(Q) = \frac{4\pi e^2}{Q^2}$, $f(Q) = \frac{1}{2} Q^2 / (Q^2 + \beta^2)$

and $\Pi_0(q) = \frac{mk_F}{2\pi^2 n^2} \left[1 + \frac{1-\eta^2}{2\eta} \ln \left| \frac{1+\eta}{1-\eta} \right| \right]$ (2.33)

β is a measure of the inverse screening length used in the Hubbard correction. Geldart and Vosko (1966, 1967) have given a prescription for determining β from the electron gas compressibility.

Having obtained the screened ion-electron interaction we can now proceed to obtain an expression for the total energy change when a pair of identical ions are introduced as imposed charges in the electron gas. For our purpose we can separate the total contribution into two parts

$$V(R) = V_d(R) + V_{ind}(R) \quad (2.34)$$

$V_d(R)$ represents the direct coulomb interaction between the ions separated by a distance R . The ions can be treated as point charges to evaluate this contribution and is given by

$$V_d(R) = \frac{Z^2 e^2}{R} = \frac{\Omega_0}{(2\pi)^3} \int U_c(Q) e^{i\mathbf{Q}\cdot\mathbf{R}} d\mathbf{Q} \quad (2.35)$$

$$\text{where } U_c(Q) = \frac{4\pi Z^2 e^2}{\Omega_0 Q^2} .$$

$V_{ind}(R)$ refers to the indirect interaction between the ions via the conduction electrons. The change of electron energy will involve the interaction of a positive charge distribution $eZ(\mathbf{r})$ with a negative charge distribution $eZ_e(|\mathbf{R}-\mathbf{r}|)$. Expressing this part of the energy in terms of the corresponding Fourier transforms

$$V_{ind}(R) = \frac{\Omega_0}{(2\pi)^3} \int \frac{4\pi e^2 Z(Q) Z_e(Q)}{Q^2} e^{i\mathbf{Q}\cdot\mathbf{R}} d\mathbf{Q}$$

Substituting the value of $Z_e(Q)$ from Eq. (2.30), we can rewrite the above expression as

$$V_{ind}(R) = \frac{\Omega_0}{(2\pi)^3} \int U_e(Q) e^{i\mathbf{Q}\cdot\mathbf{R}} d\mathbf{Q} \quad (2.36)$$

$$\text{where* } U_e(Q) = - \frac{\Omega_0 Q^2}{4\pi e^2} |w^0(Q)|^2 \left(1 - \frac{1}{\epsilon(Q)}\right) \quad (2.37)$$

Finally, the total energy for N identical ions immersed in the electron gas can be expressed as

$$\Phi = \frac{1}{2} \sum_Q S(Q) S^*(Q) U(Q), \quad U(Q) = U_c(Q) + U_e(Q) \quad (2.38)$$

The treatment of electron-phonon interaction given above follows closely that given by Cochran (1965). The results are essentially the same as presented by Harrison (1966) in his book "Pseudopotentials in the Theory of Metals" where he has emphasized the significance of the above result. Some of the approximations made here do not enter his calculations; however same general conclusions were reached. His work was mainly directed at obtaining the total energy of the crystal which includes the contribution from the free electron energy also. However, in lattice dynamics calculations, the free electron energy does not enter since it is independent of the rearrangement of the ions at constant volume.

Dispersion Curves and Interatomic Potential

The dynamical matrix, $D_{\alpha\beta}(\underline{q})$, defined by Eq. (2.9) involves summation over all direct lattice points. We can obtain an alternative form for the dynamical matrix in terms of a summation over all reciprocal lattice points.

* The present definition of $U(Q)$ differs by a factor of two from the quantity $F(Q)$ introduced by Harrison (1966). This is because Harrison's $F(Q)$ refers to energy per ion and not for a pair of ions as considered here.

If \underline{Q} is a general vector in the reciprocal space, we can take a Fourier expansion of the interatomic potential $V(\underline{R})$ between two ions separated by a distance \underline{R} :

$$V(\underline{R}) = \sum_{\underline{Q}} U(\underline{Q}) \exp(i\underline{Q} \cdot \underline{R}) \quad (2.39a)$$

If we regard the lattice potential Φ to be sum of two-body potentials $V(\underline{R}^{\ell} - \underline{R}^{\ell'})$, we have

$$\Phi_{\alpha\beta}^{\ell\ell'} = - [\partial^2 V(\underline{R}) / \partial R_{\alpha} \partial R_{\beta}]_{\underline{R}=\underline{R}^{\ell}-\underline{R}^{\ell'}} \quad (2.39b)$$

Now, substituting $\Phi_{\alpha\beta}^{\ell\ell'}$ from (2.39) and using the standard relation

$$\frac{1}{N} \sum_{\underline{l}} \exp(i\underline{Q} \cdot \underline{R}_{\underline{l}}) = \sum_{\underline{G}} \delta_{\underline{Q}, \underline{G}}$$

where \underline{G} is a reciprocal lattice vector ; we obtain

$$D_{\alpha\beta}(\underline{q}) = \frac{1}{M} \left[\sum_{\underline{G}} (\underline{q} + \underline{G})_{\alpha} (\underline{q} + \underline{G})_{\beta} U(\underline{q} + \underline{G}) - \sum_{\underline{G} \neq 0} G_{\alpha} G_{\beta} U(\underline{G}) \right] \quad (2.40)$$

For short range interaction, (2.9) converges more rapidly and for long range potential (2.40) is to be preferred. The function $U(\underline{Q})$ is a sum of two terms $U_c(\underline{Q})$ and $U_e(\underline{Q})$, as can be seen from the analysis given in the previous section. The first, $U_c(\underline{Q})$, describes the Coulomb interaction of the ions due to their valence charges and the second term describes the interaction of the conduction electrons with these ions and essentially screens the former interaction.

Evaluation of the Coulomb contribution to vibration frequencies can be made using standard procedures (Born and Huang 1954). $U_e(\underline{Q})$ depends upon the choice of model for the electron-ion potential and the nature of the approximation describing the interacting electron gas.

Toya (1958) was the first to calculate the normal mode frequencies of monovalent metals from fundamental considerations. Recently the pseudopotential approach has been successfully employed to calculate the lattice dynamics of metals. However, in some cases even though the phonon dispersion curves and the elastic constants could be explained fairly well, the calculated binding energy was far from the correct value (Cochran 1963; Harrison 1966). This deficiency was rectified in an improved pseudopotential calculation for Na and K by Wallace (1968a) where the exchange and the correlation energy of the electron gas were properly taken into account. Heine and Abarenkov (1964) have proposed a method of setting up a model pseudopotential from the spectroscopic data pertinent to the free atom. An extensive discussion of the recent theories of lattice dynamics of metals can be found in the review article by Joshi and Rajagopal (1968).

F. Disordered Alloys

(i) Crystal Dynamics of Alloys

In the preceding sections, the discussion of lattice vibrations within the framework of Born-von Kármán theory and the treatment of electron-phonon interaction with the assumption of a sharply defined Fermi surface, are valid, strictly speaking, only for a perfect periodic crystal. A departure from lattice periodicity may be expected to give rise to force constant disorder contributing to phonon life-time, and scattering of the conduction electrons due to the presence of disorder in the crystal may lead to blurring of the Fermi surface. It is therefore necessary to examine the validity of the previous results in the case of alloys.

Since the work to be described in this thesis concerns the Bi-Pb-Tl system, we shall confine our attention to the substitutional alloys where the constituent elements are neighbours on the periodic table and therefore the atomic masses are not significantly different. A substitutional alloy has lattice periodicity as a whole but the lattice points are occupied randomly by the constituent atoms. Hence, in a sense most pure metals are alloys in this category, since they are composed of isotopes which differ slightly in mass. This choice precludes the interesting topic of dilute alloys with large mass difference (Elliot and Maradudin 1965) where "resonance" modes or "localized" modes appear inside or outside the frequency distribution of the host lattice (Møller and Mackintosh 1965; Svensson et al.

1965, Nicklow *et al.* 1968).

It has been found from coherent neutron scattering experiments on binary compositions of Bi-Pb-Tl (Ng and Brockhouse 1967, 1968) and Mo-Nb alloys (Powell *et al.* 1968) that sharp and well-defined neutron groups exist in these disordered alloys. Neutron groups measured in β -brass (Gilat and Dolling 1965) also did not exhibit, in general, any anomalous broadening in going through the order-disorder transition. These results suggest that the interatomic potential in these disordered systems are well-defined as in pure metals. This can be explained qualitatively with the following argument. (Brockhouse, Hallman and Ng 1968): The interatomic force constants in two pure metals A and B may be quite different. But in the alloy AB, the A-A, B-B and A-B force constants (for a given geometrical arrangement of the pair) are specific to this alloy, having no necessary relation to the force constants in pure A or B. Hence, although the bare ion-ion interaction could fluctuate appreciably, the conduction electrons move to screen the cores in such a way that effective forces between individual pairs of ions may be quite similar. From this point of view, one can justify the application of the Born-von Kármán theory of lattice dynamics to alloys.

We may therefore make the reasonable assumption that the ionic potential consists of two parts--a periodic part which describes the normal modes of the system in exactly the same way as in pure metals and a weak non-periodic part

which gives rise to broadening of the phonons which we consider below. The non-periodic potential is also responsible for the residual resistivity in alloys.

(ii) Damping of phonons in Solid Solutions

It is clear from the preceding discussion that even for a disordered alloy, the use of the Born-von Kármán theory as a starting point for the analysis is justified. The finite phonon life-time arising from the scattering of phonons in an imperfect lattice may then be treated using time-dependent perturbation theory.

The influence of mass disorder has been discussed by Mathis (1957); Ivanov and Krivoglaz (1964) and Ng and Brockhouse (1968). For the particular case of a completely disordered binary alloy AB with a cubic lattice of the Bravais type, the spread in the phonon frequency is given by

$$\Delta\omega = \frac{\pi}{2} \frac{\omega^2 g(\omega)}{\int g(\omega) d\omega} C_A C_B \left(\frac{M_A - M_B}{\bar{M}} \right)^2 \quad (2.41)$$

$g(\omega)$ denotes the frequency distribution function of the alloy, C_A and C_B are concentrations. Hence, even for a relative mass variation $(M_A - M_B / \bar{M}) \sim 0.1$, the associated broadening of peaks $< 0.01\omega$ which is too small to be observable.

It follows from the above analysis that small mass differences have little effect. However, for alloys composed of elements of similar mass, broadening may still be caused due to atomic force constant disorder. In this case, one

can proceed by defining a configuration average (C.A.) of the force constants for a disordered alloy:

$$\bar{\phi}_{\alpha\beta}^{\ell\ell'} = \langle \phi_{\alpha\beta}^{\ell\ell'} \rangle_{\text{C.A.}}$$

The difference between the actual and the average force constants $\Delta\phi_{\alpha\beta}^{\ell\ell'}$ may be treated as a perturbation

$$\Delta\phi_{\alpha\beta}^{\ell\ell'} = \phi_{\alpha\beta}^{\ell\ell'} - \bar{\phi}_{\alpha\beta}^{\ell\ell'}$$

One obtains for the width (Ng and Brockhouse 1968)

$$\begin{aligned} \Delta\omega_j(\underline{q}) &= \frac{\pi}{2N^2 M^2 \omega^2} \sum_{\underline{q}', j'} \delta(\omega_j(\underline{q}) - \omega_{j'}(\underline{q}')) \\ &\times \left| \sum_{\substack{\alpha, \beta \\ \ell, \ell'}} \Delta\phi_{\alpha\beta}^{\ell\ell'} \xi_{\alpha j}^*(\underline{q}) \xi_{\beta j'}(\underline{q}') e^{-i\underline{q} \cdot \underline{R}_\ell} \right. \\ &\left. \times e^{i\underline{q}' \cdot \underline{R}_{\ell'}} \right|^2 >_{\text{C.A.}} \end{aligned} \quad (2.42)$$

It is seen that $\Delta\omega$ involves products of pairs of deviations of force constants from their mean values and is therefore relatively insensitive to force constant disorder. This explains why the neutron groups observed in the disordered binary alloys are usually well defined. However, we shall see later in connection with the experimental results on a ternary alloy that there could be appreciable force constant disorder in such system causing significant broadening of the neutron groups.

(iii) Pseudo-potential formalism for disordered alloys

In section E we briefly sketched the pseudopotential formulation of the indirect interaction among the ions by means of the conduction electron gas for an elemental crystal.

For the case of a binary alloy it is necessary to generalise

Eq. (2.22) for factorization of matrix elements into the structure factor $S(Q)$ and the form factor $w(Q)$; this generalization has been considered by Hayes et al. (1968).

We consider a disordered binary alloy AB, with fractional concentrations C_A and C_B of the total number of ions N arranged randomly on a Bravais lattice. w_A^0 and w_B^0 denote bare pseudopotentials of each type of ions A and B; the ions are screened with conduction electrons of the density appropriate to the alloy. Following the notation of Hayes et al. (1968): $\sigma(\underline{R}^\ell) = +1$ if the site \underline{R}^ℓ contains an A atom, $\sigma(\underline{R}^\ell) = -1$ if the site \underline{R}^ℓ contains a B atom. The matrix element of the lattice potential W as seen by the conduction electrons is

$$\begin{aligned} \langle \underline{k} + \underline{Q} | W | \underline{k} \rangle &= \frac{1}{2N} \sum_{\ell} e^{-i\underline{Q} \cdot \underline{R}^\ell} \{ (1 + \sigma(\underline{R}^\ell)) \langle \underline{k} + \underline{Q} | w_A | \underline{k} \rangle \\ &+ (1 - \sigma(\underline{R}^\ell)) \langle \underline{k} + \underline{Q} | w_B | \underline{k} \rangle \} \end{aligned} \quad (2.43)$$

w_A and w_B are the screened individual ionic pseudopotentials with screening appropriate to the alloy. We introduce an average pseudopotential (screened) for the alloy

$$\langle \underline{k} + \underline{Q} | \bar{w} | \underline{k} \rangle = C_A \langle \underline{k} + \underline{Q} | w_A | \underline{k} \rangle + C_B \langle \underline{k} + \underline{Q} | w_B | \underline{k} \rangle \quad (2.44)$$

and a difference pseudopotential

$$\langle \underline{k} + \underline{Q} | \Delta w | \underline{k} \rangle = [\langle \underline{k} + \underline{Q} | w_A | \underline{k} \rangle - \langle \underline{k} + \underline{Q} | w_B | \underline{k} \rangle] \quad (2.45)$$

Then Eq. (2.43) can be written as

$$\begin{aligned} \langle \underline{k} + \underline{Q} | W | \underline{k} \rangle &= S(\underline{Q}) \langle \underline{k} + \underline{Q} | \bar{w} | \underline{k} \rangle \\ &+ S'(\underline{Q}) \langle \underline{k} + \underline{Q} | \Delta w | \underline{k} \rangle \end{aligned} \quad (2.46)$$

where $S(\underline{Q})$ is the usual structure factor:

$$S(\underline{Q}) = \frac{1}{N} \sum_{\ell} e^{-i\underline{Q} \cdot \underline{R}^{\ell}}$$

and

$$S'(\underline{Q}) = \frac{1}{2N} \sum_{\ell} e^{-i\underline{Q} \cdot \underline{R}^{\ell}} [\sigma(\underline{R}^{\ell}) - \langle \sigma \rangle_R] \quad (2.47)$$

with

$$\langle \sigma \rangle_R = \frac{1}{N} \sum_{\ell} \sigma(\underline{R}^{\ell}) = (C_A - C_B)$$

If Born-von Kármán theory is used as a starting point for the alloys to describe the normal modes, then within that framework it will be consistent to use the average pseudopotential $\bar{w}(q)$ of the alloy for calculating the electron-ion contribution to lattice vibration. It also follows that for evaluating the direct interaction between the ions (Coulomb interaction), one uses the average ionic charge $\bar{Z} = C_A Z_A + C_B Z_B$.

On the other hand, the difference pseudopotential Δw in the alloy will contribute to finite life-time to the one-electron states. Neutron scattering study of Kohn effects in binary disordered alloys (Chapter IV(F)) suggests that, on alloying, Fermi level shifts in accordance with rigid-band model but without especially large blurring of the Fermi surface. Therefore $|w_A - w_B|$ should be small; nevertheless it should give a fair explanation of residual resistivity of such alloys. This non-periodic part (with a corresponding

contribution arising from charge fluctuation, $\Delta Z = |Z_A - Z_B|$, at the lattice sites) also gives rise to phonon broadening.

Hayes et al. (1968) have given a pseudopotential formulation for binary alloys using a second order perturbation theory. It can be seen from their work that for a proper calculation of phonon frequencies in a disordered alloy one has to consider terms of the type $\bar{w}(q)\Delta w(q)$ and $|\Delta w(q)|^2$ in addition to the leading contribution arising from $|\bar{w}(q)|^2$ (similarly for Coulomb interactions). Finally, we note that Eq. (2.42) giving phonon broadening due to force constant disorder can be cast into pseudopotential formalism involving summations over reciprocal space (Trofimenkoff 1969).

G. Damping of Phonons

(i) Anharmonic damping of phonons in solids

In the previous section, we discussed the damping of phonons in disordered alloys within the harmonic approximation. In the expansion of the potential energy (Eq. 2.1), if we take into account the terms ϕ_3 , ϕ_4 (and higher ones) explicitly, we obtain an anharmonic theory which leads to interaction of the phonons. In an anharmonic crystal, the normal modes of vibration are altered in frequency and they also have a finite life-time. The expressions for shift and width are rather involved; they can be found in the review article by Cowley (1963). Detailed numerical calculations of the anharmonic shift and widths have recently been reported for aluminum (Högberg and Sandström 1969) and for potassium (Buyers and Cowley 1969), using the pseudo-potential approach.

(ii) Damping of phonons due to the electron-phonon interaction

In metals or metallic solid solutions damping of phonons may be present due to electron-phonon interaction.

In section E the contribution to phonon frequency due to electron-phonon interaction was formulated in terms of the static dielectric constant $\epsilon(q,0)$. In a more general treatment, the expression will involve frequency dependent dielectric constant $\epsilon(q,\omega_q)$ which is complex. Now, the real part of $\epsilon(q,\omega_q)$ describes the shift of phonon frequencies and the imaginary part describes the damping. To obtain an estimate of the electron-phonon contribution to phonon width Γ (full width at half maximum), we consider the coupling of the

longitudinal phonon-field to the electrons in the jellium model (Pines and Nozieres 1966):

$$\Gamma_{\mathbf{q}}/\omega_{\mathbf{q}} = \frac{\text{Im } \epsilon(\mathbf{q}, \omega_{\mathbf{q}})}{\text{Re } \epsilon(\mathbf{q}, \omega_{\mathbf{q}})}$$

In the long wavelength limit it reduces to

$$\Gamma_{\mathbf{q}}/\omega_{\mathbf{q}} \sim (m/M)^{1/2} \sim 10^{-2}-10^{-3}.$$

We see that phonon damping as a consequence of the electron response is indeed small. This result essentially follows from the great mismatch in phonon and electron frequencies. Hence, if we assume the validity of the adiabatic approximation in the theory of metals, electron-phonon damping can be neglected.

Realistic calculation of phonon life-time due to electron-phonon interaction has been carried out for Al (Björkman et al. 1967; Högberget al. 1969) and for K (Price et al. 1970). In both the cases it was found small compared with the anharmonic damping. Further since change of electron-phonon widths with temperature is extremely small (Buyers and Cowley 1969) this effect tends to be completely masked by phonon-phonon damping at a finite temperature.

CHAPTER III

INTERACTION OF THERMAL NEUTRONS WITH SOLIDS

A. Introduction

Normally, an experiment conducted on a physical system involves the excitation of the system by an external probe and the subsequent measurement of the system's response to that probe. If the interaction between the probe and the system is sufficiently weak, the system's response is linear and it is determined entirely by the properties that the system possesses in the absence of the probe. Inelastic scattering of slow neutrons from solids offers a convenient method of studying the spectrum of elementary excitations in the many-particle system. Thermal neutrons emerging from a research reactor have simultaneously energies of the order of the characteristic energies of solids and liquids, and wavelengths of the order of interatomic spacings. These features make the study of neutron inelastic scattering a powerful tool. The interaction between a neutron and an isolated atom is partly a nuclear interaction and partly a magnetic dipole interaction between the neutron and the electrons of the atom. A very weak non-magnetic interaction with the electrons has also been observed; however this part can be ignored for the present purpose. Further if we restrict ourselves to non-magnetic materials the magnetic scattering vanishes and only the nuclear part remains. For wavelengths long compared to the linear dimension of the nucleus

the scattering is independent of scattering angle and for energies far below any resonance band of the nucleus the cross-section is also independent of the energy of the incident neutron under the assumption of a fixed nucleus. However, the scattering may differ significantly for parallel and antiparallel spins of the neutron and the nucleus.

B. Scattering Cross Section

When considering scattering by a system of interacting nuclei it would be natural to assume the interaction potential as a sum of two particle potentials

$$H_{\text{int}} = \sum_{\ell} v(\underline{R}^{\ell} - \underline{r}_n) \quad (3.1)$$

where \underline{R}^{ℓ} and \underline{r}_n are the system particle and probe (neutron) positions respectively. It is convenient to Fourier analyse as follows:

$$\begin{aligned} H_{\text{int}} &= \sum_{\ell} \sum_{\mathbf{q} \neq 0} v_{\mathbf{q}} e^{i\mathbf{q} \cdot (\underline{R}^{\ell} - \underline{r}_n)} \\ &= \sum_{\mathbf{q}} v_{\mathbf{q}} \rho_{\mathbf{q}}^+ e^{-i\mathbf{q} \cdot \underline{r}_n} \end{aligned} \quad (3.2)$$

In the above equation $v_{\mathbf{q}}$ is the Fourier transform of $v(\underline{R})$ while $\rho_{\mathbf{q}}$ is the Fourier transform of the particle density

$$\begin{aligned} \rho_{\mathbf{q}} &= \int d^3R \rho(\underline{R}) e^{-i\mathbf{q} \cdot \underline{R}} = \sum_{\ell} \int d^3R \delta(\underline{R} - \underline{R}^{\ell}) e^{-i\mathbf{q} \cdot \underline{R}} \\ &= \sum_{\ell} e^{-i\mathbf{q} \cdot \underline{R}^{\ell}} \end{aligned} \quad (3.3)$$

$\rho_{\mathbf{q}}$ describes the fluctuations of the particle density about its average value $\rho_0 = N$.

We next consider a scattering event in which the incident particle is scattered from a state $|k_0\rangle$ of energy E_0 to a state $|k'\rangle$ of energy E' and the state of the system is changed from $|\alpha\rangle$ of energy ϵ_{α} to $|\beta\rangle$ of energy ϵ_{β} . We also make the important assumption that the probe particle is weakly coupled to the many-particle system, so that the scattering act may be described within the Born approximation. The inelastic differential scattering cross section per unit solid angle per unit energy range is, per unit volume of specimen

$$\frac{d^2\sigma}{dE d\Omega} = \frac{k'}{k_0} \left(\frac{\mu}{2\pi}\right)^2 |\langle k' \alpha | H_{int} | \beta k_0 \rangle|^2 \delta(h\nu + \epsilon_\alpha - \epsilon_\beta) \quad (3.4)$$

where $E = h\nu = \hbar\omega$ is the energy transfer to the target; μ is the reduced mass of the particle and Ω denotes solid angle. Since the crystal is in thermal equilibrium before scattering, therefore there is a thermal mixture of states, the probability of state α being

$$P_\alpha = \frac{e^{-\epsilon_\alpha/kT}}{\sum_\alpha e^{-\epsilon_\alpha/kT}}$$

To get the true scattering cross section, we have to sum over all the states α with their probabilities. Further, we are not interested in the final states of the crystal, but only in that of the neutron; this means an additional sum over states $|\beta\rangle$. Finally, we arrive at the result

$$\frac{d^2\sigma}{d\Omega dE} = A_{\underline{Q}} S(\underline{Q}, \omega) \quad (3.5)$$

where

$$A_{\underline{Q}} = \frac{k'}{k_0} \left(\frac{\mu}{2\pi}\right)^2 |v_{\underline{Q}}|^2, \quad \underline{Q} = \underline{k}_0 - \underline{k}'$$

depends essentially on the two-body potential, and

$$S(\underline{Q}, \omega) = \sum_{\alpha \beta} P_\alpha |\langle \alpha | \rho_{\underline{Q}}^+ | \beta \rangle|^2 \delta(\hbar\omega + \epsilon_\alpha - \epsilon_\beta) \quad (3.6)$$

$S(\underline{Q}, \omega)$ embodies all the properties of the many-particle systems that are relevant to the scattering of the probe. It furnishes a direct measure of the excitation spectrum of the density fluctuations, being proportional to the squared matrix element for each permissible excitation energy. For neutron scattering, this important result was given by Van Hove (1954) who introduced time-dependent correlation functions. This approach has proved particularly fruitful in analysing neutron

scattering experiments on liquids and magnetic systems.

The treatment given so far is perfectly general in that it applies to any system of interacting particles (gases, fluids or crystals). We next proceed to discuss the specific case of crystals.

C. Scattering by Crystals

In the process of scattering if there is no change in energy between the incident and the scattered neutrons then the process is called elastic scattering. If the neutron and the lattice exchange energy then it is called "inelastic". As a consequence of periodicity of the structure in solids the scattered neutrons can interfere with each other coherently. Such coherent scattering can be either elastic or inelastic. On the other hand we can have spin and isotopic incoherence which can also be either elastic or inelastic. Additional incoherent scattering may be present in alloys.

The theory of neutron scattering by monatomic crystals was developed by Weinstock (1944) and extended to lattices with bases by Waller and Froman (1952). Review articles dealing with the theory have been published by Cassels (1950), Kothari and Singwi (1958), Brockhouse (1964). Since the actual nuclear interaction between the neutron and the target nucleus is unknown, it is replaced by a δ -function whose strength is adjusted to give the experimentally determined scattering length. This is the Fermi pseudopotential. The fact that the range of the nuclear interaction ($\sim 10^{-12}$ cm) is very small, compared with the neutron wavelength ($\sim 10^{-8}$ cm) makes it possible to treat the interaction as a point interaction.

(i) Harmonic Perfect Crystals

Coherent Scattering

We consider a crystal with one atom per primitive unit cell. The coherent scattering length per atom is

defined as

$$\langle b \rangle = \sum_{\ell} p_{\ell} b_{\ell}$$

where p_{ℓ} is the probability that an atom will have the scattering amplitude b_{ℓ} .

For a harmonic crystal where plane waves (normal modes) are exact eigenstates of the crystal, the differential scattering cross section can be written as (Sjolander 1958):

$$\begin{aligned} \frac{d^2\sigma}{d\Omega dE} = & \frac{1}{\hbar} \frac{(2\pi)^3 N}{v} \langle b \rangle^2 \frac{k'}{k_0} e^{-2W} \left[\delta(\omega) \sum_{\underline{G}} \delta(\underline{Q} - \underline{G}) \right. \\ & + \sum_S \sum_{\epsilon} \left(\frac{\hbar |\underline{Q} \cdot \underline{\xi}_S|^2}{2NM\omega_S} \right) \left(\frac{\text{Coth}(\beta\omega_S) + \epsilon}{2} \right) \delta(\omega + \epsilon\omega_S) \\ & \times \sum_{\underline{G}} \delta(\underline{Q} - \underline{G} + \underline{q}) \\ & + \frac{1}{2} \sum_{SS'} \sum_{\epsilon\epsilon'} \left(\frac{\hbar |\underline{Q} \cdot \underline{\xi}_S|^2}{2NM\omega_S} \right) \left(\frac{\hbar |\underline{Q} \cdot \underline{\xi}_{S'}|^2}{2NM\omega_{S'}} \right) \\ & \left(\frac{\text{Coth}(\beta\omega_S) + \epsilon}{2} \right) \left(\frac{\text{Coth}(\beta\omega_{S'}) + \epsilon'}{2} \right) \delta(\omega + \epsilon\omega_S + \epsilon'\omega_{S'}) \\ & \times \sum_{\underline{G}} \delta(\underline{Q} - \underline{G} + \underline{q}_S + \underline{q}_{S'}) \\ & + \dots \dots \dots \left. \right] \quad (3.7) \end{aligned}$$

e^{-2W} is the well known Debye-Waller factor. $\beta = \frac{\hbar}{2kT}$, S stands for the double index (\underline{q}, j) characterising a normal mode of wave-vector \underline{q} and branch j , $\underline{\xi}_S$ denotes the polarization vector satisfying the orthonormality conditions, N is the number of unit cells in the crystal, v is the volume of the unit cell, M is the mass of the atom and $\epsilon = \pm 1$ corresponding to emission and absorption of phonons.

The first term on the right hand side of the equation (3.7) represents elastic scattering (zero phonon) at any reciprocal lattice vector \underline{G} . The second term represents a one-phonon process, in which the neutron is scattered with

the creation or annihilation of one quantum. It is governed by selection rules

$$\underline{Q} = \underline{k}_0 - \underline{k}' = \underline{G} - \underline{q} \quad (3.8a)$$

$$\hbar\omega = E_0 - E' = \pm \hbar\omega_j(\underline{q}) \quad (3.8b)$$

The satisfaction of these two laws of conservation of pseudo-momentum and energy during one-phonon coherent scattering offers the possibility of determining dispersion relations in crystals. This point will be considered in more detail later.

Finally, the third term in Eq. (3.7) describes two-phonon processes which involve simultaneous creation and/or annihilation of two phonons. The selection rules are,

$$\begin{aligned} \underline{k}_0 - \underline{k}' &= \underline{G} - \underline{q}_S - \underline{q}_{S'} \\ E_0 - E' &= \pm \hbar\omega_S \pm \hbar\omega_{S'} \end{aligned} \quad (3.9)$$

Similarly, there will be higher-phonon processes. The multi-phonon process gives a continuous background under the δ -function peaks in the one-phonon energy distributions. This effect may be important if the dispersion relations are studied close to the melting point of the crystal and/or at large Q . However, there may be additional complication due to increased anharmonicity at high temperatures which leads to interference between one-phonon and multi-phonon scattering (Ambegaokar et al. 1965, Cowley and Buyers 1969).

Incoherent Scattering

If the scattering amplitudes of the atoms vary randomly in a solid then the neutron waves scattered from the individual centres will appear not to interfere with each other and this part is said to be incoherent. The expression for the incoherent cross section may be directly obtained from Eq. (3.7) with

$\langle b \rangle^2$ replaced by $(\langle b^2 \rangle - \langle b \rangle^2)$ and substituting unity for

$$\frac{(2\pi)^3}{V} \frac{\sum \delta(\dots)}{G}$$

For the particular case of monatomic cubic Bravais lattices, the differential cross-section can be expressed in a compact form:

$$\frac{d^2\sigma}{d\Omega dE} = \frac{1}{\hbar} (\langle b^2 \rangle - \langle b \rangle^2) \frac{k'}{k_0} e^{-2W} \sum_{n=0}^{\infty} \frac{(2W)^n}{n!} G_n(\omega) \quad (3.10)$$

where

$$G_0(\omega) = \delta(\omega)$$

$$G_{n+1}(\omega) = \int_{-\infty}^{\infty} h(\omega - \omega') G(\omega') d\omega', \quad n \geq 0$$

$$h(\omega) = \frac{g(\omega)}{\omega} \frac{(\hbar Q^2/2M)}{2W} \frac{(\text{Coth}(\beta\omega) - 1)}{2},$$

$$|\omega| \leq \omega_m$$

$$= 0, \quad |\omega| > \omega_m$$

Also,
$$\int_{-\infty}^{\infty} G_n(\omega) d\omega = 1$$

ω_m denotes the cut-off of the frequency spectrum $g(\omega)$.

In Eq. (3.10), $n=0,1,2,\dots$ denote zero, one and higher phonon processes respectively. Since

$$G_1(\omega) = \int h(\omega - \omega') \delta(\omega') d\omega' = h(\omega) \propto g(\omega)$$

we find that one-phonon incoherent scattering is directly related to the frequency distribution of the normal modes of a cubic crystal with one atom per unit cell. This important result was first obtained by Placzek and Van Hove (1954).

(ii) Scattering from imperfect Crystals

Coherent Scattering

In Eq. (3.7), the origin of δ -function in energy and momentum transfer in the expression for the coherent scattering cross section is the infinite life-time of the phonons. In principle, this situation holds good only for an ideally perfect crystal with harmonic interaction between atoms and in the absence of any disorder or inhomogeneity in the crystal.

Presence of anharmonicity in a crystal leads to interaction of the phonons and hence to the possibility of their decomposition into other phonons and scattering at one another. Plane waves are no longer exact eigenstates of the crystal and their life-times become finite. The corresponding indeterminacy in the energy of a phonon leads to the spreading of the one-phonon peaks of coherent neutron scattering. We expect the δ -function in the scattering amplitude replaced by

$$\delta(\omega - \omega_j(\underline{q})) \rightarrow \frac{1}{(\omega - \omega_j(\underline{q}) - \Delta_j(\underline{q})) + i\Gamma_j(\underline{q})}$$

where $\Delta_j(\underline{q})$ is the frequency shift and $\Gamma_j(\underline{q})$ the life-time of the phonons due to anharmonicity. The cross-section is expected to be

$$\frac{d^2\sigma}{d\Omega dE} \sim \frac{(\Gamma_j(\underline{q}))^2}{(\omega - \omega_j(\underline{q}) - \Delta_j(\underline{q}))^2 + (\Gamma_j(\underline{q}))^2}$$

It turns out further that the exact cross-section does not have the symmetrical Lorentz shape but there has to be added an additional term which produces an asymmetry in the cross-section (Maradudin and Fein 1962; Maradudin and Ambegaokar 1964).

In alloy crystals, damping of phonons may arise from mass and force constant disorder and this will modify the one-phonon coherent cross-section in much the same way as in anharmonic crystals. An experimental study of broadening by neutron scattering technique may give valuable information regarding the interaction of phonons with disorder present in the crystal and the relaxation times. The theory of neutron scattering by dilute alloys has been developed by Elliott and Maradudin (1965). Neutron scattering from binary alloys with finite concentration has been considered by Krivoglaz (1969).

Incoherent Scattering from Alloys

As mentioned before, the deviations in the scattering length b give rise to the incoherent scattering. In a crystal containing single chemical species, isotopic and spin incoherence may be present.

For a completely disordered binary alloy AB (generalization to alloys containing several chemical species is straightforward) with average scattering lengths $\langle b_A \rangle$ and $\langle b_B \rangle$ and concentrations C_A and C_B , the incoherent scattering cross-section per atom can be written as

$$\sigma_{\text{inc}}^{\text{AB}} = 4\pi [C_A (\langle b_A^2 \rangle - \langle b_A \rangle^2) + C_B (\langle b_B^2 \rangle - \langle b_B \rangle^2) + C_A C_B (\langle b_A \rangle - \langle b_B \rangle)^2] \quad (3.12)$$

The differential scattering cross-section is obtained from Eq. (3.10) by simply replacing $(\langle b^2 \rangle - \langle b \rangle^2)$ with $(\sigma_{\text{inc}}^{\text{AB}}/4\pi)$. If we consider the special case where the species A and B have

negligible incoherent scattering lengths and their coherent scattering lengths are nearly equal ($\langle b_A \rangle \sim \langle b_B \rangle$) then Eq. (3.12) will predict no incoherent scattering from such a system.

However, Ng (1967) has shown that there may still be an additional incoherence present arising from the fluctuation of the polarization vectors due to variation of mass and atomic force constants in the system. The expression for differential scattering cross-section is analogous to Eq. (3.10).

Krivoglaz (1969) has also considered the influence of static inhomogeneity on one-phonon incoherent scattering.

In the above discussion of the disordered alloys we have tacitly assumed that phonons are well defined excitations in the system. A departure from this ideal situation will lead to a broadening of energy levels and consequent spreading of the singularities in the frequency distribution function $g(\omega)$ which enters in the differential scattering cross-section.

D. Experimental Procedure

The frequencies of the normal modes can be determined from neutron spectroscopy measurements, very directly. It was found in section C that one-phonon coherent scattering is governed by selection rules

$$\underline{Q} = \underline{k}_0 - \underline{k}' = \underline{G} - \underline{q} \quad (3.8a)$$

$$\hbar\omega = E_0 - E' = \pm\hbar\omega_j(\underline{q}) \quad (3.8b)$$

As emphasised by Brockhouse (1961) the above equations together with the dispersion relation $\omega = \omega_j(\underline{q})$ constitute a system of five equations in four unknowns, for which solutions can be expected but rarely; i.e. the neutrons occur in groups corresponding to certain discrete values of E' .

Triple-Axis Spectrometer (Constant- \underline{Q} Method)

Crystal spectrometers as well as time of flight instruments have been used to measure phonon dispersion relations in crystals. However, a triple-axis spectrometer operated in the constant- \underline{Q} mode, first introduced by Brockhouse (1961), offers the most powerful and the direct method for mapping phonon frequencies in the Brillouin zone. In a triple-axis spectrometer there are four parameters which can be varied. They are: the incident wave-vector (\underline{k}_0), the scattered wave-vector (\underline{k}'), the angle of scattering (ϕ), the specimen orientation in the scattering plane (ψ). By varying any of the three parameters and keeping the fourth one fixed, measurements can be made at a preselected point in the reciprocal space. The natural variables of a scattering experiment are the wave-vector and energy transfers, \underline{Q} and ω

and therefore the constant- \underline{Q} method is the natural method.

In another mode of operation "Constant E" the energy transfer is kept fixed while ϕ and ψ are varied in such a way that \underline{Q} moves along a desired direction in reciprocal space (Brockhouse 1961; Stedman 1961). This method is useful for studying an extremely steep dispersion curve.

In section C the differential cross section for one-phonon coherent scattering was given (Eq. (3.7)). To obtain physical quantities the δ -functions must be integrated out over the resolution of the apparatus and the track of the experiment. For a conventional experiment in which the neutron group is integrated over the outgoing energy with the other parameters remaining fixed, the one-phonon differential cross-section per steradian per unit cell for a neutron group is given by

$$\sigma_j(\underline{k}' \rightarrow \underline{k}_0) = b_{\text{coh}}^2 \frac{k'}{k_0} \frac{\hbar}{2NM\omega_j(\underline{q})} [\underline{Q} \cdot \underline{\xi}_j(\underline{q})]^2 e^{-2W} \left(\frac{\text{Coth}(\beta\omega_S) + \epsilon}{2} \right) \frac{1}{|J|} \quad (3.13)$$

where $|J|$ is the Jacobian and has the value

$$|J| = \left| 1 + \epsilon \frac{\hbar}{2E} \underline{k}' \cdot \nabla_{\underline{q}} \omega_j(\underline{q}) \right|$$

$\epsilon = \pm 1$ corresponding to emission and absorption of phonon. In the constant- \underline{Q} method it turns out that $|J| = 1$ (Brockhouse 1961). This feature facilitates intensity measurements of neutron groups. The fact that the intensity is proportional to a factor $(\underline{Q} \cdot \underline{\xi}_j(\underline{q}))^2$ offers a means of observing a particular mode j by suitably arranging the experimental conditions.

The experimental results presented in this thesis were obtained using two different triple-axis crystal spectrometers; one at the McMaster University reactor (Rowe 1965) and the other at the NRU reactor at Chalk River (Brockhouse et al. 1968). Fig. 3.1 shows a layout of the installation at the McMaster University reactor. A schematic diagram of the spectrometer installed at hole E2 of the NRU reactor at Chalk River is shown in Fig. 3.2. However, **the** bulk of the work was carried out using the latter spectrometer at Chalk River. This spectrometer has some unusual design features in that it employs a dual monochromator deep within the beam hole. Because of the double reflection ((220) planes of copper) the final monochromatic beam can be expected to be of high purity. Further, since only the monochromatic beam emerges from the reactor hole, the shielding required is comparatively modest.

In the Constant- Q mode of operation, incident energy is kept fixed while E' , ψ and ϕ are varied. Since E' is variable, it is necessary in some cases to apply corrections for the efficiency of the analysing spectrometer. The sensitivity function of the analysing spectrometer is discussed in the appendix. Further, due to a minor fault in the design a weak contaminant is present in the primary beam, produced by double reflection from (331) planes of the monochromator. While measuring a phonon, experimental conditions are suitably adjusted to avoid any possible interference with the contaminant.

MC MASTER UNIVERSITY SPECTROMETERS

R	REACTOR COIL
B	BISMUTH PLUS
D	BEAM TUBE
G	IRON GATE
L	LATHE BED
C	COUNTER
M	MONITOR
S	BEAM STOPPER
X ₁	MONOCHROMATOR
X ₂	MONOCHROMATOR
X ₃	SAMPLE TABLE
X ₄	ANALYSER
X ₅	SAMPLE TABLE

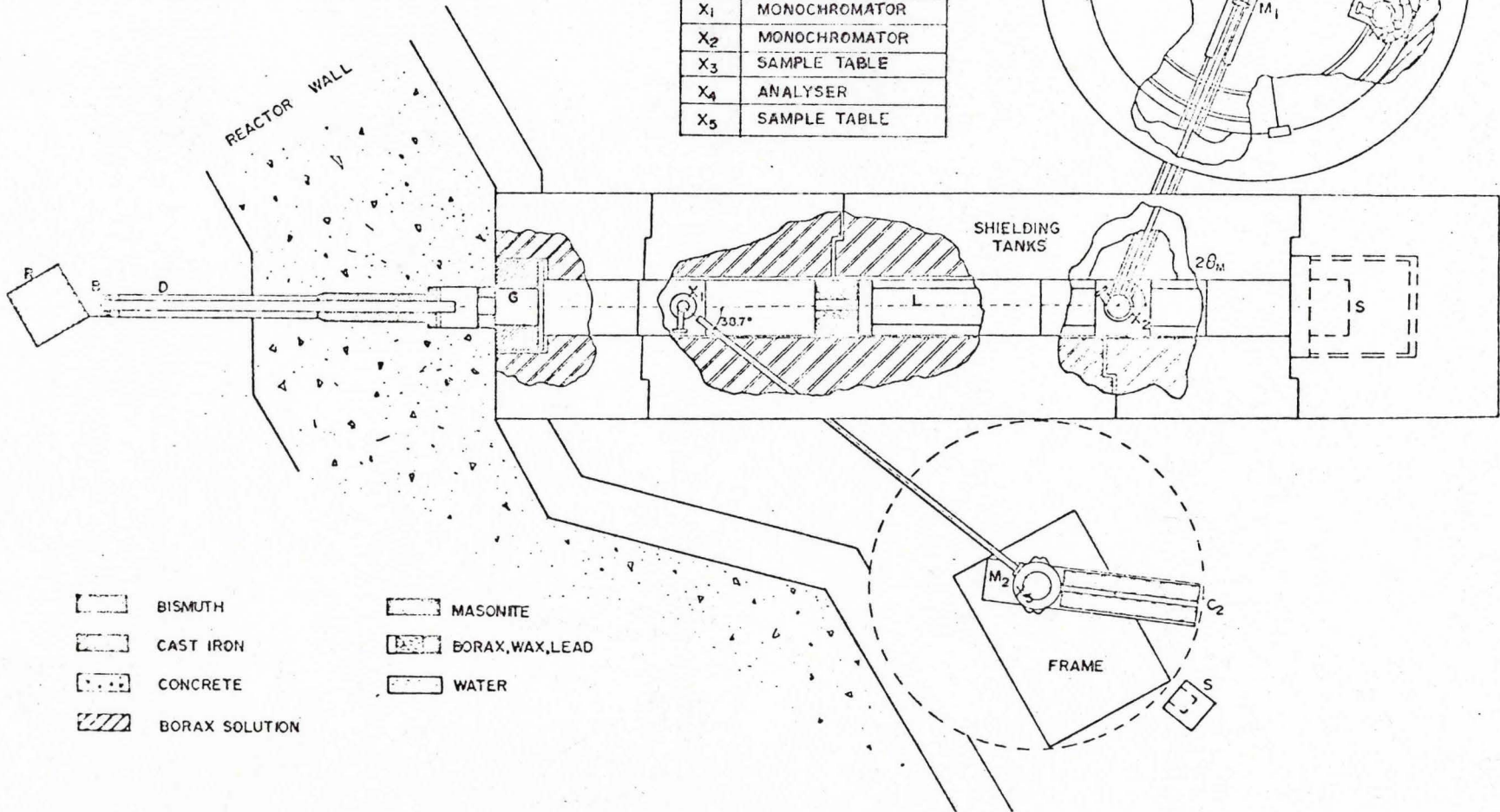


Fig. 3.1

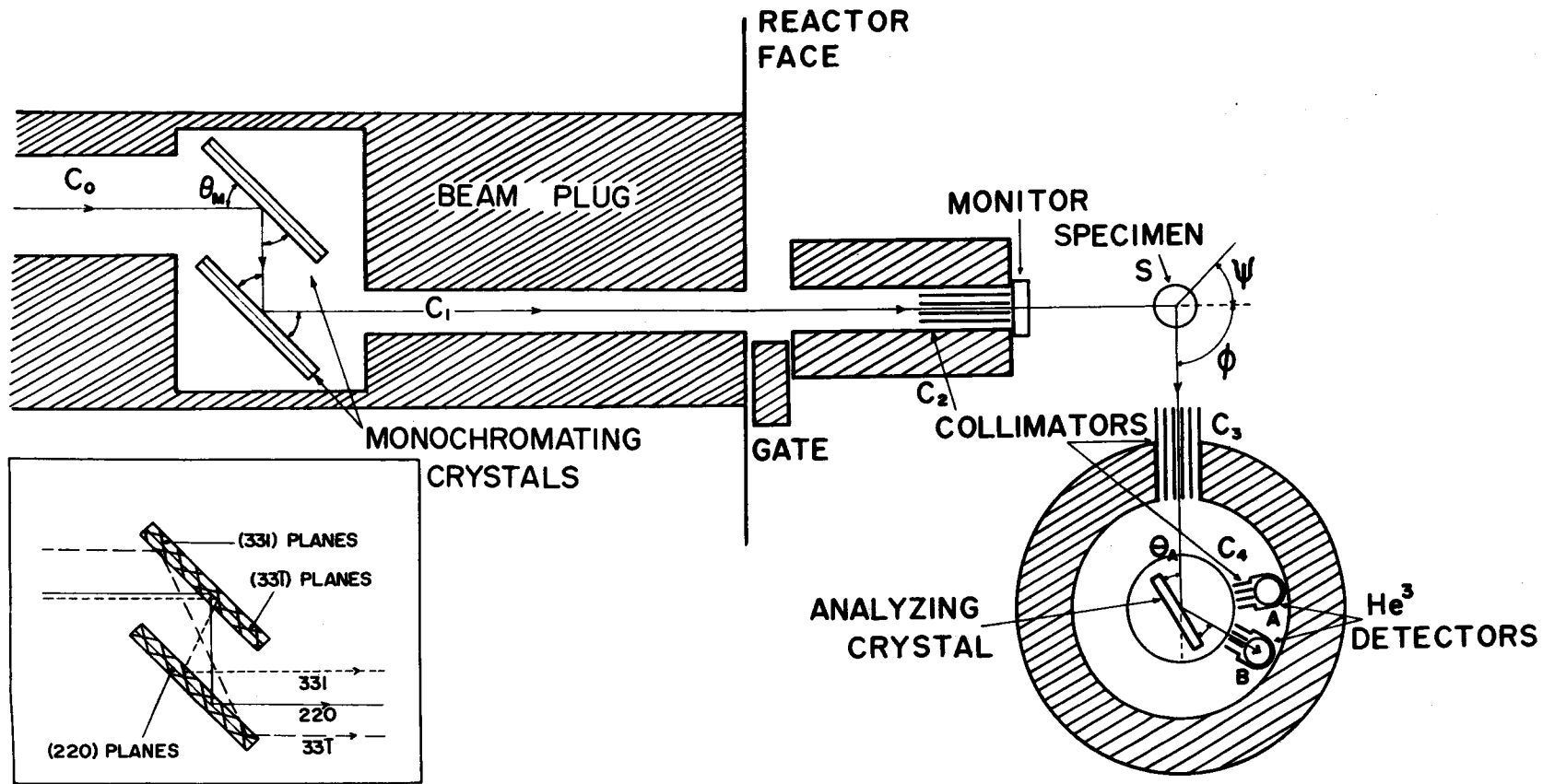


Fig. 3.2 A schematic diagram of the McMaster University triple-axis spectrometer at the NRU reactor, Chalk River. The inset illustrates the origin of the contaminant produced by the (331) planes. (Courtesy of J.R.D. Copley.)

CHAPTER IV

CRYSTAL DYNAMICS OF BI-PB-TL ALLOYS

A. Introduction

In recent years, neutron scattering studies on various alloy systems have been undertaken. These have been mainly directed towards obtaining information about the effects of differences in the masses of the constituent atoms in alloys (Svensson et al. 1965; Møller and Mackintosh 1965) or on alloys composed of different elements of similar mass to study the various effects of changes in the interatomic forces (Powell et al. 1968; Ng and Brockhouse 1967, 1968; Hallman and Brockhouse 1969).

In particular, Ng and Brockhouse (1967, 1968) have studied the atomic vibrations in face centred cubic alloys of Bi, Pb and Tl which are neighbouring elements in the Periodic table and possess favorable neutron scattering properties (Table 4.1(a)). Bismuth has five, lead four and thallium three conduction electrons per atom respectively. Hence, it is possible to vary the conduction electron concentration in a controlled way and study the effect of the electron-phonon interaction on the lattice dynamics. Six disordered binary alloys ($\text{Bi}_{15}\text{Pb}_{85}$, $\text{Pb}_{80}\text{Tl}_{20}$, $\text{Pb}_{40}\text{Tl}_{60}$, $\text{Bi}_{20}\text{Tl}_{80}$ and $\text{Bi}_{10}\text{Tl}_{90}$) were investigated. The dispersion curves measured at 100°K show a progressive change with electron concentration.

In the course of the present work, measurements have been extended to another Pb-Tl binary alloy e.g. $\text{Pb}_{33}\text{Tl}_{67}$. The above composition was chosen because according to the phase diagram (Hansen 1958) the solidus and the liquidus curves get separated for higher Tl concentrations. (An attempt to grow a single crystal of $\text{Pb}_{20}\text{Tl}_{80}$ met with failure). An additional interest lies in the fact that the Fermi surface is expected to be just empty in the third zone for the alloy $\text{Pb}_{33}\text{Tl}_{67}$ and this feature might be reflected in the lattice vibrations in some important way. The ternary alloy $\text{Bi}_{20}\text{Pb}_{60}\text{Tl}_{20}$ * was chosen since it has the same number of electrons per atom as for pure Pb. This offers an interesting possibility of studying the role of the conduction electrons on lattice vibrations. In later sections the results of experimental investigations of the anharmonic properties in Bi-Pb-Tl alloys and the force constant disorder in the ternary alloy are reported. An experimental method of obtaining the frequency distribution function from neutron scattering results for polycrystalline materials is also described.

The alloy crystals used were grown by Research Crystals Inc. of Richmond, Virginia; they were cylindrical, 1 1/4" in diameter and 3 1/2" long. Since it is desirable to know the compositions, homogeneities and mosaic spreads we describe in Appendix I these characterizations of the alloy crystals determined by neutron diffraction. Other useful physical properties are listed in Table 4.1(b).

* Initial measurements of the dispersion curves at 100°K and the Born von Kármán analysis of the results in $\text{Bi}_{20}\text{Pb}_{60}\text{Tl}_{20}$ were made in collaboration with Dr. S.C.Ng --see Ng and Brockhouse (1968).

TABLE 4.1(a)

Properties of the elements Bi, Pb, Tl

	Bi	Pb	Tl
Atomic number	83	82	81
Atomic mass (amu)	208.98	207.19	204.37
Free atom			
Ground state	$6s^2 6p^3$	$6s^2 6p^2$	$6s^2 6p$
Crystal Structure	rhomb.	F.C.C.	H.C.P.
Melting temperature ($^{\circ}$ K)	544	600	575
Superconducting			
Transition Temperature ^(a) ($^{\circ}$ K)	-	7.22	2.36
Debye temperature ^(a) ($^{\circ}$ K)	119	110	87
Neutron Scattering			
cross section ^(b) (barns)			
σ_{coherent}	9.35	11.5	10.0
$\sigma_{\text{absorption}}$	0.034	0.17	3.4
$\sigma_{\text{incoherent}}$	-----negligible-----		

(a) Am. Inst. Phys. Handbook. 1963 (McGraw-Hill Book Co., New York).

(b) Neutron Cross Sections. 1958. Edited by Hughes, D.H. and Schwartz, W.B. (Brookhaven National Lab. U.S.A.).

TABLE 4.1(b)
Properties of the Bi-Pb-Tl Alloys
(Nominal compositions are indicated)

	Bi ₂₀ Pb ₆₀ Tl ₂₀	Bi ₁₅ Pb ₈₅	Pb ₈₀ Tl ₂₀	Pb ₆₀ Tl ₄₀	Pb ₄₀ Tl ₆₀	Pb ₃₃ Tl ₆₇	Bi ₂₀ Tl ₈₀	Bi ₁₀ Tl ₉₀
Crystal Structure (a)	F.C.C.	F.C.C.	F.C.C.	F.C.C.	F.C.C.	F.C.C.	F.C.C.	F.C.C.
Specimen lattice constant at 296°K ^(b) (Å°)	4.9585	4.9646	4.9345	4.9179	4.8986	4.8917	4.9170	4.8816
Specimen mosaic spread ^(b) (F.W.H.M.)	0.85°	0.8°	0.55°	0.75°	0.5°	0.4°	0.4°	0.3°
Fusion Temp. (a) (°K)	-	512	618	635	653	653	553	573
Elastic Constants at 296°K ^(c) (10 ¹¹ dynes/cm ²)								
C ₁₁	-	-	4.576	4.329	4.157	4.148	-	-
C ₁₂	-	-	3.964	3.851	3.803	3.764	-	-
C ₄₄	-	-	1.38	1.275	1.195	1.182	-	-
Superconducting transition temp ^(d) (°K)	7.26 ^(f)	7.7	6.6	5.8	4.6	3.6	4.0	2.5
Debye Temp. (e) (°K)	103	103	109	112	116	117	112	122

(a) Hansen, M. 1958. Constitution of Binary alloys (McGraw-Hill Book Co., New York).

(b) See Appendix I.

(c) Shepard, M.L. and Smith, J.F. 1967. Acta. Met. 15, 357.

(d) Claeson, T. 1966. Phys. Rev. 147, 340.

(e) Debye temperature is estimated from the cut-off of the phonon frequency spectrum at 100°K.

(f) Dynes, R.C. and Rowell, J. M. 1969. Phys. Rev. 187, 821.

B. Phonon dispersion curves in $\text{Pb}_{33}\text{Tl}_{67}$ and $\text{Bi}_{20}\text{Pb}_{60}\text{Tl}_{20}$ at 100°K

Experimental*

The frequency-wave vector dispersion relations for the lattice vibrations were measured mainly along the four major symmetry directions at 100°K on the McMaster University spectrometer at Chalk River (Brockhouse et al. 1968). The alloy crystals were sealed in thin walled aluminium cans since thallium is toxic and were pre-aligned using the double-axis spectrometer at the McMaster University reactor. (The latter instrument was constructed by S. H. Chen (1964) and modified by E. D. Hallman (1969)). The constant- Q mode of operation was generally employed. The measurements were made in neutron-energy loss with fixed incoming energy and variable outgoing energy, in the (100) and (1 $\bar{1}$ 0) planes of the reciprocal lattice. Copper crystals with (220) and (200) planes were used as the monochromator and the analyzer respectively. The monochromating crystal was normally set at $2\theta_M = 92^\circ$ corresponding to an incident neutron frequency of 5.85×10^{12} cps. The energy resolution (F.W.H.M. of the vanadium elastic peak $\sim 0.30 \times 10^{12}$ cps) was adequate for most of the measurements. The focussing characteristics of the spectrometer (see, for example, Brockhouse (1966)) were also exploited, as far as possible, to obtain sharp neutron groups. Further, with the above choice of the incident energy it was possible to avoid spurious neutron groups arising from a weak contaminant present in the incident beam. To reduce the occurrence of spurious groups arising from higher order reflections of the monochromator and the analyzer, a

* The general experimental details given here are not specific to this section only but apply to most of the experimental work presented in this chapter, unless otherwise stated.

6" quartz single crystal filter was normally used in the incident beam. Søller collimators with horizontal divergence of about 0.7° were used in both the incoming and the outgoing neutron beams. To investigate the limiting slopes near the origin (long wavelength phonons), the constant-E technique was employed and Søller collimators were used in the vertical plane as well.

Results and Force Constant Models

Nearly one hundred phonons were measured in both $\text{Pb}_{33}\text{Tl}_{67}$ and $\text{Bi}_{20}\text{Pb}_{60}\text{Tl}_{20}$; the results are tabulated in Tables*4.2 and 4.3. Fig. 4.1 shows the dispersion curves for $\text{Pb}_{33}\text{Tl}_{67}$ in the four major symmetry directions at 100°K . The straight lines through the origin give the initial slopes of the curves as calculated from the elastic constants (Shepard and Smith 1967). Along the $[0\zeta\zeta]\text{T}_1$ branch, the phonon dispersion curve begins to depart from the line of the limiting slope quite rapidly though it probably merges with it around $\zeta = 0.1$ as suggested by the limited measurements in the long-wavelength region. Kohn anomalies are also probably seen in the $[0\zeta\zeta]\text{L}$ branch around $\zeta = 0.48$ and along the $[\zeta\zeta\zeta]\text{L}$ branch around $\zeta = 0.35$. This will be discussed in more detail in section F.

An analysis of the dispersion curves has been carried out on the basis of the Born-von Kármán theory, using the programs of Svensson et al. (1967). (The solid curves in Fig. 4.1 represent a Born-von Kármán fit to the measurements.)

* In these tables, figures and elsewhere in the text, the wave-vector \underline{q} is written in reduced units; $\underline{q} = (2\pi/a)[\zeta_1, \zeta_2, \zeta_3]$ and is usually specified by the numbers ζ_i .

TABLE 4.2

Phonon frequencies for the symmetry branches
in $\text{Pb}_{33}\text{Tl}_{67}$ at 100°K

ζ	ν	$\Delta\nu$	ζ	ν	$\Delta\nu$	ζ	ν	$\Delta\nu$
[00 ζ]T								
0.20	0.375	0.03	0.50	0.93	0.02	0.80	1.355	0.02
0.30	0.58	0.02	0.60	1.10	0.02	0.90	1.45	0.02
0.40	0.77	0.02	0.70	1.245	0.02	1.00	1.465	0.02
[00 ζ]L								
0.20	0.765	0.02	0.50	1.71	0.03	0.80	2.24	0.03
0.30	1.10	0.02	0.60	1.95	0.02	0.90	2.35	0.03
0.40	1.41	0.02	0.70	2.115	0.03	1.00	2.395	0.02
[$\zeta\zeta\zeta$]T								
0.15	0.33	0.02	0.30	0.67	0.02	0.45	0.785	0.03
0.20	0.44	0.02	0.35	0.74	0.02	0.50	0.78	0.03
0.25	0.56	0.02	0.40	0.78	0.03			
[$\zeta\zeta\zeta$]L								
0.10	0.805	0.03	0.337	2.09	0.02	0.425	2.37	0.02
0.20	1.44	0.03	0.35	2.13	0.02	0.45	2.415	0.03
0.25	1.72	0.02	0.362	2.19	0.02	0.475	2.44	0.03
0.30	1.935	0.02	0.375	2.25	0.02	0.50	2.45	0.03
0.325	2.03	0.02	0.40	2.32	0.02			
[0 $\zeta\zeta$]T ₂								
0.20	0.61	0.02	0.50	1.60	0.02	0.80	2.22	0.02
0.30	0.96	0.02	0.60	1.84	0.02	0.90	2.34	0.02
0.40	1.29	0.02	0.70	2.04	0.02	1.00	2.39	0.02
[0 $\zeta\zeta$]T ₁								
0.20	0.28	0.02	0.50	0.875	0.02	0.80	1.32	0.02
0.30	0.46	0.02	0.60	1.035	0.02	0.90	1.42	0.02
0.40	0.69	0.02	0.70	1.21	0.02			
[0 $\zeta\zeta$]L								
0.15	0.88	0.02	0.475	2.00	0.02	0.65	2.025	0.02
0.20	1.13	0.02	0.50	2.01	0.02	0.675	2.05	0.04
0.30	1.575	0.02	0.525	2.05	0.02	0.70	1.94	0.30
0.375	1.835	0.02	0.55	2.075	0.02	0.725	1.87	0.03
0.40	1.90	0.02	0.575	2.07	0.03	0.75	1.825	0.03
0.425	1.95	0.02	0.60	2.075	0.02	0.80	1.72	0.02
0.45	1.985	0.03	0.625	2.09	0.03	0.90	1.56	0.02
[0 ζ 1] Λ								
0.10	1.475	0.03	0.30	1.46	0.02	0.50	1.45	0.02
0.20	1.47	0.03	0.40	1.43	0.02			
[0 ζ 1] π								
0.10	2.375	0.02	0.40	2.065	0.02	0.70	1.68	0.02
0.20	2.30	0.02	0.50	1.95	0.02	0.80	1.58	0.02
0.30	2.20	0.02	0.60	1.81	0.03	0.90	1.50	0.02

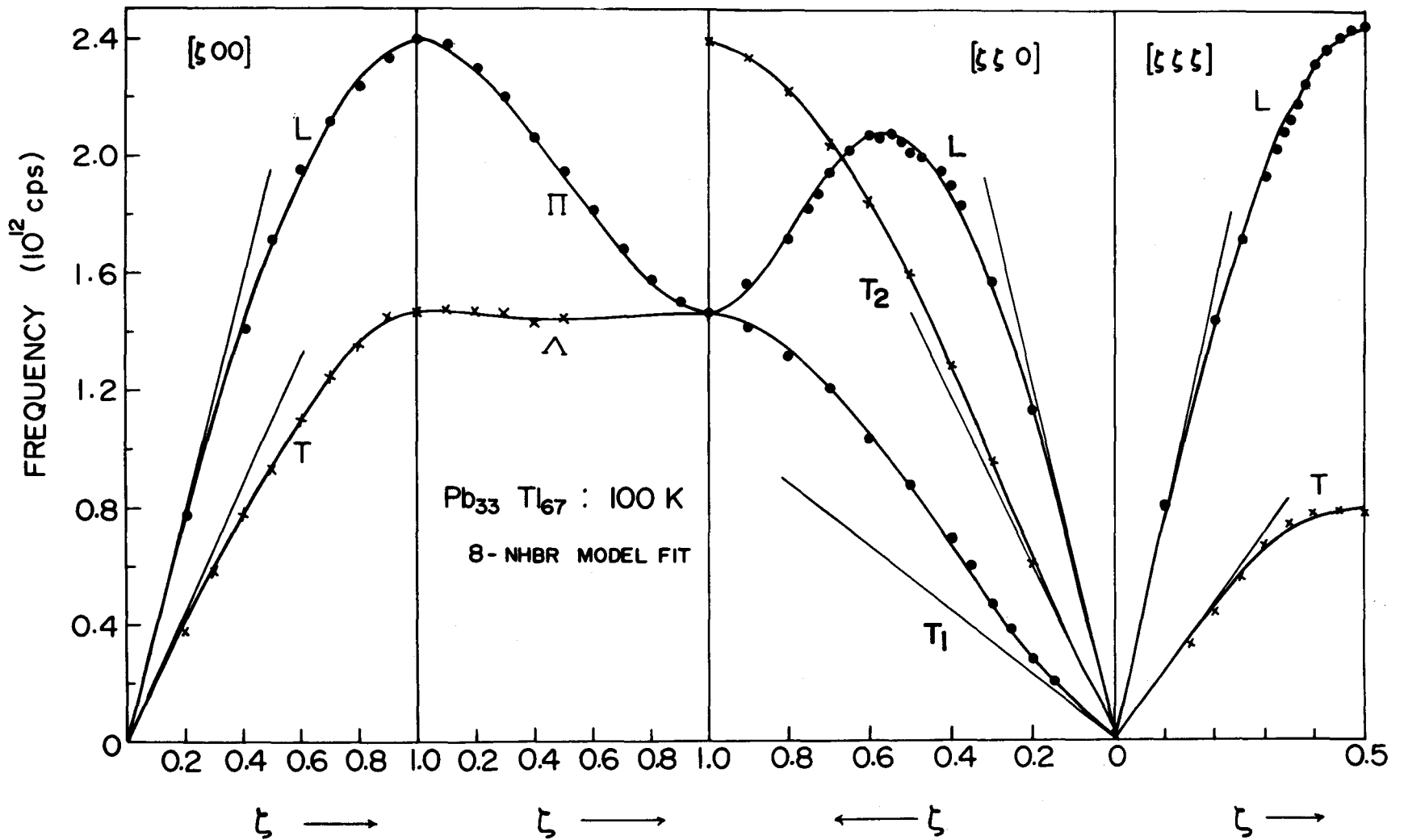


Fig. 4.1

The dispersion curves for $\text{Pb}_{33}\text{Tl}_{67}$ in the four major symmetry directions at 100°K . The solid line is an eight-neighbour Born-von Kármán fit to the experimental points. The straight lines through the origin give the initial slopes of the curves as calculated from the elastic constants.

The elastic constants were included in the fit. The atomic force constants are tabulated in Table 4.4. Good fits were obtained using an eight-neighbour model with forces from fifth to eighth neighbours constrained to be axially symmetric.

Fig. 4.2 shows a comparison between the dispersion curves for the alloy $\text{Bi}_{20}\text{Pb}_{60}\text{Tl}_{20}$ and for pure Pb, which both have the same number of electrons per atom. The results for Pb were taken from the literature (Brockhouse *et al.* 1962); to avoid confusion, the experimental points for Pb are omitted. The overall similarity between the dispersion curves is quite striking which implies that the lattice dynamics of this metallic alloy is primarily determined by the conduction electron density. The mean ratio $\langle v(\text{Bi}_{20}\text{Pb}_{60}\text{Tl}_{20}) / v(\text{Pb}) \rangle$ is 0.96 with a standard deviation of 0.05. It should be noted however, that the force constant disorder present in the ternary alloy will lead to damping as well as shift of the phonon frequencies.

The results of a force constant analysis are given in Table 4.4. The fit is less satisfactory than that obtained for $\text{Pb}_{33}\text{Tl}_{67}$. It was noted by Ng and Brockhouse (1968) that long-range forces extending beyond eighth neighbours exist for the Bi-Pb-Tl alloys; the interaction with distant neighbours becomes weaker as the electron concentration in the alloy system is reduced.

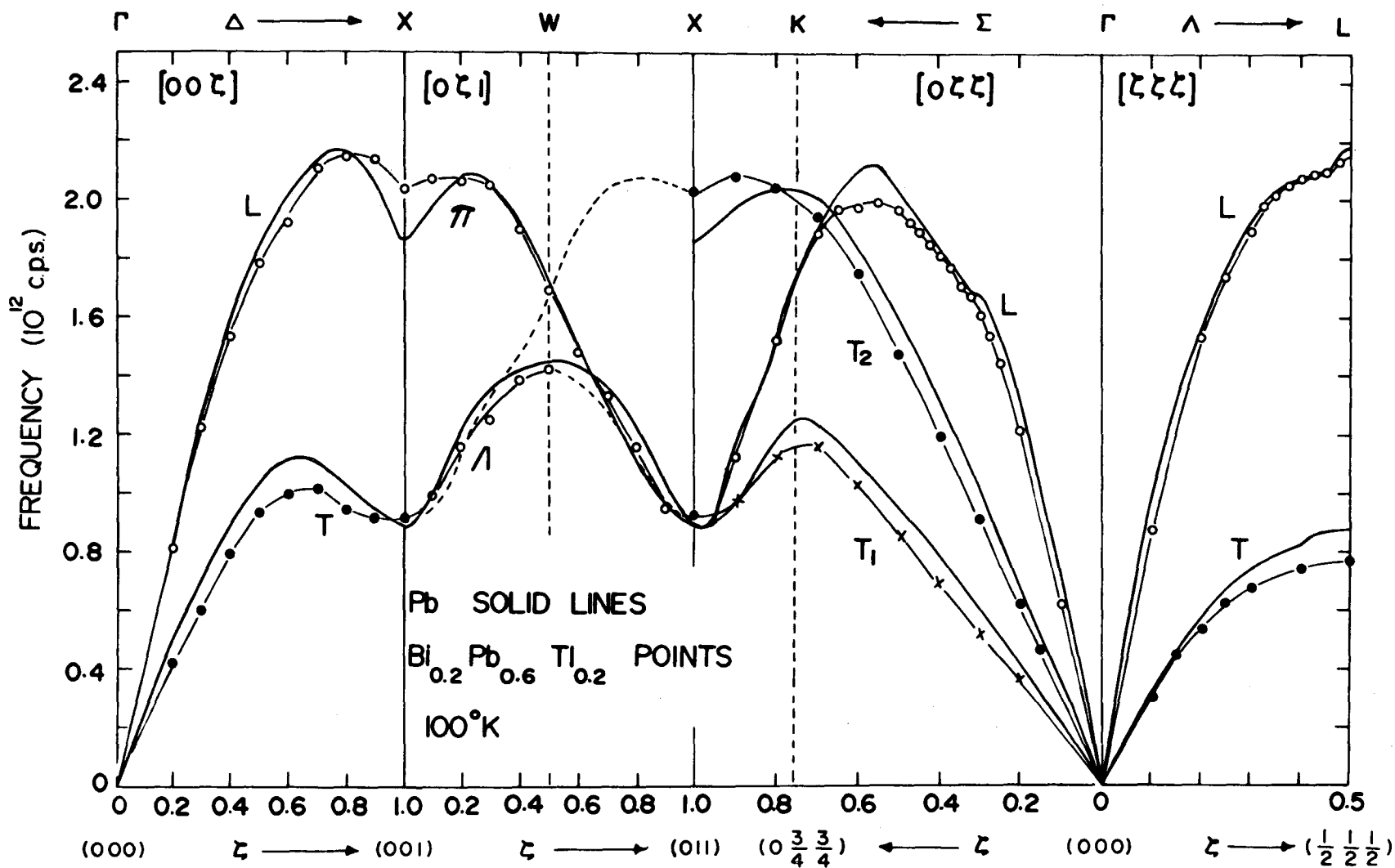


Fig. 4.2

The dispersion curves for $\text{Bi}_{20}\text{Pb}_{60}\text{Tl}_{20}$ at 100°K along the symmetry direction. Lines have been drawn through the points to serve as a guide to the eye. For comparison, the dispersion curves for Pb (Brockhouse et al. 1962) are also shown.

TABLE 4.4

Atomic force constants for $\text{Bi}_{20}\text{Pb}_{60}\text{Tl}_{20}$
and $\text{Pb}_{33}\text{Tl}_{67}$ at 100°K
in units of dyne/cm

AFC	$\text{Bi}_{20}\text{Pb}_{60}\text{Tl}_{20}$	$\text{Pb}_{33}\text{Tl}_{67}$
1XX	3687+75	4855+60
1ZZ	-1574+152	-1409+116
1XY	5037+118	5759+88
2XX	1532+100	140+77
2YY	-15+71	-38+53
3XX	-312+96	110+74
3YY	71+46	-110+38
3YZ	233+60	-24+51
3XZ	40+32	-41+25
4XX	572+37	46+28
4ZZ	25+51	-157+41
4XY	176+143	148+111
5XX	-4+86	-91+66
5YY	-221+43	51+33
5ZZ	-248+56	69+43
5XY	81+47	-53+34
6XX	-6+26	-105+21
6YZ	-88+77	12+67
7XX	-32+46	79+34
7YY	84+47	-25+37
7ZZ	-1+21	26+17
7YZ	12+14	6+13
7XZ	18+22	9+20
7XY	37+20	18+12
*8XX	144+107	-73+68
8XY	267+73	-8+46

Force Constant Matrix $\begin{pmatrix} n_{XX} & n_{XY} & n_{XZ} \\ n_{XY} & n_{YY} & n_{YZ} \\ n_{XZ} & n_{YZ} & n_{ZZ} \end{pmatrix}$

reference atoms $\frac{a}{2}(hkl)$, $h>k>l>0$

*In the mathematical fit, the eighth-neighbour force constants are affected by the termination and this is probably reflected in the values being comparatively large.

C. Temperature Dependence of Phonon Dispersion Curves
in Pb and Pb₄₀Tl₆₀

It is seen from the discussion given in the previous section that the conduction electron concentration in metals and metallic alloys plays an important role in determining the phonon frequencies. Also lattice vibrations normally exhibit temperature dependence. Therefore, it may be instructive to study the temperature dependence of the phonon frequencies* in substances with different electron concentrations. We discuss below, the dispersion curves at 100°K and 296°K in Pb and Pb₄₀Tl₆₀ which have 4 and 3.4 electrons per atom respectively.

Comprehensive measurements on lead along the major symmetry directions at 100°K were made by Brockhouse et al (1962). Limited measurements at 296°K and 425°K were also reported (Brockhouse et al.1961, 1966). Stedman et al. (1967a) have also determined the phonon frequencies at many points in reciprocal space at 80°K and at some selected points at 300°K for lead. The results of the above workers agree quite well within the assigned errors.

To make a detailed comparative study of the dispersion curves, we have measured the phonon frequencies in

*The effect of temperature on phonon-lifetime is discussed later.

Pb along the four major symmetry directions at 296°K. These are presented in Fig. 4.3 along with the dispersion curves at 100°K (Brockhouse et al. 1962). (For the sake of clarity, the experimental points at 100°K have been omitted). Fig. 4.4 shows the dispersion curves of $\text{Pb}_{40}\text{Tl}_{60}$ at two different temperatures. (The results at 100°K are due to Ng (1967)). In $\text{Pb}_{40}\text{Tl}_{60}$, all the phonon frequencies show very much the same temperature variation. The observation that the frequencies decrease as the temperature of the crystal is increased seems to apply to most of the metallic crystals studied so far; e.g. K (Buyers and Cowley 1969), Al (Larsson et al. 1961), Cu (Nicklow et al. 1967), Pd (Miiller and Brockhouse 1970), Ni (deWit and Brockhouse 1968). However, the temperature dependence of the phonon frequencies in Pb is unusual in the sense that different modes behave quite differently as to absolute magnitude, relative magnitude and even sign (Brockhouse 1966). In particular, attention may be drawn to the branch $[00\zeta]\text{T}$ and $[0\zeta 1]\text{A}$ in lead to illustrate the above statement. Also, for the $[00\zeta]\text{L}$ zone-boundary mode, the frequency seems to increase with increasing temperatures. The different kinds of frequency shifts observed in Pb and $\text{Pb}_{40}\text{Tl}_{60}$ may be related to the fact that the strengths of the electron-phonon interaction are quite different in the two materials and hence the anharmonic frequency shifts which involve the

TABLE 4.5

Phonon frequencies (in units of 10^{12} cps) for the symmetry
branches in lead at 296°K

ζ	ν	$\Delta\nu$	ζ	ν	$\Delta\nu$	ζ	ν	$\Delta\nu$
				[00 ζ]T				
0.15	0.37	0.02	0.40	0.86	0.025	0.80	1.00	0.03
0.185	0.46	0.02	0.50	0.985	0.03	0.90	0.96	0.03
0.25	0.58	0.02	0.60	1.055	0.03	1.00	0.925	0.03
0.30	0.69	0.02	0.70	1.04	0.03			
				[00 ζ]L				
0.30	1.225	0.03	0.60	1.99	0.04	0.90	2.04	0.04
0.40	1.54	0.03	0.65	2.04	0.04	0.95	1.94	0.04
0.50	1.77	0.035	0.75	21.45	0.04	1.00	1.88	0.04
0.55	1.875	0.04	0.80	2.12	0.04			
				[$\zeta\zeta\zeta$]T				
0.10	0.31	0.02	0.25	0.62	0.02	0.40	0.80	0.03
0.15	0.41	0.02	0.285	0.68	0.025	0.45	0.81	0.03
0.20	0.53	0.02	0.35	0.74	0.03	0.50	0.825	0.03
				[$\zeta\zeta\zeta$]L				
0.075	0.59	0.03	0.30	1.87	0.03	0.425	2.05	0.04
0.10	0.70	0.03	0.325	1.94	0.03	0.45	2.06	0.035
0.15	1.13	0.02	0.35	1.97	0.03	0.475	2.10	0.04
0.20	1.47	0.03	0.375	1.98	0.04	0.50	2.165	0.035
0.25	1.72	0.03	0.40	2.04	0.03			
				[0 $\zeta\zeta$]T ₂				
0.10	0.32	0.02	0.40	1.21	0.03	0.70	1.95	0.04
0.20	0.62	0.02	0.50	1.46	0.03	0.85	2.00	0.04
0.30	0.92	0.025	0.60	1.71	0.035	1.00	1.89	0.04
				[0 $\zeta\zeta$]T ₁				
0.20	0.35	0.025	0.50	0.88	0.02	0.90	0.97	0.04
0.25	0.42	0.025	0.60	1.01	0.03	0.95	0.925	0.035
0.30	0.505	0.02	0.70	1.14	0.035			
0.40	0.69	0.02	0.80	1.13	0.035			
				[0 $\zeta\zeta$]L				
0.093	0.63	0.03	0.35	1.68	0.03	0.60	2.06	0.04
0.15	0.93	0.03	0.375	1.76	0.035	0.65	2.01	0.045
0.20	1.22	0.03	0.40	1.79	0.03	0.70	1.89	0.04
0.25	1.46	0.035	0.425	1.83	0.03	0.75	1.72	0.035
0.275	1.54	0.03	0.45	1.875	0.03	0.80	1.51	0.03
0.30	1.61	0.03	0.50	1.995	0.04	0.85	1.305	0.03
0.325	1.67	0.03	0.55	2.04	0.04			
				[0 ζ 1] Λ				
0.10	1.04	0.03	0.30	1.295	0.04	0.50	1.42	0.04
0.20	1.18	0.03	0.40	1.355	0.04			
				[0 ζ 1] π				
0.10	1.96	0.04	0.40	1.92	0.03	0.70	1.30	0.03
0.20	2.05	0.04	0.50	1.68	0.035	0.80	1.14	0.025
0.30	2.025	0.04	0.60	1.47	0.03	0.90	1.00	0.03

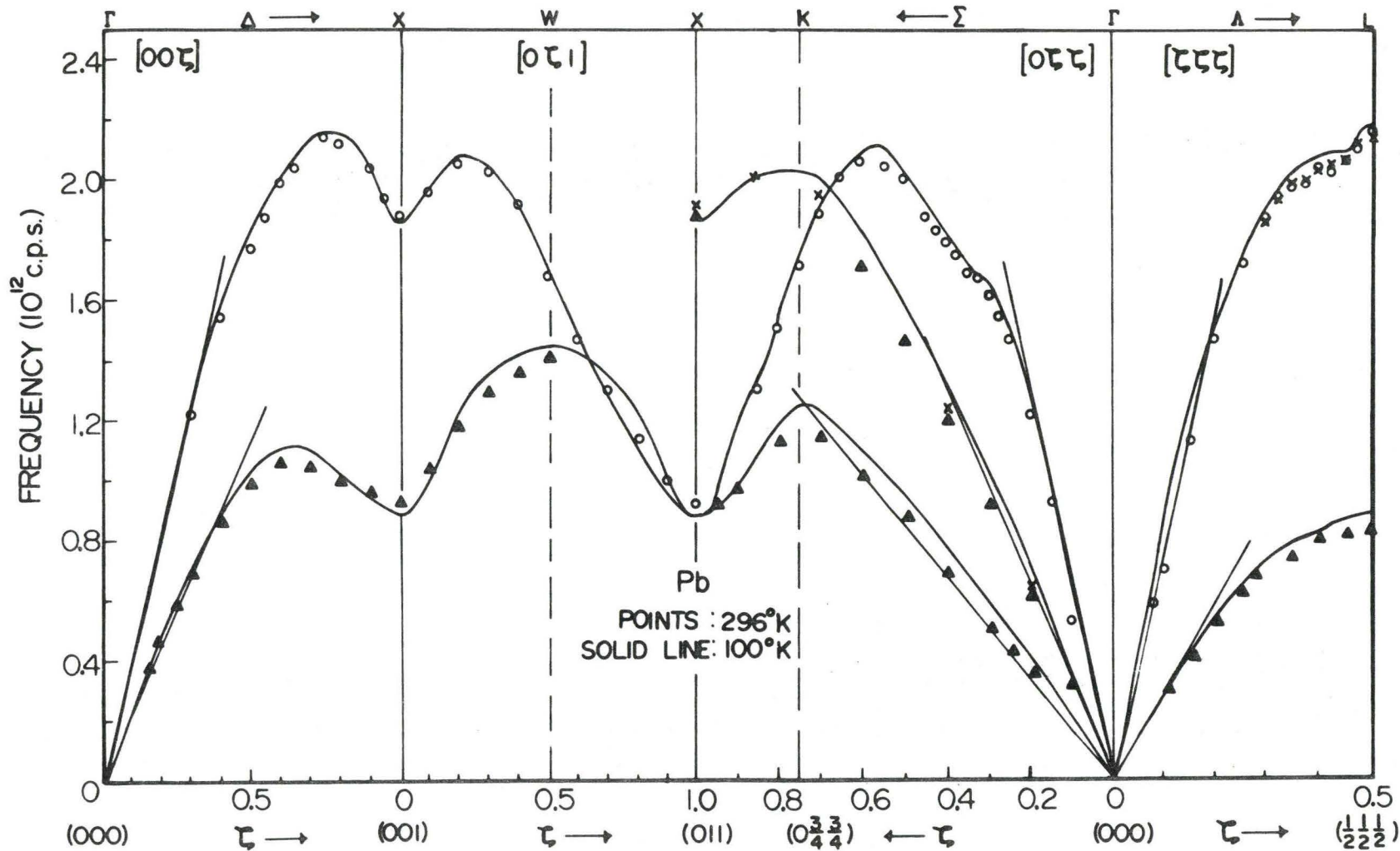


Fig. 4.3

The dispersion curves of Pb obtained at 296°K along the various symmetry directions. These measurements were done at the McMaster reactor (except the crosses which were obtained using the Chalk River spectrometer). For comparison the dispersion curves at 100°K (Brockhouse et al. 1962) are also shown.

TABLE 4.6

Phonon frequencies for the symmetry
branches in $\text{Pb}_{40}\text{Tl}_{60}$ at 100°K and 296°K

Branch	ζ	Frequency ν (10^{12} cps)	
		100°K ^(a)	296°K
[00 ζ]T	0.20	0.432+0.02	0.42+0.025
	0.30	0.626+0.02	0.595+0.03
	0.40	0.81 +0.02	0.78 +0.03
	0.50	0.965+0.02	0.92 +0.035
	0.60	1.122+0.02	1.09 +0.035
	0.70	1.275+0.02	1.235+0.045
	0.80	1.37 +0.03	1.31 +0.05
	0.90	1.45 +0.03	1.38 +0.04
	1.00	1.455+0.03	1.41 +0.04
[00 ζ]L	0.30	1.155+0.03	1.15 +0.04
	0.40	1.46 +0.03	1.44 +0.04
	0.50	1.74 +0.03	1.685+0.04
	0.60	1.975+0.03	1.91 +0.04
	0.70	2.13 +0.04	2.08 +0.04
	0.80	2.24 +0.03	2.20 +0.045
	0.90	2.33 +0.04	2.30 +0.04
	1.00	2.38 +0.03	2.34 +0.04
[$\zeta\zeta\zeta$]T	0.15	0.383+0.02	0.375+0.03
	0.20	0.485+0.03	0.47 +0.04
	0.30	0.675+0.02	0.65 +0.03
	0.35	0.742+0.02	0.72 +0.035
	0.40	0.784+0.02	0.75 +0.035
	0.45	0.777+0.02	0.765+0.035
	0.50	0.77 +0.02	0.74 +0.035
[$\zeta\zeta\zeta$]L	0.10	0.76 +0.02	0.715+0.04
	0.15	1.125+0.03	1.09 +0.04
	0.20	1.45 +0.04	1.41 +0.04
	0.25	1.70 +0.03	1.66 +0.04
	0.30	1.94 +0.04	1.89 +0.04
	0.35	2.105+0.04	2.06 +0.045
	0.40	2.29 +0.05	2.265+0.045
	0.45	2.37 +0.04	2.37 +0.04
0.50	2.42 +0.04	2.39 +0.045	

cont'd next page

Table 4.6 cont'd

Branch	ζ	$\nu (10^{12} \text{ cps})$	
		$100^\circ\text{K}^{(a)}$	296°K
[$\zeta\zeta\zeta$]L	0.10	0.76 +0.02	0.715+0.04
	0.15	1.125+0.03	1.09 +0.04
	0.20	1.45 +0.04	1.41 +0.04
	0.25	1.70 +0.03	1.66 +0.04
	0.30	1.94 +0.04	1.89 +0.04
	0.35	2.105+0.04	2.06 +0.045
	0.40	2.29 +0.05	2.265+0.045
	0.45	2.37 +0.04	2.37 +0.04
	0.50	2.42 +0.04	2.39 +0.045
[0 $\zeta\zeta$]T ₂	0.15		0.45 +0.03
	0.20	0.63 +0.02	0.625+0.03
	0.30	0.967+0.02	0.925+0.025
	0.40	1.32 +0.02	1.26 +0.025
	0.50	1.59 +0.02	1.535+0.03
	0.60	1.85 +0.03	1.77 +0.03
	0.90	2.32 +0.03	2.27 +0.05
	(1.00)	(2.38 +0.03)	(2.34 +0.04)
[0 $\zeta\zeta$]T ₁	0.15		0.23 +0.03
	0.20	0.325+0.02	0.30 +0.025
	0.30	0.492+0.01	0.47 +0.02
	0.40	0.745+0.02	0.71 +0.03
	0.50	0.93 +0.02	0.88 +0.025
	0.60	1.098+0.02	1.06 +0.03
	0.70	1.25 +0.02	1.22 +0.04
	0.80	1.37 +0.02	1.30 +0.045
	(1.00)	(1.455+0.03)	(1.41 +0.04)
[0 $\zeta\zeta$]L	0.15	0.915+0.03	0.85 +0.04
	0.20	1.155+0.03	1.12 +0.03
	0.30	1.57 +0.02	1.535+0.03
	0.40	1.905+0.03	1.87 +0.03
	0.50	2.01 +0.02	1.96 +0.04
	0.60	2.09 +0.02	2.035+0.035
	0.70	1.965+0.03	1.93 +0.035
	0.80	1.725+0.04	1.69 +0.04
	0.90	1.55 +0.03	1.515+0.04
(1.00)	(1.455+0.03)	(1.41 +0.04)	
[0 ζ 1] Λ	0.10	1.465+0.03	1.41 +0.035
	0.30	1.45 +0.03	1.42 +0.03
	0.50	1.45 +0.03	1.42 +0.035
[0 ζ 1] π	0.20	2.305+0.03	2.31 +0.04
	0.40	2.095+0.03	2.05 +0.04
	0.60	1.845+0.03	1.78 +0.035

(a) Ng (1967)

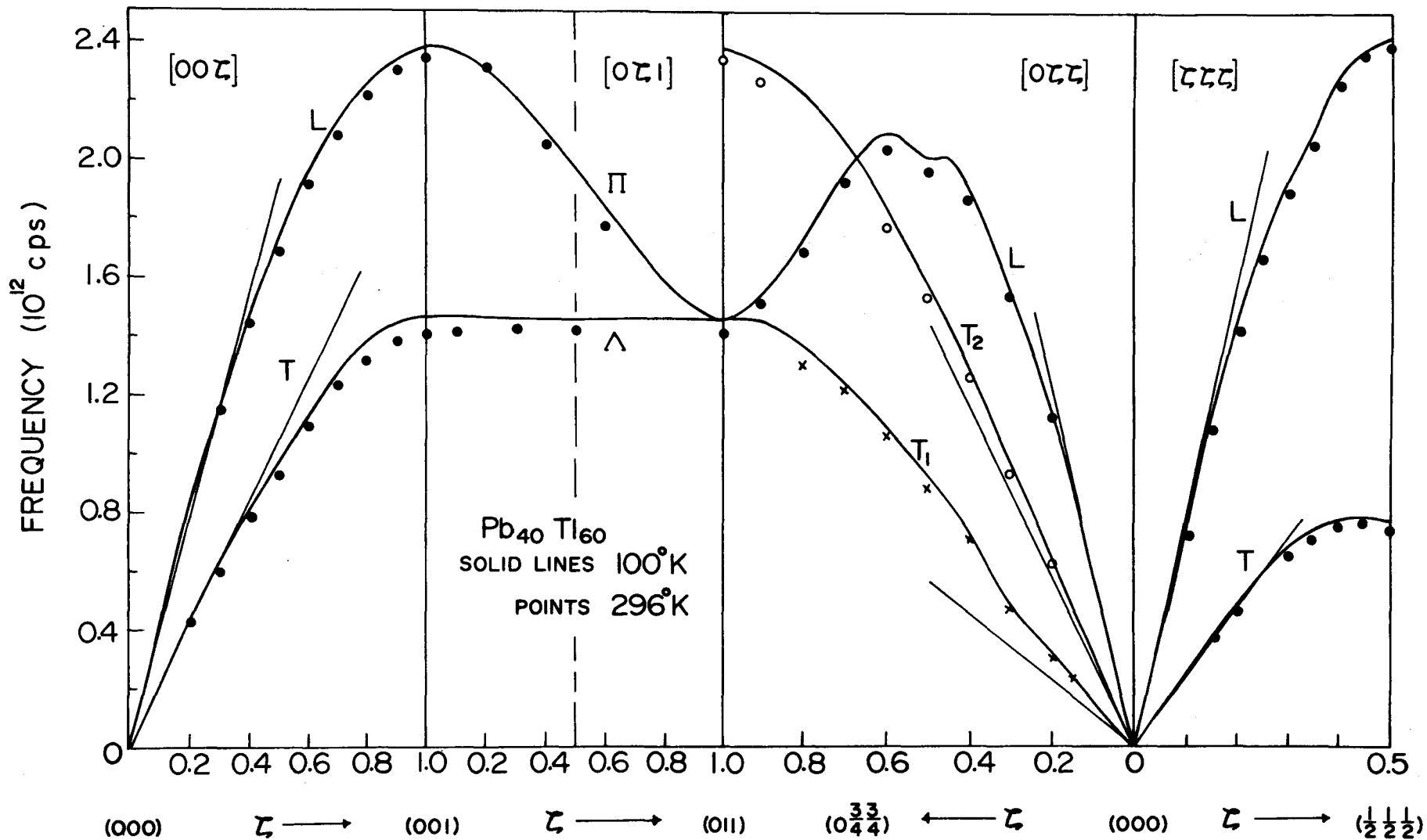


Fig. 4.4

The dispersion curves for $\text{Pb}_{40}\text{Tl}_{60}$ along the symmetry directions at 296°K and 100°K . The results for 100°K are taken from the work of Ng and Brockhouse (1968). The initial slopes determined by elastic constants at 296°K are also indicated.

electron-phonon matrix element may be quite different.

Brockhouse et al. (1961, 1962) analyzed the dispersion curves of Pb in terms of Fourier components (interplanar force constants). The analysis indicated existence of very long range forces in Pb - the range of the forces apparently decreasing with increasing temperature. For $\text{Pb}_{40}\text{Tl}_{60}$, an adequate description of the dispersion curves can be obtained using an eight-neighbour force constant model within the framework of the Born-von Kármán formalism. The above statements about the range of the force constants should be qualified by the remark that since the force constants are determined from dispersion curves measured at finite temperatures they contain anharmonic contributions. Now, for $T > \Theta_D$, the shift of the phonon frequency is expected to be a linear function of temperature (Leibfried and Ludwig 1961). In view of this, it has been suggested by Hahn (1963) and by Leibfried and Ludwig (1961), that the dispersion curves measured as a function of temperature (for $T > \Theta_D$) may be extrapolated linearly to $T = 0$ to obtain the dispersion curves for the harmonic crystal at 0°K and these may then be analyzed to yield information about the range of the harmonic force constants.

Fundamental calculation of the dispersion curves

In Chapter II (section E), we outlined the procedure of calculating the phonon frequencies of simple metals from

an effective interaction between ions arising from the direct Coulomb interaction between the ions and the conduction-electron response to the ion motion. Such a fundamental calculation for Pb was done by Vosko et al. (1965). Fair qualitative agreement was obtained; however quantitative agreement could not be expected since the Fermi surface was assumed to be completely spherical in reciprocal space and the spin-orbit effect (which is appreciable for a heavy element like lead) was neglected.

For $\text{Pb}_{40}\text{Tl}_{60}$, the calculation of the phonon frequencies may be expected to be comparatively simpler since the electron-screening contribution is relatively small compared with that in lead. This is illustrated in Fig. 4.5 where we have plotted the bare-ion frequencies (in the absence of the conduction-electron response) and the experimental frequencies. Dynes et al. (1969) obtained the electron-ion pseudopotential form factor (see Eq. (2.24)) for $\text{Pb}_{40}\text{Tl}_{60}$, based on the Heine-Abarenkov model potential (Heine and Abarenkov 1964). The model potential consists of a square well of radius $r = R_M$ and equals Z/r for $r > R_M$. The potential is characterized basically by three parameters; A_0 , A_1 and A_2 (Animalu and Heine 1965). This bare potential is then screened in the local approximation as outlined in Chapter II (section E) and the phonon frequencies were calculated in the standard way

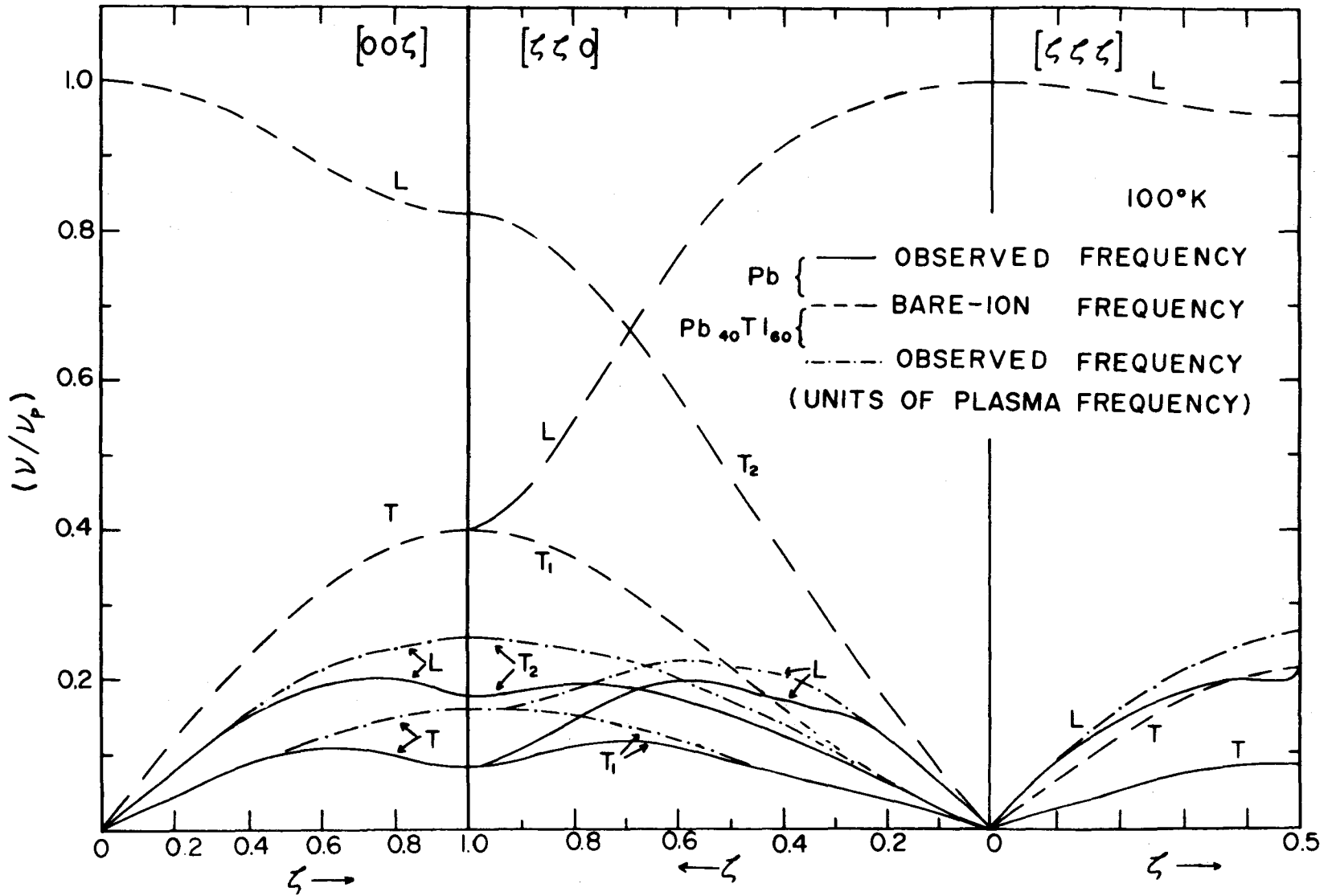


Fig. 4.5

Bare-ion Coulomb frequencies and the renormalized phonon frequencies in Pb and Pb₄₀Tl₆₀ along various symmetry directions to illustrate the influence of screening by electron-phonon interaction.

(Eq. (2.40)). The well depth parameters A_0 , A_1 and A_2 and the screening parameters β (Eq. (2.33)) were adjusted to give reasonable fits to some selected zone-boundary phonon frequencies at 100°K. The fitted pseudopotential form factor is shown in Fig. 4.6. The following values have been used for the various parameters*.

$$A_0 = 1.61, \quad A_1 = 1.61, \quad A_2 = 1.52, \quad \beta = 1.47$$

(atomic units)

For comparison, we also show in Fig. 4.6 the pseudopotential obtained by adding the bare model-potentials of Pb and Tl (calculated in the local approximation using the parameters given by Animalu and Heine (1965)) in proper concentrations (40 atomic % and 60 atomic % respectively) and then screened appropriate to the alloy $\text{Pb}_{40}\text{Tl}_{60}$ (i.e. $Z = 3.4$).

The phonon dispersion curves computed along major symmetry directions using the fitted pseudopotential exhibit good agreement with the experimental measurements at 100°K (Dynes et al. 1969). Therefore, it may be of interest to calculate the volume dependent frequency shifts in the pseudopotential theory. For calculating the frequencies corresponding to a different equilibrium volume, the volume dependence of the parameters A_0 , A_1 and A_2 characterizing

* The author is grateful to Dr. D. W. Taylor for the computer programme and for his advice.

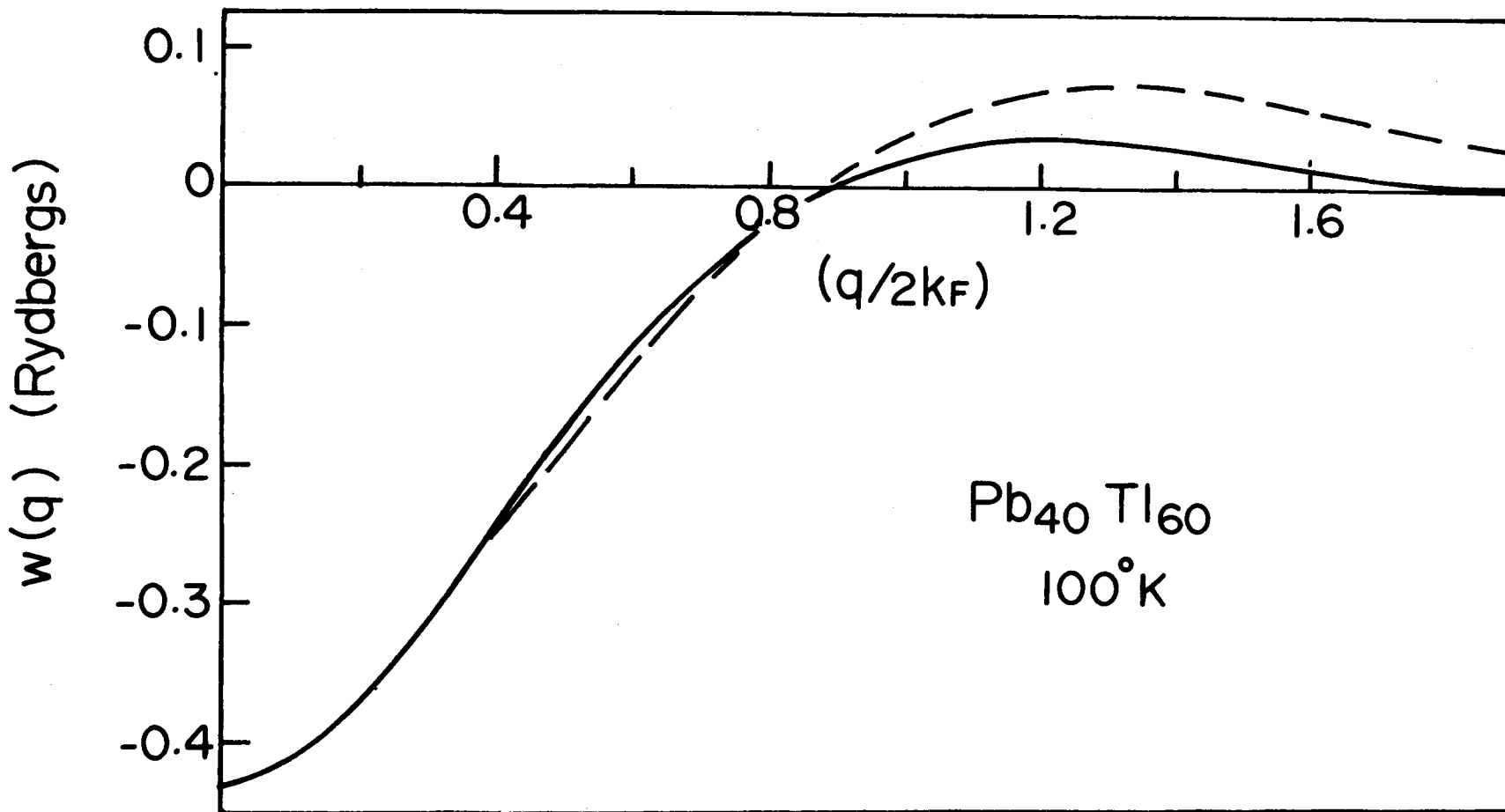


Fig. 4.6

The solid curve gives the (Heine-Abarenkov) screened form factor obtained by fitting to the $[\zeta 00]$ zone boundary phonon frequencies of $Pb_{40}Tl_{60}$ at $100^\circ K$. The dashed line represents an 'average' form factor for $Pb_{40}Tl_{60}$ obtained from the bare pseudopotentials of Pb and Tl with screening appropriate to the alloy.

the bare model-potential can be neglected (Trofimenkoff and Carbotte 1970; Coulthard 1970). The variation of the HA potential arises mainly from the explicit volume factor in the bare potential (Animalu and Heine 1965) and the change in the dielectric function $\epsilon(q)$ with Fermi momentum k_F . The shift to the phonon frequencies arising from the direct ion-ion interaction (Coulomb) is easily incorporated in the calculation as the relevant Grüneisen parameter $\gamma_{\text{Coulomb}} = \frac{1}{2}$. The results of the calculations are shown in Fig. 4.7. The phonon dispersion curves for $\text{Pb}_{40}\text{Tl}_{60}$ have been computed using the crystal volumes appropriate to 100°K and 296°K; the parameters for the model-potential were fixed by fitting to the $[00\zeta]$ zone-boundary phonon frequencies at 100°K as explained before.

The experimental measurements were made with the $(1\bar{1}0)$ axis of the crystal vertical. For a given q , the phonon frequencies were measured at the two different temperatures at identical points in reciprocal space and under identical spectrometer calibrations to eliminate systematic errors in obtaining the frequency shifts as far as possible. These limited measurements agree with the frequencies listed in Table 4.6 well within assigned errors. It is seen that the computed frequency shifts are in fair agreement with the experimental values. No quantitative agreement was anticipated since in the calculation we have

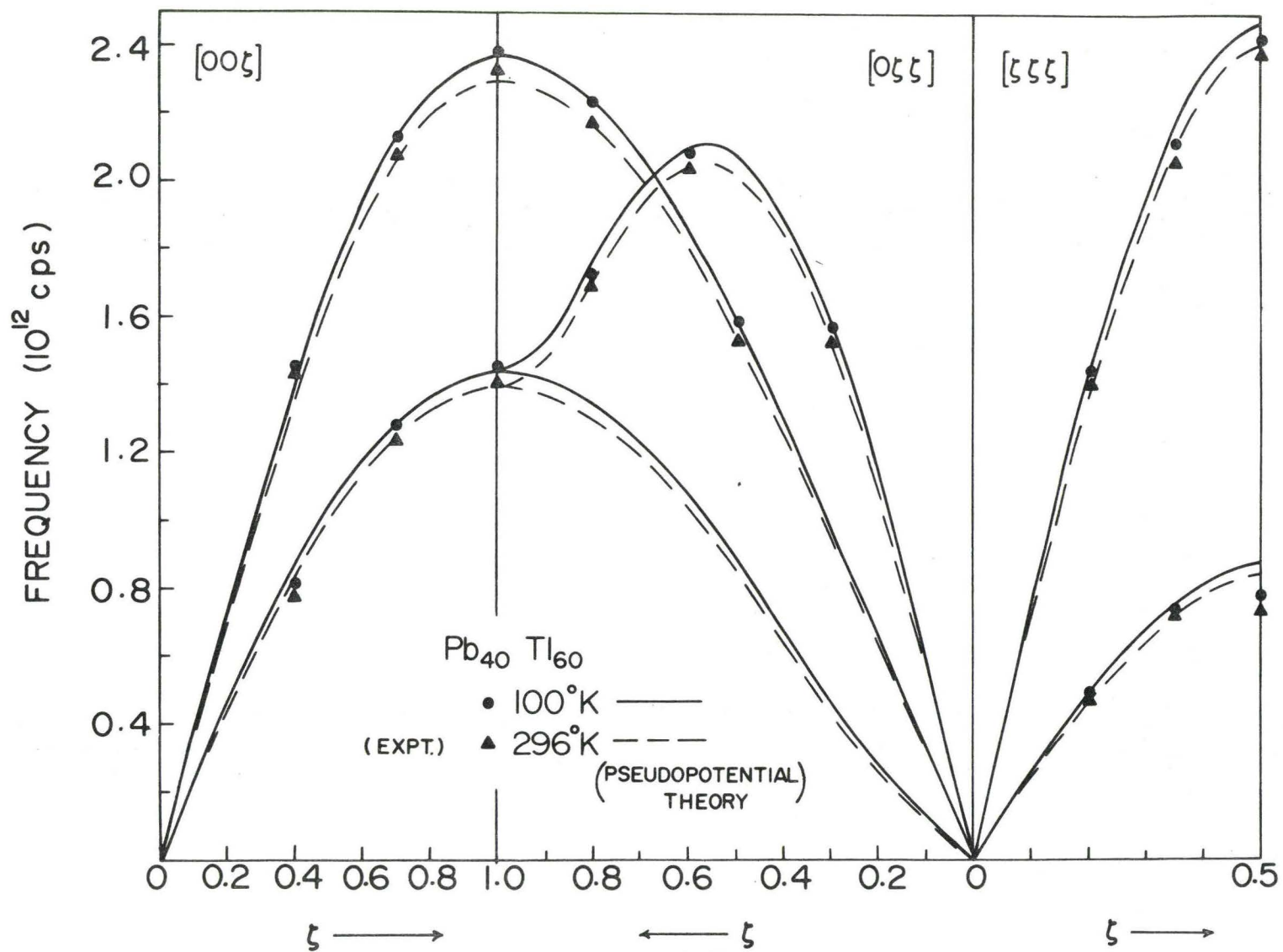
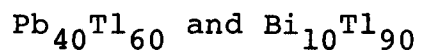


Fig. 4.7

The dispersion curves calculated at 100°K and 296°K using the Heine-Abarenkov model pseudopotential. Experimental measurements at a few selected points are also shown.

included the contribution arising from the "thermal strain" only (quasi-harmonic approximation) and neglected the explicit temperature shift caused by the anharmonic terms in the potential energy. However, the principal anharmonic contributions come from the third and the fourth order terms (Maradudin and Fein 1962) and these are often of opposite signs and partially cancel (Cowley and Cowley 1965). However, it can not be stated with certainty that this situation applies to $\text{Pb}_{40}\text{Tl}_{60}$ unless detailed anharmonic calculations are made (Buyers and Cowley 1969).

D. Anharmonic damping of phonons in



Introduction

For a harmonic crystal the peaks in the coherent one-phonon scattering for a particular q are δ -functions in energy broadened by the resolution of the apparatus. In a crystal in which the interaction between the atoms are anharmonic the wave trains of the lattice vibration are limited in time. As a result, the form of the one-phonon cross section is approximately a Lorentzian. (This follows from a simple analogy with the decay of radioactive atoms; Fourier transform of an exponential decay in time gives rise to a Lorentzian line shape in energy.) Therefore, the observed neutron group is the convolution of the instrumental resolution function (assumed to be a Gaussian) as a function of Q and ω with a Lorentzian line shape of the one-phonon excitation. In addition to the problem of deconvolution to obtain the natural width of the phonon; the experiments to study line broadening is complicated by the fact that often the neutron groups at elevated temperatures are superposed on a strong background.

Experimental Energy Widths in $\text{Pb}_{40}\text{Tl}_{60}$

Phonons were studied in $\text{Pb}_{40}\text{Tl}_{60}$ at 100°K and 296°K to investigate the anharmonic effects. The temperature dependent frequency shifts observed in $\text{Pb}_{40}\text{Tl}_{60}$ were considered in the earlier section. In this section we discuss the frequency widths of phonons.

Fig. 4.8 shows the neutron groups along the $[\zeta\zeta 0]L$ branch for $\zeta=0.3$ at two different temperatures measured under identical settings of the spectrometer using the same counting period as regulated by the monitor in the incident beam. At $296^\circ K$, the one-phonon group is observed to sit on a strong and sloping background arising from multi-phonon scattering and from multiple-event inelastic scattering processes, both of which increase markedly with temperature. To obtain the true phonon-widths it is necessary to subtract the above background and correct the neutron group for resolution.

The separation between one-phonon and multiphonon scattering may not be well defined for an anharmonic crystal. Ambegaokar et al. (1965) pointed out that anharmonicity gives rise to an interference between the sharp one-phonon peak and the diffuse multi-phonon background. This interference modifies the shape as well as the intensity of the one-phonon peak. Numerical calculations by Maradudin and Ambegaokar (1964) indicated that the former effect is very small. However, it has been recently shown that the interference effect on the intensity of the one-phonon peak is larger (Cowley and Buyers 1969) and has also been observed experimentally in KBr (Cowley, Svensson and Buyers 1969). In view of this, it was necessary to examine the intensities of the neutron groups more closely. The procedure followed for the subtraction of the background will be illustrated by referring to the neutron groups shown in Fig. 4.8.

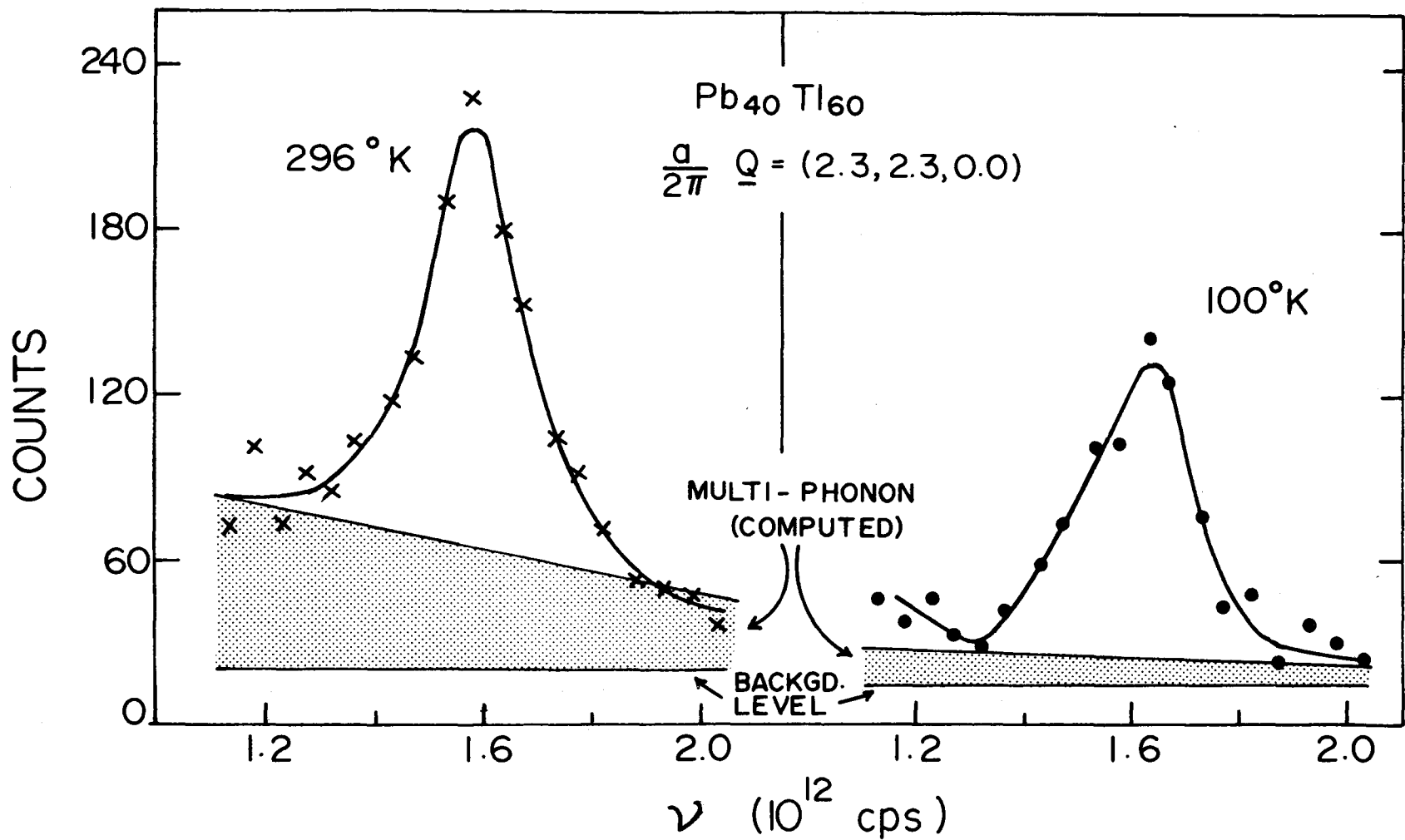


Fig. 4.8

Neutron groups at two different temperatures illustrating the temperature dependent background arising from the multiphonon processes. The general background level as estimated from the "background counter" is also shown.

We first calculate the multi-phonon cross-section as a function of the wave-vector and energy transfer in the neighbourhood of the one-phonon peak at 100°K , in the incoherent approximation for a harmonic crystal (Eq. (3.10)). At this temperature, all the higher phonon processes except the two-phonon cross-section are negligible. The computed cross-section is folded with the resolution function of the spectrometer and the effect of the analyzer sensitivity is also included (Appendix II). The coherence effects in multi-phonon processes are averaged out to a large extent (Eq. (3.9); see also Sjolander (1958)). Further, since the observed spectrum is heavily smeared by the resolution, the calculation of the two-phonon coherent cross-section in the incoherent approximation is expected to be reasonably valid.

The computed cross-section is then normalized to the observed multi-phonon background at 100°K . The drawing of the background line is somewhat arbitrary; however the neutron groups are quite well defined at this temperature (100°K) and therefore the uncertainty is not large. Using this intensity scale factor obtained from the above normalization at 100°K , the multi-phonon contribution is fixed at 296°K and is used to draw the background line under the neutron group at 296°K . (See Fig. 4.8.)

It should be mentioned that for large specimens* used in the neutron-scattering experiments, multiple-event inelastic scattering processes are also present—either two-phonon scattering followed or preceded by Bragg scattering, or

* The transmission of the specimen crystal was about 45% at 296°K --a rather low value. However, the transmission was 60% at 100°K and was suitable for measuring the dispersion relations.

two one-phonon scattering events (successive energy gain and/or energy loss). However, for both the above processes, the shape of the spectrum is roughly the same as that of the single-event two-phonon scattering (simultaneous energy gain and/or loss) and therefore the two-event scattering processes mentioned above are also included in the calculation in an approximate way.

Finally, the integrated intensities of the background subtracted neutron groups are compared with the calculated one-phonon cross-sections (Eq. (3.13)). From the measured transmissions of the specimen at the two temperatures, a correction for self-absorption in the specimen was made in all the above calculations. No deviations from the calculations based on the harmonic theory were found outside the limits of the experimental uncertainty for the phonons investigated at 100°K and 296°K.

Fig. 4.9 shows typical neutron groups corrected for the analyzer sensitivity in the $[\zeta\zeta 0]_L$ and $[\zeta 0 0]_T$ directions, at 100°K and 296°K. The background lines were drawn from the considerations given before and the integrated intensities of the neutron groups were consistent with the one-phonon cross sections calculated using Eq. (3.13). It may be remarked that this procedure involves the assumption that the energy broadening does not affect the integrated cross-section. If the anharmonic width and shift are small compared with the phonon frequency then the above assumption can be shown to be valid (Brockhouse 1966).

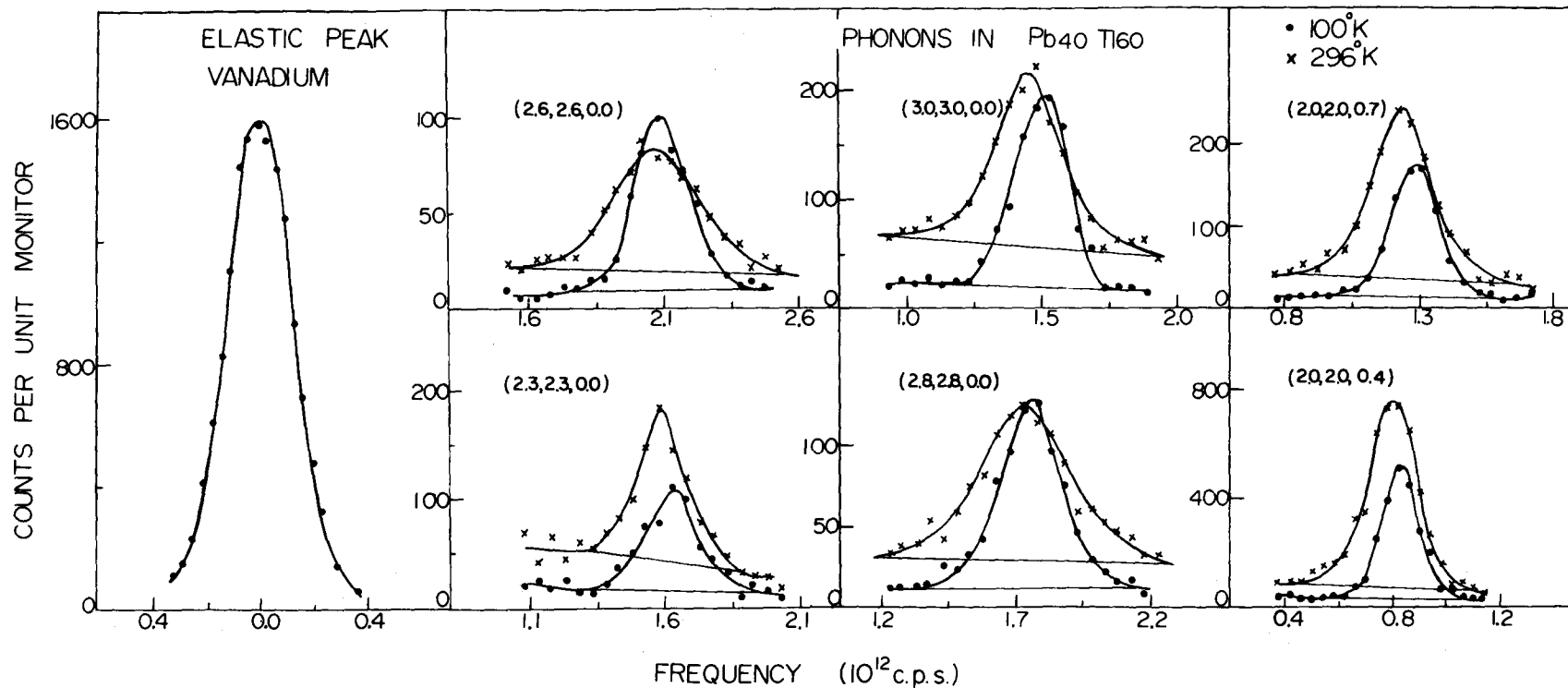


Fig. 4.9

Typical neutron groups, corrected for the analyzer sensitivity, corresponding to the $[\zeta\zeta 0]L$ and $[\zeta 00]T$ branches in $Pb_{40}Tl_{60}$ at $100^{\circ}K$ and $296^{\circ}K$. The points of observation in reciprocal space are also shown. The integrated intensities of the neutron groups (for a given q) at the two different temperatures are compatible with the cross-section formula (Eq. (3.13)). The background lines are also indicated.

The natural line width of a group at 296°K may be deduced by comparison with the width of the corresponding group at 100°K. However, at 100°K some anharmonic broadening is also present. In Fig. A2.4 (App.II) we have plotted the widths of neutron groups at 100°K corresponding to the zone-boundary phonons ($[\zeta 00]T$ and L) in Pb , $Pb_{40}Tl_{60}$ and $Bi_{10}Tl_{90}$. The resolution of the spectrometer as a function of the energy transfer is estimated from the observed vanadium width at the zero energy transfer. Since, for the zone boundary phonons ($\text{grad}_{\underline{q}} \nu = 0$) the gradient focussing is virtually absent, we may conclude from Fig. A2.4 that the resolution widths are approximately 90% of the widths of the corresponding resonances at 100°K.* We next make the reasonable assumption that the above procedure of obtaining the resolution widths from the corresponding measured widths at 100°K holds true for the phonons measured at other values of \underline{q} also. ($\text{Grad}_{\underline{q}} \nu$ does not change much with temperature). Fig. A2.4 also shows that we may disregard any additional broadening⁺ that may be present in the neutron groups for $Pb_{40}Tl_{60}$ and $Bi_{10}Tl_{90}$ caused by force constant disorder. This statement is consistent with the observation of Ng and Brockhouse (1967, 1968) that the neutron groups in these binary alloys are as sharp and well formed as for pure metals.

To extract the natural width at 296°K tables of Lorentz functions folded with Gaussian resolution function (Rose et al.) were employed. The results are presented as

* The machine calculation of the instrumental widths (App.II) indicates that the resolution widths are 80-90% of the observed line widths in $Pb_{40}Tl_{60}$ at 100°K

+ The electron-phonon damping may be ignored (Chap.II(G)).

triangles in Fig. 4.10. A more extensive but somewhat less reliable result for the widths are shown as filled circles. These were obtained from another independent set of measurements made at room temperature (296°K) only. Therefore to obtain the true widths it was necessary to calculate the resolution function of the spectrometer as a function of energy and momentum transfer. A proper consideration of the focussing characteristics of the spectrometer is rather involved (see also Appendix II). The computations, based on the work of Cooper and Nathans (1967), were done in the McMaster University CDC-6400 computer. (The programme was written by Mr. A. Larose; the author is grateful to him for a copy of the computer programme.)

Large errors are introduced in the deconvoluting process, particularly when the line width is comparable with the resolution width. When the broadening is large the Lorentzian line shape is not necessarily expected to hold. (Incidentally this fact introduces little uncertainty in the extraction of the widths provided the width is significantly larger than the resolution width.) According to the detailed theories (Maradudin and Fein 1962; Kokkedee 1962; Cowley 1963) the damping turns out to be a function of the frequency; it is a constant only when the anharmonic interaction and thus the damping itself is very small. In view of these, we have not shown the errors on the individual widths since many of the widths may not be significant by themselves. However; the overall trend of any group of results is likely to be significant.

F. W. H. M. (10^{12} cps)

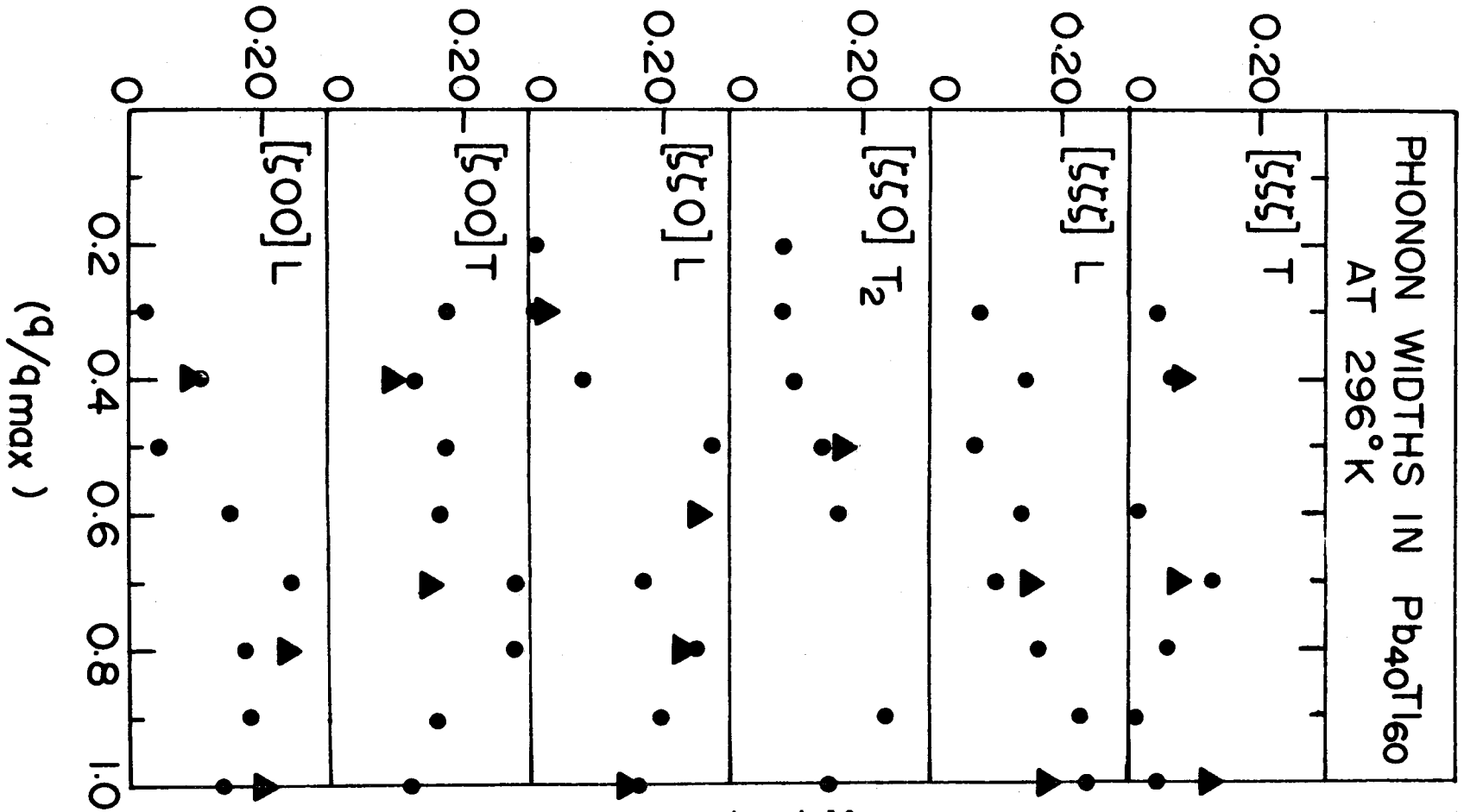


Fig. 4.10

Phonon widths at 296°K arising mainly from anharmonic broadening. The filled circles were obtained after correcting for the instrumental width which was estimated following Cooper and Nathans (1967). The triangles were determined from a comparative study of neutron groups at 100°K and 296°K.

Frequency Shifts and Widths in $\text{Bi}_{10}\text{Tl}_{90}$

The measurements were made at 100°K and 296°K in the $[\zeta 00]$ direction only, for the longitudinal and the transverse branches. The widths at 296°K were obtained from a comparative study of widths at 100°K, as discussed for $\text{Pb}_{40}\text{Tl}_{60}$. Fig. 4.11 shows the results for the widths and shifts in $\text{Bi}_{10}\text{Tl}_{90}$. Along the $[\zeta 00]L$ branch widths are unusually large in the neighbourhood of $\zeta=0.7$.* This is illustrated in Fig. 4.12 where some of the neutron groups are shown at 100°K and 296°K. It is interesting to note that the frequency shifts are also probably large in that region. These effects could be inter-related and may be associated with a singularity in the phonon-phonon interaction there. Unfortunately, proper calculation of these anharmonic properties calls for a major effort of computation; it is only very recently that such detailed calculations have appeared in the literature. (Buyers and Cowley 1969; Sandström and Högberg 1970; Koehler et al. 1970).

Nevertheless, we may analyze the results in terms of an extension to the Born-von Kármán theory of lattice dynamics following Brockhouse et al. (1961). If we include dissipative forces depending linearly on the relative velocities of the ions then for a branch in the symmetry direction the energy width

* The dispersion curves ($[\zeta 00]L$) for $\text{Bi}_{10}\text{Tl}_{90}$ and $\text{Bi}_{20}\text{Tl}_{80}$ show some structure in this region which is not readily interpretable in terms of Kohn kinks. However, the neutron groups at 100°K do not exhibit any anomalous width along this branch.

Fig. 4.11

Phonon widths and shifts in $\text{Bi}_{10}\text{Tl}_{90}$. The solid lines drawn in (a) represent fits to the widths from simple theoretical consideration. (For the $[\zeta 00]$ T zone-boundary mode, the phonon widths were determined at two different positions in reciprocal space and are shown by the filled and the open circles. The measured frequency shifts were identical (See Table 4.9).)

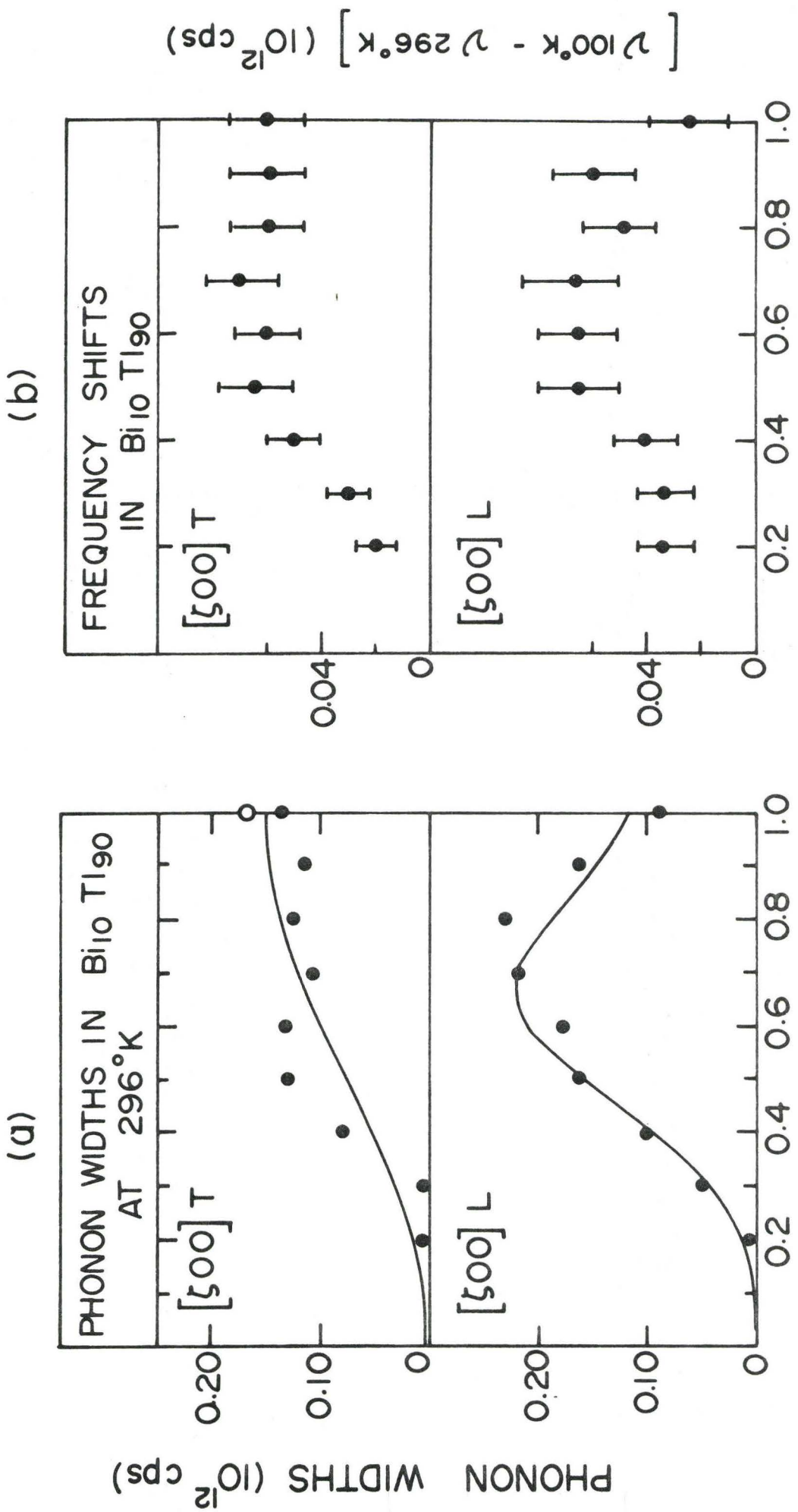


Fig. 4.11

TYPICAL NEUTRON GROUPS IN $\text{Bi}_{10}\text{Tl}_{90}$ $[\zeta 00]L$

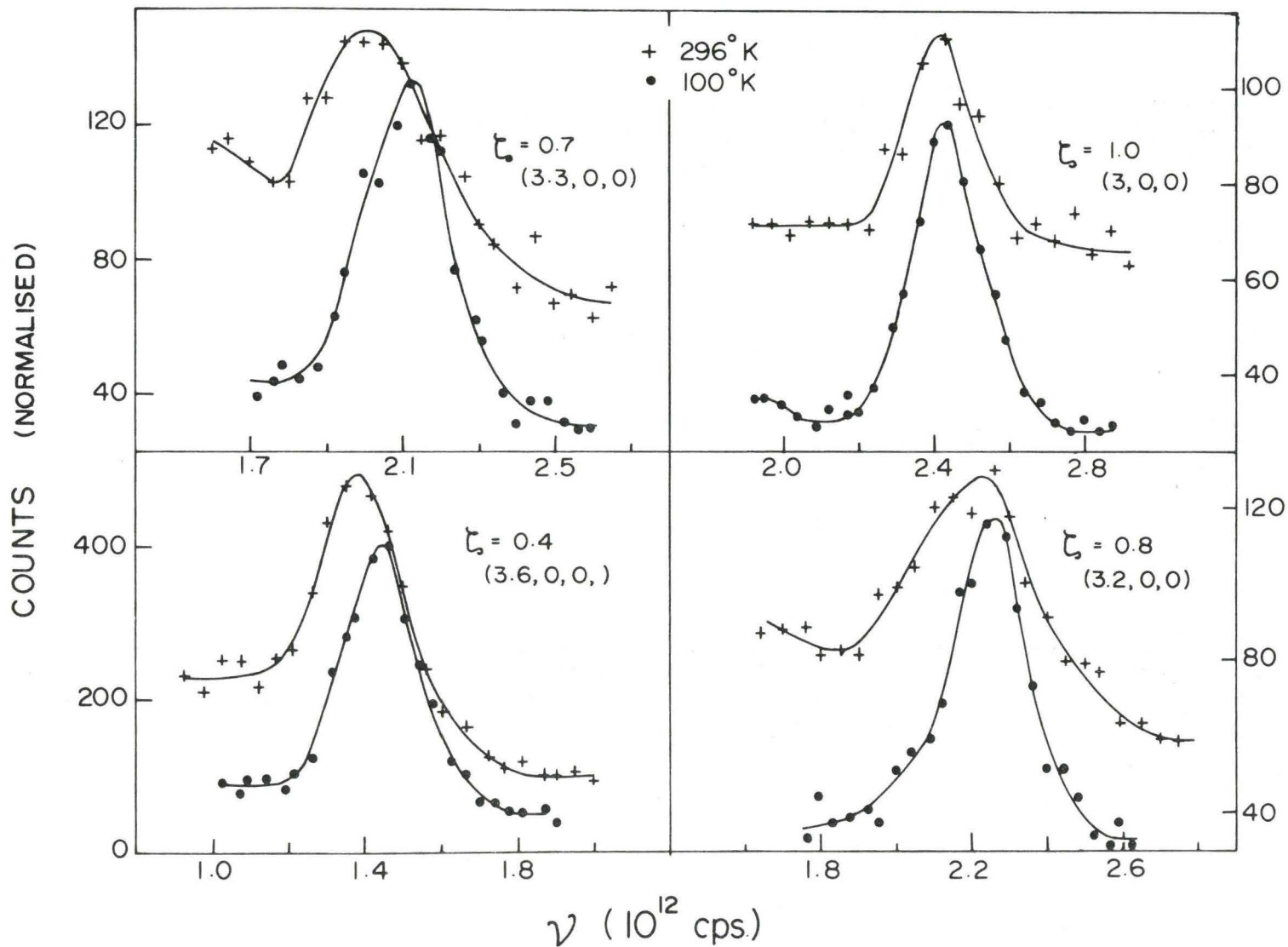


Fig. 4.12

Typical neutron groups in $\text{Bi}_{10}\text{Tl}_{90}$ at 100°K and 296°K along the $[\zeta 00]L$ symmetry direction.

of a phonon, $W = \hbar\gamma$, can be expressed as (Brockhouse et al. 1961)

$$\gamma = \sum_{n=1}^N \Gamma_n (1 - \cos n\pi q/q_M) \quad (4.1)$$

where Γ_n are effectively the dissipative force constants between planes of atoms. The index n indicates the n th plane of atoms and the summation is carried out to a value $n=N$ beyond which Γ_n effectively vanishes. The solid lines shown in Fig. 4.11(a) show the best fits to expressions of the form of Eq. (4.1) with $N=1$ for the $[\zeta 00]T$ branch and $N=3$ for the $[\zeta 00]L$ branch.

Before concluding this section it may be relevant to mention that the anharmonic broadening in Pb was studied by Brockhouse et al. (1961) at 425°K and by Stedman et al. (1967a) at 300°K. A comparison of the widths along various symmetry directions between Pb and $Pb_{40}Tl_{60}$ at 300°K shows similar trends---the damping in lead being probably somewhat larger, in general. Since the damping of phonons is mainly governed by the cubic term in the potential energy and the thermal expansion also involves the cubic anharmonic term to the lowest order, it may not be unreasonable to argue that Pb and $Pb_{40}Tl_{60}$ should have similar thermal expansion coefficients. We discuss the measurements of thermal expansion of the alloys in the next section. It may be recalled here that the temperature dependent frequency shifts for certain modes show quite different trends in the two materials which, however, does not contradict the above discussion in any direct way.

TABLE 4.7(a)
Phonon frequencies in $\text{Bi}_{10}\text{Tl}_{90}$
along the $[\zeta 00]$ symmetry direction.

ζ	$\nu (10^{12} \text{ cps})$			
	Transverse		Longitudinal	
	100°K	296°K	100°K	296°K
0.20	0.440	0.420	0.770	0.735
0.30	0.635	0.605	1.115	1.080
0.40	0.820	0.770	1.430	1.390
0.50	0.995	0.930	1.720	1.655
0.60	1.155	1.095	1.945	1.880
0.70	1.280	1.210	2.105	2.040
0.80	1.355	1.295	2.240	2.190
0.90	1.415	1.355	2.390	2.330
1.00	1.420	1.360	2.440	2.410

For the purpose of calculating the frequency shifts, errors of 0.5-1% were assigned to the frequencies. It should be pointed out, however, that the absolute error for any particular measurement is considerably higher than this.

TABLE 4.7(b)
 Phonon widths (F.W.H.M.) at 296°K
 corrected for resolution, in $\text{Bi}_{10}\text{Tl}_{90}$ along the
 $[\zeta 00]$ symmetry directions

ζ	Phonon Widths (10^{12} cps)	
	Transverse	Longitudinal
0.20	0 \pm 0.05	0 \pm 0.05
0.30	0 \pm 0.06	0.05 \pm 0.05
0.40	0.08 \pm 0.05	0.10 \pm 0.05
0.50	0.13 \pm 0.04	0.16 \pm 0.05
0.60	0.13 \pm 0.05	0.18 \pm 0.06
0.70	0.10 \pm 0.05	0.22 \pm 0.06
0.80	0.13 \pm 0.05	0.23 \pm 0.05
0.90	0.11 \pm 0.06	0.16 \pm 0.05
1.00	{ 0.14 \pm 0.05	0.08 \pm 0.05
	{ 0.17 \pm 0.04	

The error in the natural width was obtained by changing the observed width of the neutron group by its error and repeating the deconvoluting procedure. Because of large errors, many of the widths are not significant by themselves, however, the over-all trend of any group of results may be expected to be significant.

E. Anharmonic Effects in Thermodynamic Properties

(i) Thermal Expansion of Bi-Pb-Tl Alloys (experimental)

Introduction

In a harmonic theory the equilibrium positions of the ions are those defined by the minimum of the potential energy, independent of temperature. However, the fact that solids exhibit thermal expansion implies that equilibrium positions are temperature dependent and this effect is related to anharmonic terms in the expansion of the potential energy with respect to the displacements of the atoms. Therefore, experimental information on thermal expansion in solids is useful in the investigation of anharmonic properties. In this section we describe experimental measurements of thermal expansion of Bi-Pb-Tl alloys over a temperature range of 100°K-400°K.

Experimental Details and Results

The characterization and lattice constant measurements at room temperature of the alloy single crystals by neutron diffraction is described in Appendix I. Expansion coefficients can be obtained by measuring lattice constants as a function of temperature. All the specimens were previously annealed. Because the large neutron beam penetrates almost the whole ingot, the effect arising from any quenching stress present on the surface layers may be expected to be negligible. Further most of the alloy crystals were fairly homogeneous in composition as can be seen from Table (A1.1).

The experiments were carried out at the McMaster triple axis spectrometer (Rowe 1965). Neutrons with incoming wavelength of 2.330 \AA were used throughout the experiment. A "perfect" Cu(220) analyzer ($2\theta_{\text{A}} \sim 132^\circ$) was employed with a mosaic spread of $8'$ (FWHM) to ensure high resolution in the scattered beam. Back angle reflection (400) off the specimens were measured to improve the sensitivity; the scattering angles were in the range of 140° - 150° . Effect on lattice constant arising from mislocating the crystal on the spectrometer table was investigated by deliberately displacing the specimen from the centre of rotation of the ψ -table. It was found that displacement along the scattering vector of the Bragg reflection plane has virtually no effect. In a direction perpendicular to the scattering vector a shift of $\frac{1}{2}$ " (diameter of the specimen ~ 1 ") amounted to a change of 0.0015 \AA in lattice constant. However, it should be noted that this effect does not contribute any appreciable error to the measurement of thermal expansion. The accuracy in measuring a lattice constant was estimated to be about one part in 10^4 .

Specimen single crystals were mounted in a cryostat and were aligned using neutron beam either with (100) or ($1\bar{1}0$) axis vertical. The crystals used have cylindrical geometry ($1-1\frac{1}{2}$ " in dia and $3\frac{1}{2}$ " long) with the angle between the cylindrical axis and the crystallographic axis varying from 0° to 20° . The alignment was probably good to within a few minutes of arc. All the specimen crystals were enclosed in tight fitting aluminum cans ($1/32$ " thickness) and

insulated heating elements were wrapped round the base of the can. Temperatures were recorded at two points across the length of the crystal using calibrated copper-constantan thermocouples screwed on to the aluminum can. Radiation shields were placed around the specimen to ensure thermal equilibrium with the temperature bath. For measurements below room temperature, liquid nitrogen and dry ice were used along with the heater for other intermediate temperatures. When the specimen is cooled the aluminum can enclosing it contracts less than does the specimen, thus resulting in poor thermal contact. For this reason, the specimen was allowed to cool for five to six hours before starting a low temperature run (liquid nitrogen or dry ice bath). Temperatures were measured probably to within an accuracy of 2-3°K. For the runs carried out at intermediate temperatures using heaters, temperature measurements were less accurate--temperatures recorded at two ends of the specimen indicated a gradient of ~6°K across the length of the crystal. These measurements are indicated by crosses in Fig. 4.13. In particular, for both the Bi-Tl alloys, namely Bi₁₀Tl₉₀ and Bi₂₀Tl₈₀ there were serious discordances for the measurements at intermediate temperatures and consequently they have been omitted from the plot. It may be noted that for the measurements made above room temperature good thermal contact between the aluminum can and the specimen was automatically insured as the coefficients of expansion of the alloys are about one and half times greater than the expansion coefficient of aluminum

Fig.4.13 shows a plot of lattice constants as a function of temperature for various alloys as well as for pure lead. It is seen that for lead, the present limited measurements agree with other more accurate measurements (interferometric measurements (Nix and McNair 1942) are shown from 85°K to 296°K and X-ray measurements (Stokes and Wilson 1941) from 296°K extending to higher temperatures) within limits of the experimental accuracy. This comparison provides a valuable and important check of the temperature scale as well as on the measurement of lattice constant. The lines drawn through the experimental points of the alloys represent a least square fit of the form $a(T) = a_0 + a_1T + a_2T^2$. The coefficients are tabulated in Table 4.8 along with values of lattice constants at a few selected temperatures. Since the measurements were confined to temperatures ranging from θ_D and above, a_0 probably gives a measure of the extrapolated lattice constant at 0°K for the harmonic lattice. It is seen that alloys have more or less similar thermal expansion coefficients which would probably imply (to some extent) similar anharmonic interactions (cubic term) too. However, for the $\text{Bi}_{20}\text{Pb}_{60}\text{Tl}_{20}$ alloy, the curvature of the fitted line is negative whereas for the rest of the alloys it is positive.

In addition to measuring thermal expansion there was some additional interest with the Bi-Tl alloys. According to the phase diagram for $\text{Bi}_{10}\text{Tl}_{90}$ and $\text{Bi}_{20}\text{Tl}_{80}$ there is some indication for the existence of a new phase boundary above 55°C and ~85°C respectively (Hansen 1958). Search was

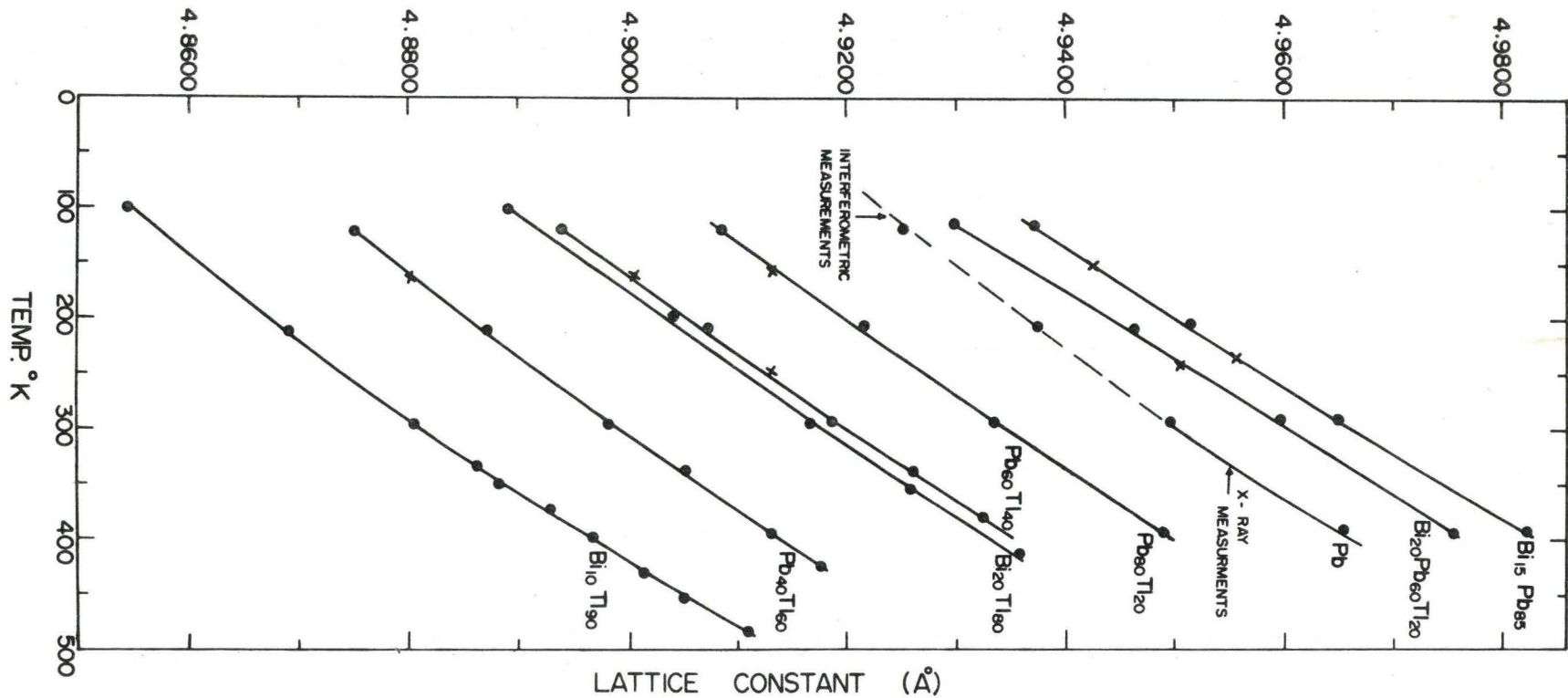


Fig. 4.13

Lattice constants measured as a function of temperature for the Bi-Pb-Tl alloys. The size of the points is a fair measure of the experimental accuracy. The crosses have somewhat larger errors than the circles. For the alloys, the solid lines represent least square fits to the experimental points as explained in the text. For Pb, the interferometric (Nix and McNair 1942) and X-ray (Stokes and Wilson 1941) measurements are shown.

TABLE 4.8

Materials	Temp°K (+2°)	Lattice Const. a (Å°) (+0.0005 Å°)	a ₀	a ₁ ⁴ (x10 ⁴)	a ₂ ⁸ (x10 ⁸)	Linear Expansion coefficient (at 300°K) (10 ⁻⁶ deg ⁻¹)*
Pb	395	4.9656 (4.9651) ¹				
	296	4.9499 (4.9498) ¹	4.9108	1.14	6.1	30.5 (28.8) ⁺
	121	4.9255 (4.9260) ²				
Bi ₂₀ Pb ₆₀ Tl ₂₀	398	4.9757				
	296	4.9597	4.9100	1.74	-2.3	32.1
	117	4.9300				
Bi ₁₅ Pb ₈₅	398	4.9824				
	296	4.9651	4.9204	1.40 ₄	3.8	32.9
	118	4.9374				
Pb ₈₀ Tl ₂₀	396	4.9491				
	296	4.9336	4.8919	1.36	2.0	30.1
	122	4.9087				

* The coefficients of expansion were calculated from the parameters a₀, a₁ and a₂ which were obtained by fitting to the measured lattice constants. The errors in the expansion coefficients are probably 6% or slightly more.

+ Interferometric measurements (Nix and McNair 1942).

Table 4.8 cont'd

	Temp°K (+2°)	Lattice Const. a (A°) (+0.0005 A°)	a ₀	a ₁ ¹⁴ (x10 ⁴)	a ₂ ⁸ (x10 ⁸)	Linear Expansion coefficient (at 300°K) (10 ⁻⁶ deg ⁻¹)
Pb ₆₀ Tl ₄₀	382	4.9326				
	295	4.9189	4.8781	1.30	3.1	29.6
	120	4.8941				
Pb ₄₀ Tl ₆₀	396	4.9133				
	296	4.8982	4.8606	1.15	4.6	29.1
	122	4.8752				
Bi ₂₀ Tl ₈₀	417	4.9358				
	296	4.9169	4.8760	1.31	2.8	30
	101	4.8893				
Bi ₁₀ Tl ₉₀	430	4.9015				
	296	4.8807	4.8438	1.03 ₃	7.2	30
	100	4.8547				

1. Interpolated from X-ray measurements (Stokes and Wilson 1941).

2. Interpolated from interferometric measurements (Nix and McNair 1942).

Pb was taken as standard; a=4.9499 A° at 296°K (Pearson 1958). a₀, a₁ and a₂ are the coefficients of the least square fit $a(T)=a_0+a_1T+a_2T^2$ to the experimental points.

for any anomalous change in lattice constant above and below the transition temperature with negative result.

(ii) Calculation of thermodynamic properties

in Pb₄₀Tl₆₀

Thermal Expansion

We found in Section C that for Pb₄₀Tl₆₀, since the electron-phonon interaction is not too strong, a simple pseudopotential calculation of the phonon frequencies gave reasonably good results. Therefore, it may be of interest to calculate anharmonic properties using this pseudopotential and compare them with experimental results. We describe below the calculation of thermal expansion.

The quasiharmonic lattice dynamical contribution to thermal expansion can be written as (Eq. 2.15):

$$\frac{\beta_0 v_0}{3k\chi_T} = \frac{1}{3N} \sum_{\mathbf{qj}} \gamma_j(\mathbf{q}) (h\nu/kT)^2 \bar{n}_{\mathbf{qj}} (\bar{n}_{\mathbf{qj}} + \frac{1}{2}) \quad (4.2)$$

All the quantities appearing in the above equation have been defined earlier in Chapter II(D)--the subscript T on χ implies isothermal compressibility and β_0 is the volume expansion coefficient corrected thermodynamically to a fixed volume v_0 . The phonon frequencies were calculated within the irreducible volume of the Brillouin zone on a uniform mesh of \mathbf{q} -points using the pseudopotential fitted to the dispersion curves at 100°K (section C). Proper weights were assigned to the surface points. The Gruniesen parameters, $\gamma_j(\mathbf{q}) = (\partial \ln \nu_j(\mathbf{q}) / \partial \ln v)$, were found by calculating the frequencies as a function of volume and determining the limiting slope.

The comparison of the calculation with the measured quantity is shown in Fig. 4.14. The experimental value of the coefficient of expansion β was determined from a least square fit to the lattice constants measured as a function of temperature described in the previous section. It was further necessary to correct the measured (zero pressure) thermal expansion coefficient $\beta(v, T)$ to a fixed volume coefficient $\beta(v_0, T)$ (Barron et al. 1964). This was done by using the following thermodynamic relation (Wallace 1968b)

$$\beta_0 \equiv \beta(v_0, T) = \beta(v, T) - \left(\frac{v-v_0}{v_0}\right) \left(\frac{d \ln \chi_T}{dT}\right)$$

The adiabatic compressibility χ_s was determined from the experimental data on elastic constants (0-300°K) (Shepard and Smith 1967) using the following expression

$$\frac{1}{\chi_s} = \frac{1}{3} (C_{11} + 2C_{12})$$

The isothermal compressibility was found from the relation

$$\frac{\chi_T}{\chi_s} = 1 + \frac{\beta^2 T v}{\chi_s C_p}$$

where C_p is the heat capacity. (The calculation of C_p is described later.)

Fig. (4.14) shows a discrepancy of about 10% between the theory and the experiment. This could be attributed to the neglect of the explicit anharmonic free energy (see, for example, Cowley 1968) and the electronic contribution. (The latter contribution is, however, expected to be negligible except at very low temperatures.)

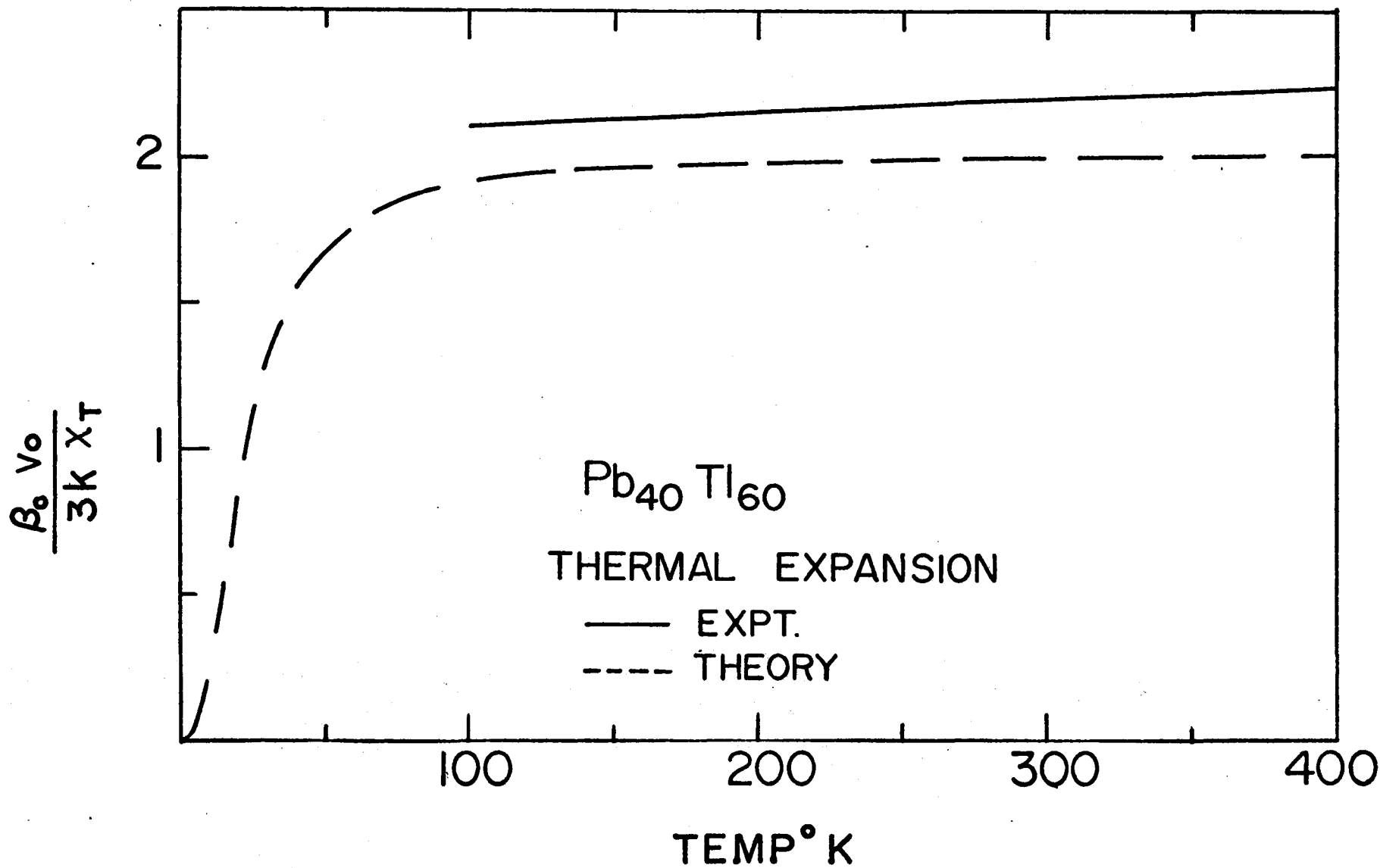


Fig. 4.14

Calculated (dashed line) and measured (solid line) curves of thermal expansion coefficient in the form of $(\beta_0 \Omega_0 / 3kX)$ at fixed volume, for $\text{Pb}_{40}\text{Tl}_{60}$.

Frequency distribution function and heat capacity

From the measurement of the phonon dispersion curves along symmetry directions in $\text{Pb}_{40}\text{Tl}_{60}$ at 100°K and 296°K , it was found that the frequency shifts in different modes were rather similar (Section C). This behaviour may be expected to hold reasonably well for the off-symmetry modes also. In Fig. 4.15, we show the frequency distribution functions of $\text{Pb}_{40}\text{Tl}_{60}$ at 100°K and 296°K (model calculation using an eight nearest neighbour fit to the dispersion curves measured along the four major symmetry directions). These distributions should be accurate*enough to use in calculating lattice specific heats since the force constant model can reproduce the phonon frequencies along both symmetry and non-symmetry directions to within 2% of the experimental results (Ng and Brockhouse 1968).

We next proceed to calculate the total lattice specific heat (harmonic + anharmonic) of $\text{Pb}_{40}\text{Tl}_{60}$ at constant pressure (essentially zero pressure) using the method outlined in Chapter II(D). The reference temperature T_0 was chosen as 100°K . From the measured phonon frequencies at 100°K and 296°K (Table 4.6), the frequency ratio defined with respect to the reference temperature T_0 was found to be

$$G(296^\circ\text{K}) = \left\langle \frac{\nu(296^\circ\text{K})}{\nu(100^\circ\text{K})} \right\rangle = 0.973 \pm 0.003$$

* The sharp singularities in the computed frequency spectra are artificial to some extent for a disordered alloy, like $\text{Pb}_{40}\text{Tl}_{60}$. See section G for a discussion of the effect of the phonon life time on the singularities.

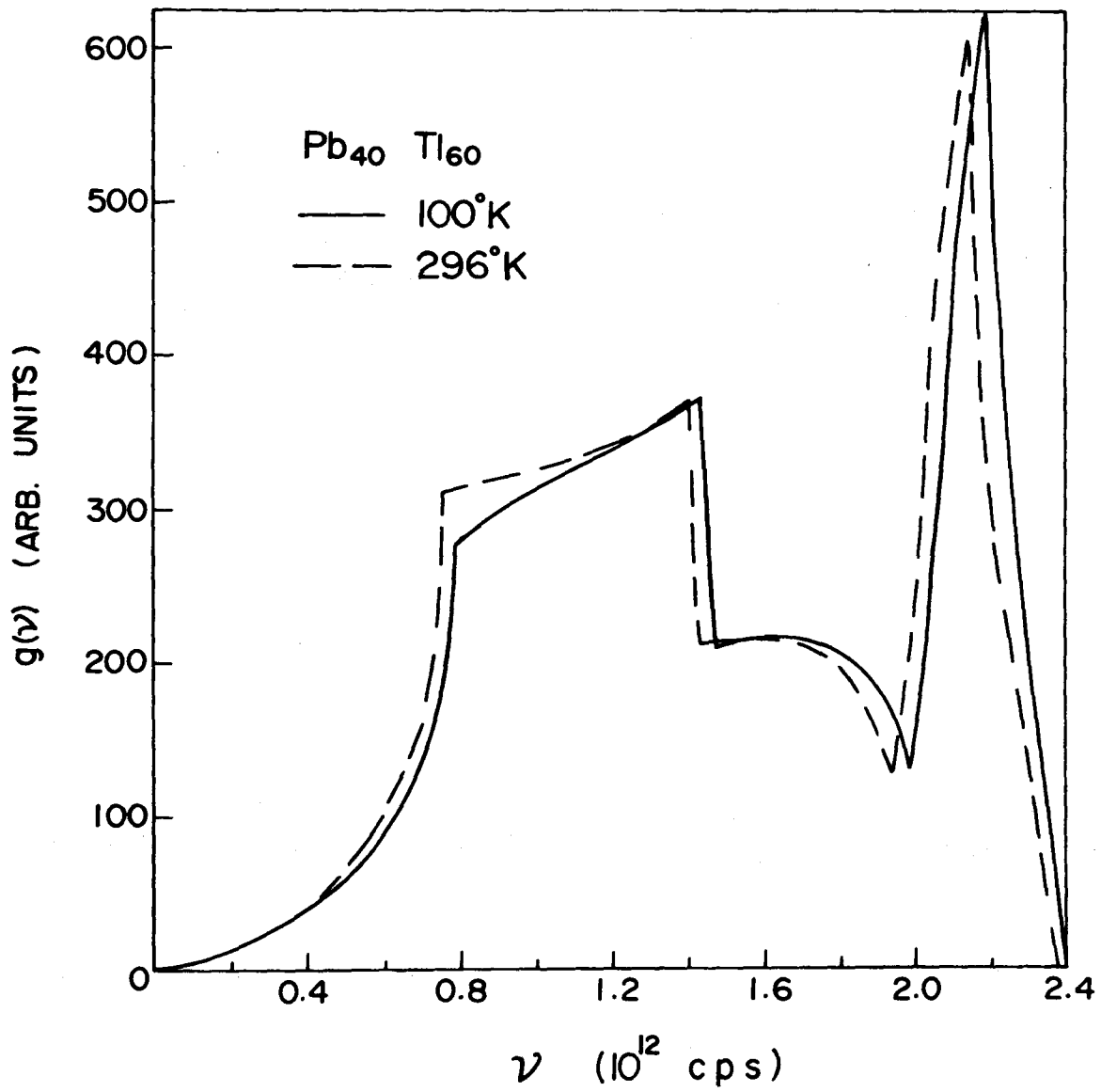


Fig. 4.15

Frequency distribution functions of $\text{Pb}_{40}\text{Tl}_{60}$ at 100°K and 296°K , computed using an eight-neighbour force constant model. The two distributions are normalized to the same area.

Since, for $T > \theta_D$, the shift of the phonon frequency is expected to be a linear function of temperature (Leibfried and Ludwig 1961) we make the assumption that $(dG(T)/dT)$ is a constant above 100°K ($\sim \theta_D$) and therefore $G(T)$ at any temperature above T_0 is readily obtained from $G(296^\circ\text{K})$. For temperatures less than 100°K , dG/dT is temperature dependent and tends to zero near 0°K . dG/dT may be estimated from the known temperature variation of the elastic constants assuming that $(d \ln \nu / dT) \sim \frac{1}{2} (d \ln C / dT)$ where C is an appropriate elastic constant. From the experimental elastic constants (Shepard and Smith 1967), $(d \ln C / dT)$ was evaluated in the symmetry direction $[\zeta 0 0]$, $[\zeta \zeta 0]$ and $[\zeta \zeta \zeta]$ for all the acoustic branches, as a function of temperature in the range $0-100^\circ\text{K}$. A simple average of $(d \ln C / dT)$ over all the above branches was used to evaluate $G(T)$ and dG/dT . Finally, the heat capacity was computed from Eq. (2.20). Fig. 4.16 shows the results of the calculation. The harmonic specific heat is calculated by using an effective frequency distribution corresponding to 0°K and assuming that the normal mode frequencies are temperature independent. No calorimetric measurements of the heat capacity for Pb-Tl alloys are available. Therefore, we have taken the experimental heat capacities of Pb and Tl from the literature (Hultgren et al. 1963) and added them in proper concentrations; these

are shown as filled circles in Fig. 4.16 for comparison.* If we subtract the electronic specific heat contribution (Calculated in the free electron model) from the experimental points the agreement with the calculated curve (the solid line in Fig. 4.16) will be excellent. However, the above method of obtaining the heat capacity of the alloy by adding the heat capacities of the constituent elements is admittedly very crude and no physical significance can be attached to the agreement obtained.

* According to Neumann-Kopp's rule, the heat capacity of an alloy may be calculated additively from the heat capacities of the components. This rule is obeyed to within +3% for various intermetallic compounds and alloys (Smithe I 1962).

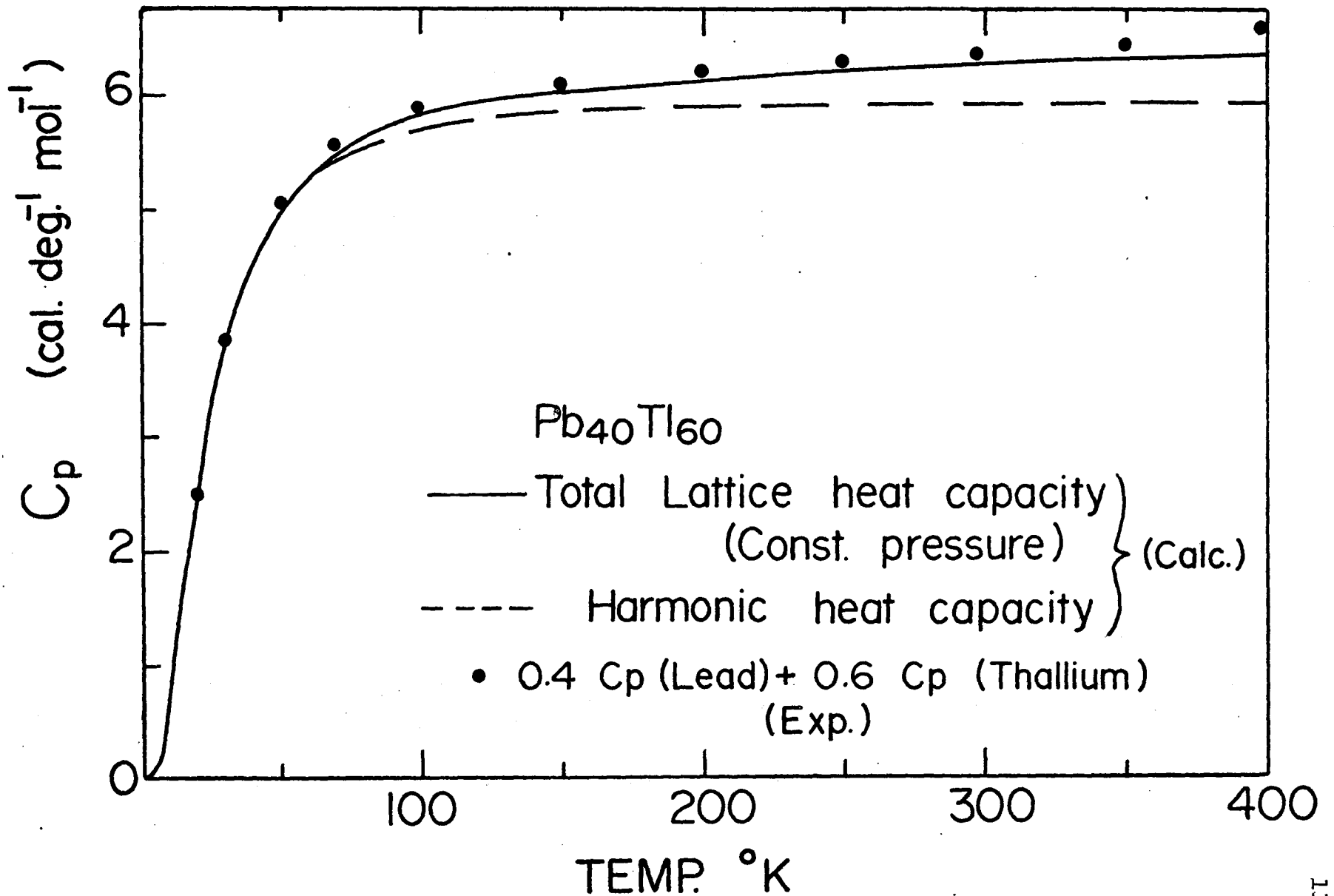


Fig. 4.16

The solid line represents the calculated lattice specific heat of $Pb_{40}Tl_{60}$ at constant pressure including the anharmonic contribution. The points were obtained by adding the experimental heat capacities of Pb and Tl in the ratios as indicated in the figure.

F. Kohn Anomaly and Electron-phonon Interaction in Bi-Pb-Tl Alloys

(i) Kohn Anomaly and Fermi Surface in Pb-Tl alloys

Introduction

It was first pointed out by Kohn (1959) that the interaction of lattice vibrations with the conduction electrons in a metal should cause anomalies in the phonon spectra. This was first experimentally demonstrated for lead by Brockhouse et al. (1961). Kohn anomalies have subsequently been seen in the transition metals of columns V and VI of the periodic table (Woods and his collaborators 1965; Walker and Egelstaff 1969), aluminum (Stedman and Nilsson 1965), zinc (Iyengar et al. 1968), Nb-Mo alloys (Powell, Martel and Woods 1968) and Bi-Pb-Tl alloys (Ng and Brockhouse 1967, 1968). It is interesting to note that all the above materials are superconductors* We will return to this point later.

Although the neutron method is perhaps less accurate than the conventional electrodynamic methods for studying Fermi surfaces, it has the advantage that it does not require very low temperatures or particularly pure samples. In fact it is the only tool available for investigating the Fermi surface in disordered alloys. This was mainly the motivation for undertaking a somewhat detailed study of the Fermi surface in $\text{Pb}_{80}\text{Tl}_{20}$ which will be described in this section

Origin of the Anomalies

The Kohn effect results from an abrupt change in the ability of the electrons to screen the ionic motions. When the wavevector transfer exceeds an extremal distance across the

* The Kohn anomalies have been recently observed in Pd, a material which is not a superconductor (Miiller 1969).

Fermi surface, the electrons can not be scattered with conservation of energy as the phonon energy is negligible compared with the typical Fermi energy in metals. Therefore, sudden variation of transition density occurs for pair of points where the tangent planes are parallel. For a diametral transition one has the relation

$$2k_F = |\underline{G} \pm \underline{q}|$$

where k_F is the Fermi radius.

Size of the Anomalies

For diametral transitions, with the assumption of a spherical Fermi surface, the anomalies will be mainly governed by the magnitude of the electron-phonon matrix element at $Q=2k_F$. However, even for a nearly free electron metal the Fermi surface departs appreciably from the appropriate spherical shape near a Bragg reflection plane. As a result, the detailed dependence of the electron-phonon interaction, on the magnitude of the momentum transfer corresponding to a particular transition (diametral or non-diametral), plays an important role in determining the size of the anomaly. The strength of the anomaly also depends on (i) the multiplicity of the transitions (eg. some particular transition across the Fermi surface may be produced from several reciprocal lattice points) (ii) phonon polarization $\xi_j(\underline{q})$ and the momentum transfer Q through the factor $(Q \cdot \xi_j(\underline{q}))^2$ and (iii) the density of states on the Fermi surface and the local curvature.

Taylor (1963) suggested that the relative sizes of the effects in different materials (neglecting Fermi surface shape effects) should be governed by the factor $F=Z^3 \rho / M \sigma T$

where the various quantities are defined as: Z valence; ρ density; M atomic weight; σ electrical conductivity; T absolute temperature. σ appears in the expression because nearly the same electron-phonon matrix element as used in phonon frequency, determines the resistivity. This reasoning also indicates why superconductors which display strong electron-phonon coupling are likely candidates for observing the Kohn effect. We give below the value of F for a few substances (Taken from a table given by Taylor (1963) and Sharp (1969)), in which Kohn anomalies have been studied.

	Cu	Zn	Al	Pb	Nb
$F \times 10^8$ (CGS units)	0.08	1.83	2.63	25.4	60.8

Though these values should not be taken too literally, they nevertheless give an idea of the relative magnitudes of the Kohn effect.

In Chapter II-D, it was found that the bare-ion frequencies are renormalized when the electron response is taken into account. As a consequence, anomalies in the phonon dispersion curves may arise from singularities present in the dielectric function $\epsilon(Q)$. This can be seen immediately by writing the contribution of the electron-phonon interaction to the dynamical matrix $D_{\alpha\beta}(Q)$:

$$\frac{1}{M} \sum_{\underline{G}} (\underline{q} + \underline{G})_{\alpha} (\underline{q} + \underline{G})_{\beta} U_e(\underline{q} + \underline{G})$$

Now, $U_e(Q)$ contains $\epsilon(Q)$ (Eq. (2.37)). For free electrons with spherical Fermi surface $\epsilon(Q)$ is given by Eq. (2.29).

We see that $\epsilon(Q)$ has a logarithmic singularity at $Q = 2k_F$.

The first derivative near $2k_F$ is given by

$$\nabla_Q \epsilon \sim \frac{me^2}{4\pi\hbar^2 k_F^2} \ln \left| 1 - \frac{Q}{2k_F} \right|$$

and

$$\nabla_Q \omega^2(Q) \Big|_{Q \sim 2k_F} \propto [\nabla_Q \epsilon(Q) / \epsilon^2(Q)]_{Q \sim 2k_F}$$

Now, $\nabla_Q \epsilon(Q)$ is infinitely negative ($\ln 0 = -\infty$) at $Q = 2k_F$.

Furthermore $\epsilon(Q)$ is positive for $Q = 2k_F$: therefore as we follow the phonon wavevector path from the inside to the outside of the sphere $Q = 2k_F$, the frequency increases rapidly. This is called an upward anomaly (Brockhouse et al. 1961; Woll and Kohn 1962). If we cross from outside to the inside, the frequency drops infinitely rapidly--a downward anomaly. However, it should be noted that $\epsilon(Q)$ is well behaved and if one plots $\epsilon(Q)$ as a function of Q one finds only a slight inflection in the neighborhood of $Q = 2k_F$. The remarkable smallness of a logarithmic singularity is rather striking.

For evaluating the magnitudes of Kohn anomalies, one needs an accurate knowledge of the electron-phonon matrix element. Stedman et al. (1967c) estimated the sizes and senses of Kohn anomalies in Pb for a nearly spherical surface. It was found that the experimentally observed heights of the anomalies were higher by a factor of seven even after suitably adjusting the value of electron-phonon matrix element. This discrepancy is attributed to the departure of the Fermi surface from a spherical shape which arises from the interaction of the electrons with the periodic ionic potential in the

crystal--the distortion of the Fermi surface being greatest near a Bragg plane.

Afansev and Kagan (1963) have shown that for a circular cylinder of radius k_F

$$\epsilon(Q) = 1 + \frac{me^2}{\pi k_F h^2 \eta^2} [1 - (1-\eta^2)^{1/2}]$$

The cylindrical Fermi surface therefore, has a square-root singularity in $\nabla_Q \omega^2$ and is much more pronounced than the logarithmic singularity for the spherical case.

Kaganov and Semenenko (1966) have considered parabolic, elliptic and hyperbolic surfaces. For a planar Fermi surface, the singularity is like $|Q-2k_F|^{-1}$, thus very sharp.*

Experimental Observation of Anomalies

Kohn anomalies were seen in Pb-Tl alloys by Ng and Brockhouse (1967, 1968) along the symmetry directions corresponding to those observed for Pb in the $[\zeta\zeta 0]L$ and $[\zeta\zeta\zeta]L$ branches. They found that their results correlate well with the Fermi surfaces deduced from the band structure of Pb determined by Anderson and Gold, using the rigid band model.

In the present work, measurements have been extended to another Pb-Tl alloy-- $Pb_{33}Tl_{67}$. The results are tabulated below along with the results for the other alloys, for the sake of completeness, taken from the paper by Ng and Brockhouse (1968).

*Near a singularity, in addition to an anomalous change in phonon frequency, damping of phonons may also arise from the electron-phonon interaction. This has been observed in Pd (Miiller 1969).

Fermi Surface Diameters (units $2\pi/a$)

	Face diameter	Body diameter	Free electron diameter
Pb	2.38 \pm 0.02	2.50 \pm 0.02	2.48
Pb ₈₀ Tl ₂₀	2.28	2.44	2.44
Pb ₆₀ Tl ₄₀	2.21	2.39	2.40
Pb ₄₀ Tl ₆₀	2.16	2.34	2.34
Pb ₃₃ Tl ₆₇	2.15	2.34	2.336

It is seen that for Pb₃₃Tl₆₇ along the face diagonal (110) the Fermi radius is $\sim 1.075(2\pi/a)$ and is smaller than the free electron radius by about 8%. Since the third zone starts from the point K ($\Gamma K \sim 1.06(2\pi/a)$) along this direction, it follows that it is virtually empty in this alloy.

A comparatively more elaborate study of the Fermi surface was carried out for Pb₈₀Tl₂₀. Fig. 4.17 shows a section through the Fermi surface of Pb₈₀Tl₂₀ in the (1 $\bar{1}$ 0) plane deduced from the Fermi surface of Pb determined by Anderson and Gold (1965), using the rigid band model. Filled circles indicate points obtained from the neutron scattering experiments discussed below. We also show in Fig. 4.17 the (1 $\bar{1}$ 0) plane of the reciprocal lattice. The directions along which measurements were carried out are labelled by capital letters. Results along the symmetry direction ΓL and ΓK were obtained earlier by Ng (1967). Phonon dispersion relations along AB and PQ are shown in Figs. 4.18 & 4.19. For locating the anomalies, a curve of $(\Delta v/\Delta \zeta)$ versus ζ was drawn. The values of the slope were taken from pairs of

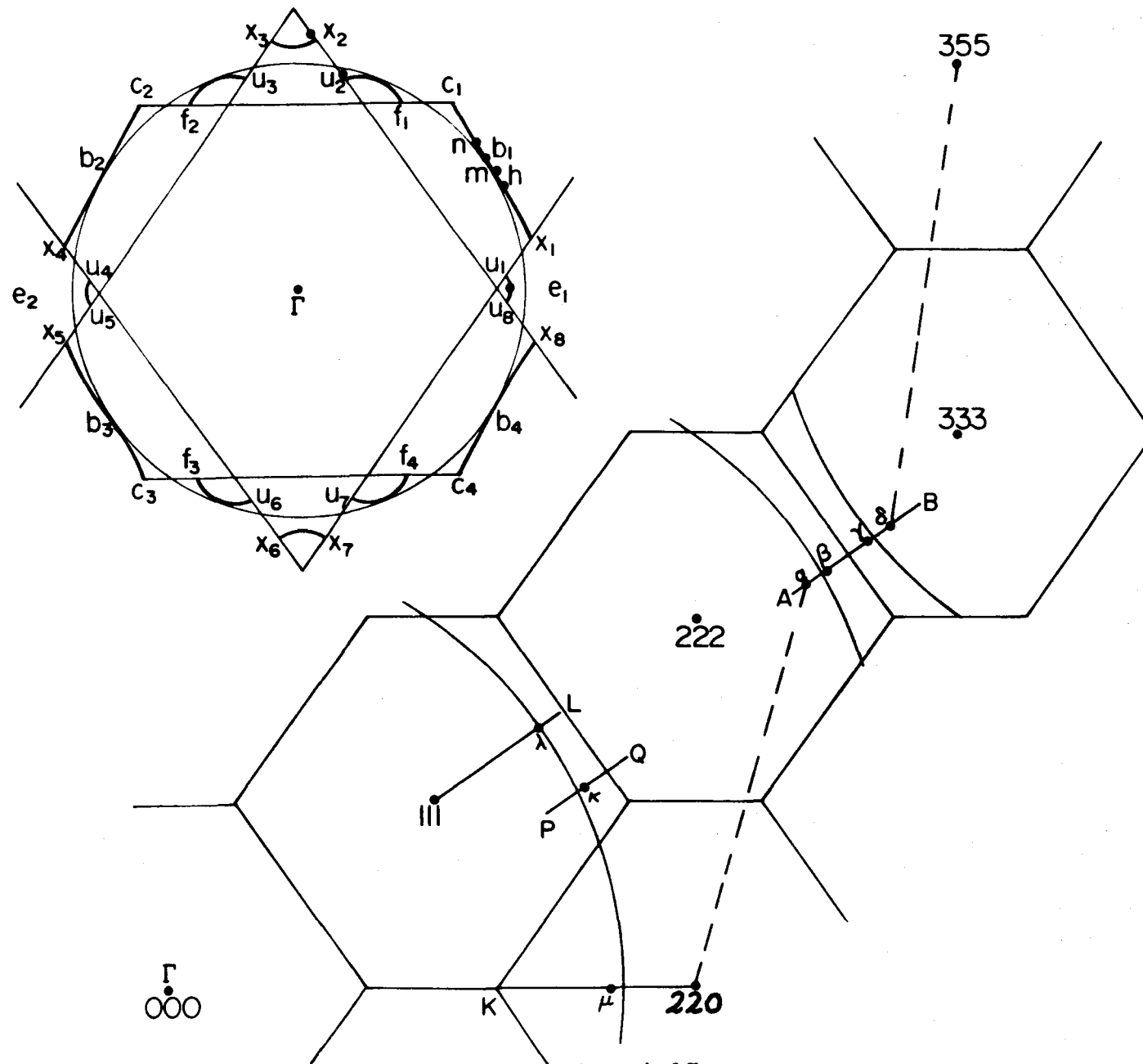


Fig. 4.17

The $(1\bar{1}0)$ plane of the reciprocal lattice: the filled circles labelled by small greek letters indicate positions of the observed anomalies in $Pb_{80}Tl_{20}$ at $100^\circ K$. Arcs of radii $Q=2k_F$ have also been drawn from various reciprocal lattice points. The anomalies are remapped (as filled circles) on to the Fermi surface of $Pb_{80}Tl_{20}$ shown in the $(1\bar{1}0)$ plane (bold line). The section of the free electron Fermi sphere is indicated by a light line.

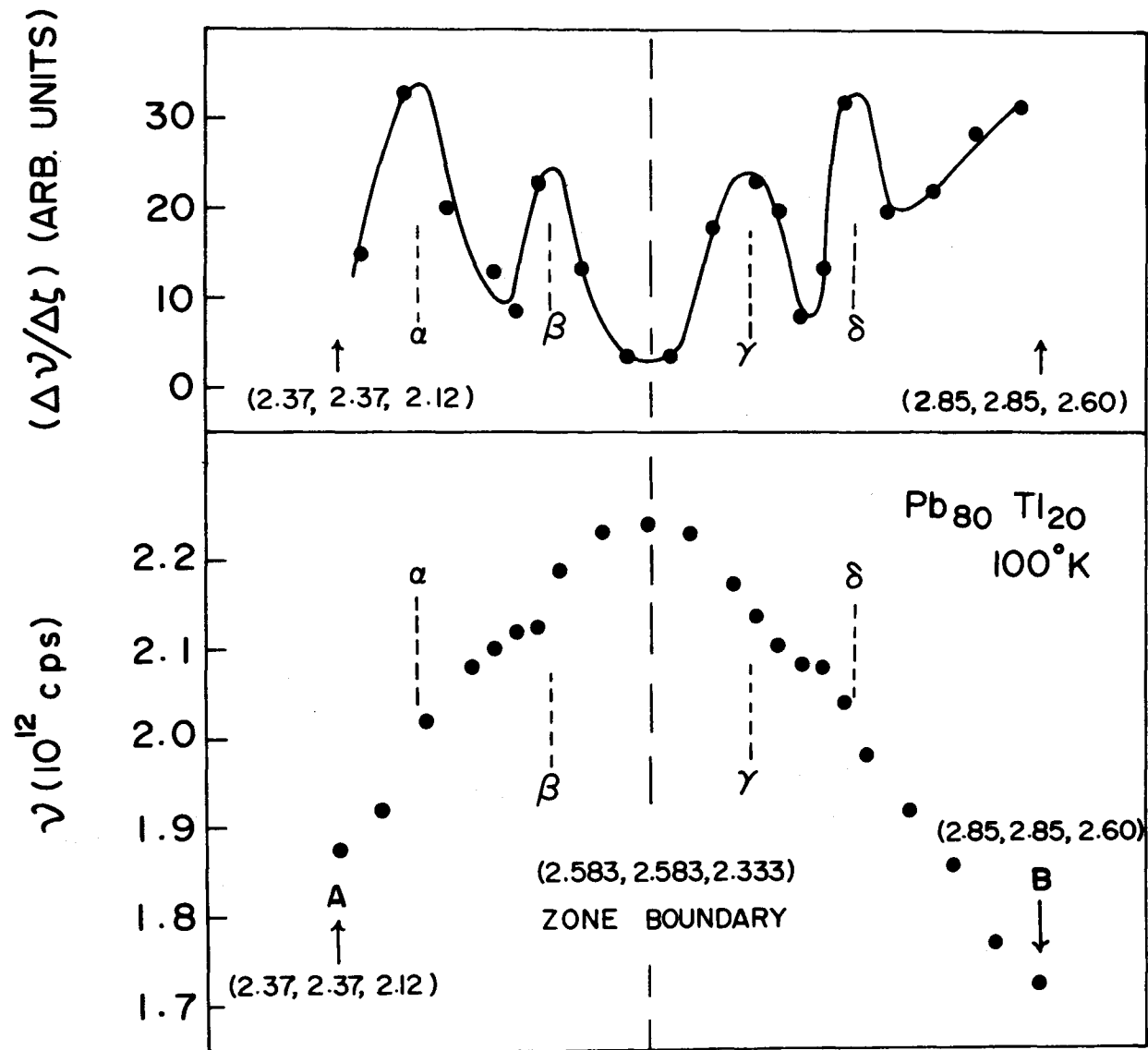


Fig. 4.18

Phonon dispersion relation and $\text{grad}_q v$ along AB in the reciprocal space (see Fig. 4.17).

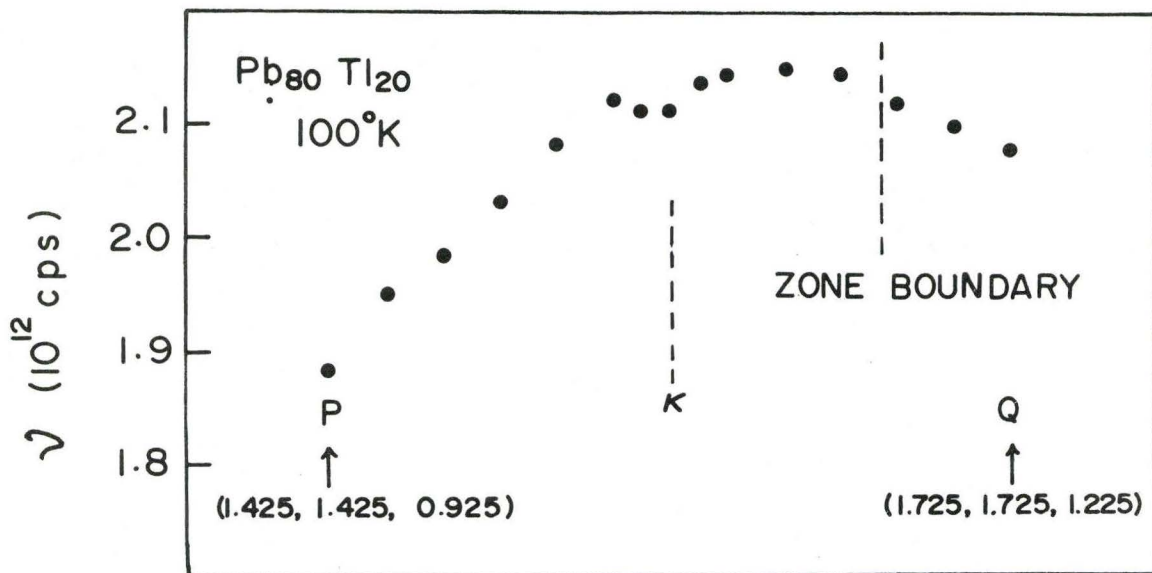


Fig. 4.19. Observation of Kohn anomaly along an off-symmetry direction in $\text{Pb}_{80}\text{Tl}_{20}$

adjacent measurements. An example of such a curve is also shown for the direction AB in Fig. 4.18. Even though the errors get magnified in a plot of $(\Delta\nu/\Delta\zeta)$, it should be noted that the errors in the curve are not ordinarily mutually independent errors. The anomalies as observed in the phonon dispersion relations measured along various directions in the reciprocal space are labelled by Greek letters.

Mapping of the anomalies μ and λ on to the Fermi surface has been discussed earlier by Brockhouse et al. (1962) in connection with their work on Pb. They arise from transitions of the type e_1e_2 and b_1b_3 respectively. We consider next the anomaly β observed along the non-symmetry direction AB at $\frac{a}{2\pi} \underline{Q} = (2.514, 2.514, 2.264)$. This corresponds to an extremal dimension* of the Fermi surface of $|\underline{Q} - \underline{G}_{111}| = \frac{2\pi}{a} (2.489)$ and is defined with respect to the (111) direction by the angle

* A general figure for the uncertainty in these dimensions for our results is ± 0.015 .

$$\alpha = \cos^{-1}((\underline{Q} \cdot \underline{G}_{111}) / (|\underline{Q}| \cdot |\underline{G}_{111}|)) = 4.6^\circ.$$

The points γ and κ can be similarly mapped by referring them with respect to the lattice point (444) and (000) respectively. The anomaly marked α arises from the diametral transitions in the neighborhood of u_2u_6 referred to the lattice point (220) (Fig. 4.17). Similarly, one can relate the anomaly δ to non-diametral transitions near x_2u_6 (or u_2x_6) referred to the lattice point (335) (Fig. 4.17). The transition ux differs from the ones previously considered in the sense that it corresponds to a non-diametral transition between two non-equivalent points u and x on the Fermi surface which belong to the third and the second energy band respectively. It was noted by Taylor (1963) that states that are actually on the zone boundary possess definite symmetry characteristics and consequently transitions between states that are on the same zone boundary but in different bands will be inhibited. In the present case u and x are situated on Bragg planes and they belong to different bands but they are both general points (unlike U or X) on Bragg planes and therefore transitions are not expected to be forbidden. Further, the phonons may have the proper symmetry for compatibility. We also note that the anomalies arising from the transitions uu and ux considered before are quite strong and this is probably due to the high density of states of the electrons near a Bragg plane. The fact that the density of states play an important role in determining the magnitude of the Kohn kinks was pointed out earlier by Brockhouse *et al.* (1962). As noted

by Stedman et al. (1967c), Taylor's formulas include this effect through the term $|v_a - v_b|^{-1}$ where v_a and v_b are the electron velocities at the points a and b. As the component of the electron velocity perpendicular to the Bragg plane has to be small, it follows that $|v_a - v_b|^{-1}$ may be quite large near a Bragg plane.

Transitions of the type cc, cf and ff may be expected to give rise to structures in the $[\zeta\zeta 0]L$ branch, beyond $\frac{aq}{2\pi} = 1.24$. Unfortunately, detailed measurements are not available in that region. However, we note that the marked depression of this branch near zone boundary observed experimentally for lead (Brockhouse et al. 1962, Stedman et al. 1967a) and lead rich alloys (Ng and Brockhouse, 1968), may be interpreted in terms of these transitions as the third zone of the Fermi surface plays an important role.

On the basis of the results described above, it is seen that for $Pb_{80}Tl_{20}$ there is fair agreement between the Fermi surface deduced from the rigid band model and that obtained from the present neutron scattering experiments.

Smearing of the Kohn Anomalies

A finite temperature as well as various scattering mechanisms of the electrons lead to a smoothing out of the singularities.

Kaganov and Semenenko (1966) have considered spreading of the anomaly, Δ , arising from finite temperature effects. For our purpose we can express their result in the form $\Delta = 2k_F(T/T_F)$ where T_F is the Fermi temperature of the conduction electrons. Since $T_F \sim 10^5$ °K we find that this will

have a negligible effect for cases of interest.

The role of scattering leads to the result that the minimum value which the parameter Δ can take is \hbar/ℓ where ℓ is the smallest of the mean free paths of the electrons or phonons with wavevector $Q=2k_F$. In a pure metal at 0°K , $\ell \rightarrow \infty$ consequently singularity will be ideally sharp. At a finite temperature electron mean path will be limited by electron-phonon scattering. For lead at 100°K , the broadening can be estimated from the observed electrical resistivity to be $\sim (0.007) \frac{2\pi}{a}$ which is still quite small. At higher temperatures, one must also consider the phonon-phonon interaction which will limit the phonon mean free path. Buyers and Cowley (1969) find that the temperature dependence is given by the well known Debye-Waller factor. Fig. 4.20 shows the Kohn kinks as observed in Pb along the $[\zeta\zeta\zeta]L$ branch at 100°K and 296°K . There is an indication that the anomaly gets weaker with increasing temperature in accordance with the preceding discussion.

In a disordered alloy mean free path of the electrons will be further modified due to lack of perfect periodicity, thus spreading out the singularity (Ng and Brockhouse 1968). From deGennes's work (1964) we see that for $2\ell k_F > 20$, one still has the Kohn singularity at $Q=2k_F$ while for $2\ell k_F < 20$ the singularity tends to wash out. From the available resistivity measurements at room temperature we can set a lower limit of $2\ell k_F \sim 40$ for the Pb-Tl alloys and therefore the anomalies should be observable. This qualitative argument

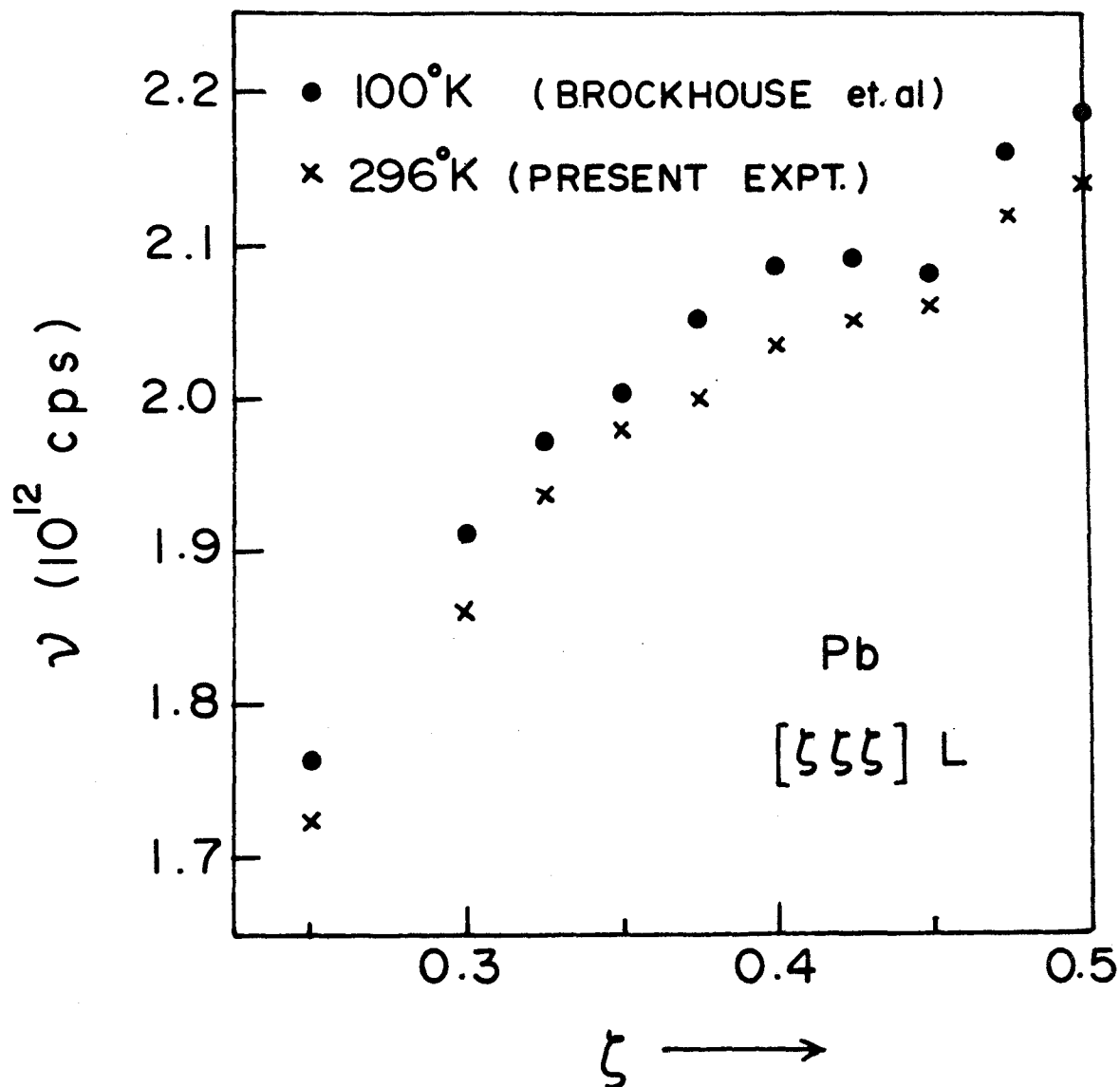


Fig. 4.20. Temperature dependence of Kohn anomaly in Pb.

is consistent with the experimental findings of Ng and Brockhouse (1968). However, it should be noted that the relative strengths of the anomalies in the different alloys are directly related to the strengths of the electron-phonon matrix element at $Q=2k_F$. In the pseudopotential theory it appears that it decreases monotonically as electron concentration is decreased in going from Pb to $Pb_{40}Tl_{60}$ --the reduction being roughly by a factor of two at $Q=2k_F$.

(ii) Comparative Study of the electron-phonon interaction in Bi-Pb-Tl alloys.

In the preceding section, we mentioned the fact that the Kohn anomaly, which is a manifestation of the electron-phonon interaction in lattice vibrations, grows weaker in Bi-Pb-Tl alloys with decreasing electron concentration (Ng and Brockhouse 1968). The superconducting transition temperature T_c and the superconducting gap edge Δ_0 have been measured by Claeson (1966) and Dynes et al. (1969) respectively. Their results show that T_c and Δ_0 decrease with electron concentration indicating again a similar trend in the electron-phonon coupling strength.

It was mentioned in Chapter II(D) that for metals with small non-overlapping cores, the frequencies of lattice vibrations can be separated into two parts

$$v^2 = v_c^2 - v_e^2 \quad (4.2)$$

where v_c^2 arises from the Coulomb interaction between the bare ions with a uniform non-responsive conduction electron background and v_e^2 is the contribution from the indirect interaction via the electrons due to their response to the ion motion. To compare the observed frequencies in Bi-Pb-Tl alloys which have different valences and slightly different mass, we may express the observed frequencies in terms of the "plasma frequency" $v_p = (1/2\pi)(4\pi Z^2 e^2 / M\Omega_0)^{1/2}$. In Fig. 4.21, the second moments of the frequency distribution function (the average of v^2 over the whole frequency distribution) in units of plasma frequency are plotted as a function of the average

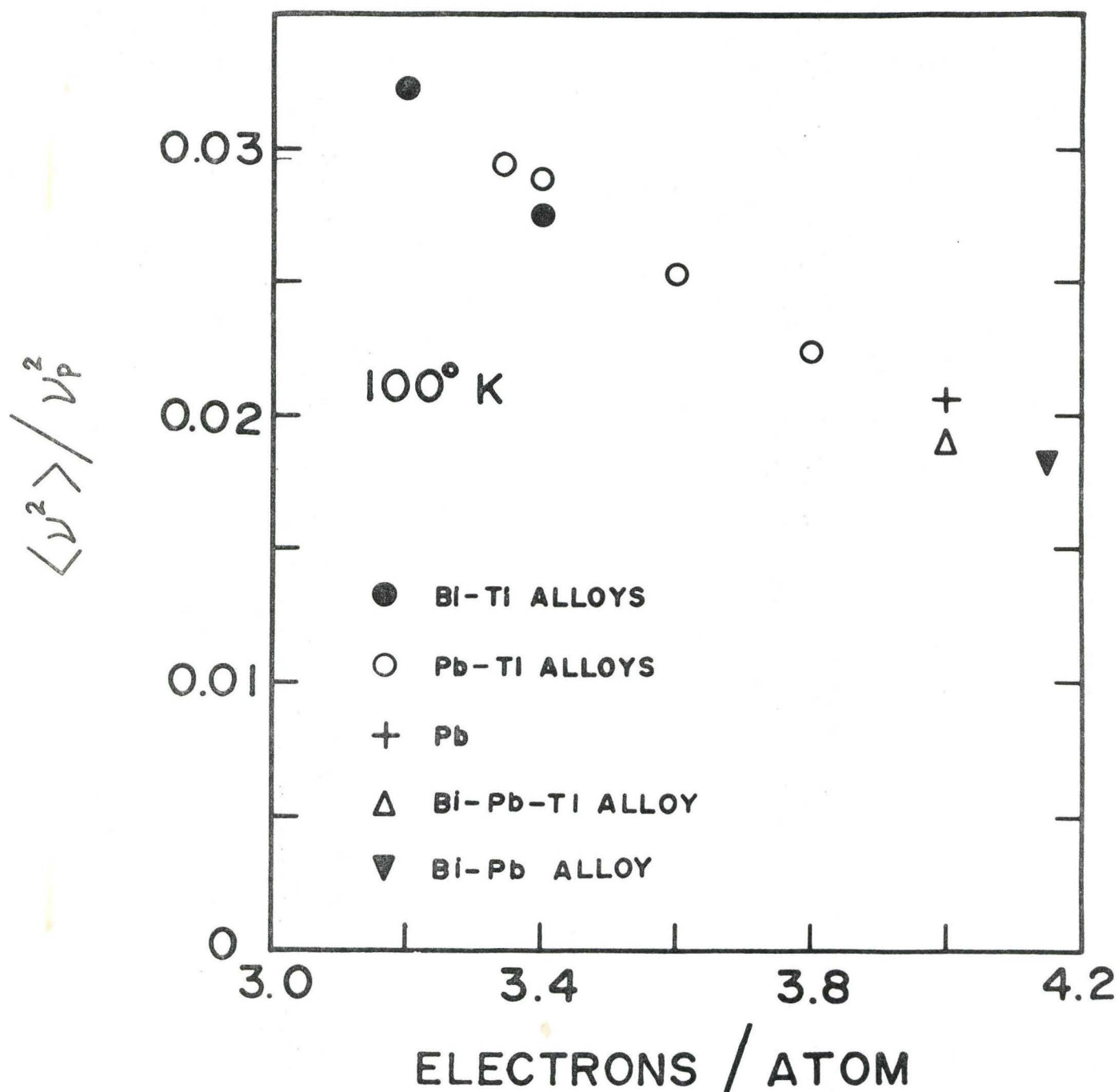


Fig. 4.21

The second moments of the frequency distributions for Bi-Pb-Tl alloys (in units of plasma frequency for the ions), plotted as a function of the average valence. (after Ng and Brockhouse 1968).

valence. (This figure is taken from Ng and Brockhouse (1968); an additional point corresponding to the alloy $\text{Pb}_{33}\text{Tl}_{67}$ has been added in the figure.) This figure shows that the average of the phonon frequencies squared decrease with increase in electron concentration. In other words, the contribution from the indirect interaction and hence the electron-phonon coupling strength increases with electron concentration; in agreement, with the conclusion stated previously.

It may also be illuminating to focuss our attention to a specific mode which exhibits large electron-phonon interaction. It was pointed out in Section C that for certain modes in Pb and in particular, the $[\zeta 00]\text{T}$ zone boundary mode, the phonon frequency increases with temperature (Fig. 4.3)-- a rather unusual feature in the sense that a similar behaviour has not been observed in any other metallic crystal studied so far. It is also worth mentioning that for this mode, the electron screening contribution v_e^2 cancels off 96% of v_c^2 , a particularly high value. It may be recalled here that for $\text{Pb}_{40}\text{Tl}_{60}$ (Fig. 4.4), the sign of the frequency shift for this mode is opposite to that in Pb and we also note that the cancellation of v_c^2 is 85% in this case. In an attempt to relate these observations to the electron concentration in a systematic way, we describe below an experimental study of the temperature induced frequency shifts for the $[\zeta 00]\text{T}$ zone boundary mode in Bi-Pb-Tl alloys.

The general experimental details were essentially the same as outlined in Section B. The specimen crystal was mounted in a cryostat and the measurements were made at liquid nitrogen temperature and room temperature using the same set-up thus eliminating systematic errors in determining the frequency shifts to a large extent which might otherwise arise from the spectrometer calibration and/or slight misalignment of the crystal. $\text{Bi}_{15}\text{Pb}_{85}$, Pb and $\text{Bi}_{10}\text{Tl}_{90}$ had the (100) crystallographic axis vertical and for the rest the measurements were made in the (1 $\bar{1}$ 0) plane of the reciprocal lattice. For liquid-nitrogen runs, the temperature of the specimen crystals, as recorded by a calibrated copper-constantan thermocouple were $\sim 100^\circ\text{K} (+3^\circ\text{K})$ except for $\text{Pb}_{80}\text{Tl}_{20}$ and $\text{Bi}_{20}\text{Tl}_{80}$ for which the temperatures were $\sim 115^\circ\text{K}$. This difference arose because of the use of a different cryostat in the latter measurements. However, the slight temperature difference is of no significance since shifts of frequency from 100°K to 115°K are expected to be less than 0.1 of the shifts from 100°K to 297°K (room temperature) and are therefore well within the errors. The neutron groups as measured for the $[\zeta 00]\text{T}$ zone-boundary mode at two different temperatures in the Bi-Pb-Tl alloys are shown in Fig. 4.22. From some alloys, the measurements were repeated at a different point in reciprocal space. All the experimental results are given in Table 4.9.

To gain some insight into the results, we have presented the experimental information in Fig. 4.23 in a form which is suggested by Eq. (4.2). The Coulomb frequency

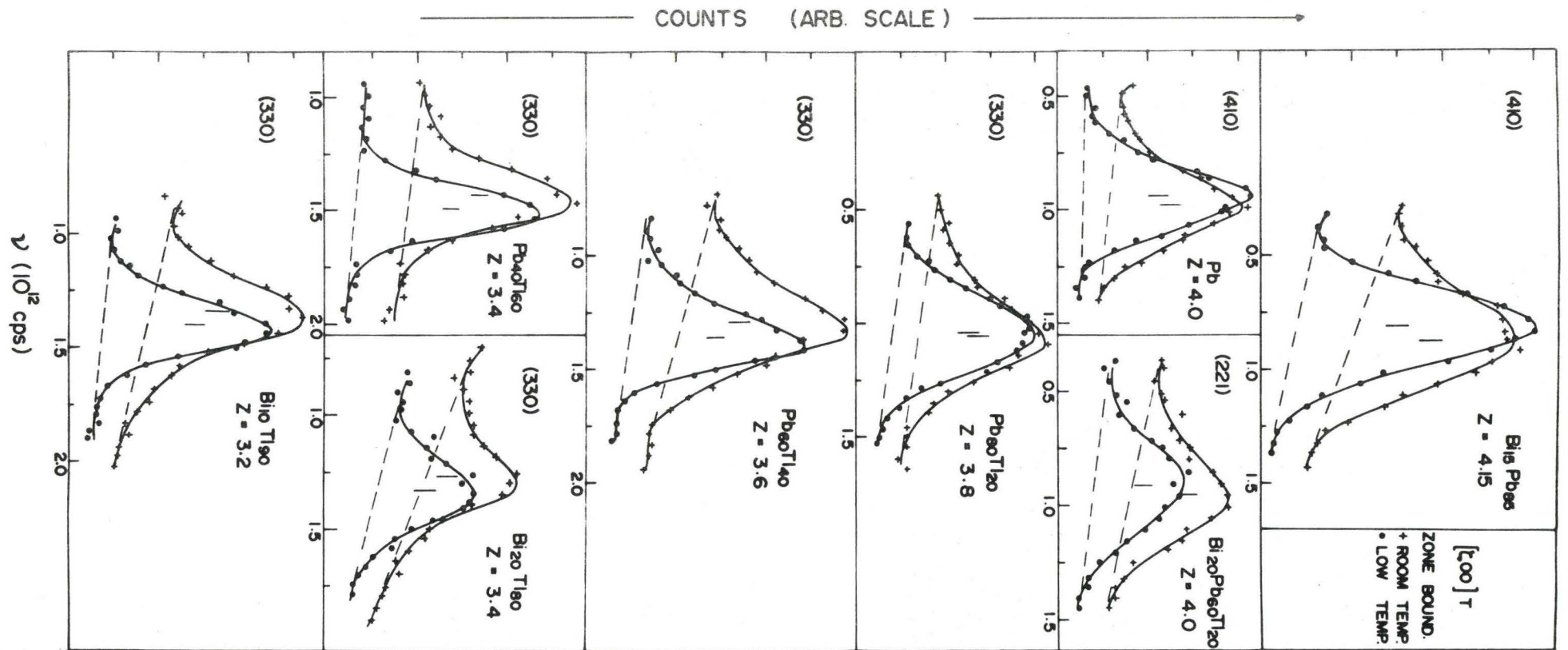


Fig. 4.22

Neutron groups for some Bi-Pb-Tl alloys at two different temperatures, for the $[100]T$ zone-boundary mode. The low temperature runs were carried out at $115^\circ K$ for $Pb_{80}Tl_{20}$ and $Bi_{20}Tl_{80}$ and at $100^\circ K$ for the rest--the room temperature was around $297^\circ K$. The points in reciprocal space where the measurements were made are also indicated (units $\frac{2\pi}{a}$).

TABLE 4.9

[100]T zone-boundary phonon frequencies in the Bi-Pb-Tl alloys measured at different temperatures.

	$(\frac{a}{2\pi})\underline{Q}$	Frequency (10^{12} cps)	
Bi ₁₅ Pb ₈₅	(4.0, 1.0, 0.0)	0.805 (101°K)	0.870 (297°K)
	(3.0, 3.0, 0.0)	0.805 (101°K)	0.865 (297°K)
Bi ₂₀ Pb ₆₀ Tl ₂₀	(2.0, 2.0, 1.0)	0.92 (100°K)	0.96 (298°K)
Pb	(4.0, 1.0, 0.0)	0.890 (100°K)	0.930 (296°K)
Pb ₈₀ Tl ₂₀	(2.0, 2.0, 1.0)	1.045 (115°K)	1.060 (296°K)
	(3.0, 3.0, 0.0)	1.040 (115°K)	1.055 (296°K)
Pb ₆₀ Tl ₄₀	(2.0, 2.0, 1.0)	1.350 (100°K)	1.285 (296°K)
	(3.0, 3.0, 1.0)	1.360 (100°K)	1.295 (296°K)
Pb ₄₀ Tl ₆₀	(3.0, 3.0, 0.0)	1.470 (98°K)	1.415 (296°K)
Bi ₂₀ Tl ₈₀	(2.0, 2.0, 1.0)	1.315 (115°K)	1.260 (297°K)
	(3.0, 3.0, 0.0)	1.330 (115°K)	1.280 (297°K)
Bi ₁₀ Tl ₉₀	(4.0, 1.0, 0.0)	1.420 (100°K)	1.360 (296°K)
	(3.0, 3.0, 0.0)	1.400 (100°K)	1.340 (296°K)

Note: To estimate errors in the frequency shifts [$v_{\text{exp}}^2(300^\circ\text{K}) - v_{\text{exp}}^2(100^\circ\text{K})$], it was assumed that the frequencies at 100°K were known to an accuracy of 1% and those at 300°K to an accuracy of 1.5%. However, it may be seen that the frequency shifts obtained from measurements at two different positions in reciprocal space indicate better accuracy.

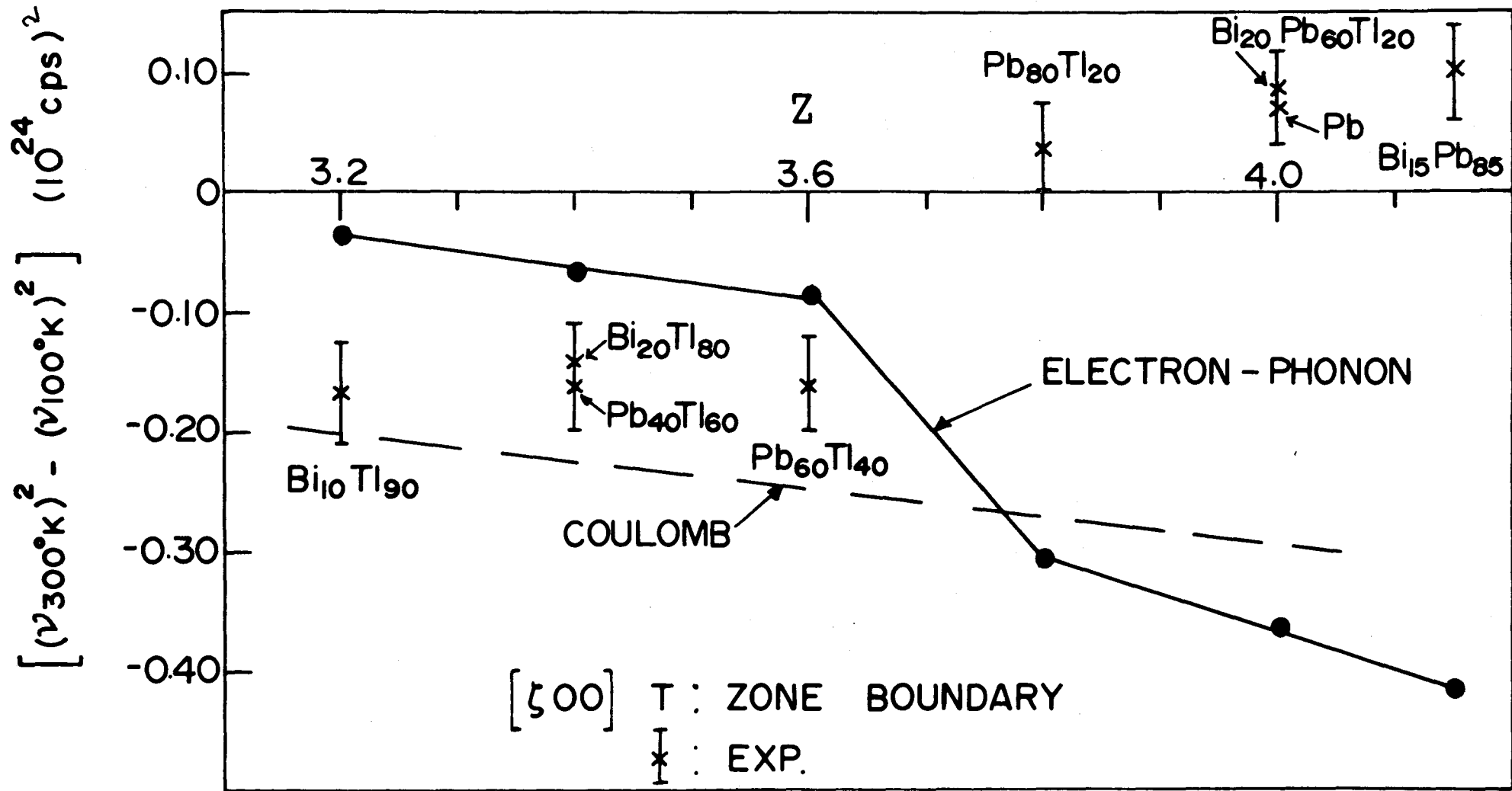


Fig. 4.23

Temperature shifts of the $[\zeta 00]T$ zone-boundary phonon frequencies for the Bi-Pb-Tl alloys. Note the abrupt variation as z changes from 3.8 to 3.6.

(The contribution arising from the direct interaction between ions) can be simply expressed in terms of the plasma frequency v_p and for this particular mode (i.e. $[\zeta 00]T$ zone-boundary)

$$v_c^2 = 0.161 v_p^2$$

Hence the coulomb contribution to the frequency shift may be written as

$$\begin{aligned} v_c^2 &\equiv [v_c^2(300^\circ K) - v_c^2(100^\circ K)] \\ &= 0.161 [v_p^2(300^\circ K) - v_p^2(100^\circ K)] \end{aligned}$$

and is shown as the dashed line in Fig. 4.23. Finally, the electron-phonon contribution is obtained from

$$\Delta v_e^2 = \Delta v_c^2 - \Delta v_{\text{exp}}^2$$

We note in Fig. 4.23 that there is a strong indication of an abrupt change in the measured frequency shifts (accompanied with a change in sign also) as Z changes from 3.8 to 3.6 and since the Coulomb contribution is rather smooth this feature is also reflected in the electron-phonon term. It is instructive to make a similar plot of the phonon frequencies themselves. Such a plot for the alloys is shown in Fig. 4.24 for the $[\zeta 00]T$ zone-boundary mode at $100^\circ K$; the respective Coulomb and electron-phonon contributions are also indicated. (The experimental results are due to Ng (1967).) It is interesting to find a sudden change in the electron-phonon interaction again in the region $Z=3.8-3.6$. (It should be noted that in Fig. 4.24, $v_{\text{el-phonon}}^2$ is plotted on a rather compressed scale and the uncertainty in its value for any particular alloy, arising from the uncertainty in v_{exp}^2 , is probably less than the size of the triangle drawn in the figure.)

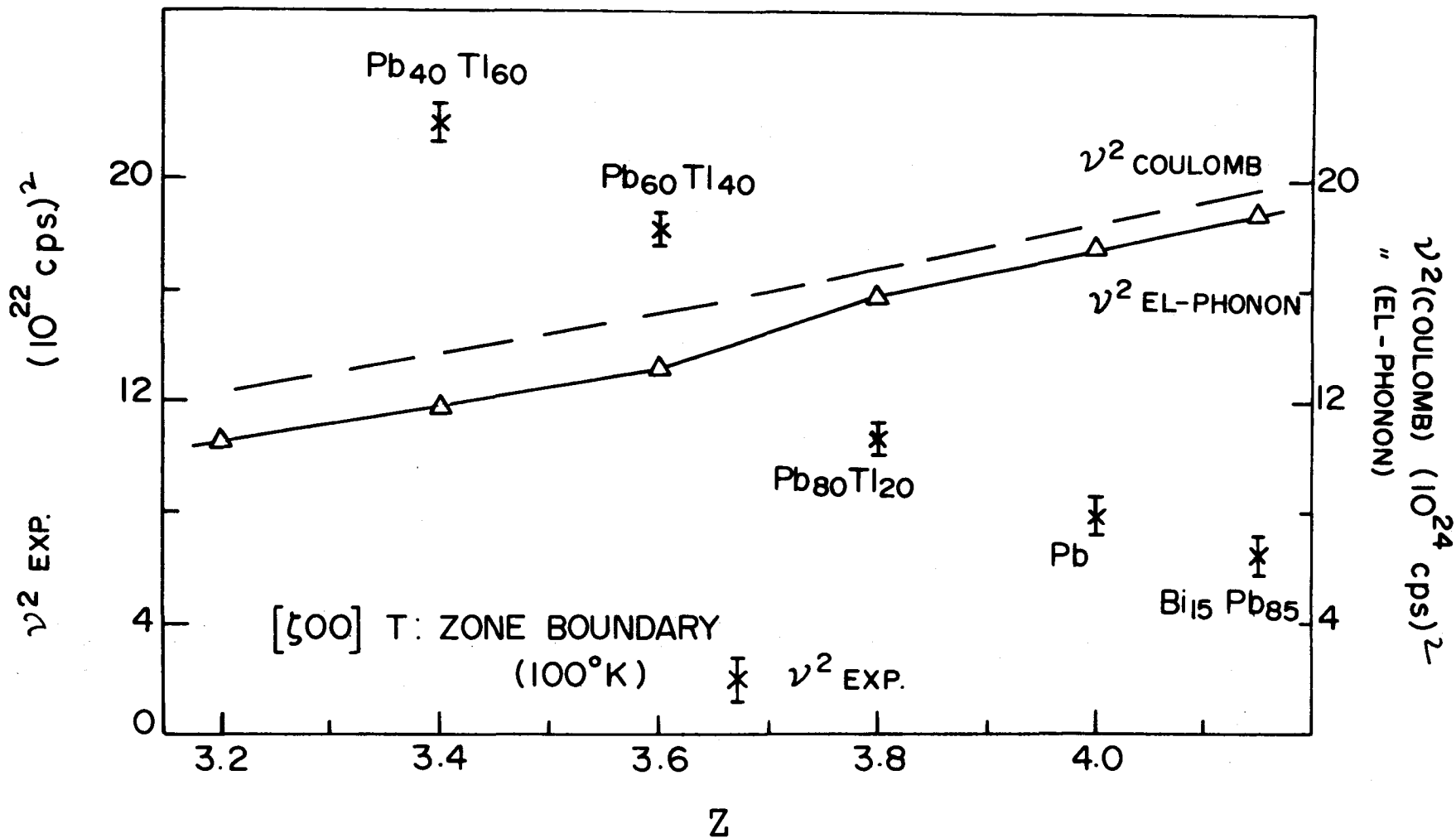


Fig. 4.24

Plot of ν^2_{exp} ($[500]T$ zone-boundary) against average valence for some alloys. Coulomb and electron-phonon contributions are also indicated. Note the abrupt change in ν^2_{exp} as Z changes from 3.8 to 3.6

The interpretation of the results presented in Fig. 4.23 is incomplete in the sense that the anharmonic effects have not been considered explicitly. However, in Section C it was shown that the temperature dependence of the phonon dispersion curves in $\text{Pb}_{40}\text{Tl}_{60}$ could be explained within the quasiharmonic approximation and therefore the approach used here is perhaps justified for alloys with similar electron concentrations. For higher electron concentrations (≥ 4.0), the situation is less clear. For Pb, very limited measurements of the pressure induced frequency shifts are available (Lechner and Quittner 1966). All the modes (including the $[\zeta 00]$ T zone-boundary mode) were found to have positive Grüneisen constant, in other words, frequency increases with decreasing volume.* This suggests that the consideration of the explicit temperature dependent anharmonic contribution may be necessary. At present, it does not seem to be feasible to carry out a reliable anharmonic calculation in metals which exhibit very strong electron-phonon interaction, like Pb. Nevertheless, the fact that the discontinuous change in the observed frequency shift occurs precisely in the region where also the electron-phonon interaction undergoes a sudden change (Fig. 4.24) lends some support to the interpretation given for the experimental results presented in Fig. 4.23.

*In these experiments, the absolute magnitude of the frequency shifts were rather small. For example, along the $[\zeta 00]$ T branch, for $\zeta=1.0$, $|\Delta\nu|\sim 0.02$ and $\zeta=0.65$, $|\Delta\nu|\sim 0.007$. For both these modes, the temperature dependent frequency shifts give negative Grüneisen constants.

G. Coherent Inelastic Scattering of Neutrons from
Polycrystalline Materials*

Lattice Frequency Spectra of Pb and Pb₄₀Tl₆₀

Introduction

For Bravais lattices with cubic symmetry, the frequency distribution function $g(\nu)$ of the lattice vibrations is directly related to the one-phonon incoherent partial differential scattering cross section of monoenergetic neutrons scattered by a single or poly crystal (Placzek and Van Hove 1954). For coherent scatterers fairly accurate curves of $g(\nu)$ can be calculated provided one can obtain a satisfactory force-constant model by fitting to the dispersion curves measured (along symmetry directions) by neutron inelastic scattering from a single crystal. For superconductors information about $g(\nu)$ is furnished by tunneling experiments also (McMillan and Rowell 1965).

Because of extremely long range forces present in lead (Brockhouse et al., 1962) it is not possible to obtain a detailed description of the force constants in the Born-von Kármán theory for this material. Serious discrepancies are observed if one compares the frequency distribution presented by Gilat (1965) (Model calculation using an eight-nearest neighbour fit to the dispersion curves measured along high symmetry directions by coherent inelastic slow-neutron scattering) with that obtained from the tunneling data (McMillan and Rowell 1965). These discrepancies are attributed to inadequacy of the force constant model in predicting off-symmetry phonon frequencies (Dynes et al. 1968; Stedman et al. 1967b). A

* The work described in this section is now published--
Roy and Brockhouse (1970).

realistic frequency distribution for lead was constructed by Stedman et al. (1967b) by measuring a limited number of phonon frequencies in off-symmetry directions using neutron spectroscopy and making interpolation throughout the cell utilising symmetry conditions. However, an adequate sampling of frequencies in the whole Brillouin zone by this technique requires considerable time and effort. For lead, the distribution presented by Stedman et al. (1967b) compares favorably with that obtained from the tunneling data (Rowell et al. 1969; Franck et al. 1969). However, there is a small but significant discrepancy regarding the position of the principal maximum arising from the longitudinal phonons. It is true that in the tunneling experiment one obtains the product $\alpha^2(\nu)g(\nu)$ where $\alpha^2(\nu)$ is the electron-phonon coupling strength. However, $\alpha^2(\nu)$ is thought to be a rather slowly varying function of frequency and therefore positions of the critical points are expected not to be affected. This is readily seen by referring to Fig. 3 of the paper by Dynes et al. (1969).

For the $\text{Pb}_{40}\text{Tl}_{60}$ alloy, an eight-neighbour tensor force model can reproduce the phonon frequencies along both symmetry and non-symmetry directions to within 2% of the experimental results (Ng and Brockhouse 1967, 1968). However, the frequency spectrum calculated within the framework of the Born-von Kármán model does not represent the true physical situation as it neglects the phonon life time broadening in a disordered alloy crystal (Ng and Brockhouse 1968).

In the light of the preceding discussion, we thought it worthwhile to obtain the frequency spectra of lead and the lead-thallium alloy directly using a different experimental technique which is described below.

Principle of the Experimental Method

It was remarked earlier that one-phonon incoherent inelastic neutron scattering is directly related to the density of states $g(\nu)$. For coherent scattering, when collective atomic motions in the system are dominant, it is necessary to ensure a high degree of averaging of the interference pattern. By using a polycrystalline target one essentially averages the scattering cross-section over all directions of momentum transfer with respect to a fixed crystal orientation. Further, to provide a more adequate sampling of the reciprocal space one can superpose the energy distribution of slow neutrons scattered coherently from a polycrystalline sample over a wide range of magnitudes of momentum transfer. Finally, $g(\nu)$ can be obtained from the superposed data in the incoherent approximation (Placzek and Van Hove 1954). A notable feature of this experiment is that one can profitably use relatively thick specimens to enhance the intensity. Normally, multiple scattering is considered undesirable, however, in this type of experiment double scattering events which involve successive creation (or annihilation) of one phonon and elastic scattering or vice versa contribute significantly to the intensity and improve the sampling.

Though it seems reasonable to assume that the method described above is capable of giving frequency spectra for coherent scatterers to a fair approximation, this approach has not been justified rigorously in theory. According to a prescription given by Egelstaff (1953) the polycrystalline coherent one-phonon cross section is written as a product of incoherent inelastic cross-section and an energy dependent structure factor. Marshall and Stuart (1961) have examined the validity of Placzek's incoherent approximation (Placzek 1954) for calculating the total inelastic coherent scattering. The limitation of these approaches has been discussed recently by deWette and Rahman (1968). They carried out computer calculations of the one phonon coherent polycrystalline cross-section for a monatomic crystal assuming a Lennard-Jones (6-12) potential of interaction between the atoms for values of momentum transfer $|\underline{Q}|$ comparable with the dimensions of the Brillouin zone. Results were presented in terms of a function $f(\underline{Q}, \nu)$ defined as

$$f(\underline{Q}, \nu) = \left\langle \sum_{j=1}^3 [\underline{Q} \cdot \underline{\xi}(\underline{Q}, j)]^2 \delta(\nu - \nu(\underline{Q}, j)) \right\rangle,$$

where $\underline{\xi}(\underline{Q}, j)$ is the polarization vector of a phonon with wave vector \underline{Q} and frequency $\nu(\underline{Q}, j)$, $j = 1, 2, 3$, and $\langle \dots \rangle$ denotes averaging over all directions of \underline{Q} . In our experiment, the average value of the momentum transfer was about 6.5 \AA^{-1} , much larger than the linear dimension of the Brillouin zone ($\sim 1.3 \text{ \AA}^{-1}$) and in such cases $f(\underline{Q}, \nu)$ may be expected to resemble the density of states, $g(\nu)$. However, the importance of adequate sampling in reciprocal space for obtaining a

reliable $g(\nu)$ must be borne in mind. Obviously if Q-points are sampled uniformly over just one Brillouin zone, the quantity within $\langle \dots \rangle$ is proportional to $Q^2 g(\nu)$. Even for single scattering events only, the region of reciprocal space sampled in the present experiment may be estimated to be roughly one hundred times the volume of the first Brillouin zone. For coherently scattering polycrystalline substances, as pointed out earlier, double scattering events, involving coherent zero-phonon and one-phonon scattering, play an important role in enhancing the degree of sampling (Fig. 4.25). Bredov et al. (1967) have considered the influence of multiple coherent elastic reflection on the inelastic coherent scattering from polycrystalline sample. Various authors¹ have studied time-of-flight spectra of polycrystalline substances using chopper or beryllium filtered cold neutrons. For strong coherent scatterers, structures appear in the spectra arising from interference effects because proper averaging is not effected in these methods. Therefore, any attempt to extract the frequency distribution function in the incoherent approximation might lead to incorrect results. For example, the $g(\nu)$ spectrum obtained by Mozer et al. (1963) for palladium by the above procedure deviates appreciably from the true spectrum (Miiller and Brockhouse 1970). Similar conclusions were reached by Schmunk et al. (1965) and Larsson et al. (1965) in connection with their work on polycrystalline aluminum which

¹ See, for example, Proceedings of Neutron Inelastic Scattering in Solids and Liquids. 1961, 1963, 1965, 1968 (IAEA, Vienna).

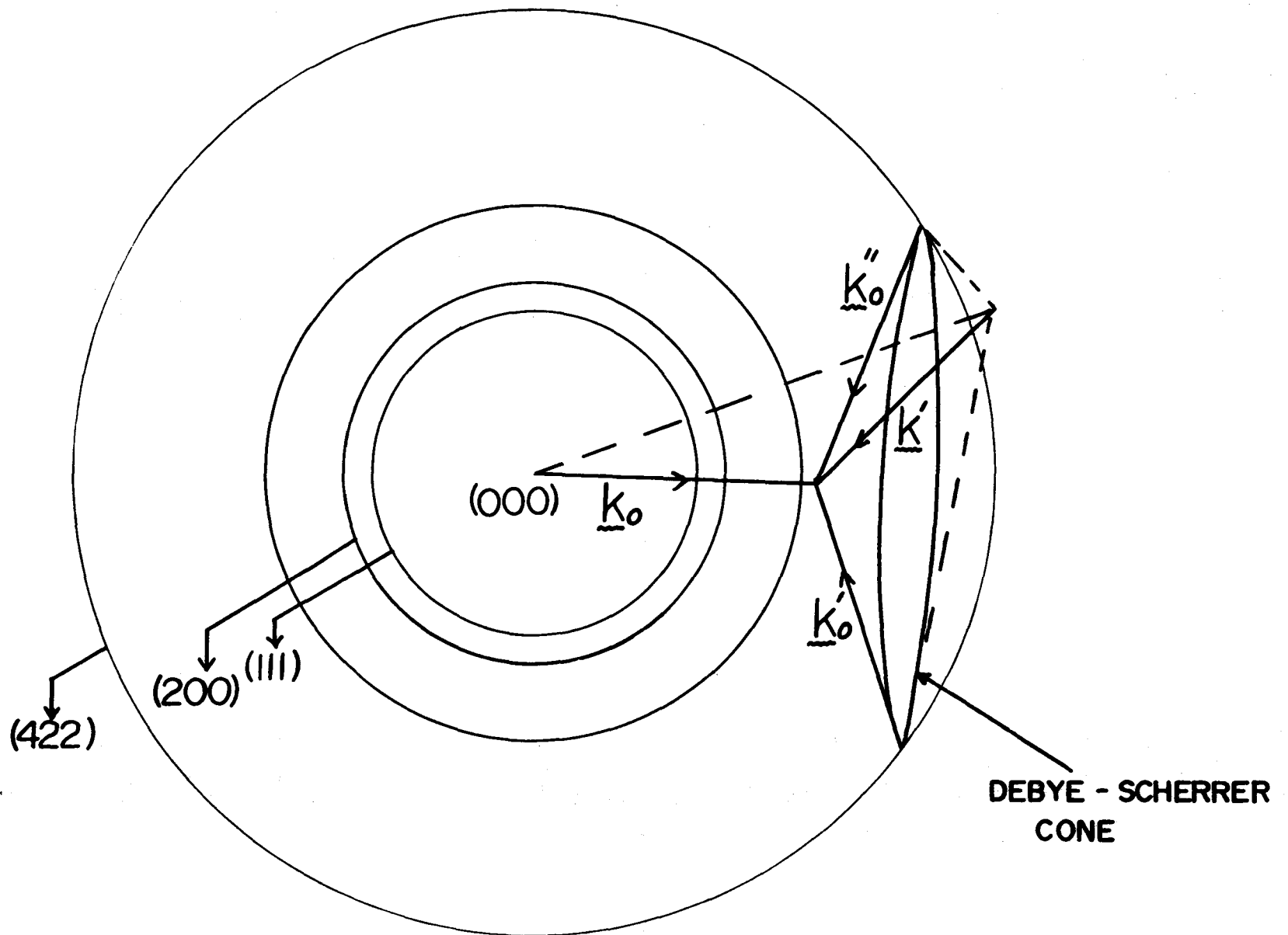


Fig. 4.25 Reciprocal space diagram illustrating double scattering events. The incident beam \underline{k}_0 is first elastically scattered (422) and the scattered beam can lie anywhere on the Debye-Scherrer cone. It finally emerges in the direction \underline{k}' after an inelastic scattering event. It may be seen from the figure that the magnitude of the momentum transfer for the inelastic event can vary over a large range.

is again a substance which scatters coherently. Bredov et al. (1967) and Kotov et al. (1968) have also studied the frequency spectrum by coherent inelastic scattering of cold neutrons from polycrystalline materials - aluminium, lead and tellurium.

In addition to the interest in the detailed results through comparison of $g(\nu)$ from neutron scattering with $\alpha^2(\nu)g(\nu)$ from tunneling, a motivation for the present work was to actually attack this long-posed problem of obtaining a good $g(\nu)$ from neutron scattering results for polycrystalline material.

Experimental Details

The lead sample was in the form of shots, about 2.5 mm in diameter, with a nominal purity of 99.99%. The lead-thallium alloy was in the form of granules. Neutron diffraction measurements were used to characterise the composition and bulk homogeneity of the alloy. By comparing the positions of Debye-Scherrer lines ((220) and (311)) of the alloy with those of pure lead powder (Fig. 4.26) the composition was estimated to be $\text{Pb}_{41.5}\text{Tl}_{58.5}$ (with an accuracy of ± 3 atomic %) from the known behaviour of the lattice constant as a function of alloy concentration (Pearson 1958). Further, the alloy peaks did not show any appreciable broadening compared with the lead powder peaks, a fact which implies that the alloy was quite homogeneous.

A cylindrical aluminium container (3" long and 1" in diameter) was used for both specimens. Transmission of the lead specimen was 60%. The experiments were carried out using the McMaster triple-axis spectrometer installed at the NRU

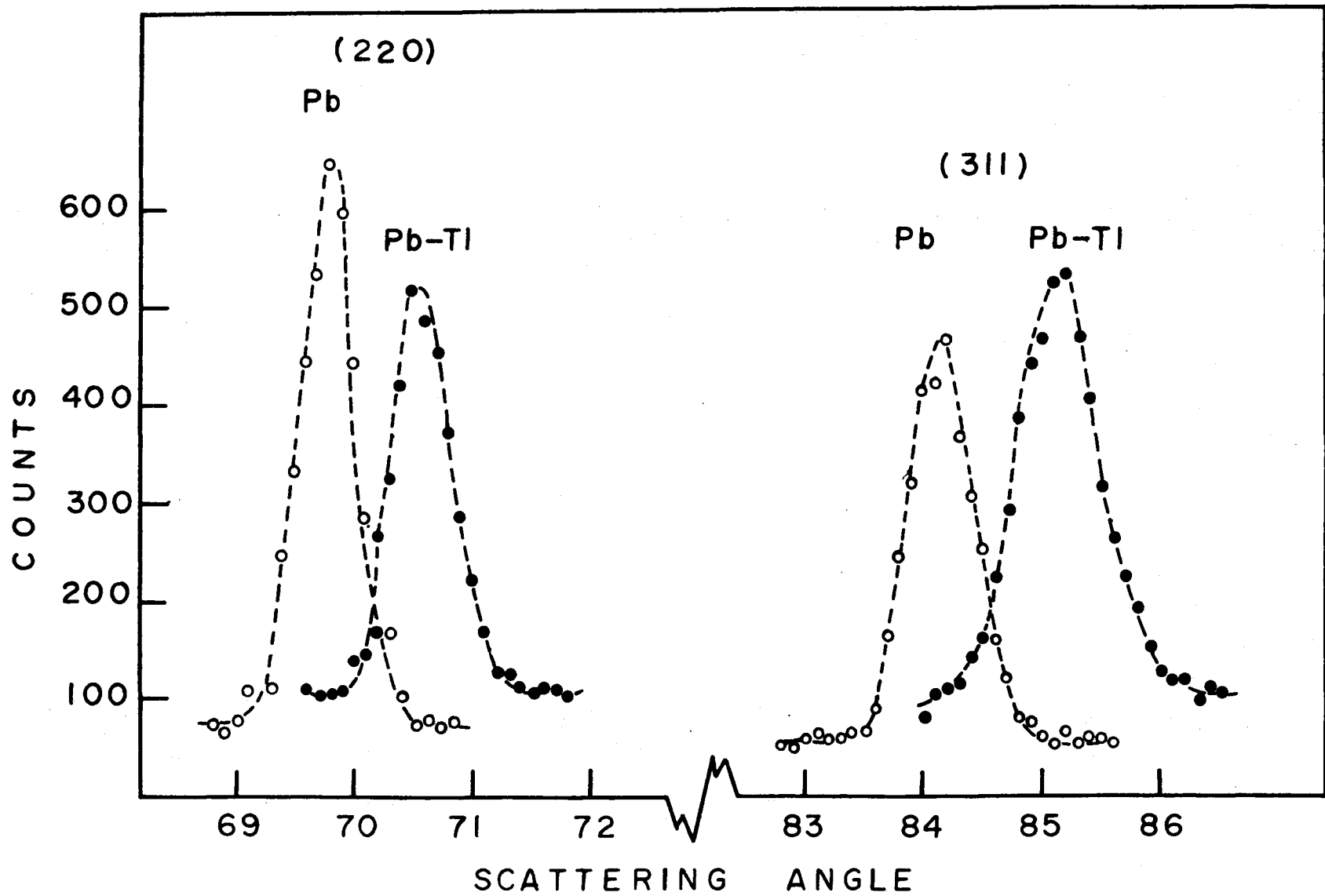


Fig. 4.26 Debye-Scherrer lines at 296°K from polycrystalline specimens of Pb and the Pb-Tl alloy.

reactor at the Chalk River Nuclear Laboratories (Brockhouse, deWit, Hallman and Rowe 1968). Neutrons with incoming frequency of 7.0×10^{12} cps were used throughout the experiment. The energy distribution of the outgoing neutrons was measured over a range of frequency transfer of 3.2×10^{12} cps for eleven different scattering angles ranging from 142° to 90° , with neutron energy loss (phonon creation). Measurements were made at temperatures within five degrees of 90°K . Ideally the experiments should have been done in the Constant- $|Q|$ mode; however this was not feasible as Debye-Scherrer lines from the sample interfered with the inelastic spectrum by rescattering from the analyzing crystal.

Results and Analysis

The raw data for lead is shown in Fig. 4.27. The sharp peaks appearing in the patterns taken at scattering angles 134° , 110° and 90° at the frequency 2.5×10^{12} cps are spurious and were smoothed out. They arise from a very weak contaminant present in the main beam which happens to produce a Debye-Scherrer line by scattering off the specimen at these scattering angles and finally is Bragg reflected by the analyzer. For the $\text{Pb}_{40}\text{Tl}_{60}$ alloy similar peaks appeared at scattering angles 131° and 107° for the same energy transfer of 2.5×10^{12} cps and could be accounted for in exactly the same way.

Background was monitored in another counter which was placed at an angle of 40° with respect to the signal counter (Brockhouse et al. 1968). In addition to this, in

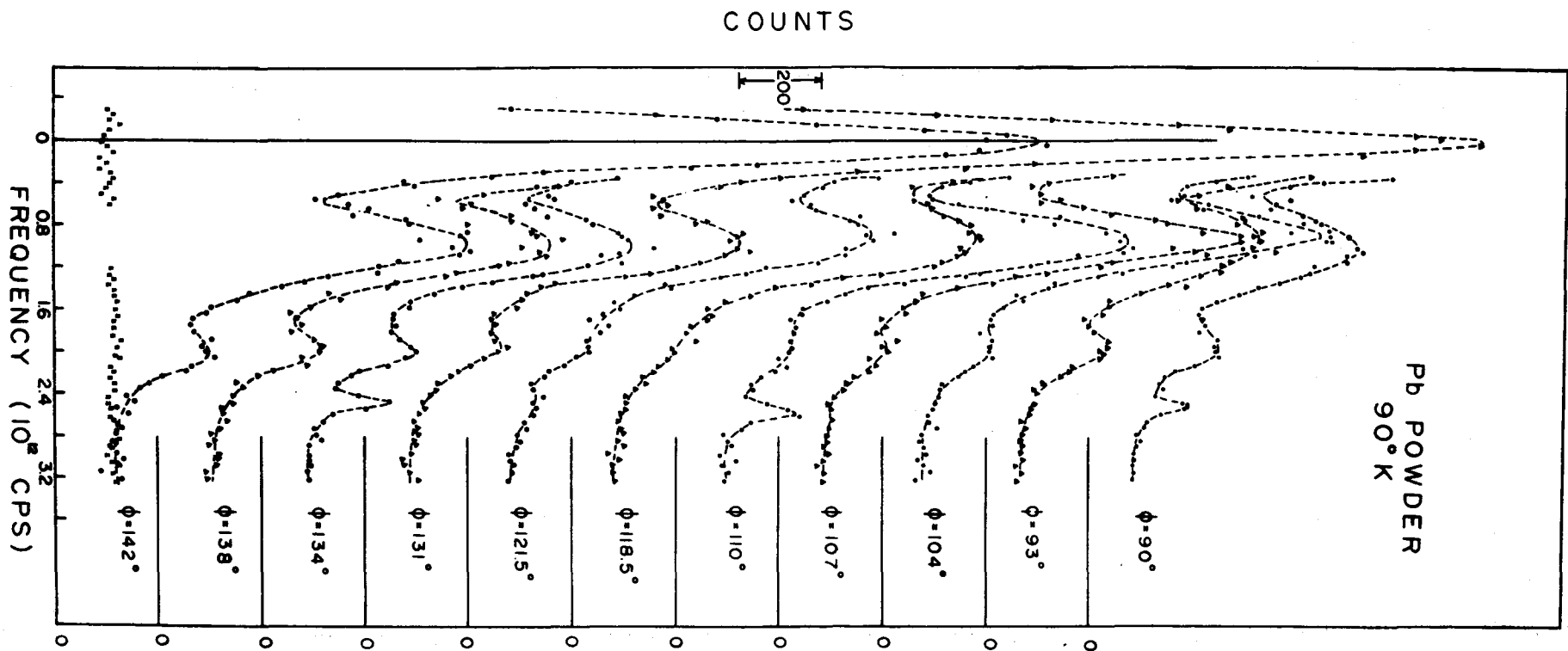


Fig. 4.27 Observed neutron spectra scattered from Pb powder at 90°K over an energy transfer of 3.2×10^{12} cps and an angular range of 90-142°. The background recorded for one angle (142°) is also shown.

some instances background counts were recorded in the signal counter by flipping the analyzer from the Bragg position. Also runs were carried out for a few selected scattering angles to ascertain the contribution from the empty aluminium sample holder and the cryostat. After correcting for general background effects it was necessary to further correct the data for multiphonon and multiple-event inelastic processes. As the experiments were done at liquid nitrogen temperature, all higher phonon processes except the two phonon process were negligible. The two-phonon contribution (simultaneous creation and/or annihilation of two phonons), in this (coherent scattering) case, is quite well described by the incoherent approximation. It is further necessary to consider the effect of the following multiple scattering events on the observed inelastic spectrum. They are (a) creation of one phonon in a scattering event followed by the annihilation or creation of another phonon in another scattering event i.e. successive energy loss and gain and successive energy loss, and (b) single two-phonon events (simultaneous creation or creation and annihilation of two phonons) followed or preceded by elastic scattering. It is interesting to note that for both the above processes (a) and (b) the shape of the energy spectrum is about the same as that of the single two-phonon event mentioned earlier. Therefore, subtraction of the contributions arising from these multiple scattering events do not present any additional problem. A rough estimate of the relative importance of these processes can be easily made by calculating the following quantity:

$$\left(\begin{array}{l} \text{Single-event scattering:} \\ \text{Two-phonon} \end{array} \right. \quad \left. \begin{array}{l} \text{Two-event scattering:} \\ + \text{(i) One-phonon, one-phonon} \\ \text{(ii) two phonon, elastic} \end{array} \right)$$

$$\left(\begin{array}{l} \text{Single-event scattering:} \\ \text{One-phonon} \end{array} \right. \quad \left. \begin{array}{l} \text{Two-event scattering:} \\ + \text{one-phonon, elastic} \end{array} \right)$$

$$\sim \frac{[\beta e^{-2W} \frac{1}{2}(2W)^2 + (\beta e^{-2W})^2 (2W)^2]}{[\beta e^{-2W} 2W + (\beta e^{-2W})^2 (2W)]}$$

In the above expression, $\beta = \log_e(1/T)$ where T is the transmission of the sample and e^{-2W} is the Debye-Waller factor. For the lead specimen $\beta \sim 0.50$ and $e^{-2W} \sim 0.75$. Substituting these values we get the ratio 0.18. The cross-sections referred to above, essentially imply integration over the whole range of energy transfer. To apply correction to the data it is necessary to evaluate the energy-dependent partial differential cross sections in the incoherent approximation.

The two-phonon differential scattering cross-section was evaluated for a mean scattering angle of 116° assuming an approximate frequency distribution function (Sjolander 1958). It was then folded with the resolution function of the spectrometer. The ratio of the integrated two-phonon cross section to the one-phonon cross section was fixed by the analysis given before. Fig. 4.28 shows the accumulated data for Pb and $\text{Pb}_{40}\text{Tl}_{60}$ obtained from superposition of all the individual runs recorded at various scattering angles ranging from 142° to 90° and the estimated two-phonon contribution. It can be seen that the calculated two-phonon partial differential cross section

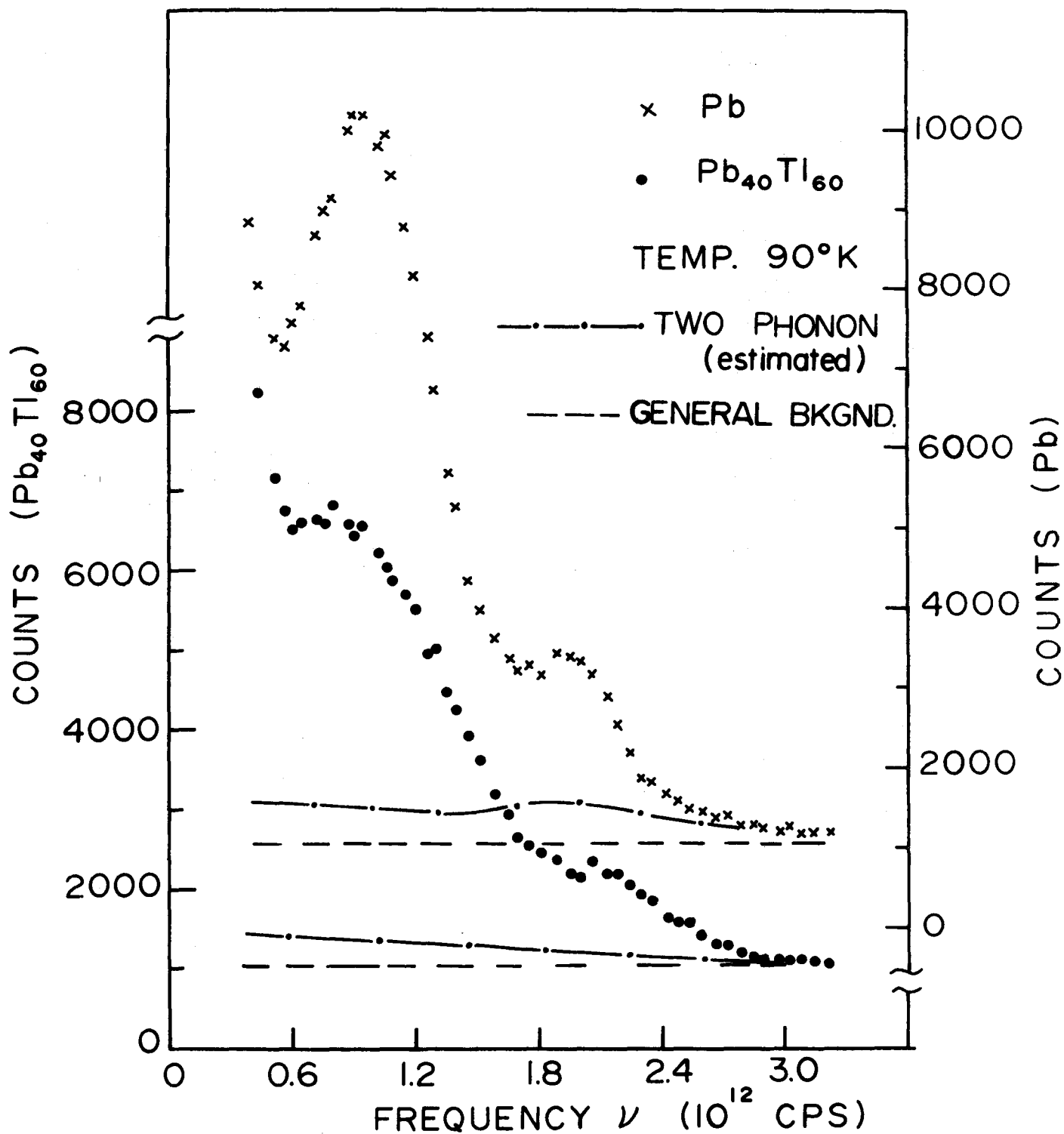


Fig. 4.28

Accumulated data for Pb and Pb₄₀Tl₆₀ obtained from superposition of all the individual runs recorded at various scattering angles. General background and the estimated two-phonon contribution are also shown.

fits reasonably well in the tail region (from 2.8×10^{12} cps to 3.2×10^{12} cps) which is beyond the cut off of the one-phonon spectrum. After subtracting the calculated two-phonon cross section, normalised as described above, from the experimental data, the frequency distribution function is extracted in the incoherent approximation. As uncertainty is introduced in the average magnitude of the momentum transfer $|Q|$ at a given energy transfer and angle of scattering by multiple scattering we did not attempt to weight the individual angular patterns with the factor $[Q^2 \exp(-2W)]$ before adding them; rather we used mean values of momentum transfer determined by the angular range covered in the various runs.

Finally, correction had to be applied to the data to take into account the variation in the reflectivity of the analysing crystal over the range of the energy transfer measured. The determination of the sensitivity function of the analyzing spectrometer is discussed in Appendix II. It was found to vary approximately linearly by about 30% over the energy range covered in the present experiment.

Discussion

We show in Fig. 4.29 the frequency distribution function of lead obtained from the present experiment. For comparison we also show the tunneling data (Rowell et al. 1969) and the neutron scattering results of Stedman et al. (1967a), in each case broadened by the resolution function of our spectro-

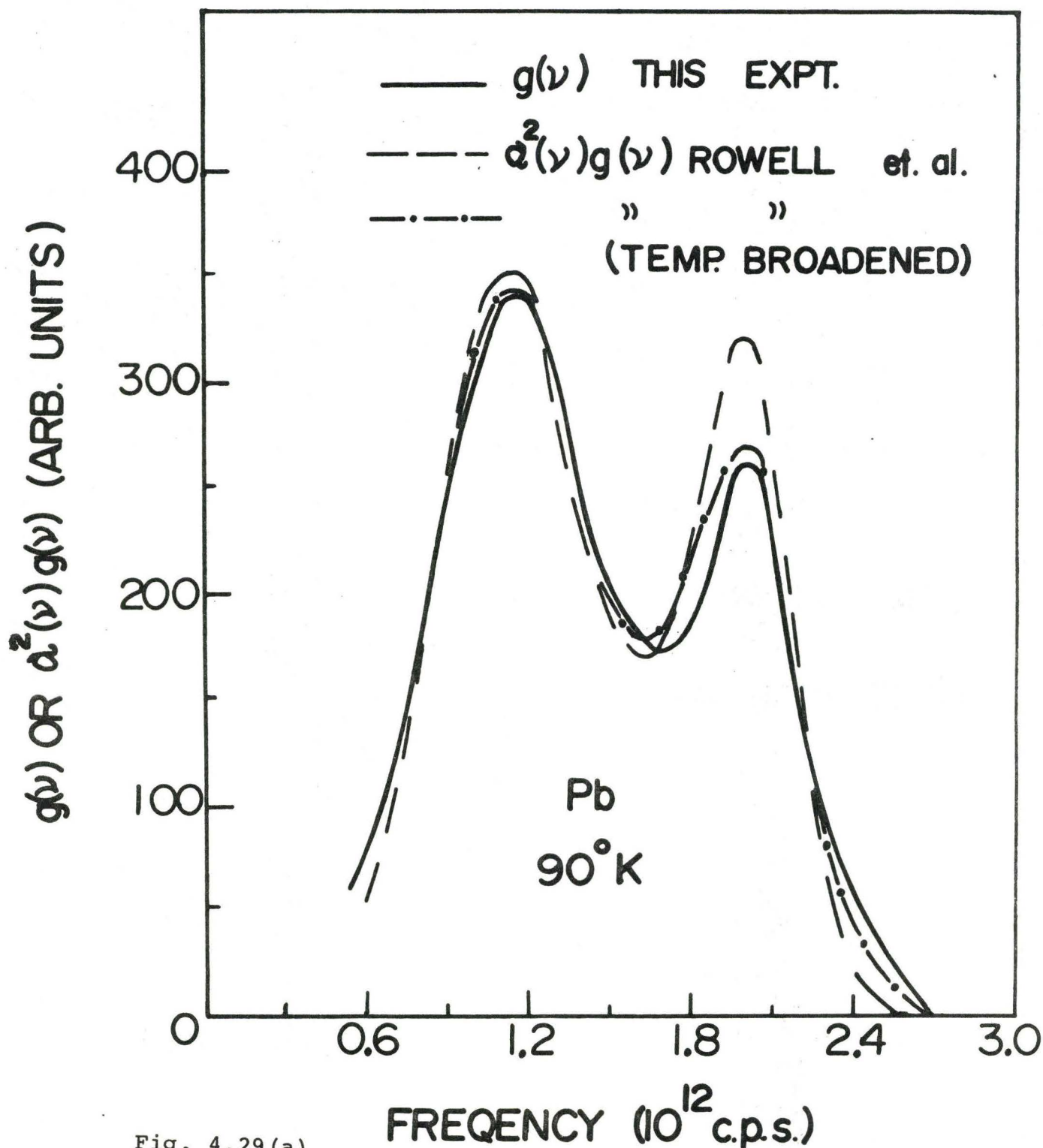


Fig. 4.29 (a)

Comparison of $g(\nu)$ for Pb obtained from the powder experiment with $\alpha^2(\nu)g(\nu)$ from tunneling measurements of Rowell et al. (1969) (-----). Additional Lorentzian broadening of $\Delta\nu/\nu=0.05$ is shown by the (-.-.-.) line. The tunneling spectra have been folded with the resolution function of the spectrometer. All the distributions (also in Fig. 4.29(b) and 4.30) are normalized to the same area.

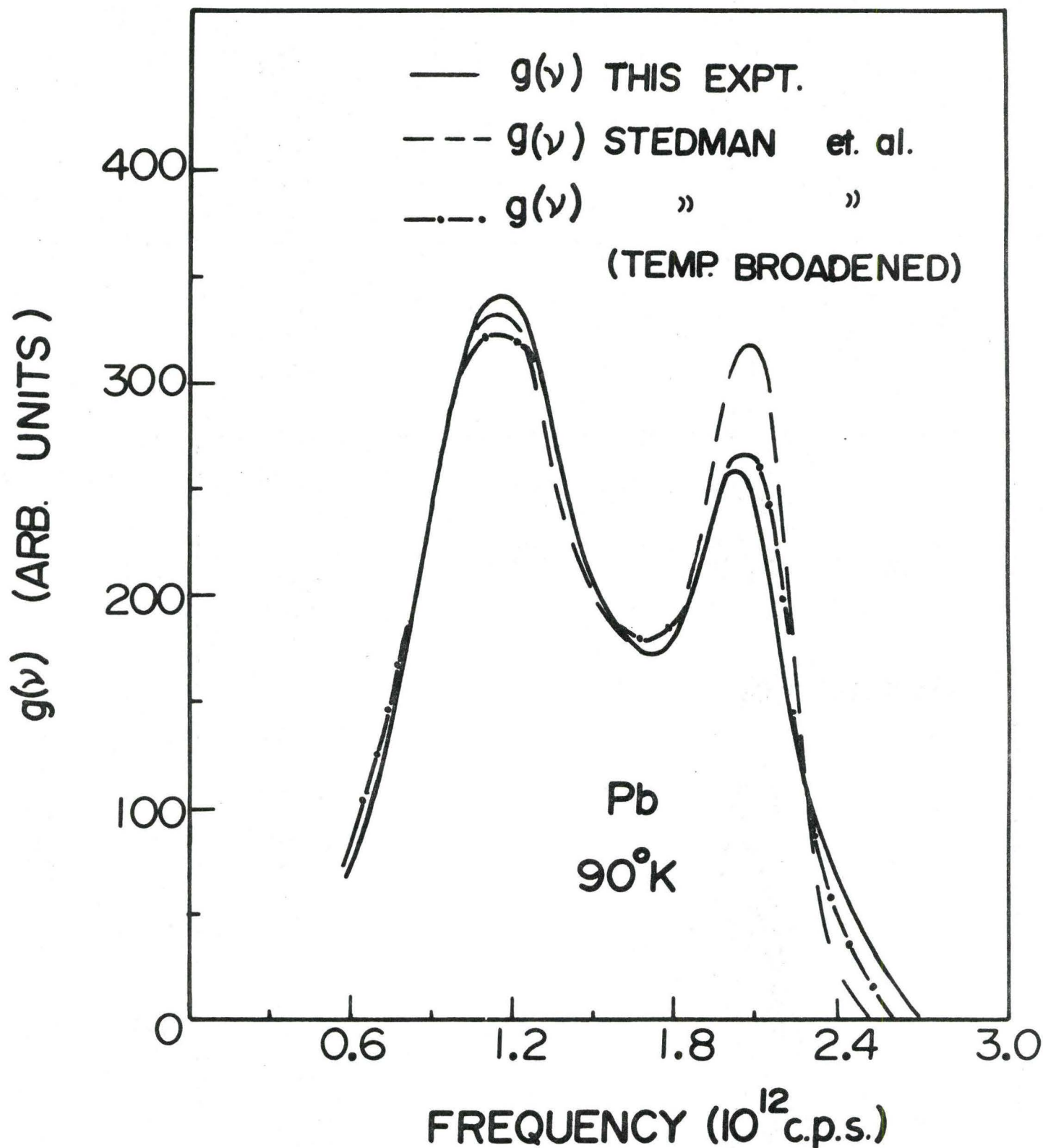


Fig. 4.29(b)

Comparison of $g(\nu)$ for Pb obtained from the powder experiment with that from the neutron scattering results of Stedman et al. (1967) (----). Additional Lorentzian broadening of $\Delta\nu/\nu = 0.05$ is shown by the (-.-.-) line. The effect of the resolution function of the spectrometer has been taken into account as explained in the text.

meter¹ (assumed to be Gaussian). We find that the position of the longitudinal peak agrees particularly well with the tunneling result. The high energy tail appearing in the powder experiment can be attributed to an inadequate correction for the multiphonon effects or to some inherent broadening present in the experimental result. The tunneling spectrum corresponds to a temperature of 1°K, whereas the present neutron scattering experiment was carried out at 90°K. Therefore some anharmonic broadening should be present in our result. This effect is particularly important for the short wavelength longitudinal modes (Brockhouse et al. 1961; Stedman et al. 1967a); as the longitudinal peak in the $g(\nu)$ spectrum is relatively sharp, any additional broadening appreciably modifies the peak height. Similarly, although the frequency distribution given by Stedman et al. (1967b) refers to 90°K, the effects of the finite lifetimes of the phonons at this temperature were not incorporated by them in their $g(\nu)$. Stedman et al. (1967a) estimate the broadening ($\Delta\nu/\nu$) to be about 5%; for the sake of comparison we show in Fig. 4.29 the effect of this additional broadening assuming that the phonon lifetimes have a Lorentzian distribution.

¹ Their frequency distribution functions were first used to calculate the one-phonon cross-section in the incoherent approximation which was then folded with the resolution function of the spectrometer. Frequency spectra computed from the folded cross section are plotted in Fig. 4.29.

We find in Fig. 4.30 that for $\text{Pb}_{40}\text{Tl}_{60}$ (unlike Pb) $\alpha^2(\nu)$ tends to decrease in the longitudinal region. We may explain this behaviour qualitatively on the simplified assumption that whereas for Pb both the normal and the umklapp processes contribute to $\alpha^2(\nu)$ for the longitudinal modes and only umklapp processes for the transverse modes, the sharp distinction between the normal and the umklapp processes no longer exists for a disordered lattice like $\text{Pb}_{40}\text{Tl}_{60}$. Fig. 4.30 clearly indicates the strong effect of energy smearing on the strengths of narrow peaks in the density of states. The anharmonic broadening tends to be masked by the broadening caused by force constant disorder of the alloy. In a recent paper Dynes and Rowell (1969) have demonstrated smearing of the fine structure in the product function $\alpha^2(\nu)g(\nu)$ for the alloy system $\text{Bi}_x\text{Pb}_{1-2x}\text{Tl}_x$.

If it is assumed that the phonon lifetimes have a Lorentzian distribution in the alloy and that the relative linewidth $\Delta\nu/\nu$ remains a constant then we can easily incorporate the effect of the finite lifetime in the frequency spectrum computed from the force constant model. It is seen from Fig. 4.30(b) that for a value of $\Delta\nu/\nu = 0.10$, the experimentally observed broadening is well reproduced in the calculated distribution.

The various discordances remaining in Figs. 4.29 and 4.30 are probably also contributed to by inadequate sampling. Inspection of Fig. 4.27 shows that very considerable differences exist between the patterns for the different angles of

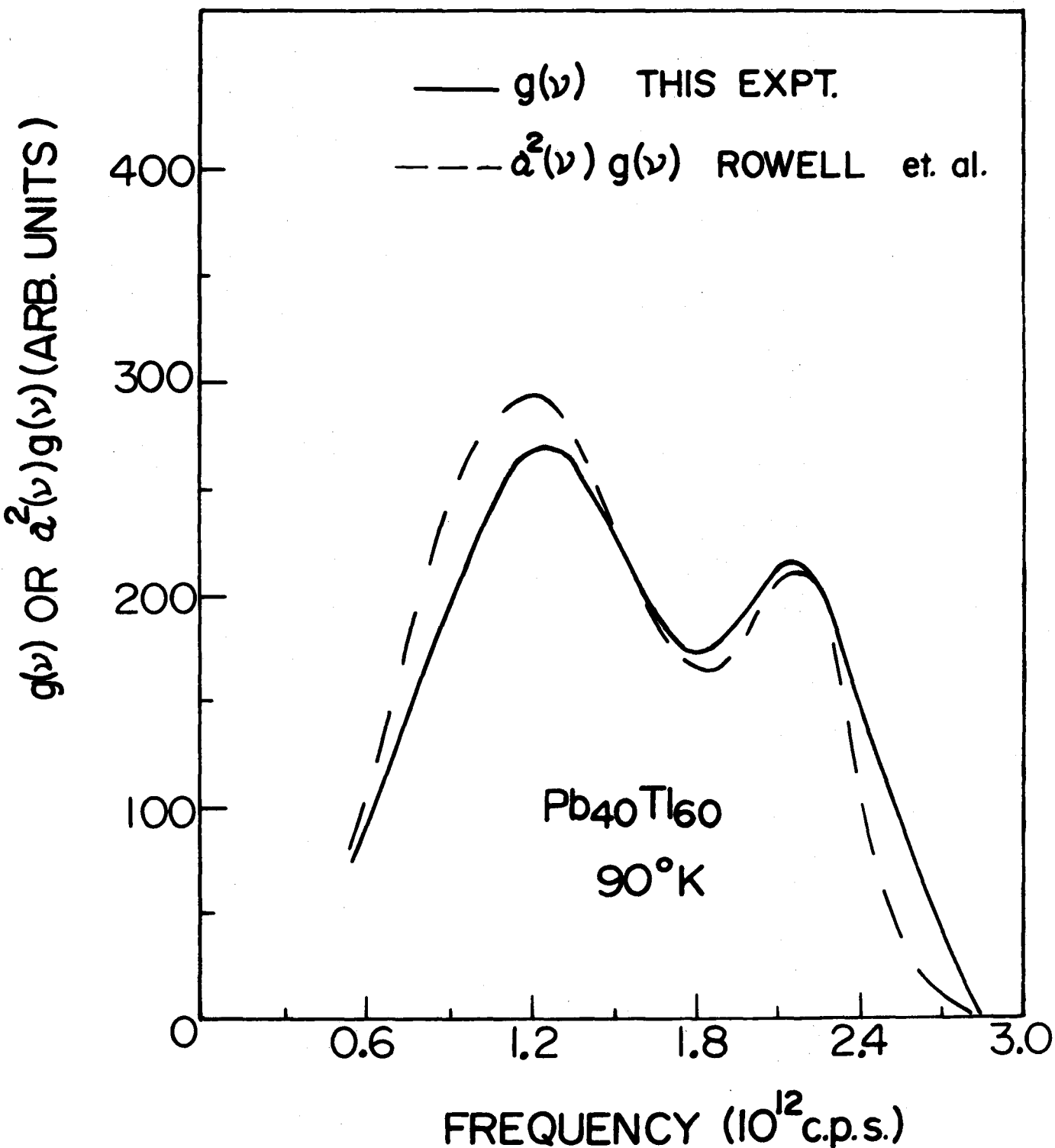


Fig. 4.30(a)

Comparison of $g(\nu)$ for Pb₄₀Tl₆₀ obtained from the powder experiment with $\alpha^2(\nu)g(\nu)$ from the tunneling measurements (folded with the resolution function of the spectrometer).

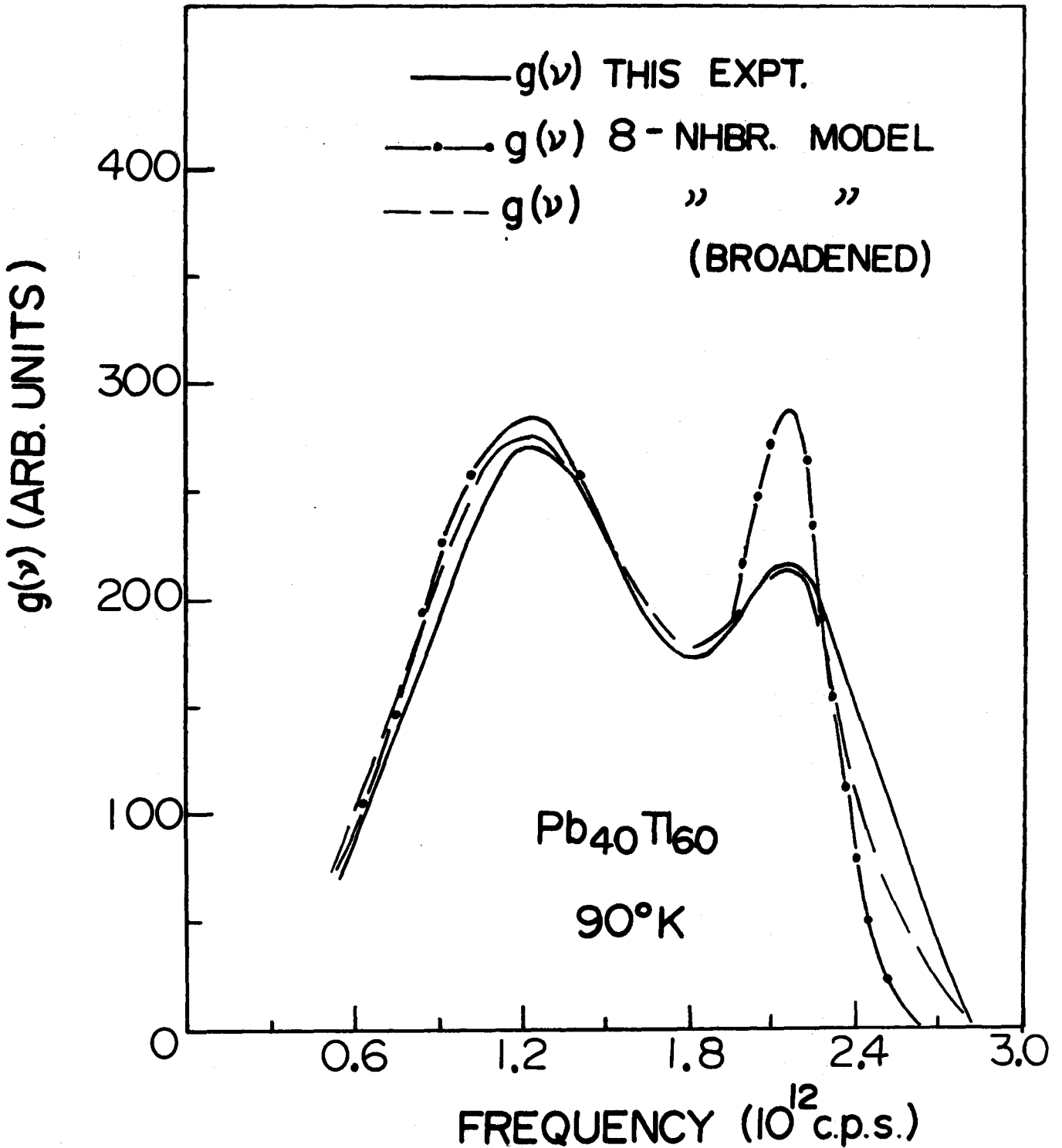


Fig. 4.30(b)

Comparison of $g(\nu)$ for $Pb_{40}Tl_{60}$ obtained from the powder experiment with $g(\nu)$ computed from an eight neighbour tensor force model (-·-·-) and a smeared $g(\nu)$ (- - -) with an additional Lorentzian broadening of $\Delta\nu/\nu = 0.10$. The computed frequency spectra are further modified by the resolution function of the spectrometer as explained in the text.

scattering. Attention should be particularly focussed on the varying prominence of the longitudinal peak at $\sim 2.0 \times 10^{12}$ cps in the various patterns. The reason for the observed fluctuation in the intensity of the longitudinal peak may be qualitatively understood by referring to Fig. 4.31. The scattering diagrams drawn in reciprocal space correspond to an energy transfer of 2×10^{12} cps. The intensity of the longitudinal peak at any particular scattering angle depends on the relative positions of the end point of the scattering vector \underline{k}' with respect to the Debye-Scherrer lines (with due consideration of the multiplicity). It is obvious that averaging over eleven patterns is not really sufficient to satisfactorily delineate this peak in the "average" pattern. An increase in the number of patterns taken and the angular range covered ought to improve the situation. It may be noted that the resolution of the neutron crystal spectrometer is inadequate to reveal all the fine details of the frequency spectrum. However, the principal maxima in the spectra are clearly resolved for Pb and $\text{Pb}_{40}\text{Tl}_{60}$, the substances studied in the present work. In $\text{Pb}_{40}\text{Tl}_{60}$ we see direct evidence of energy smearing arising from the finite lifetimes of the phonons caused by force constant disorder of the alloy.

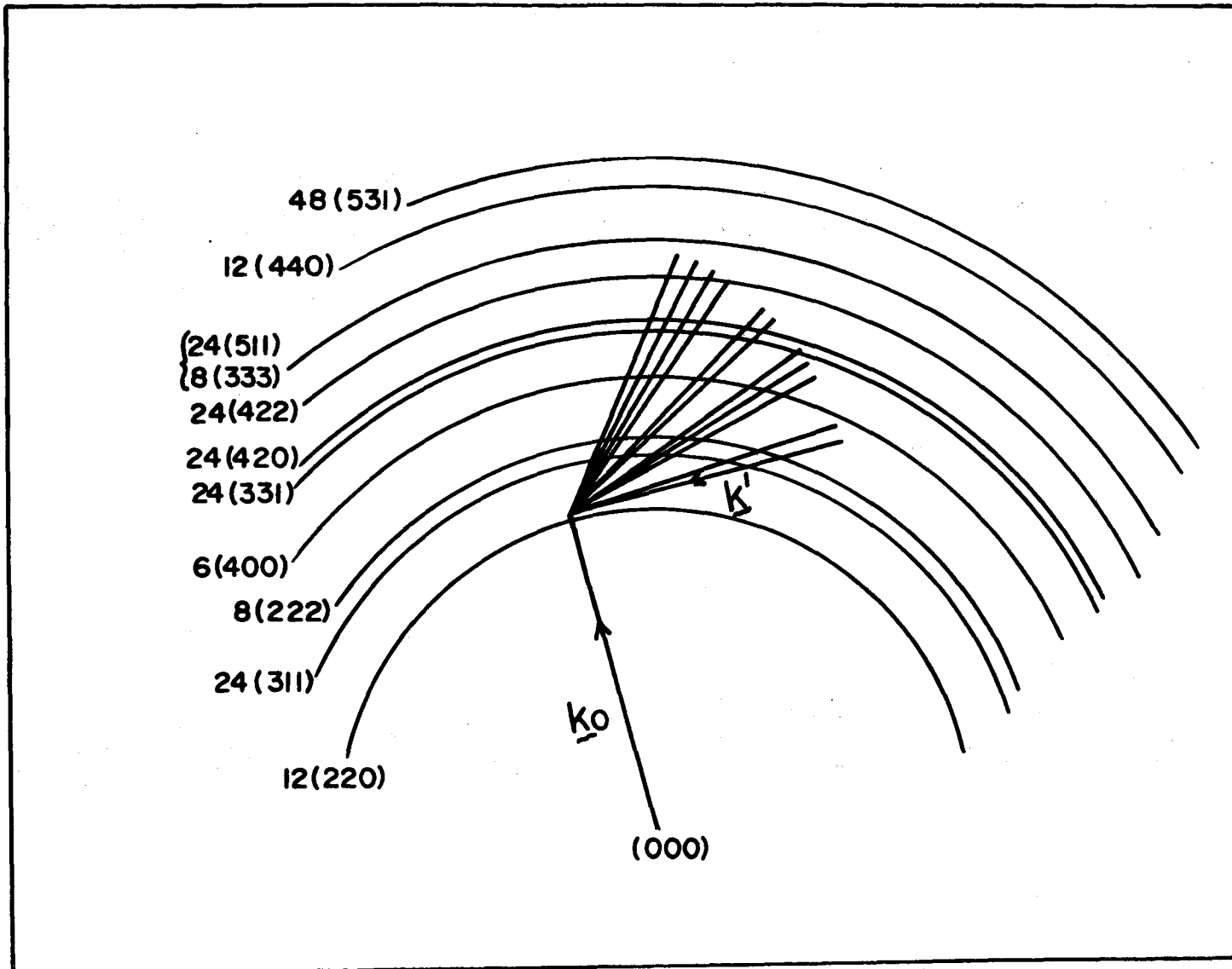


Fig. 4.31 A Schematic reciprocal space diagram showing the Debye-Scherrer lines (multiplicities are also indicated), \underline{k}_0 and \underline{k}' represent the incident and the scattered neutron wave-vectors respectively. The energy transfer corresponds to the main longitudinal peak of $g(\nu)$ in Pb.

H. Force Constant Disorder in Alloys

It was stated in Chapter II(F) that in alloys composed of different elements of similar mass, the neutron groups from coherent scattering are expected to be reasonably sharp and well defined. This is because the widths of the neutron groups involve products of pairs of deviations of force constants from their mean values and therefore are relatively insensitive to force constant disorder. This explains qualitatively the observation that for the binary alloys $\text{Pb}_{40}\text{Tl}_{60}$ and $\text{Bi}_{10}\text{Tl}_{90}$, the broadening caused by force constant disorder was very small (see section D and also Fig. A2.4). In this section, we describe the neutron scattering studies from the ternary alloy, $\text{Bi}_{20}\text{Pb}_{60}\text{Tl}_{20}$, for which the force constant disorder is found to be significantly larger.

It should be remarked here that force constant disorder also leads to a spreading of the singularities in the frequency distribution function $g(\nu)$, as was shown in Section G. The fact that the longitudinal peak in the frequency spectrum is relatively sharp makes it possible to observe the effect of the energy smearing.

Neutron Scattering from $\text{Bi}_{20}\text{Pb}_{60}\text{Tl}_{20}$

Fig. 4.32 shows the scattered neutron spectrum as a function of the energy transfer observed at the point $(a/2\pi)\underline{Q} = (222)$. Neutrons with incoming frequency of 5.45×10^{12} cps were used and the measurements were made at temperatures within five degrees of 100°K , with neutron energy loss, employing the Const-Q technique. Since the point of observation is a reciprocal lattice point, no coherent one-phonon process is expected. Hence, the observed intensity is mainly arising from the incoherent inelastic processes. However, Bi, Pb and Tl--the constituent elements of the alloy--all have negligible incoherent cross sections and the coherent cross-sections are almost identical. The fluctuation of the polarization vectors as a result of variation of the atomic

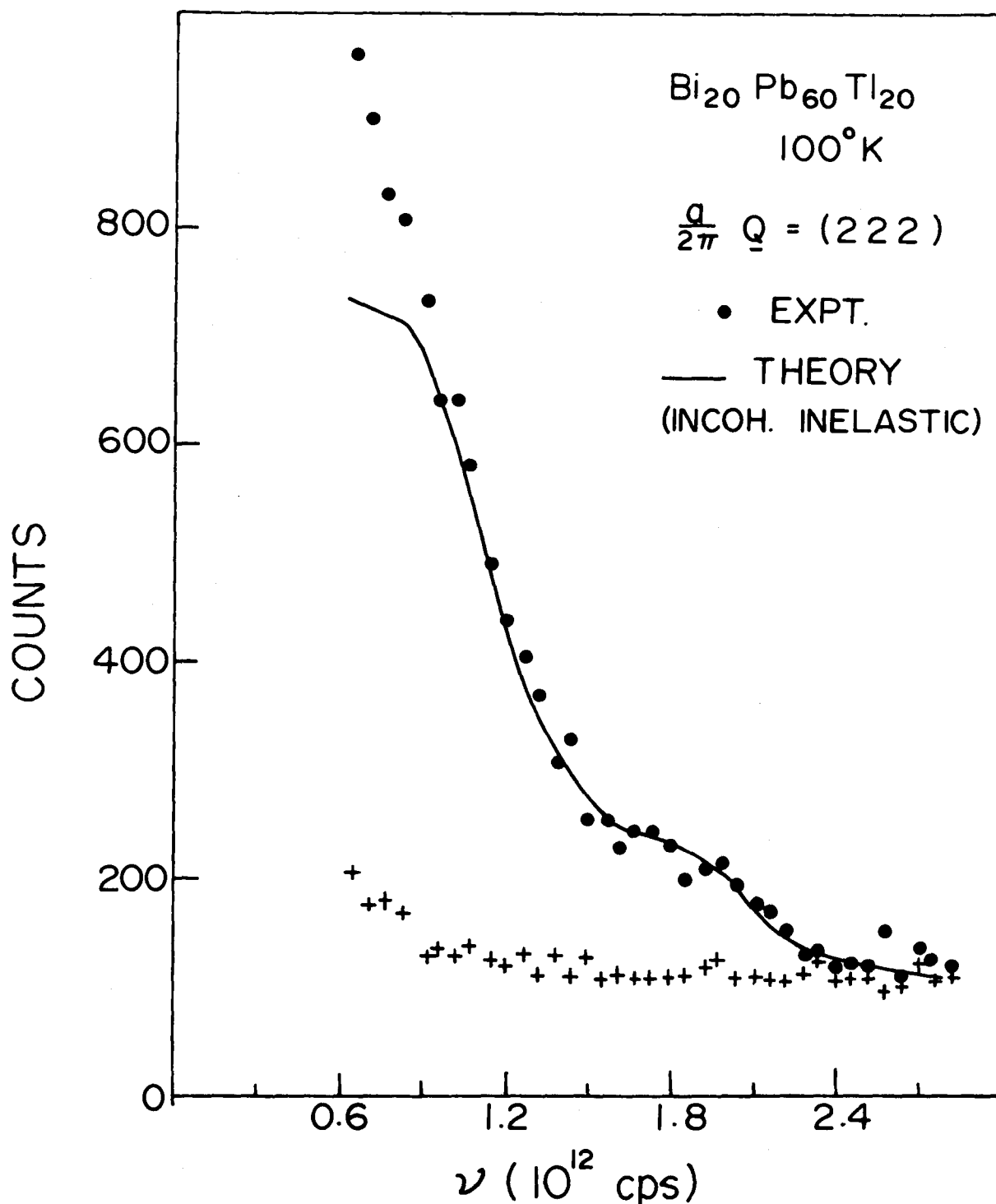


Fig. 4.32

Observed neutron spectrum at the reciprocal lattice point (222). The solid line represents a theoretical calculation of the inelastic spectrum (one phonon + two phonon) in the incoherent approximation, arbitrarily normalized to the tail region of the experimental spectrum.

force constants may be expected to give rise to an incoherent scattering from the system. It is fairly straightforward to calculate the one-phonon incoherent inelastic cross-section (Eq. (3.10)) using the smeared frequency spectrum shown in Fig. 4.33. The calculated curve (the effect of the analyzer sensitivity was taken into account--Appendix II) is shown in Fig. 4.32, arbitrarily normalized to the tail region of the experimental spectrum. The contribution of the two-phonon processes (coherent + incoherent) was estimated to be 10-15% of the one-phonon incoherent inelastic cross section. It is interesting to note that the longitudinal peak in $g(\nu)$ is reflected in the experimental spectrum as should be expected. In the region of small energy transfer, the departure of the experimental points from the calculated curve is marked. This may be partly spurious because of the contamination from the strong Bragg peak as evidenced by the observed rise in background also, in that region. It should be added here that since the specimen crystal was large ($\sim 50\%$ transmission) and the mosaic width (50' F.W.H.M.) was appreciable; multiple-event scattering processes also contribute to the observed spectrum. A typical pattern, for $(a/2\pi)\underline{Q} = (2.5, 2.5, 2.5)$ is shown in Fig. 4.34 (filled circles) for which only the $[\zeta\zeta\zeta]$ zone-boundary longitudinal phonon should appear. ($(\underline{Q}\cdot\underline{\xi})^2$ is zero for the transverse mode at the point of observation, see Eq (3.13).) However, a strong group appears at a frequency corresponding to the $[\zeta\zeta\zeta]$ zone-boundary transverse mode. This anomalous neutron group may be ascribed to a double scattering process

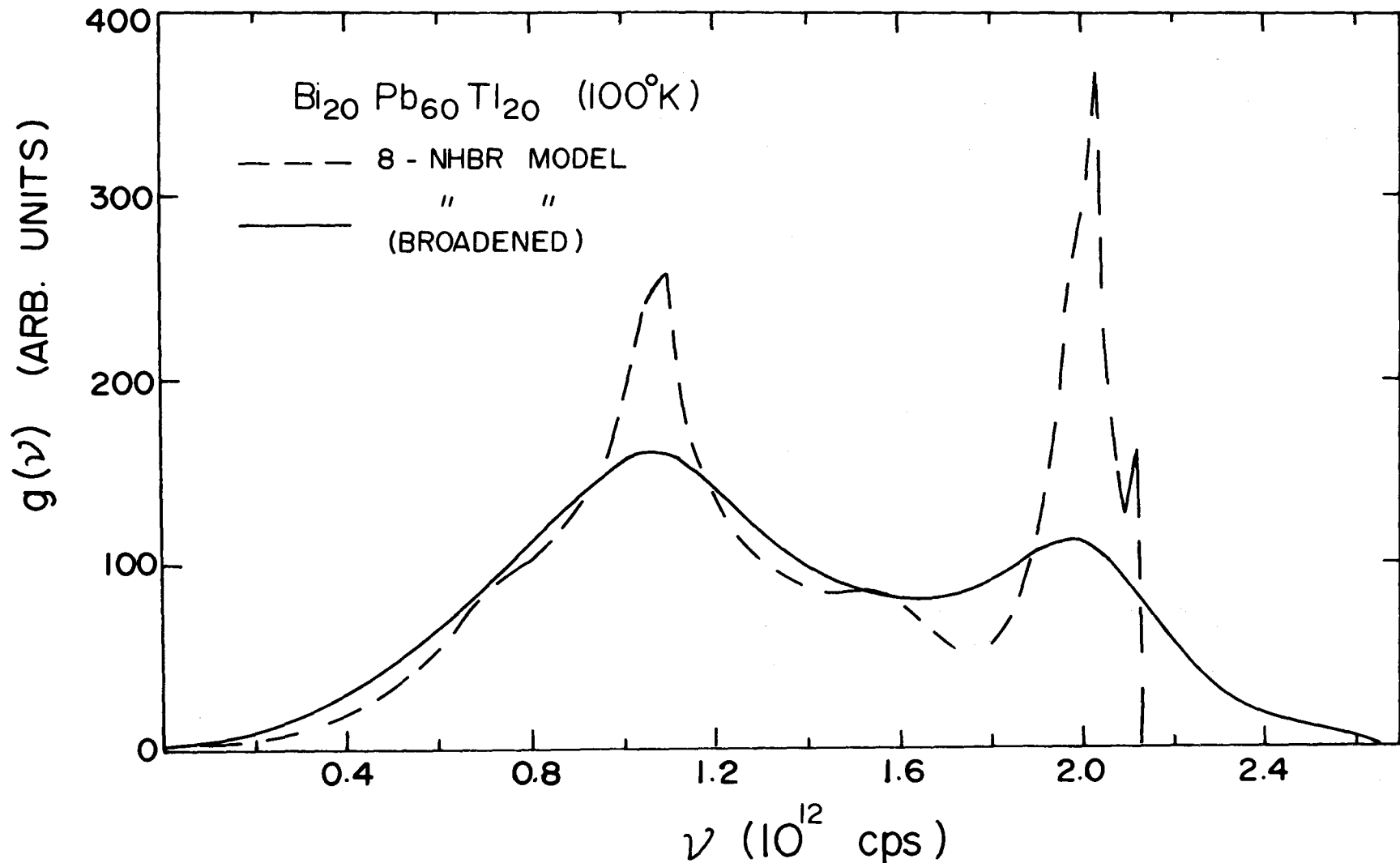
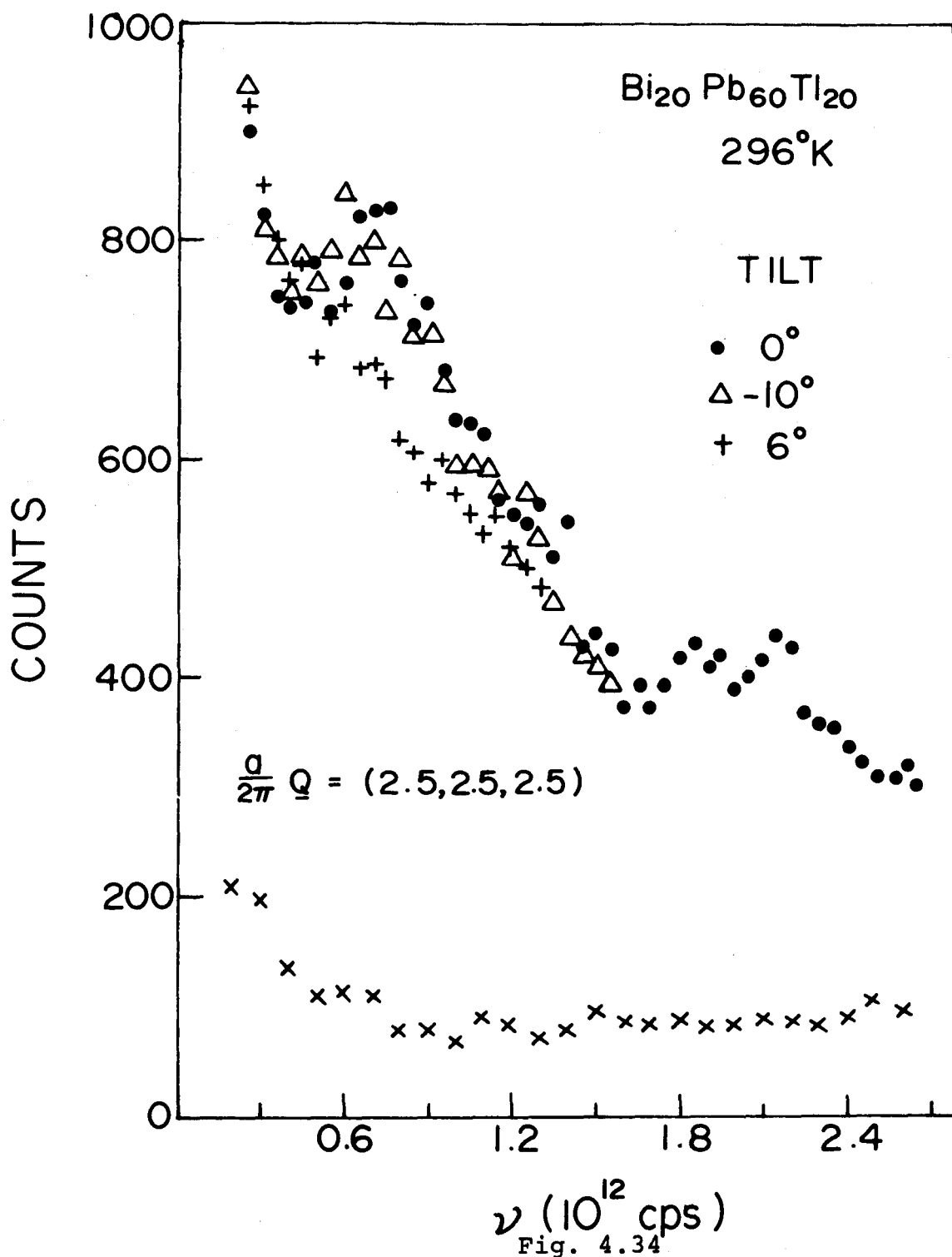


Fig. 4.33

The dashed line gives the frequency distribution function for $\text{Bi}_{20}\text{Pb}_{60}\text{Tl}_{20}$ at 100°K , calculated using an eight-neighbour force constant model. The solid line is obtained after a Lorentzian broadening of $\Delta\nu/\nu \approx 0.13$ (to simulate the energy smearing caused by force constant disorder in the alloy) and then folded with the resolution function of the spectrometer. Both the distributions are normalized to the same area.



Constant- \underline{Q} measurement at $\frac{2\pi}{a}(2.5, 2.5, 2.5)$ where only the longitudinal mode ($\nu \approx 2.07 \times 10^{12}$ cps) is expected to be excited. For 0° tilt, the $(1\bar{1}0)$ axis is vertical; the peak at $\nu \approx 0.8 \times 10^{12}$ cps is probably the transverse mode appearing as a result of multiple scattering processes. By rotating the crystal about the (111) direction which leaves the point of observation invariant, the peak disappears for a tilt of 6° .

(Brockhouse et al. 1962) in which the neutrons involved in the one-phonon group have been Bragg scattered before or after the single phonon scattering. Then, if \underline{k}'' is the neutron wave vector after the first scattering and \underline{k}' after the second scattering,

$$\underline{k}_0 - \underline{k}'' = \underline{G}_1$$

$$\underline{k}'' - \underline{k}' = \underline{G}_2 - \underline{q}$$

Adding we have

$$\underline{k}_0 - \underline{k}' = (\underline{G}_1 + \underline{G}_2) - \underline{q} = \underline{G}_3 - \underline{q}$$

since the sum of two reciprocal lattice vectors \underline{G}_1 and \underline{G}_2 is itself a reciprocal lattice vector.

On the other hand,

$$E_0 - E' = \hbar v_j(\underline{q})$$

Therefore, the reduced wave-vector \underline{q} is not changed but the position in reciprocal space at which the neutron group is observed is changed. Thus, the intensities need no longer satisfy the one-phonon theoretical expression as to polarization dependence. To demonstrate experimentally the influence of Bragg scattering, we also show in Fig. 4.34 the patterns obtained after rotating the crystal about the (111) axis which lies in the plane defined by the incident and the final scattered neutron wave vectors \underline{k}_0 and \underline{k}' respectively. By this procedure, the point of observation (2.5,2.5,2.5) remains unaltered, always lying in the plane of \underline{k}_0 and \underline{k}' . However, the relative orientations of the Bragg planes with respect to \underline{k}_0 and \underline{k}' are changed and hence also the probability of Bragg

scattering. It is seen, for example, that for a tilt of 6° the transverse peak is virtually absent. However, for a tilt of -10° (the minus sign simply indicates that the tilt was applied in a sense opposite to the previous one) the transverse peak reappears. Consideration of the probability of occurrence of the double scattering leads to the conclusion that the process may be the rule rather than the exception for large crystals which are efficient Bragg scatterers (Brockhouse et al. 1962).

Damping of Phonons caused by Disorder

It was mentioned earlier that the presence of force constant disorder in alloys leads to the damping of phonons, although, for the binary alloys, the damping is relatively small. Considerable broadening of the neutron groups beyond the resolution of the instrument is observed in $\text{Bi}_{20}\text{Pb}_{60}\text{Tl}_{20}$ which implies the existence of significant force constant disorder in this ternary alloy. Fig. 4.35 shows the neutron groups in $\text{Pb}_{80}\text{Tl}_{20}$ and $\text{Bi}_{20}\text{Pb}_{60}\text{Tl}_{20}$ for the $[\zeta\zeta\zeta]$ zone-boundary modes at 100°K . The resolution widths (incident neutron frequency $\sim 5.8 \times 10^{12}$ cps) may be calculated easily at these points ($\nabla_{\underline{q}}\nu=0$) since the focussing characteristics of the spectrometer need not be considered; the effect of the mosaic spread of the specimen also can be neglected. The instrumental widths were estimated to be about 85% of the widths of the neutron groups observed for $\text{Pb}_{80}\text{Tl}_{20}$. The natural line width of the phonon was obtained by finding the width of the Lorentzian curve that must be convoluted with the

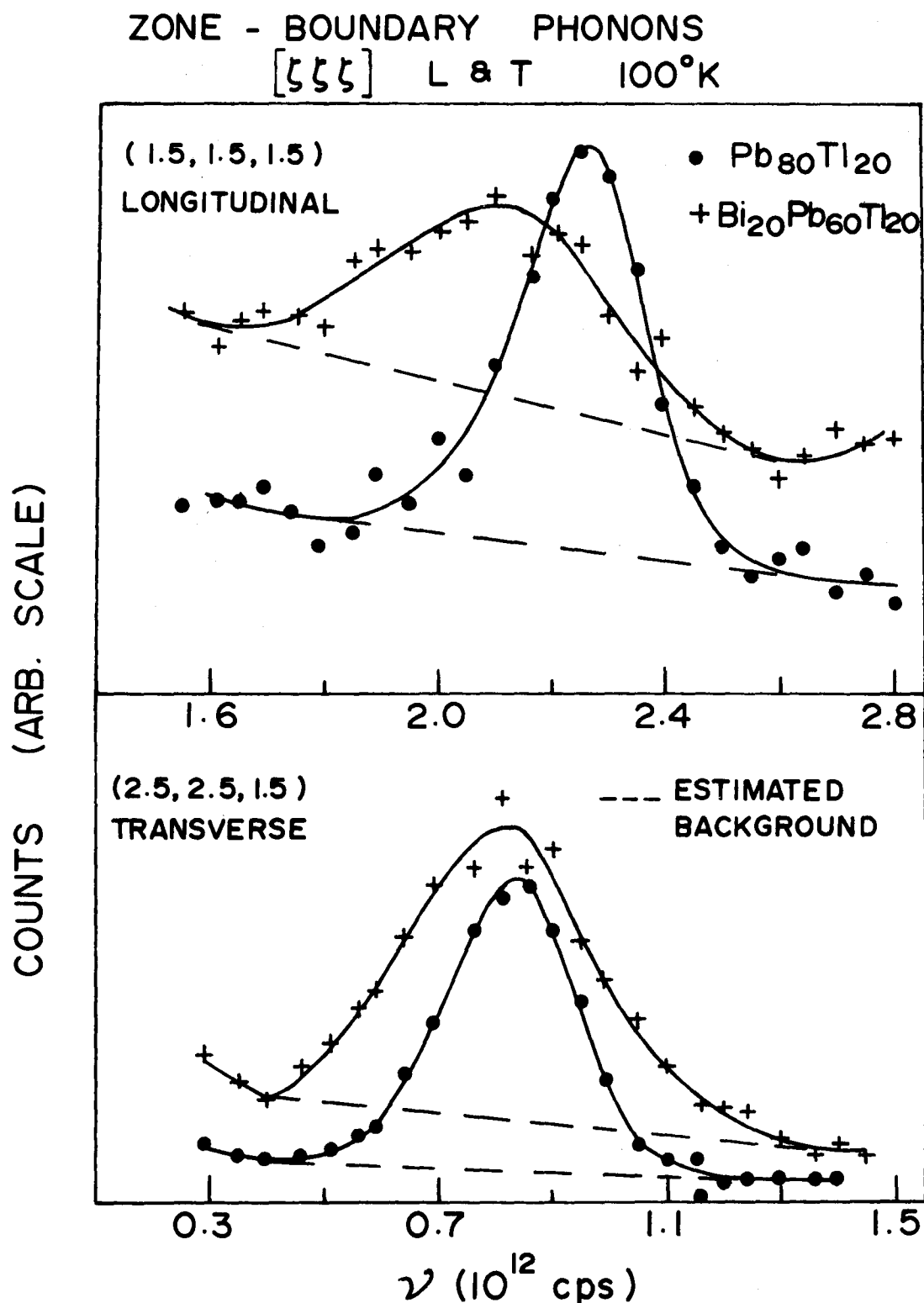


Fig. 4.35

Comparison of neutron groups in Pb₈₀Tl₂₀ and Bi₂₀Pb₆₀Tl₂₀. This figure illustrates significant broadening, present in the ternary alloy, caused by force constant disorder.

resolution function (assumed to be Gaussian) so as to give the observed width. The extracted width contains a small contribution from the anharmonic broadening present at 100°K which is probably less than the uncertainty introduced by the deconvoluting process. We give in Table 4.10 the phonon widths (F.W.H.M.), corrected for resolution, for the zone boundary points X and L.

It is also interesting to study the dependence of the phonon broadening as a function of the phonon wave vector \underline{q} . We show in Fig. 4.36 the phonon widths along the symmetry direction $[\zeta 00]$ for the transverse mode. The instrumental widths were calculated following Cooper and Nathans (Appendix II). The effect of mosaic structure of the specimen crystal on the width of the neutron group was also taken into account. The contribution from the mosaic structure can be written as $\eta(\nabla_{\underline{q}} \nu \times \underline{Q})$ where η is the mosaic spread. For longitudinal phonons this contribution can be small because it is possible to choose \underline{Q} along a symmetry direction but for transverse phonons (particularly if $\text{grad}_{\underline{q}} \nu$ is large) it may be appreciable.

We find in Fig. 4.36 that for small wave vectors, the phonons are relatively sharp. It also follows from Eq. (2.42) that $\Delta\nu$ approaches zero as \underline{q} tends to zero; it is perhaps intuitively obvious that sound waves should propagate freely in the continuum limit. For the short wavelength phonons, the lifetime is quite short. If we define the lifetime as $\tau = \hbar/\Gamma$ where Γ is the energy width then at zone-boundary the lifetime is only about half the period of vibration!

Table 4.10

Phonon widths (F.W.H.M.) for the zone-boundary modes in $\text{Bi}_{20}\text{Pb}_{60}\text{Tl}_{20}$ at 100°K , obtained after correction for resolution widths

	$(\frac{a}{2\pi})\underline{Q}$	Polarization	Frequency	Phonon Width (± 0.10)
[$\zeta\zeta\zeta$]	(1.5,1.5,1.5)	Longitudinal	2.14	0.36
	(2.5,2.5,1.5)	Transverse	0.78	0.25
[$\zeta 00$]	(0.0,0.0,3.0)	Longitudinal	2.05	0.31
	(2.0,1.0,0.0)	Transverse	0.91	0.31

(units 10^{12} cps)

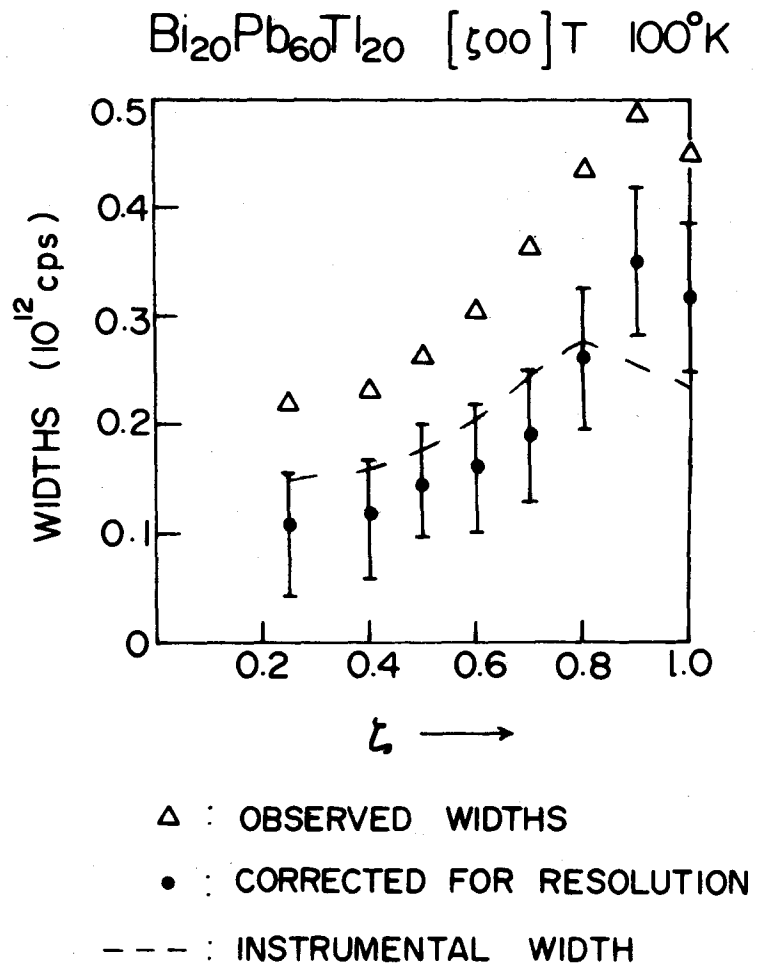
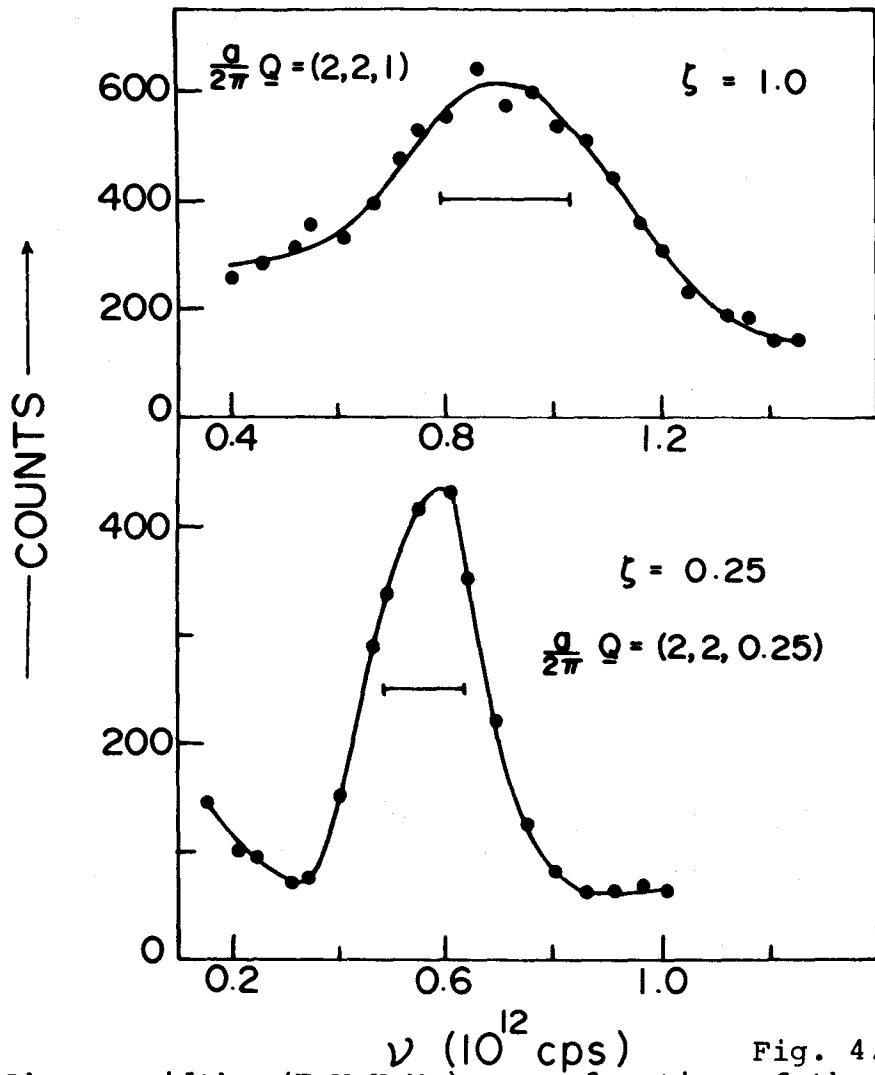


Fig. 4.36 Phonon widths (F.W.H.M.) as a function of the wave-vector along the [$\zeta 00$]T branch in $\text{Bi}_{20}\text{Pb}_{60}\text{Tl}_{20}$. Typical neutron groups are shown--the corresponding resolution widths are also indicated.

An estimate of force constant disorder at the zone-boundary can be made from Eq. (2.42). The contribution from the second neighbours vanishes by symmetry ($(\exp i(\underline{q} \cdot \underline{R}^{\ell}) - 1) = 0$) and we may assume that the contribution from the distant neighbours is negligible. Further, since the polarization vectors are fixed by symmetry ($[\zeta 00]$ direction), we arrive at the simple result

$$\frac{\Delta v}{v} \sim \frac{3\pi v g(v)}{2 \int g(v) dv} \left(\frac{\Delta \phi}{\phi}\right)^2$$

This expression yields a force constant disorder of $\sim 30\%$.

Before concluding this chapter mention should be made of the recent tunneling work in the alloy system $\text{Bi}_x\text{Pb}_{1-2x}\text{Tl}_x$ (Dynes and Rowell 1969). The product function $\alpha^2(v)g(v)$ was determined experimentally for the ternary alloys where $\alpha^2(v)$ is a measure of the electron-phonon coupling strength and $g(v)$ is the frequency distribution function. It was found that the calculated $\alpha^2(v)g(v)$ function (in the absence of force constant disorder) with a Lorentzian broadening of $\Delta v/v = 0.16$ agrees with the experimentally determined distribution for $\text{Bi}_{20}\text{Pb}_{60}\text{Tl}_{20}$. Considering the fact that this smearing is somekind of an average over the frequency distribution function, the above value of phonon broadening is not in disagreement with the values we presented before from a study of the line-shapes of the coherently scattered one-phonon neutron groups. They (Dynes and Rowell) also calculated the frequency spread Δv as a function of v from Eq. (2.42) by averaging over \underline{q} . The calculated phonon width in the longitudinal region is larger by a factor of three compared with that in the transverse region. However, we note from Table 4.10 that the

zone-boundary longitudinal and transverse modes have similar energy broadening. It is doubtful, if for a highly disordered system, like $\text{Bi}_{20}\text{Pb}_{60}\text{Tl}_{20}$, such a simple perturbation calculation, as carried out by these authors using the density of states appropriate to the unperturbed crystal, is valid.

APPENDIX I

Lattice Constant Measurements and Characterisation of the Specimen

Characterisation of large alloy single crystals by neutron diffraction has been discussed by Ng, Brockhouse and Hallman (1966). Because of large area, the neutron beam essentially samples the whole crystal and therefore measurement of lattice constant specifies the composition if variation of the lattice constant with composition for an alloy system is known from other methods (e.g. X-ray diffraction). Fig. A-1.1 shows a plot of lattice constant variation with composition for the Bi-Pb-Tl system as determined by X-ray methods (Pearson 1958).

The lattice constant of an alloy is determined by running a family of rocking curves for a given lattice plane of the specimen at different closely spaced scattering angles. A plot of the peak intensity for each rocking curve vs the scattering angle establishes the scattering angle for the Bragg condition. For calibration purposes, a similar procedure is carried out on a single crystal of a pure metal whose lattice constant is close to that of the alloy. The lattice constant of the alloy is then given by

$$a_A = a_M \frac{\sin(\phi_M/2)}{\sin(\phi_A/2)}$$

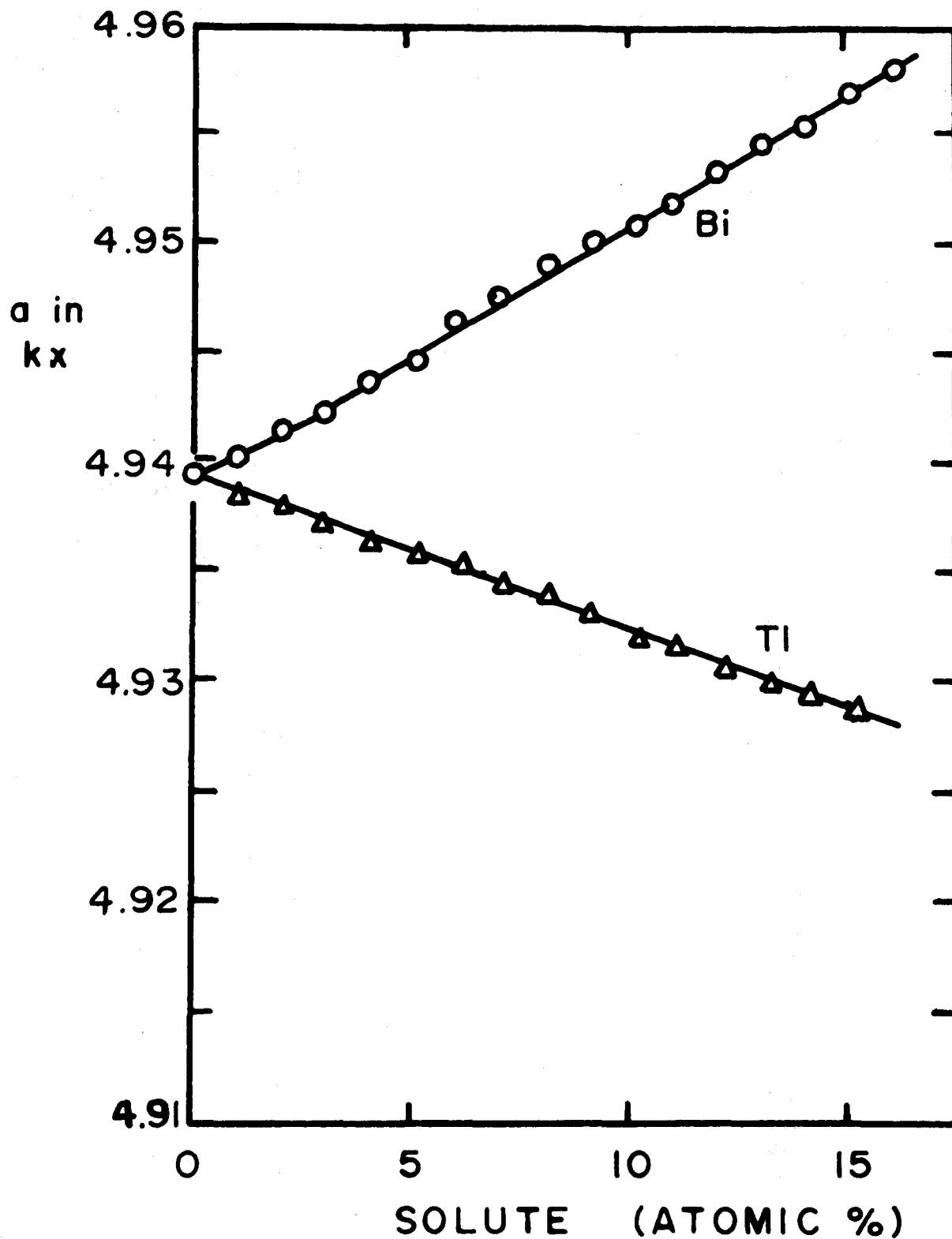


Fig. A1.1

Lead solutions (Pb-Tl and Pb-Bi) lattice spacing at 20°C. (After Pearson (1958).)

where ϕ_A and ϕ_M are the scattering angles of the alloy and pure metal respectively and a_M is the accurately known lattice constant of the pure metal. Further, inhomogeneity of the alloy crystal can be estimated from the broadening observed in the plot of peak intensity vs scattering angle in comparison to that for pure metals.

The alloy crystals described here were cylindrical, $1\frac{1}{4}$ " in diameter and roughly $3\frac{1}{2}$ " long. Preliminary results on the characterisation of these alloys were published by Ng et al. (1966) and subsequently improved data were reported by Ng (1967). The results presented here were obtained more recently using the McMaster Triple axis spectrometer (E2) at Chalk River under high resolution.

Copper (220) was used as the monochromator and $2\theta_M$ was about 125° . Soller collimators having a horizontal divergence of 0.18° FWHM were placed both in the incident and the scattered beam. Quartz (300) was used as the analyser because it has a very narrow mosaic width ($4'$ FWHM). $2\theta_A$ was 107° thus almost matching the energy resolution of the incident beam. (400) reflections were employed for the alloys and the scattering angles were in the range of 130 - 140° . Resolution widths were determined by measuring Cu(220), Ni(220), Pb(400) and Mg(202) reflections. Lattice constant of lead was used as the standard for calibration.

A typical family of rocking curves for $\text{Bi}_{10}\text{Tl}_{90}$ (400) is shown in Fig. (A-1.2). Fig. (A-1.3) shows a plot of peak intensity vs lattice constant for the alloys and a plot of the observed width (FWHM) vs lattice plane spacing is given

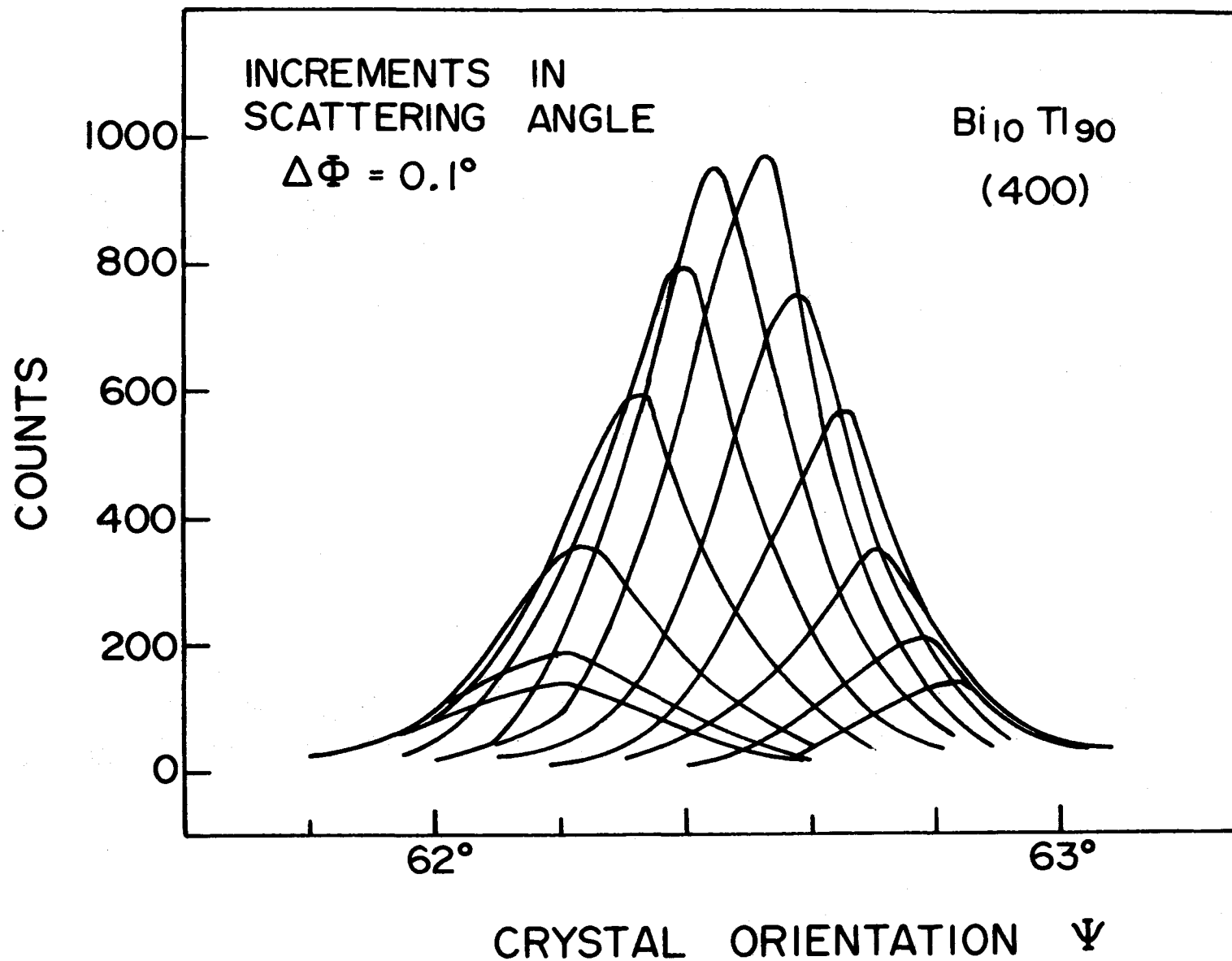


Fig. A1.2 A family of rocking curves for $\text{Bi}_{10}\text{Tl}_{90}$ -- (400) reflection.

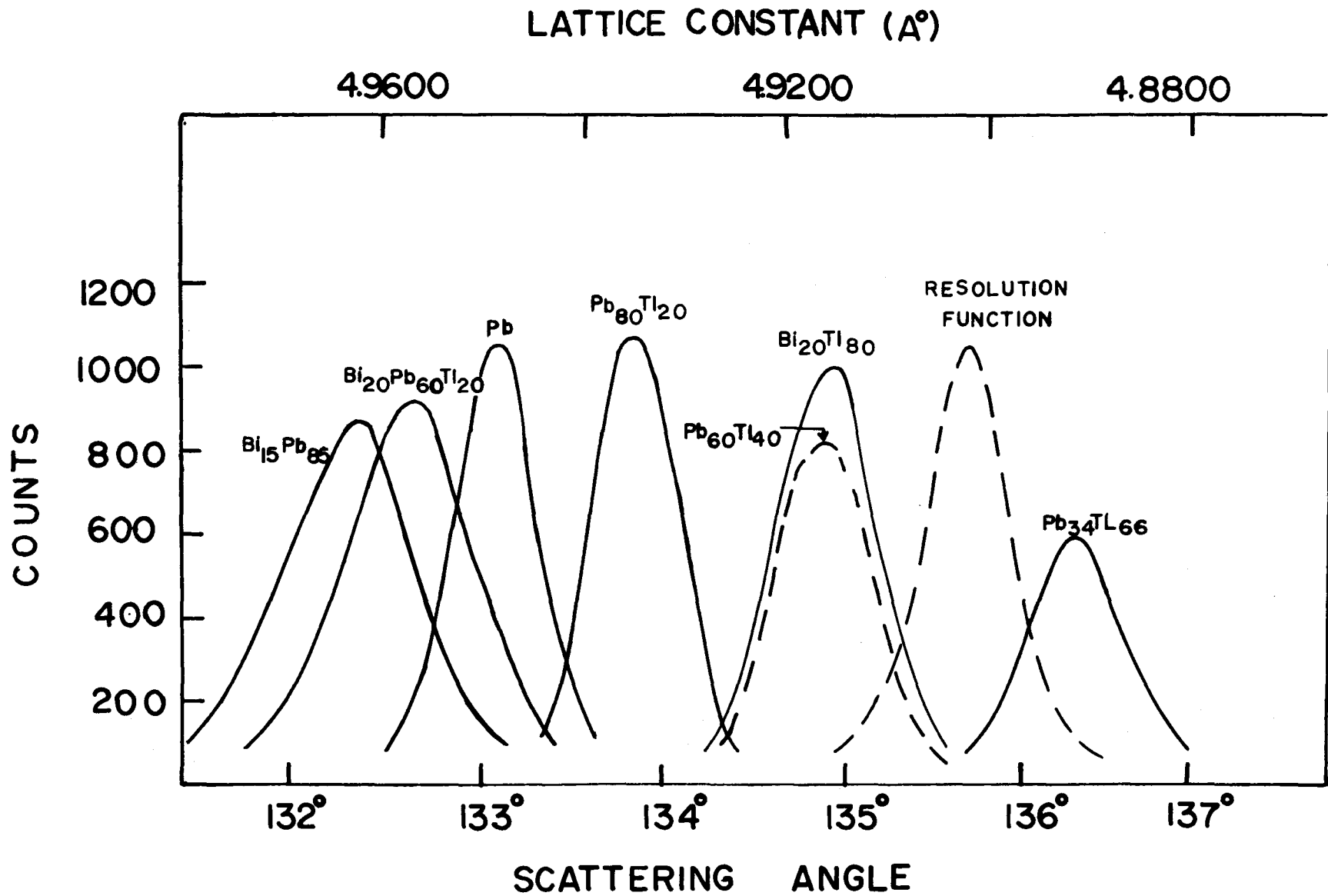


Fig. A1.3 Plots of the maximum intensity of the ψ rocking curves for some of the alloy crystals, as a function of the scattering angle.

in Fig. (A-1.4). It is clear from the plot that among the alloys $Pb_{80}Tl_{20}$, $Pb_{40}Tl_{60}$ and $Bi_{10}Tl_{90}$ are highly homogeneous. On the other hand $Bi_{15}Pb_{85}$, $Bi_{20}Pb_{60}Tl_{20}$ have appreciable inhomogeneity present whereas $Pb_{60}Tl_{40}$ and $Bi_{20}Tl_{80}$ fall inbetween.

The results of characterisation are tabulated in Table A-1.1. The X-ray results were interpolated from those given in the literature* (Pearson 1958). Average compositions were determined by comparing the present results with those in the literature for similar alloys. Inhomogeneity was estimated from the spread in the lattice constant.

It may be worthwhile mentioning here that $Bi_{15}Pb_{85}$ exhibited a width (FWHM) of $0,85^\circ$ (After taking out the resolution width) when the first set of measurements was carried out in Chalk River during Sept. 1967. In a subsequent measurement undertaken during July 1968, the same crystal showed a FWHM of 0.60° whereas other alloy crystals (which are comparatively older) exhibited more or less similar widths as observed in the previous measurement. It may be thought that at room temperature which is an appreciable fraction of the fusion temperature of the alloy ($\sim 500^\circ K$), considerable diffusion is going on inside the crystal thus reducing the inhomogeneity. In view of this, the $Bi_{15}Pb_{85}$ crystal was annealed in a furnace for two weeks, maintained at a temperature of $450^\circ K$. The crystal was then reexamined for any change in the width. No change was detected within the limits of the experimental accuracy.

* For the Bi-Tl alloys, an anomaly in the lattice parameter at about 14at.% Bi in Tl has recently been reported (Claesson and Ostklint 1970). The anomaly is very sharp and could have been easily missed in the present experiments.

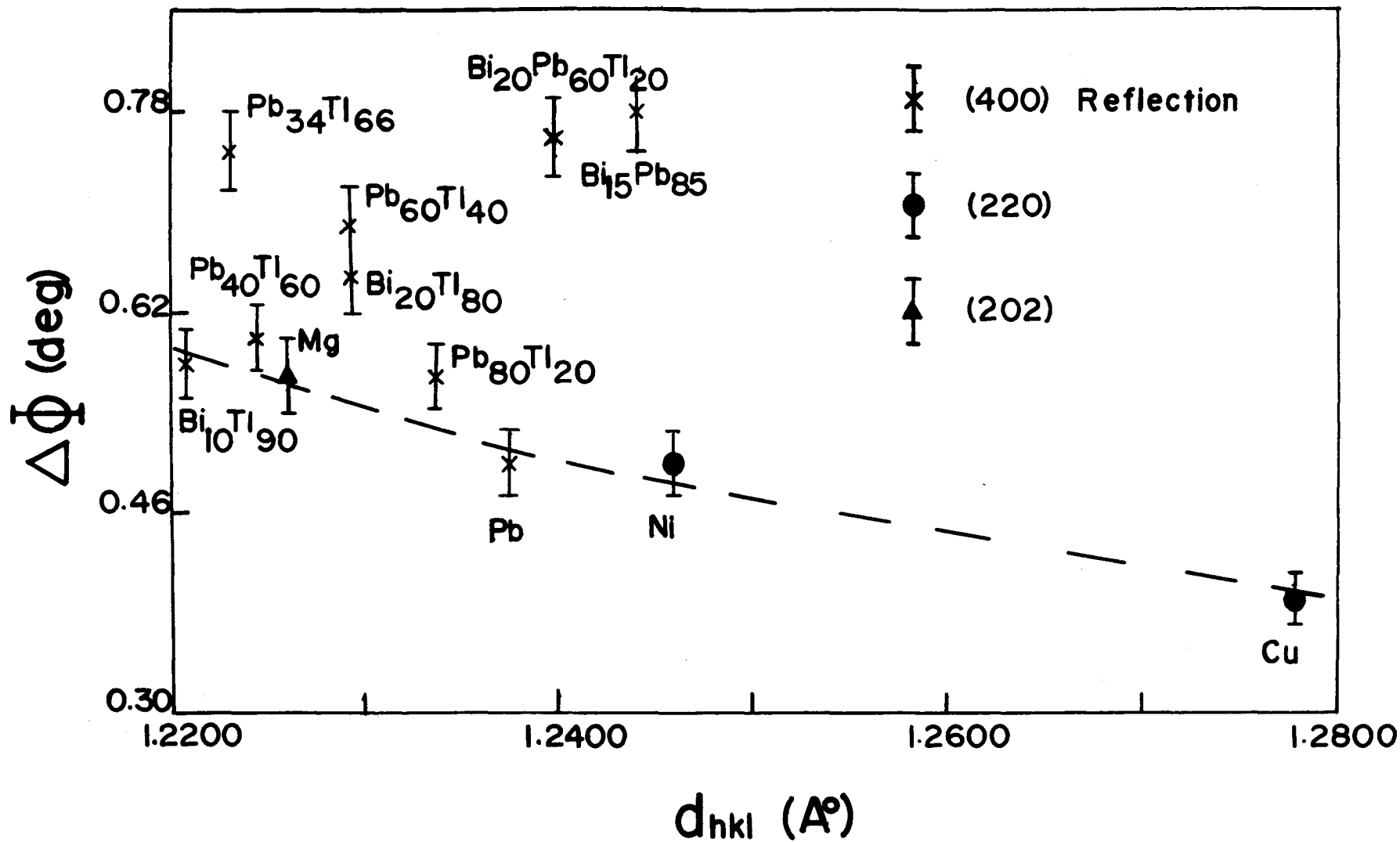


Fig. A1.4 Observed widths vs lattice plane spacing.

TABLE A 1.1

Nominal Composition	Average Lattice Const. (23°C)	Spread in Lattice Const. (+0.0014 Å°)	Average Composition (+0.5%)	Inhomogeneity (+1%)	Mosaic Width (FWHM)
Bi ₂₀ Pb ₆₀ Tl ₂₀	4.9585 Å°	0.0056 Å°	-	-	0.85°
Bi ₁₅ Pb ₈₅	4.9646	0.0057	12.5%Bi	+4.5%Bi	0.8 °
Pb ₈₀ Tl ₂₀	4.9345	0.0027	21 %Tl	+2.5%Tl	0.55°
Pb ₆₀ Tl ₄₀	4.9179	0.0040	42 %Tl	+3.5%Tl	0.75°
Pb ₄₀ Tl ₆₀	4.8986	0.0017	62 %Tl	+2 %Tl	0.5 °
Pb ₃₄ Tl ₆₆	4.8917	0.0048	67 %Tl	+3 %Tl	0.4 °
Bi ₁₀ Tl ₉₀	4.8816	0	88 %Tl	0	0.3 °
Bi ₂₀ Tl ₈₀	4.9170	0.0036	78.5%Tl	+1.5%Tl	0.4 °

Pure metal for calibration: Pb a = 4.9499 Å° (23°C)

Appendix II

Sensitivity function and the resolution function of
the triple-axis spectrometer.

Sensitivity function: As mentioned before, the bulk of the work described in this thesis was carried out using the McMaster University spectrometer installed at the NRU reactor, Chalk River. Since the experiments were done with fixed incoming energy and variable outgoing energy, it was necessary to apply corrections to the data to take into account the variation in the reflectivity of the analyzing crystal particularly if a wide range of energy transfer was covered. The sensitivity function was determined following an approach first used by Brockhouse (1958). In principle, the method consists in producing a Maxwellian spectrum and a comparison of this energy distribution as measured by the instrument with the theoretical spectrum.

Fig. A2.1 shows the measured spectra emitted from the interior of a large block of paraffin placed on the specimen table into which monoenergetic neutrons were incident. The triangles were obtained using incoming neutrons of frequency 5.85×10^{12} cps and the filled circles correspond to the frequency 16×10^{12} cps. The dips in the spectra arise from the simultaneous Bragg reflection processes in the analyzing crystal. The fact that the measured spectra agree quite well over a large energy range, indicates that the monochromatic neutrons were well thermalized in the paraffin block. The deviation in the high energy region is also understandable since the slowing down of the neutrons by the

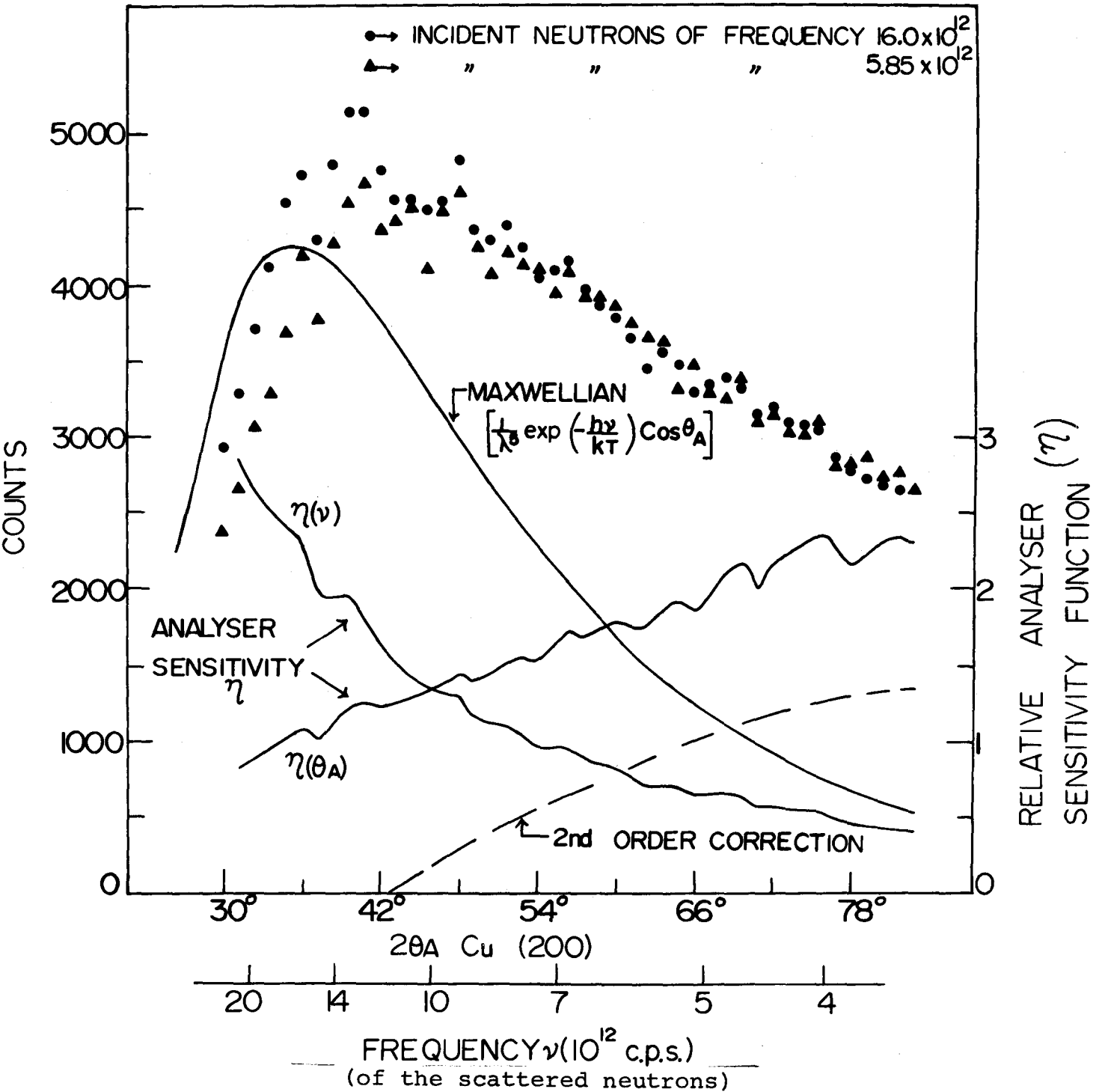


Fig. A2.1

Neutron spectra as measured after thermalization of monoenergetic neutron beams incident on a large paraffin block. Sensitivity function of the analyzing spectrometer obtained from these measurements is also shown.

moderator is relatively more efficient. (The energy distribution represented by the filled circles was used in the analysis.)

The experimental distributions shown in Fig. A2.1 consist of two spectra measured in the first and second orders of the analyzing crystal. The relative sensitivities of the analyzing crystal in the first and second order were calculated for several different energies (The author would like to thank Mr. R. Dymond regarding the computations. An experimental check on the calculation was also made from measurements on the elastic scattering of vanadium using the Cu(200) and Cu(400) reflections of the analyzer) and therefore, the correction to the measured spectrum arising from the second order component could be estimated. This is shown as the dashed line in Fig. A2.1. Finally, the instrumental sensitivity function ($\eta(\theta_A)$) is obtained by dividing the corrected spectrum by the assumed Maxwellian distribution. We also show the energy sensitivity function $\eta(v)$, defined by the relation,

$$\eta(v)dv = \eta(\theta_A)d\theta_A$$

$\eta(v)$ is the appropriate quantity while applying corrections to the data (for example, the distribution shown in Fig. 4.28) for the analyzer sensitivity.

Fig. A2.2 shows a comparison of the present work with the measurements of Dymond and Brockhouse (1970)*. In their

* To appear in the Proceedings of the Panel on Instrumentation for Neutron Inelastic Scattering Research, (IAEA, Vienna). The authors are thanked for permission to include their results.

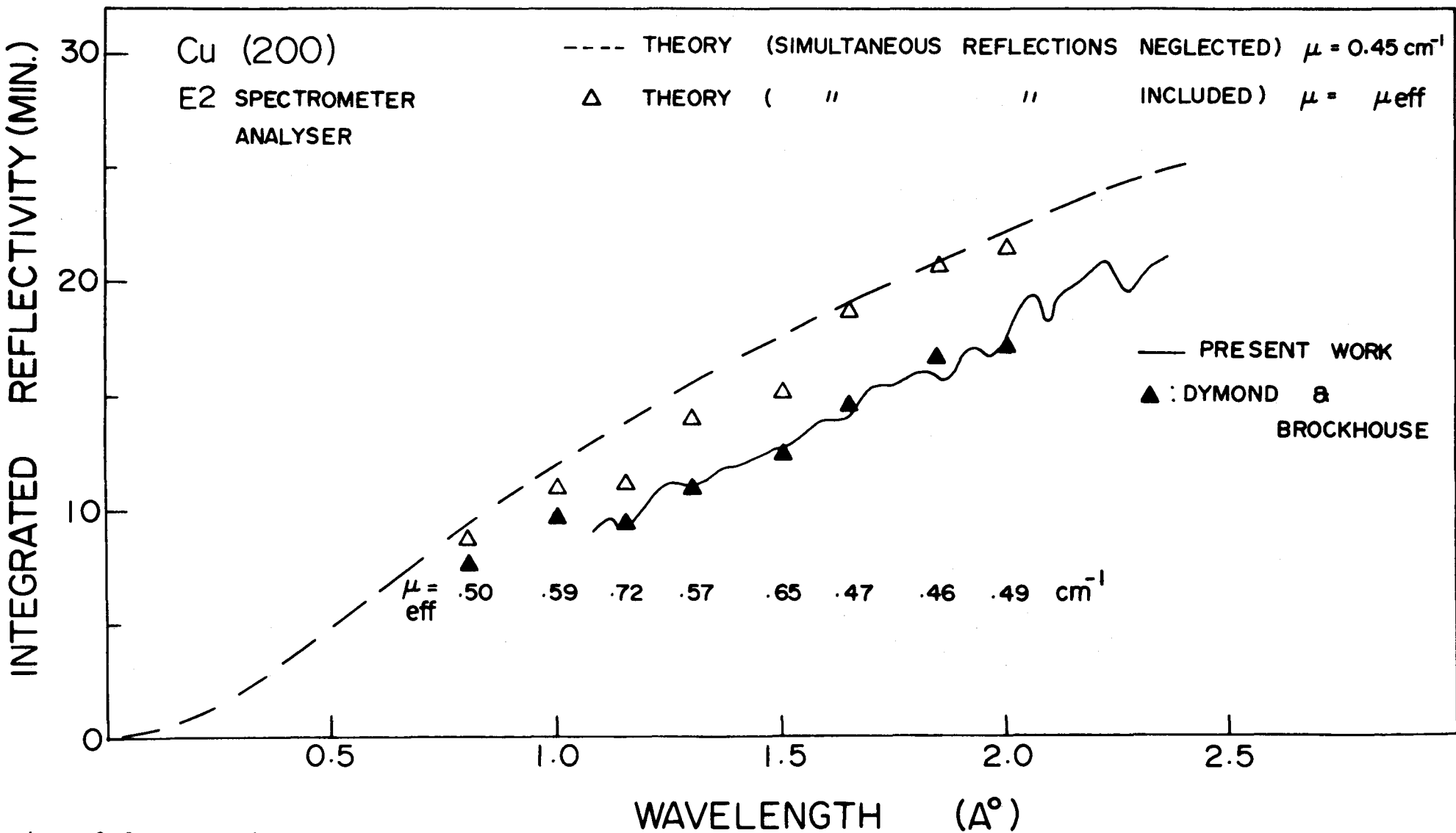


Fig. A2.2 Comparison of the present work with the experimental results and the theoretical calculations of Dymond and Brockhouse (1970); μ denotes the linear absorption coefficient of the analyzing crystal.

experiment, a Ge single crystal was used to obtain a monochromatic beam of neutrons which was then passed through an aperture into the analyzer. For several different wavelengths, the integrated reflectivities were measured by rocking the analyzing crystal. For comparison, the theoretical curves are also reproduced from their paper; in these calculations μ denotes the linear absorption coefficient.

Resolution function of the triple-axis spectrometer

We found in Chapter III that the coherent one-phonon process is governed by the energy and momentum conservation conditions (Eq. (3.8)). The presence of finite collimation in the spectrometer introduces a spread in the energy and momentum of the neutrons detected at the same setting. Accordingly, we may define the resolution function of the instrument as the probability of detection of neutrons as a function of $\Delta\omega$ and ΔQ when the instrument has been set to measure a scattering process corresponding to the point ω, Q .

The crystal spectrometers show some interesting but complicated focusing characteristics that make it difficult to calculate the line shapes of the neutron groups. Approximate treatment of the problem has been considered by Collins (1963), Peckham (1964), Bergsma and Van Dijk (1965) and by others. A more complete discussion has been recently given by Cooper and Nathans (1967). They have derived an analytic expression for the resolution function, $R(\omega, Q)$ assuming Gaussian mosaic and collimation function--the loci of constant probability are shown to be ellipsoids.

The observed intensity for a given scattering cross-section $\sigma(\omega, \underline{Q})$ can be expressed as (Cooper and Nathans(1967))

$$I(\omega, \underline{Q}) = \int R(\omega + \Delta\omega, \underline{Q} + \Delta\underline{Q}) \sigma(\omega + \Delta\omega, \underline{Q} + \Delta\underline{Q}) \Delta\omega \Delta\underline{Q} \quad (\text{A2.1})$$

For a Bragg reflection, $\sigma(\omega, \underline{Q}) \sim \delta(\omega) \delta(\underline{Q} - \underline{G})$. Therefore, by mapping the Bragg reflected intensities as a function of the settings of the spectrometer one can obtain the resolution function $R(\omega, \underline{Q})$ near a reciprocal lattice point and for essentially zero energy transfer*. Constant energy scans were made (for energies on both sides of the elastic scattering position $\omega=0$) along a symmetry direction which passed through a reciprocal lattice point (i.e. a Bragg reflection) of the specimen ($\text{Pb}_{40}\text{Tl}_{60}$). Plots of the frequency of the scan vs the \underline{q} values for which each peak has fallen to half of its maximum are shown in Fig. A2.3 corresponding to the transverse and longitudinal scans with respect to the lattice points (220) and (002) respectively. The "half-intensity contours" were calculated from the analytic expressions given by Cooper and Nathans**(1967) using the appropriate instrumental parameters (see Table A2.1). The good agreement obtained between the calculated and the experimentally determined resolution function gives confidence in calculating the resolution function at any point in ω, \underline{Q} space.

* Apparently, this was first suggested by Møller (Ph.D. thesis, Univ. of Copenhagen (1967)); see also Nielsen and Møller. 1968. Acta Cryst. A25, 547.

** The computations were done in the McMaster CDC-6400 computer. The author is grateful to Mr. A. Larose and Mr. J.R.D. Copley for the relevant computer programme.

TABLE A2.1

The instrumental parameters used in the calculation of the resolution function.

Horizontal mosaic spread (effective)		
of the monochromator (Cu(220))	~ 22'	(F.W.H.M.)
Horizontal mosaic spread		
of the analyzer (Cu(200))	~ 30'	(F.W.H.M.)
Collimations (F.W.H.M.):		
	Horizontal Collimation angle	Vertical Collimation angle
In-pile region	No Soller-slit collimation	
Monochromator to sample	~ 45'	~ 1°15'
Sample to analyzer	~ 45'	~ 3°
Analyzer to detector	No Soller-slit collimation	

The experimental results shown in Fig. A2.3 were obtained using neutrons with incoming frequency $\nu_0 = 5.8 \times 10^{12}$ cps (or $\omega_0 = 3.7 \times 10^{13}$ rad/sec).

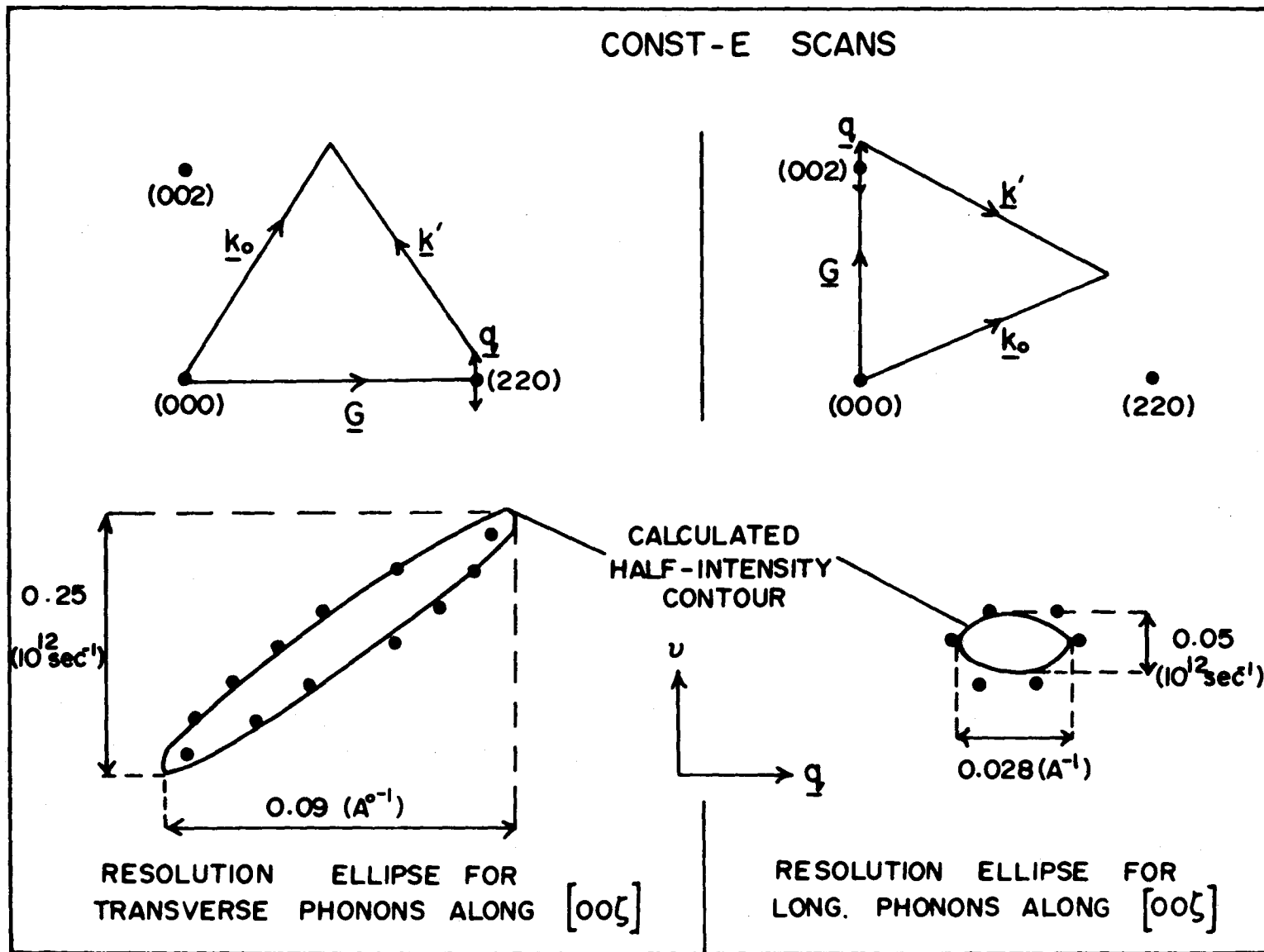


Fig. A2.3 Comparison between the calculated and the experimentally determined sections of the resolution ellipsoid. The correlation between v and q gives rise to the focusing effects.

Application to Phonon Measurements

The intensity corresponding to a one-phonon coherent scattering process for a given setting of the instrument $(\omega_0, \underline{Q}_0)$ is given by the convolution of the dispersion surface with the resolution function centred at $\omega_0, \underline{Q}_0$ (eq. (A2.1)). To simplify the calculation, the dispersion surface was assumed to be planar; the effect of the sample mosaic was also incorporated. It is seen from Fig. A2.3 that the resolution ellipsoid is extremely aspherical and it is this property which gives rise to the focusing effects. It is clear that if transverse phonons are measured from the lattice point (220) along the $[00z]$ symmetry direction then marked focusing or defocusing can occur depending on the relative orientation of the ellipse with respect to the dispersion surface. On the McMaster University spectrometer, installed at the NRU reactor, Chalk River, the transverse phonons are usually studied with \underline{q} in the anti-clockwise sense from a reciprocal lattice point to achieve the gradient focusing. Focusing effects are far less for longitudinal phonons with $\text{grad}_{\underline{q}} \nu$ along \underline{Q} . It also follows that the width of a phonon peak will depend on the type of scan in ω, \underline{Q} space used. The "Const- \underline{Q} " mode of scan was normally adopted. (Computer programs which produce punched cards to operate the spectrometer in the usual "Constant- \underline{E} " or "Constant- \underline{Q} " modes, were originally written by Dr. E.C. Svensson for the triple-axis spectrometer at the McMaster reactor. They have been modified, including changes required for use on the Bendix G20 and CDC-6600 computers at Chalk River, by Mr. J.R.D. Copley and also by Mr. A. Larose.) Comparison of

the calculated line shape* with the measured one-phonon neutron groups at 100°K in $\text{Pb}_{40}\text{Tl}_{60}$ and $\text{Bi}_{10}\text{Tl}_{90}$ showed good general agreement. However, in almost all the cases, the calculated line widths were found to be 80-90% of the observed widths. This difference can be attributed, at least partly, to the presence of the anharmonic and disorder broadening in the experimental neutron groups. In view of the above agreement it was felt that the computed line widths may be used in analyzing the observed widths of the neutron groups. This approach was used to obtain the anharmonic line broadening in $\text{Pb}_{40}\text{Tl}_{60}$ at 296°K (Chapter IV (D)) and in the investigation of the broadening caused by force constant disorder in $\text{Bi}_{20}\text{Pb}_{60}\text{Tl}_{20}$ (Chapter IV (H)).

Energy Resolution of the Spectrometer

We have, so far, considered the resolution function of the spectrometer as a function of the energy transfer ω and momentum

* In these calculations, it was assumed that the component of \underline{Q} normal to the scattering plane is not correlated with the other two components of \underline{Q} , or with ω . In other words, we consider the resolution function in three dimensions, that is, the energy transfer ω and momentum transfer in the scattering plane. This assumption is a good one if measurements are made in the mirror plane of the crystal and if the curvature of the dispersion surface is small. If the two branches of a dispersion curve are degenerate along a symmetry direction but split for any adjacent wavevector (eg $[\zeta\zeta\zeta]$ T branch) then relaxed vertical collimation may lead to broadened or double neutron groups (Cowley, E.R. and Pant, A.K. 1969. (To be published)). Spurious neutron groups have also been observed in Na and Rb along the $[00\zeta]$ symmetry direction where the longitudinal and the transverse branch are very close and have similar origin (Copley, J.R.D. Private communication).

transfer Q . In the study of line widths and line shapes involving incoherent scattering (also the powder experiment described in Chapter IV (G)) or for lines for which $\text{grad}_{\underline{q}} v=0$, the dependence of the resolution function on Q can largely be ignored. This makes it rather simple to estimate the resolution width as a function of the energy transfer.

The instrumental width corresponding to the zero energy transfer is determined by using an incoherent scatterer (for example, vanadium). The energy resolution of the monochromatic beam may be expressed as (here all width factors refer to widths at half-maximum)

$$\left(\frac{\Delta E_M}{E_0}\right) = 2(\text{Cot}\theta_M(\alpha^2 + \eta^2))^{1/2} \quad (\text{A2.2})$$

where, E_0 (or ν_0) : Incident neutron energy (or frequency)

θ_M : Monochromator angle

α : Horizontal collimation in the incident beam

η : Mosaic width of the monochromator

The resultant width of the instrument may be taken as the convolution (in Gaussian approximation) of the widths contributed by the monochromator and the analyzer. The energy width of the analyzing system corresponding to the elastic scattering (denoted by $\Delta E_A(E_0)$) may, therefore, be obtained from the measured elastic width and Eq. (A2.2). Since the experiments are usually done with neutron energy loss employing fixed incoming energy, ΔE_M remains constant. However, ΔE_A decreases with energy transfer (energy loss) and this may be estimated from $\Delta E_A(E_0)$ using the known dependence on $\text{Cot}\theta_A$. Finally, the energy resolution of the spectrometer at a given energy transfer is obtained by adding (root mean squares) ΔE_M and ΔE_A

The result of such a calculation is shown in Fig. A2.4 as the solid line. For comparison, the observed widths of some zone-boundary neutron groups (gradient focusing is absent for these phonons) are also shown. It may be mentioned here that the energy resolution calculated using the Cooper-Nathans programme (setting $\text{grad}_{\mathbf{q}} v=0$) agreed quite well with the simple calculation presented here.

- : VANADIUM ELASTIC ($\nu_0 = 5.85 \times 10^{12}$ cps)
 - : Pb
 - ▲ : Pb₄₀Tl₆₀
 - + : Bi₁₀Tl₉₀
- } Observed neutron groups at 100°K
 [500] T & L ZONE-BOUND. ($\nabla_{\mathbf{q}} \nu(\mathbf{q}) \sim 0$)

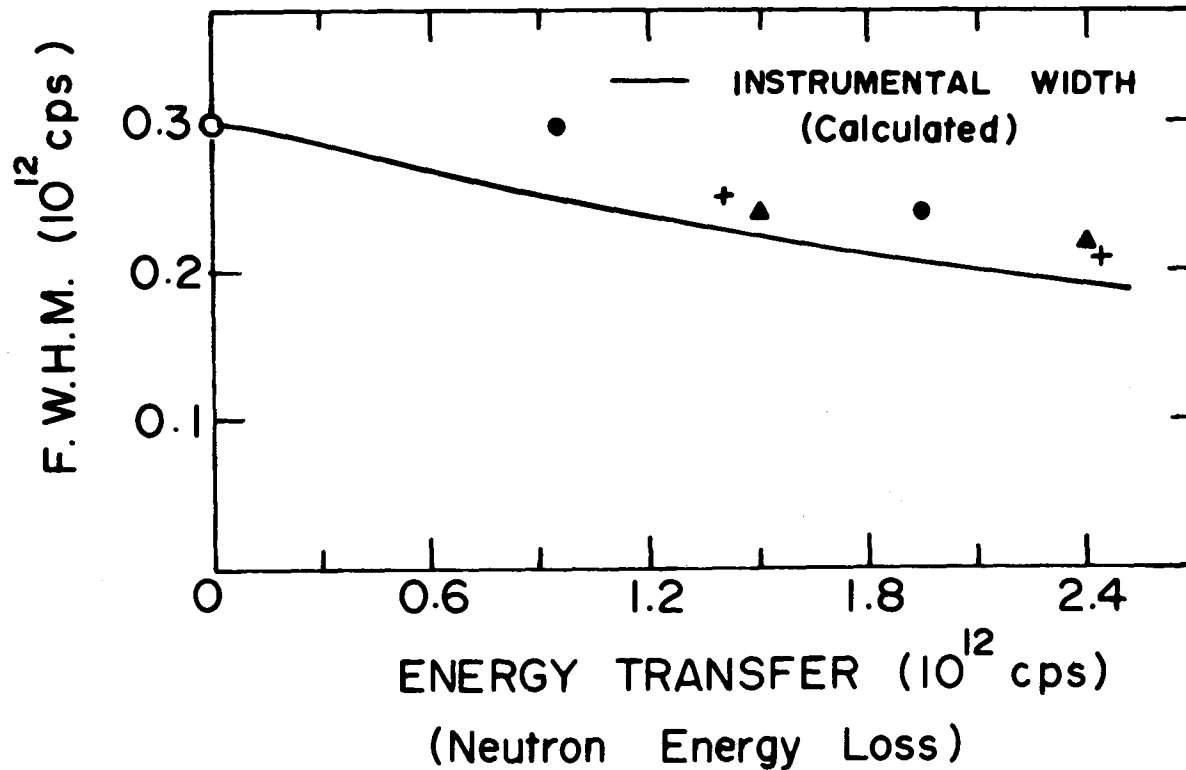


Fig. A2.4 Energy resolution of the Chalk River spectrometer for $2\theta_M \sim 92^\circ$ (Cu(220) monochromator and Cu(200) analyzer). Gradient focusing is not considered in the calculation. Widths of typical neutron groups at 100°K corresponding to the zone-boundary phonons are also plotted for comparison.

APPENDIX III

Temperature variation of the frequency of longitudinal inter-planar oscillations in pyrolytic graphite

The temperature dependence of the zone-boundary longitudinal phonon frequency, propagating along the hexad axis in pyrolytic graphite, has been studied by neutron spectrometry over a range of 200° to 900°K. The measurements were made using the McMaster University triple-axis spectrometer, at the NRU reactor at Chalk River (Brockhouse et al. 1968). The pyrolytic graphite specimen consisted of a square sheet of approximately 2" on edge and 3/8" thick. The sample used has a mosaic spread about the hexad axis of approximately 10°, F.W.H.M.; it is commercial material obtained from the General Electric Company.

The temperature of the specimen was measured by an iron-constantan thermocouple. An internal check on the temperature scale was provided by measuring the lattice constants (Ng et al. 1967) at two different temperatures. Fig.A3.1 shows plots of the maximum intensity of the crystal rocking curves for the (008) reflection as a function of scattering angle. From the observed peak shift of $\Delta\phi = 2.52^\circ$, the temperature difference with respect to the room temperature (296°K) is given by $\Delta T \sim \frac{1}{\alpha} (\cot \frac{\phi}{2}) (\frac{\Delta\phi}{2}) \sim 384^\circ\text{K}$ where α , the coefficient of linear expansion along the hexagonal direction is taken as $28 \times 10^{-6} \text{ deg}^{-1}$. The probable error

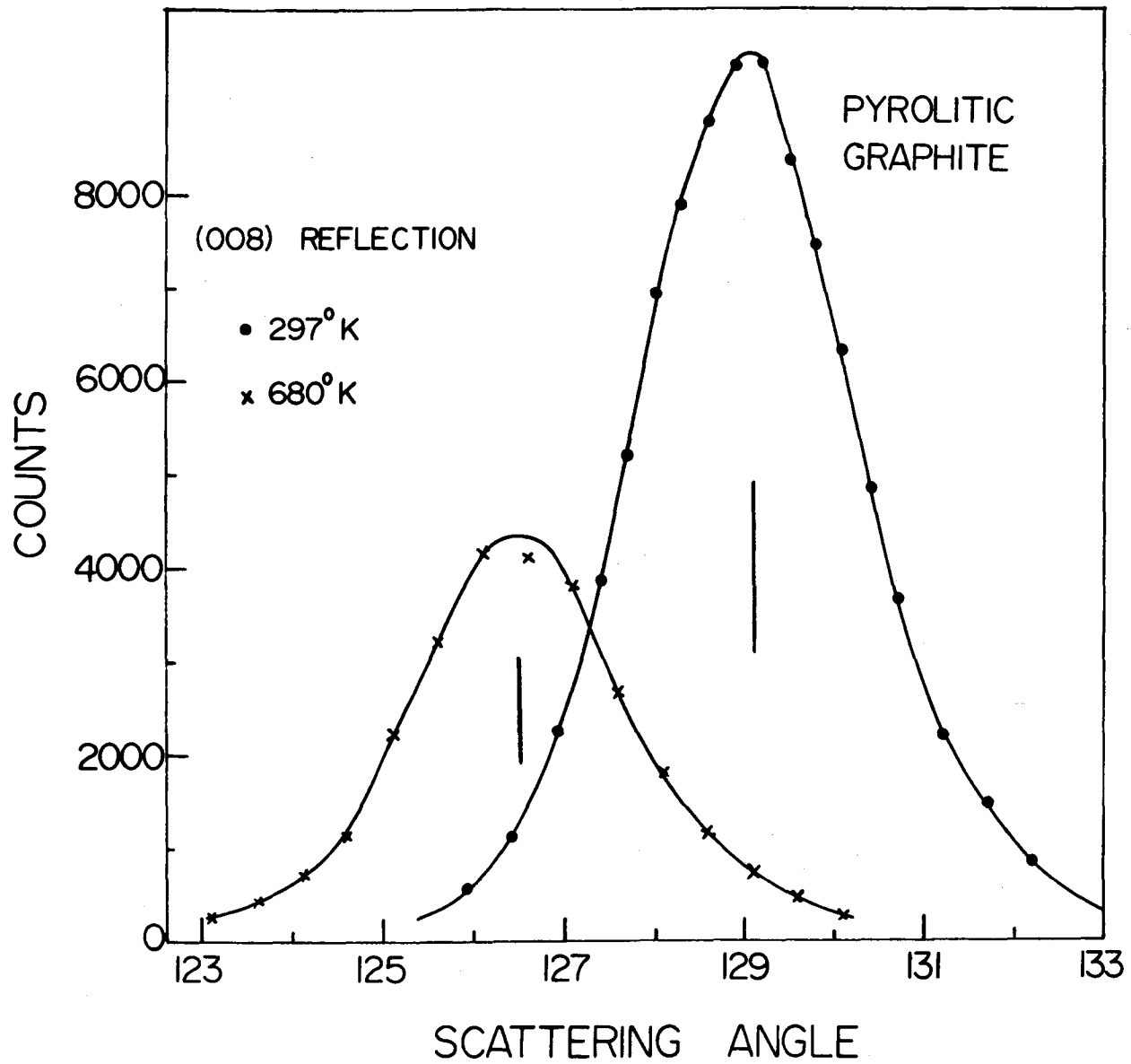


Fig. A3.1 Plots of the maximum intensity of the crystal rocking curves as a function of the scattering angle at two different temperatures.

in measuring the thermal expansion is estimated to be about 3 parts in 10^4 which amounts to an uncertainty of $\pm 10^\circ\text{K}$ in the temperature of the specimen. The temperature of the specimen, as recorded by the thermocouple, was found to be 685°K .

The phonons were measured at the point $\frac{c}{2\pi} Q = (003)$, where c (6.70 \AA at 296°) is the lattice constant along the hexagonal direction. At this point in reciprocal of space one measures the longitudinal vibration propagating along the c -axis with wavevector at the zone boundary (point A in group theoretical notation). This mode involves vibrations of neighbouring 'rigid' hexagonal planes of carbon atoms against each other. It has been studied previously at room temperature (Dolling and Brockhouse, 1962), who give the rationale as to why these modes are measurable in pyrolytic graphite.

The phonons were well defined and sharp and did not exhibit measurable changes in natural line width over the temperature range studied (Fig.A3.2). The line width is roughly that expected from instrumental resolution. The mosaic spread of 10° F.W.H.M. broadens the point of observation $Q = \frac{2\pi}{c} (0,0,3)$ into a distribution $\frac{2\pi}{c} (0.18,0.18,3)$ about the hexad axis. (In the basal plane, the Brillouin zone may be taken as bounded by a linear dimension of $\frac{2\pi}{a} (\frac{1}{\sqrt{3}})$ where $a = 2.456 \text{ \AA}$ is the lattice constant in the basal plane. Thus the Q -space resolution spread is about 15% of the zone

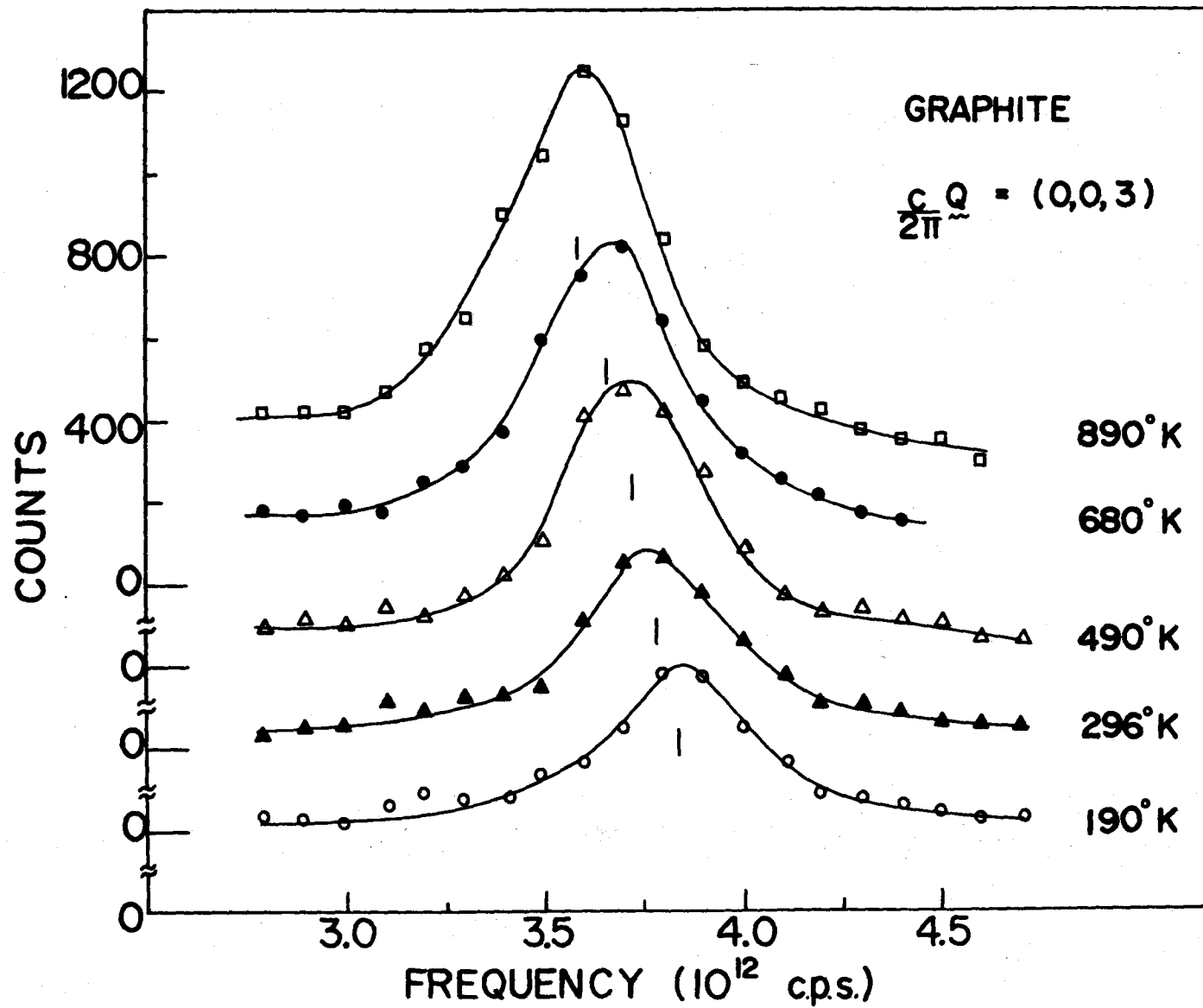


Fig. A3.2 Neutron groups observed at the point $(c/2\pi)\underline{Q} = (003)$ at various temperatures.

dimension in the basal plane. The branch under observation appears to be "flat" enough that this does not give a measurable effect¹.)

The phonon frequencies are given in Table A3.1 along with calculated values for the lattice constant (c). The relative frequency shifts are believed to have an accuracy of better than $\pm 0.02 \times 10^{12}$ cps. However, the independent frequency measurements probably have somewhat larger errors because of the large mosaic spread as discussed above. In the present case, the effect of finite resolution will be to shift the observed frequencies to higher values. It may be seen that the phonon frequencies display strong temperature dependence even though the highest temperature reached was only a small fraction of the melting temperature of graphite ($> 3800^\circ\text{K}$). From the observed frequency shifts the average Grüneisen constant γ for this zone boundary mode, defined as $(-d\ln\nu/d\ln V)$ where ν is the frequency and V is the crystal volume, is found to be 3.6.

Further, assuming that the [0001] longitudinal mode is adequately described by a sine wave (Dolling and Brockhouse 1962), the elastic constant C_{33} is estimated to vary by about 11% over the entire temperature range, from 0.37 at 190°K to 0.33 at 890°K in units of 10^{12} dynes/cm².

¹Recent measurements by Nicklow et al (1970) indicate that the transverse modes propagating in the basal plane and polarized along the c -axis are essentially isotropic.

TABLE A3.1

Phonon frequencies ν measured at
 $Q = \frac{2\pi}{c}(003)$ as a function of temperature T.

T (°K)	c* (Å°)	ν (10^{12} cps)
190	6.688	3.84
296	6.708	3.79
490	6.744	3.725
680	6.780	3.66
890	6.821	3.59

* Coefficient of linear expansion along
 c-axis was taken from AIP Handbook, 1963.
 2nd Ed. (McGraw-Hill, New York).

- Afansev, A. M. and Kagan, Yu. 1963. Soviet Phys. JETP
(English Transl., 16, 1030.
- Ambegaokar, V., Conway, J. and Baym, G. 1965. In Lattice Dynamics edited by R. F. Wallis (Pergamon Press Inc., N.Y.), p. 261.
- Anderson, J. R. and Gold, A.V. 1965. Phys. Rev. 139, A1459.
- Animalu, A.O.E. and Heine, V. 1965. Phil. Mag. 12, 1249.
- Bardeen, J. 1937. Phys. Rev. 52, 688.
- Barron, T.H.K., Leadbetter, A.J. and Morrison, J. A. 1964.
Proc. Roy. Soc. A279, 62.
- Barron, T.H.K. 1965. In Lattice Dynamics, edited by
R. F. Wallis (Pergamon Press Inc., N.Y.), p. 247.
- Bergsma, J. and Van Dijk, C. 1965. Reactor Centrum Nederland,
RCN34.
- Bjorkman, J., Lundqvist, B.I. and Sjolander, A. 1967.
Phys. Rev. 159, 551.
- Blackman, M. 1935. Proc. Roy. Soc. A149, 117.
————— 1941. Reports. Prog. Physics 8, 11.
- Bon Mardion, G., Goodman, B.B. and Lacaze, A. 1965.
J. Phys. Chem. Solids, 26, 1143.
- Born, M. and von Kármán, T. 1912. Physik. Z. 13, 297.
- Born, M. and Oppenheimer, J.R. 1927. Ann. Physik. 84, 457.
- Born, M. and Huang, K. 1954. Dynamical Theory of Crystal Lattices (Clarendon Press, Oxford).

- Bredov, M. M., Kotov, B.A., Okuneva, N.M. and Shakh-Budagov, A.L. 1967. Sov. Phys. Solid State [English Transl.], 9, 214.
- Brockhouse, B.N. 1958. Nuovo Cimento, Supp. 9, 45.
- Brockhouse, B.N. 1961. In Inelastic Scattering of Neutrons (IAEA, Vienna), p. 113.
- Brockhouse, B. N., Arase, T., Caglioti, G., Sakamoto, M., Sinclair, R.N. and Woods, A.D.B. 1961. In Inelastic Scattering of Neutrons (IAEA, Vienna) p. 531.
- Brockhouse, B. N., Rao, K. R. and Woods, A.D.B. 1961. Phys. Rev. Lett. 7, 93.
- Brockhouse, B. N., Arase, T., Caglioti, G., Rao, K. R. and Woods, A.D.B. 1962. Phys. Rev. 128, 1099.
- Brockhouse, B. N. 1964. In Phonons and Phonon Interactions edited by T. A. Bak (W. A. Benjamin Inc., N.Y.), p. 221.
- Brockhouse, B. N. 1966. In Phonons in Perfect Lattices and in Lattices with Point Imperfections, edited by R.W.H. Stevenson (Oliver & Boyd, London), p. 110.
- Brockhouse, B. N., deWit, G.A., Hallman, E.D. and Rowe, J.M. 1968. In Inelastic Scattering of Neutrons, Vol. II (IAEA, Vienna), p. 259.
- Brockhouse, B. N., Hallman, E.D. and Ng. S.C. 1968. In Magnetic and Inelastic Scattering of Neutrons by Metals, edited by T. J. Rowland and P. A. Beck (Gordon and Breach Inc., N.Y.), p. 161.

- Buyers, W.J.L. and Cowley, R. A. 1969. Phys. Rev. 180, 755.
- Caglioti, G. 1964. Acta Cryst. 17, 1202.
- Cassels, J.M. 1950. In Progress in Nuclear Physics, Vol. I, edited by O. Frisch (Academic Press, Inc., N.Y.), p.185.
- Chen, S. H. 1964. Ph.D. Thesis (McMaster University, Hamilton, Canada) Unpublished.
- Chester, G.V. 1961. Advan. Phys. 10, 357.
- Claeson, T. 1966. Phys. Rev. 147, 340.
- Claeson, T. and Ostklint, O. 1970. Solid State Commun. 8, 851.
- Cochran, W. 1963. Proc. Roy. Soc. A276, 308.
- Cochran, W. 1965. In Inelastic Scattering of Neutrons Vol. I. (IAEA, Vienna), p. 3.
- Collins, M. F. 1963. Brit. J. Appl. Phys. 14, 805.
- Cooper, M. J. and Nathans, R. 1967. Acta Cryst. 23, 357.
- Coulthard, M.A. 1970. J. Phys. C. (Solid State), 3, 820.
- Cowley, E. R. and Cowley, R. A. 1965. Proc. Roy. Soc. A287, 259.
- Cowley, R. A. 1963. Advan. Phys. 12, 421.
- Cowley, R. A. 1968. Reports Prog. Phys. 31, 123.
- Cowley, R. A. and Buyers, W.J.L. 1969. J. Phys. C. (Solid State) 2, 2262.
- Cowley, R. A., Svensson, E. and Buyers, W.J.L. 1969. Phys. Rev. Lett. 3, 525,
- Debye, P. 1912. Ann. Phys. 39, 789.

- de Gennes, P.G. 1964. In Metallic Solid Solutions, edited by J. Friedel (Benjamin, N.Y.), p. VI-1.
- DeWette, F. W. and Rahman, A. 1968. Phys. Rev. 176, 784.
- deWit, G. A. and Brockhouse, B. N. 1968. J. Appl. Phys. 39, 451.
- Dolling, G. and Brockhouse, B.N. 1962. Phys. Rev. 128, 1120.
- Dolling, G. and Woods, A.D.B. 1965. In Thermal Neutron Scattering, edited by P. A. Egelstaff (Academic Press, London and N. Y.), p. 193.
- Dynes, R. C., Carbotte, J.P. and Woll, E.J. Jr. 1968. Solid State Commun. 6, 101.
- Dynes, R. C., Carbotte, J.P., Taylor, D.W. and Campbell, C.K. 1969. Phys. Rev. 178, 713.
- Dynes, R. C. and Rowell, J. M. 1969. Phys. Rev. 187, 821.
- Egelstaff, P. A. 1953. AERE, Harwell, England, Report No. N/R 1164.
- Einstein, A. 1907. Ann. Phys. 22, 180.
- Elliott, R. J. and Maradudin, A. A. 1965. In Inelastic Scattering of Neutrons, Vol. I (IAEA, Vienna) p. 231.
- Foreman, A.J.E. and Lomer, W.M. 1957. Proc. Phys. Soc. (London) B70, 1143.
- Franck, J.P., Keeler, W.J. and Wu, T.M. 1969. Solid State Commun. 7, 483.
- Friedel, J. 1952. Phil. Mag. 43, 153.
- Geldart, D.J.W. and Vosko, S. J. 1966. Can. J. Phys. 44, 2137; *ibid* 1967. 45, 2229 (E).

- Gilat, G. 1965. Solid State Commun. 3, 101.
- Gilat, G. and Dolling, G. 1965. Phys. Rev. 138a, 1053.
- Grüneisen, E. 1926. In Handbuch der Physik, Vol. 10
(Springer, Berlin), p. 22.
- Hahn, H. 1963. In Inelastic Scattering of Neutrons, Vol. I
(IAEA, Vienna), p. 37.
- Hallman, E. D. and Brockhouse, B.N. 1969. Can. J. Phys.
47, 1117.
- Hallman, E.D. 1969. Ph.D. Thesis (McMaster Univ., Hamilton,
Canada) Unpublished.
- Hansen, M. 1958. Constitution of Binary Alloys (McGraw
Hill Book Co., N.Y.).
- Harrison, W. A. 1962. Phys. Rev. 126, 497.
- Harrison, W. A. 1966. Pseudopotentials in the Theory of
Metals (W. A. Benjamin Inc., N.Y.).
- Hayes, T.M., Brooks, H. and Bienenstock, A. 1968. Phys.
Rev. 175, 699.
- Heine, V. and Abarenkov, I. 1964. Phil. Mag. 9, 451.
- Högberg, T. and Sandström, R. 1969. Phys. Stat. Solidi.
33, 169.
- Hultgren, R., Orr, R. L., Anderson, P.D. and Kelley, K.K.
1963. Selected Values of Thermodynamic Properties of
Metals and Alloys (John Wiley and Sons Inc., N.Y.).
- Ivanov, M. A. and Krivoglaz, M.A. 1964. Soviet Phys. Solid
State [English Transl.] 6, 159.

- Iyengar, P. K., Venkataraman, G., Gameel, Y. H. and Rao, K.R. 1968. In Inelastic Scattering of Neutrons, Vol. I. (IAEA, Vienna), p. 195.
- Joshi, S. K. and Rajagopal, A.K. 1968. In Solid State Physics, Vol. 22; edited by F. Seitz and D. Turnbull (Academic Press Inc., N. Y.), p. 160.
- Kaganov, M.I. and Semenenko, A. I. 1966. Soviet Phys. JETP [English Transl.] 23, 419.
- Koehler, T., Gillis, N. S. and Wallace, D.C. 1970. Phys. Rev. B1, 4521.
- Kohn, W. 1959. Phys. Rev. Lett. 2, 393.
- Kokkedee, J.J.J. 1962. Physica, 28, 374.
- Kothari, L.S. and Singwi, K. S. 1958. In Solid State Physics, Vol. 8, edited by F. Seitz and D. Turnbull (Academic Press Inc., N.Y.). p. 109.
- Kotov, B. A., Okuneva, N.M. and Shakh-Budagov, A.L. 1968. Sov. Phys. - Solid State [English Transl.] 9, 2011.
- Krivoglaz, M. A. 1969. Theory of X-ray and Thermal Neutron Scattering by Real Crystals, (Plenum Press, N.Y.).
- Langer, J.S. and Vosko, S.H. 1959. J. Phys. Chem. Solids, 12, 196.
- Larsson, K. E., Holmryd, S. and Dahlborg, U. 1961. In Inelastic Scattering of Neutrons, (IAEA, Vienna), p. 587.
- Larsson, K. E., Dahlborg, U. and Jovic, D. 1965. In Inelastic Scattering of Neutrons, Vol. II (IAEA, Vienna), p. 117.

- Lechner, R. and Quittner, G. 1966. Phys. Rev. Lett. 17, 1259.
- Leibfried, G. and Ludwig, W. 1961. In Solid State Physics,
Vol. 12, edited by F. Seitz and D. Turnbull (Academic
Press Inc., N. Y.), p. 276.
- Ludwig, W. 1967. Recent Developments in Lattice Theory,
(Springer-Verlag, Berlin and N.Y.).
- Maradudin, A. A. and Fein, A.E. 1962. Phys. Rev. 128, 2589.
- Maradudin, A. A., Montroll, E.W. and Weiss, G.H. 1963.
Theory of Lattice Dynamics in the Harmonic Approximation,
(Academic Press, N.Y.).
- Maradudin, A. A. and Ambegaokar, V. 1964. Phys. Rev. 135, A1071.
- Marshall, W. and Stuart, R. 1961. In Inelastic Scattering of
Neutrons (IAEA, Vienna), p.75.
- Mathis, D.C. 1957. Phys. Rev. 106, 721.
- McMillan, W. L. and Rowell, J.M. 1965. Phys. Rev. Lett. 14, 108.
- Migdal, A.B. 1958. Soviet Phys. JETP [English Transl.] 7, 966.
- Miiller, A.P. and Brockhouse, B.N. 1968. Phys. Rev. Lett. 20,
798.
- Miiller, A.P. 1969. Ph.D. Thesis, (McMaster University, Hamilton,
Canada) Unpublished.
- Miiller, A.P. and Brockhouse, B.N. 1970. (To be published.).
- Møller, H.B. and Mackintosh, A.R. 1965. Phys. Rev. Lett. 15,
623.
- Mozer, B. and Otnes, K. 1963. In Inelastic Scattering of Neutrons,
Vol. II, (IAEA, Vienna) p. 167.
- Ng. Sc. 1967. Ph.D. Thesis (McMaster University, Hamilton,
Canada). Unpublished.

- Ng, S.C. and Brockhouse, B.N. 1967. Solid State Commun. 5, 79.
----- . 1968. In Inelastic Scattering of Neutrons, Vol. I (IAEA, Vienna), p. 253.
- Ng, S.C. Brockhouse, B. N. and Hallman, E.D. 1967. Mater. Res. Bull. 2, 69.
- Nicklow, R. M., Gilat, G., Smith, H.G., Raubenheimer, L.J. and Wilkinson, M. K. 1967. Phys. Rev. 164, 922.
- Nicklow, R. M., Vijayaraghavan, P. R., Smith, H.G., Dolling, G. and Wilkinson, M. K. 1968. In Neutron Inelastic Scattering, Vol. I (IAEA, Vienna), p. 47.
- Nicklow, R., Wakabayashi, N. and Smith, H. J. 1970. Bull. Am. Phys. Soc. 15, 383.
- Nix, F. C. and McNair, D. 1942. Phys. Rev. 61, 74.
- Pearson, W. B. 1958. Handbook of Lattice Spacings and Structure of Metals and Alloys (Pergamon Press, N.Y.).
- Peckham, G. 1964. AERE, Report No. 4380.
- Phillips, J.C. and Kleinman, L. 1959. Phys. Rev. 116, 287.
- Pines, D. and Nozières, P. 1966. The Theory of Quantum Liquids (W. A. Benjamin Inc., N.Y.).
- Placzek, G. 1954. Phys. Rev. 93, 897.
- Placzek, G. and Van Hove, L. 1954. Phys. Rev. 93, 1207.
- Powell, B. M., Martel, P. and Woods, A.D.B. 1968. Phys. Rev. 155, 619.
- Price, D. L., Singwi, K.S. and Tosi, M.P. 1970. Phys. Rev. (To be published).

- Rose, M. E., Miranker, W., Leak, P., Rosenthal, L. and Hendrickson, J.K. Westinghouse Electric Corporation, Atomic Power Division, Report WAPD SR-506.
- Rowe, J. M. 1965. Ph.D. Thesis (McMaster Univ., Hamilton, Canada) Unpublished.
- Rowell, J. M., McMillan, W. L. and Feldman, W.L. 1969. Phys. Rev. 178, 897.
- Roy, A. P. and Brockhouse, B. N. 1970. Can. J. Phys. 48, 1781.
- Sandström, R. and Högberg, T. 1970. J. Phys. Chem. Solids, 31, 1595.
- Schmunk, R. E., Brugger, R.M. and Randolph, P.D. 1965. In Inelastic Scattering of Neutrons, Vol. I (IAEA, Vienna), p. 379.
- Sham, L. J. and Ziman, J. M. 1963. In Solid State Physics, Vol. 15; edited by F. Seitz and D. Turnbull (Academic Press Inc., N.Y.), p. 223.
- Sham, L.J. 1965. Proc. Roy. Soc. (London) A283, 33.
- Sharp, R.I. 1969. J. Phys. C. (Solid State), 2, 432.
- Shepard, M.L. and Smith, J.F. 1967. Acta Met. 15, 357.
- Sjölander, A. 1958. Arkiv Fysik, 14, 315.
- Smithells, C.J. 1962. Metals Reference Book (Butterworths, London).
- Stedman, R. 1961. Quoted in the article by Brockhouse (1961).
- Stedman, R. and Nilsson, G. 1965. Phys. Rev. Lett. 15, 634.
- Stedman, R., Almqvist, L., Nilsson, G. and Raunio, G. 1967a. Phys. Rev. 162, 545.

- Stedman, R., Almqvist, L. and Nilsson, G. 1967b. Phys. Rev. 162, 549.
- Stedman, R., Almqvist, L., Nilsson, G. and Raunio, G. 1967c. Phys. Rev. 163, 567.
- Stokes, A.R. and Wilson, A.J.C. 1941. Proc. Phys. Soc. 53, 658.
- Svensson, E.C., Brockhouse, B.N. and Rowe, J.M. 1965. Solid State Commun. 3, 245.
- Svensson, E.C., Brockhouse, B.N. and Rowe, J.M. 1967. Phys. Rev. 162, 549.
- Takano, K. and Sato, J. 1965. J. Phys. Soc. Japan, 20, 13.
- Taylor, P. L. 1963. Phys. Rev. 131, 1995.
- Toya, T. 1958. J. Res. Inst. Catalysis, Hokkaido Univ. 6, 161, 183.
- Trofimenkoff, P. N. 1969. Ph.D. Thesis (McMaster Univ., Hamilton, Canada) Unpublished.
- Trofimenkoff, P. N. and Carbotte, J.P. 1970. Phys. Rev. B1, 1136.
- Van Hove, L. 1954. Phys. Rev. 95, 249.
- Vosko, S.H., Taylor, R. and Keech, G. H. 1965. Can. J. Phys. 43, 1187.
- Walker, C. B. and Egelstaff, P.A. 1969. Phys. Rev. 177, 1111.
- Wallace, D.C. 1968a, Phys. Rev. 176, 832.
- Wallace, D.C. 1968b. Phys. Rev. 176, 827.
- Waller, I. and Froman, P.O. 1952. Arkiv Fysik, 4, 183.

Weinstock, R. 1944. Phys. Rev. 65, 1.

Woll, E.J. Jr. and Kohn, W. 1962. Phys. Rev. 126, 1693.

Woods, A.D.B. 1965. In Inelastic Scattering of Neutrons,

Vol. I (IAEA, Vienna), p. 87; and the references therein.

Ziman, J. M. 1964. Advan. Phys. 13, 89.